

Electronic Thesis and Dissertation Repository

3-22-2024 2:30 PM

Value of Service-Oriented Multi-Service Provisioning and Resource Allocation in Integrated Localization, Sensing and Communication Systems

Biwei Li, *Western University*

Supervisor: Wang, Xianbin, *The University of Western Ontario*

A thesis submitted in partial fulfillment of the requirements for the Doctor of Philosophy degree in Electrical and Computer Engineering

© Biwei Li 2024

Follow this and additional works at: <https://ir.lib.uwo.ca/etd>



Part of the [Systems and Communications Commons](#)

Recommended Citation

Li, Biwei, "Value of Service-Oriented Multi-Service Provisioning and Resource Allocation in Integrated Localization, Sensing and Communication Systems" (2024). *Electronic Thesis and Dissertation Repository*. 9962.

<https://ir.lib.uwo.ca/etd/9962>

This Dissertation/Thesis is brought to you for free and open access by Scholarship@Western. It has been accepted for inclusion in Electronic Thesis and Dissertation Repository by an authorized administrator of Scholarship@Western. For more information, please contact wlsadmin@uwo.ca.

Abstract

The unprecedented proliferation of wireless infrastructures and their ongoing convergence with diverse industrial Internet of Things (IoT) applications introduce new demands for upcoming wireless networks. In response to such diversity of demands, envisioned future wireless networks must have multiple beyond communication capabilities, such as localization and sensing. To efficiently utilize, allocate, and manage these capabilities, the integration of localization, sensing, and communication (ILSAC) within a unified wireless system structure is of utmost importance. However, the seamless integration of ILSAC into intricate network infrastructures is encumbered by critical challenges, including high-accuracy localization/sensing algorithm, efficient resource management and allocation scheme, and robust optimization method under dynamic situations. Therefore, this thesis introduces a value-driven, multi-objective ILSAC system design mechanism.

Firstly, to extend the applicability of wireless localization into 3D environments targeting objects with six degrees of freedom, while simultaneously enhancing localization accuracy and extracting valuable environmental information from received signals, a rigid body joint localization and environment sensing scheme is proposed. Specifically, a two-step hierarchical compressive sensing algorithm is proposed to extract the angular and distance information of the line-of-sight (LOS) (if available) and single-bounce specular reflections. Then a particle swarm optimization (PSO) based method is derived to recover the posture of the rigid body and the location of reflection points. The simulation results demonstrate that the proposed scheme can achieve high accuracy in rigid body localization and locate the reflection points around the rigid body even under obstructed line-of-sight (OLOS) conditions in an indoor scene.

Secondly, to address the challenge of integrative resource allocation among coexisting functions and services within an integrated system, a service-oriented ILAC system is presented to allocate radio resources for diverse service provisioning under both static and dynamic environments. A novel concept, termed Value of Service (VoS), is coined to maximize the unified performance of the ILAC system for diverse service provisioning including localization accu-

racy and communication data rate. In the static scenario, the bandwidth and temporal resource allocation problem is formulated as a mixed-integer nonlinear problem for ILAC to maximize its VoS. In a dynamic scenario, a deep-reinforcement learning (DRL) based adaptive resource allocation update algorithm is developed for long-term system gain maximization. Simulation results demonstrate the significant superiority of our proposed VoS evaluation metric and resource allocation method in the ILAC system under both static and dynamic scenarios.

Thirdly, to tackle the dual challenge of the environment-dependent and resource-intensive nature of wireless sensing, along with managing the varied resource requirements of multiple users, we introduce a VoS-driven resource allocation scheme for cooperative service provisioning in a multi-user ISAC system. We formulate the multi-user resource allocation problem as a bargaining game-based model and address it using an iterative algorithm to attain the Nash equilibrium solution. In each iteration, power and bandwidth resources are allocated by solving the Lagrangian dual problem. Numerical simulations are performed under varying resource conditions, service demands, and channel states. The results highlight the superiority of our proposed scheme over non-collaborative alternatives and the other two benchmark schemes.

Keywords: Integrated localization and communication (ILAC), integrated sensing and communication (ISAC), resource allocation, localization and sensing, particle swarm algorithm (PSO), game theory, deep reinforcement learning, value of service (VoS).

Lay Summary

The rapid proliferation of intelligent devices, further driven by the emergence of next-generation vertical applications, including augmented reality (AR), smart factories, and autonomous robotics, has brought explosively growing demands for wireless networks to possess capabilities beyond the traditional role of data transmission. Among these capabilities, integrated localization, sensing, and communication (ILSAC) will greatly empower applications that require environmental understanding and perception alongside communication. Nonetheless, integrating localization and sensing services into existing communication systems significantly increases the complexity of system design and affects the efficiency of resource allocation. To address these challenges, this thesis developed a series of value-oriented mechanisms to guide the ILSAC system design, resource allocation and localization/sensing state recovery. Firstly, to extend the applicability of wireless localization into 3D environments targeting objects with six degrees of freedom, while simultaneously enhancing localization accuracy and extracting valuable environmental information from received signals, a rigid body joint localization and environment sensing scheme is proposed. Secondly, to address the challenge of integrative resource allocation among coexisting functions and services within an integrated system, a Value of Service (VoS) guided ILAC system is presented to allocate radio resources for diverse service provisioning under both static and dynamic environments. Thirdly, to tackle the dual challenge of the resource-intensive and environment-dependent nature of sensing, along with managing the varied resource requirements of multiple users, we introduce a VoS-driven resource allocation scheme for cooperative service provisioning in a multi-user ISAC system.

Acknowledgements

I would like to express my deep appreciation to Dr. Xianbin Wang for his exceptional guidance and support throughout my doctoral journey. Dr. Wang's mentorship has played a pivotal role in both my academic and personal development. His insightful feedback, encouragement, patience and guidance have elevated the quality of my work, and I am thankful for the opportunities to contribute to meaningful research projects under his supervision.

Thanks go to all present and former members of our research group for the time that we spent both at work and after work. I would give my best regards for their success in both study and life. I would like to extend my thanks to all my friends at Western University. The last four years have been full of fun and warmth because of your accompany and friendship. As always, I wish to thank my family for their love, support, and encouragement throughout these years.

Contents

Abstract	ii
Lay Summary	iv
Acknowledgements	v
List of Figures	x
List of Tables	xii
List of Appendices	xiii
List of Abbreviations	xiv
1 Introduction	1
1.1 Overview of Integrated Localization, Sensing and Communication Systems . . .	1
1.2 Challenges Faced by ILSAC Systems	6
1.3 Research Objective of Thesis	8
1.4 Contributions of the Thesis	10
1.5 Thesis Outlines	12
2 Challenges and Existing Solutions of Resource Allocation in ILSAC Systems	14
2.1 Background of ILSAC Systems	15
2.1.1 Wireless Localization and Sensing Technologies	15
2.1.2 Integrated Localization, Sensing and Communication	17
2.2 Existing Solutions of Resource Allocation and Their Challenges in ILSAC systems	19
2.2.1 System Mechanism and Evaluation Metric	19
2.2.2 Resource Allocation Technologies	21
2.3 Chapter Summary	23
3 5G mmWave based Joint Localization and Environment Sensing	24
3.1 Introduction	24
3.2 System Model	28
3.2.1 Environment Model	28
3.2.2 Joint Rigid Body and Reflection Points Localization Model	28
3.3 Proposed Joint Rigid Body and Reflection Points Localization Scheme	31

3.3.1	Channel Parameters Estimation	31
3.3.1.1	H-DCS-SOMP	32
3.3.1.2	Fine Estimation	35
3.3.2	Joint Rigid Body and Reflection Points Localization	37
3.3.3	Complexity Analysis	39
3.3.3.1	Channel Parameter Estimation	39
3.3.3.2	Joint Position Estimation	40
3.4	Fundamental bounds	41
3.5	Simulation Results	46
3.5.1	Simulation Setup	46
3.5.2	Rigid Body Posture Estimation	47
3.5.3	Reflection Points Location Estimation	51
3.6	Chapter Summary	53
4	Value of Service Maximization in ILAC System through Joint Resource Allocation	55
4.1	Introduction	55
4.2	System Model	59
4.2.1	Architecture of ILAC System	59
4.2.2	VoS of Communication	61
4.2.3	VoS of Localization	64
4.2.4	Problem Formulation	67
4.3	Proposed Resource Allocation Scheme	68
4.3.1	Bandwidth Allocation	68
4.3.1.1	Continuous Bandwidth Allocation	69
4.3.1.2	Discretization	71
4.3.2	Time Slot Allocation	72
4.3.3	Joint Resource Allocation Scheme	75
4.3.4	Complexity Analysis	77
4.4	Simulation Results	78
4.4.1	Evaluation of Metrics	78
4.4.2	Evaluation of Resource Allocation	80
4.4.2.1	Influence of Service Number	81
4.4.2.2	Influence of Resources	83
4.4.2.3	Complexity Analysis	86
4.4.3	Influence of Localization Weight	86
4.5	Chapter Summary	87
5	Successive Resource Allocation in Multi-User ISAC System through Deep Reinforcement Learning	88
5.1	Introduction	88
5.2	System Model	90
5.2.1	Architecture of Successive ISAC System	90
5.2.2	Sensing Model	91
5.2.3	Communication Model	94
5.2.4	Problem Formulation	95

5.3	Resource Allocation with DRL	96
5.3.1	Deep Reinforcement Learning	96
5.3.1.1	State space	97
5.3.1.2	Action space	97
5.3.1.3	Reward space	98
5.3.2	DRL-based Resource Allocation	98
5.4	Simulation Results	102
5.4.1	Parameter Setting of DRL	104
5.4.2	Effect of Available Resources	105
5.4.3	Effect of Service Request Number	106
5.4.4	Effect of Dynamic Situation	107
5.5	Chapter Summary	108
6	Value of Service Maximization in Multi-User ISAC Systems through Collaborative Resource Allocation	109
6.1	Introduction	109
6.1.1	Motivations	109
6.1.2	Related Work	111
6.1.3	Contributions	112
6.2	System Model	113
6.2.1	Communication Model	115
6.2.2	Sensing Model	118
6.2.3	Problem Formulation	121
6.3	Methodology	123
6.3.1	Collaborative Resource Allocation Game Formulation	123
6.3.2	Power Allocation Update	125
6.3.3	Bandwidth Allocation Update	127
6.3.4	Iterative Algorithm Design	129
6.4	Simulation Results	130
6.4.1	Influence of Resources	132
6.4.2	Influence of Service Number	133
6.4.3	Performance Analysis	134
6.4.3.1	Fairness Analysis	134
6.4.3.2	Robustness Analysis	136
6.5	Chapter Summary	138
7	Conclusion and Future Works	140
7.1	Conclusion	140
7.2	Future Works	142
	Bibliography	145
A	Proofs of Theorems in Chapter 3	159
A.1	The FIM of Channel Parameters in (3.38)	159
A.2	The Entries in (3.48)	160

B Proofs of Theorems in Chapter 6	162
B.1 Derivation of CRLB of $\boldsymbol{\eta}_{k,m,m'}$	162
B.2 Derivation of PEB from CRLB of $\boldsymbol{\eta}_{k,m,m'}$	163
B.3 Proof of Proposition 1	164
B.4 Proof of Proposition 2	165
Curriculum Vitae	166

List of Figures

1.1	Diverse applications with heterogeneous service requirements in industrial IoT scenarios are facilitated by multiple advanced capabilities, including localization, sensing and communication.	2
1.2	The illustration of structure, enablers and the ultimate goal of ILSAC system.	4
2.1	Examples of two types of wireless-based localization methods. (a) Localization method based on RSS or TOA, and (b) localization method using angular estimation (AOA/AOD).	16
2.2	Schematic illustration of (a) bi-static and (b) mono-static wireless sensing. The Tx and Rx are located at different devices in bi-static sensing. The Tx and Rx are co-located at BS in mono-static sensing.	16
3.1	Schematic illustration of signal transmission between anchor node and rigid body.	29
3.2	Dictionary construction in H-DCS-SOMP procedure.	34
3.3	The CDF of rigid body localization RMSE (left) and rigid body rotation angle RMSE (right) of three methods when SNR is 20 dB.	48
3.4	The CDF of rigid body localization RMSE (left) and rigid body rotation angle RMSE (right) of of three methods when SNR is 0 dB.	48
3.5	The rigid body localization RMSE (top) and rigid body rotation angle RMSE (bottom) of DCS-SOMP, H-DCS-SOMP, modified H-DCS-SOMP and corresponding theoretical bound vs different SNRs.	49
3.6	In the OLOS situation, the rigid body localization RMSE (top) and rigid body rotation angle RMSE (bottom) of modified H-DCS-SOMP and corresponding theoretical bound vs different SNRs.	50
3.7	The average AOA/AOD RMSE of the NLOS paths and their corresponding theoretical bounds under different SNRs.	52
3.8	The reflection points localization RMSE of DCS-SOMP, modified H-DCS-SOMP with GA method, modified H-DCS-SOMP with PSO method and corresponding theoretical bound vs different SNRs.	53
4.1	Illustration of joint resource allocation in ILAC system for tailored service provisioning.	60
4.2	The localization accuracy (top) and communication data rate (bottom) deviation with the three metrics as the objective function.	80
4.3	The VoS (top left), VoS of communication (top right), VoS of localization (bottom) of JRA, NJRA and RRA under different service numbers.	82

4.4	The comparison of JRA-GA algorithm and JRA-PSO algorithm vs average running time under different service numbers.	83
4.5	The CDF of VoS (top left), VoS of communication (top right), VoS of localization (bottom) with JRA, NJRA and RRA under different resource conditions.	84
4.6	The VoS (top left), VoS of communication (top right), VoS of localization (bottom) with JRA, NJRA and RRA under varied temporal resource conditions.	85
4.7	The allocated PRB number for localization (left) and VoS (right) with JRA, NJRA and RRA under different required localization weights.	87
5.1	Illustration of successive resource allocation in multi-user ISAC system for tailored service provisioning.	91
5.2	Illustration of the interaction between actor and critic network.	99
5.3	Average reward performance versus episodes under different learning rates.	105
5.4	The VoS versus different resource conditions: different power constraints (left) and bandwidth constraints (right) with four different methods.	106
5.5	The VoS versus service request number with four different resource allocation methods.	107
5.6	The CDF of VoS under different resource conditions with DRL method.	108
6.1	Illustration of collaborative sensing service provisioning in a multi-user ISAC system. Users within a group can collaborate in sensing and sharing the results.	114
6.2	Illustration of position error bounds with collaborative and non-collaborative sensing scheme (D_1 : Sensing PEB without collaboration; D_2 : Sensing PEB with collaboration).	121
6.3	The VoS of four schemes under different bandwidth resources (left) and power resources (right).	133
6.4	The VoS of four schemes under different service numbers.	134
6.5	The data rate and achievable sensing accuracy of four schemes under different service numbers.	135
6.6	The individual VoS of each user with non-collaborative and collaborative schemes with respect to bandwidth (left) and power resources (right).	136
6.7	The individual VoS of each user with non-collaborative and collaborative scheme.	137
6.8	CDF of VoS with variable service requests.	137
6.9	Achievable sensing accuracy vs. average rate trade-off using three different schemes.	138
6.10	The VoS of three schemes under different SNR.	139

List of Tables

2.1	Resource allocation strategies in ISAC systems.	19
4.1	System parameters in chapter 4.	78

List of Appendices

Appendix A Proofs of Theorems in Chapter 3	159
Appendix B Proofs of Theorems in Chapter 6	162

List of Abbreviations

2D Two Dimension

2G Second Generation

3D Three Dimension

5G Fifth Generation

AOA Angle of Arrival

AOD Angle of Departure

AWGN Additive White Gaussian Noise

CDF Cumulative Distribution Function

CRLB Cramer-Rao Lower Bound

CS Compressive Sensing

CSI Channel State Information

DCS-SOMP Distributed Compressed Sensing-Simultaneous Orthogonal Matching Pursuit

DRL Deep Reinforcement Learning

GA Genetic Algorithm

GCS Global Coordinate System

GNSS Global Navigation Satellite Systems

ILAC Integrated Localization and Communication

ILSAC Integrated Localization, Sensing and Communication

IML Maximum Likelihood

IoT Internet of Things

ISAC Integrated Sensing and Communication

JCR Joint Communication and Radar

JRA Joint Resource Allocation

KKT Karush-Kuhn-Tucker

LOS Line-of-sight

MDP Markov Decision Process

mmWave millimeter Wave

MIMO Multi Input Multi Output

mMIMO massive MIMO
NLOS Non-line-of-sight
OFDM Orthogonal Frequency Division Multiplexing
OLOS Obstructed-line-of-sight
PSO Particle Swarm Algorithm
QoS Quality of Service
RBCS Rigid Body Coordinate System
RBL Rigid Body Localization
RMSE Root Mean Square Error
RoI Range of Interest
SNR Signal-to-Noise-Ratio
TOA Time of Arrival
TDOA Time Difference of Arrival
URA Uniform Rectangular Array
VoS Value of Service
XR Extended Reality

Chapter 1

Introduction

1.1 Overview of Integrated Localization, Sensing and Communication Systems

With the rapid convergence of wireless infrastructure and vertical applications, the integration of multiple capabilities into existing wireless networks is envisioned as an inevitable trend in the development of future 6th-generation (6G) wireless networks. This trend is pivotal in supporting ubiquitous Internet of Things (IoT) applications, including factory automation, extended reality (XR), intelligent transportation and smart home systems. To enable functionalities such as remote monitoring and intelligent control in diverse application scenarios, there is an unprecedented proliferation of heterogeneous devices with stringent service requirements. To meet these evolving requirements and fully unlock the potential of intelligent applications, future wireless systems must provide not only high-quality connectivity between devices but also extend their capabilities beyond traditional communication. In contrast to current communication-centric 5G networks, numerous new capabilities, including wireless localization and sensing, will play more significant roles than ever before [1, 2]. Here, we introduce two promising industrial IoT applications that necessitate the wireless network to possess multiple capabilities, as shown in Fig. 1.1.

- Smart manufacturing demands situation-aware coordination and interaction among all involved entities to effectively and intelligently achieve operational goals. For instance,

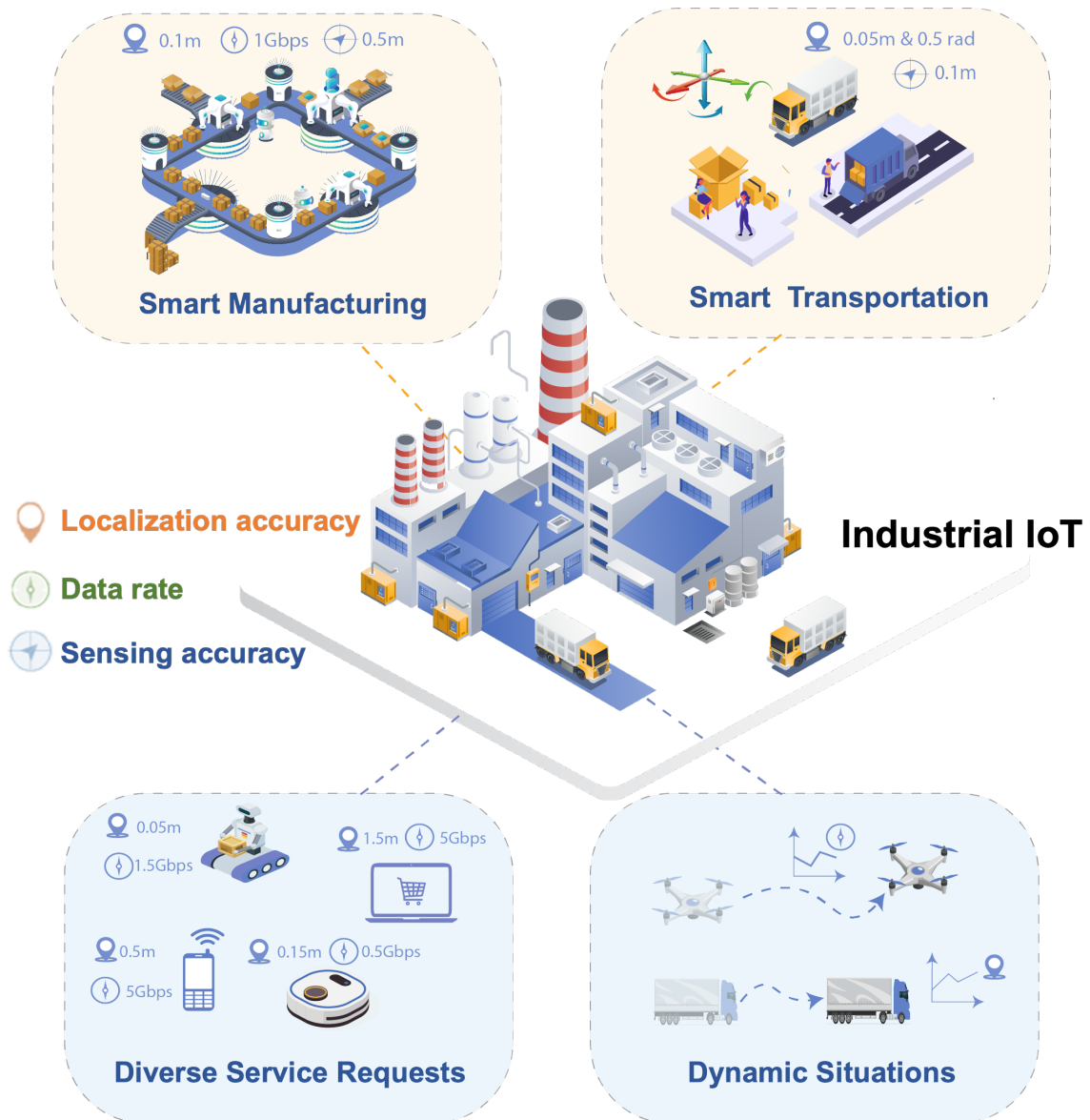


Figure 1.1. Diverse applications with heterogeneous service requirements in industrial IoT scenarios are facilitated by multiple advanced capabilities, including localization, sensing and communication.

collaborative robotics, widely employed in smart factories, exhibits substantial potential for autonomously executing a diverse set of labour-intensive tasks with heightened safety and efficiency. However, achieving intelligent operations within a group of robotics introduces new requirements for wireless networks. These requests cover extreme reliability system operation, precise positioning and sensing, and low-latency communication, which are well beyond the capabilities of existing 5G communication networks.

- Smart transportation aims to establish a seamless and interconnected mobility system, optimizing the efficient and safe movement of vehicles/objects. Within a smart transportation system, real-time localization is critical for making timely decisions to avoid collisions. Additionally, communication services play a vital role in data exchange between vehicles and the infrastructure, as well as with other connected devices in the vicinity. To meet such stringent service requirements, the wireless system must be capable of timely switching between localization, sensing and communication services, surpassing the capabilities of current 5G networks [3].

As observed from these two application scenarios, there is an urgent and critical need for an integrated wireless system that can effectively and intelligently incorporate multiple functionalities to support diverse requests from coexisting heterogeneous users. Naturally, a new design paradigm named integrated localization, sensing and communication (ILSAC) enters the field of vision.

Integrating localization service into existing wireless communication systems has been a natural progression. Starting from the second-generation cellular network (2G) [2], localization has been incorporated into wireless networks to estimate the physical position of target devices using wireless signals. For 5G and beyond, wireless localization has emerged as an essential component, providing fundamental support for a wide range of location-based services, including tracking in industrial environments and navigation in smart transportation. A significant advantage of wireless localization, especially in cluttered or indoor environments, lies in its ability to achieve sub-meter or even centimeter-level positioning accuracy, greatly surpassing the capabilities of global navigation satellite systems (GNSS). This high accuracy performance is critical in various emerging applications. For example, achieving submeter-level localization accuracy is necessary for efficient support and cooperation with various intelligent devices in automated factories. Therefore, accurately localizing a device in two-dimensional (2D) or even three-dimensional (3D) space with the assistance of wireless signals is one of the major requirements for forthcoming wireless systems.

Nevertheless, device-based localization, restricted to merely pinpointing the location of a specific object with a smart device, falls short in adequately supporting broader IoT scenarios. To overcome this limitation, a recent concept of "sensing as a service" was proposed, which

aims to integrate sensing capability into wireless networks, enabling the extraction of spectroscopic and geometric information from the surrounding environment [4]. Generally, wireless sensing includes the detection, localization, and tracking of physical objects within a given scenario. To distinguish it from wireless localization, wireless sensing focuses on device-free object sensing, meaning the targeted objects do not carry any electronic devices, as shown in Fig. 1.2. Advancements in wireless communication technologies, such as large-scale antenna systems, have played a pivotal role in enabling the development of reliable and real-time sensing capabilities for various IoT applications. In applications like robotics and automatic vehicles, dependable sensing of surrounding environments is critical to ensure safe and efficient operations. Consequently, the integration of wireless sensing into the current wireless network is emerging as a new trend to effectively support various vertical applications.

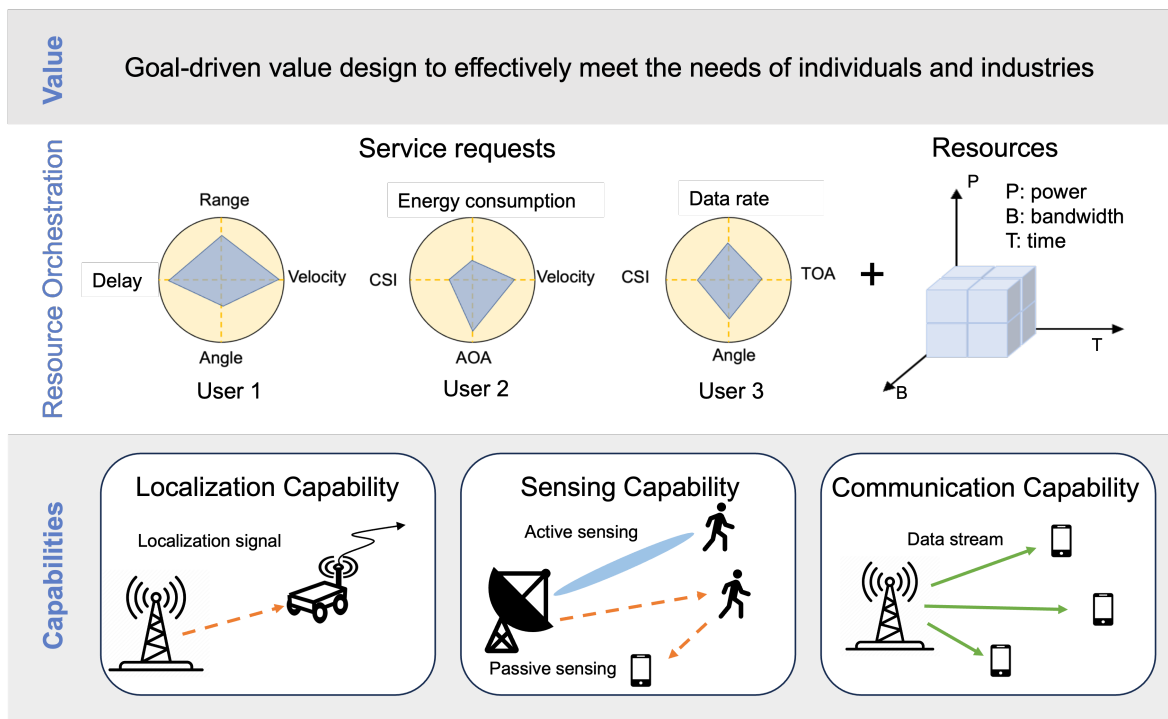


Figure 1.2. The illustration of structure, enablers and the ultimate goal of ILSAC system.

Through the integration of localization, sensing and communication services, ILSAC enables the concurrent exchange of data and localization/sensing information over the same wireless network. ILSAC not only expands the boundary and scope of wireless network services but also elevates the system’s integration to a new level.

- **Level 1 – Shared signal:** The swift advancement of massive MIMO (mMIMO) [5] and millimeter-wave (mmWave) [6] technologies constitutes a foundation for ILSAC, employing a shared signal [7] to cater to the diverse requests of users. Wireless sensing/localization and communication exhibit similarities in their channel characteristics and signal processing approaches, especially as their operating frequencies extend into the mmWave band [5]. For instance, extracting channel characteristics such as channel state information (CSI) can provide mutual benefits to both communication and sensing services. Consequently, wireless infrastructures and devices for communication can effectively perform sensing/localization through radio emission and signalling, establishing the technical foundation and rationale of ILSAC [4].
- **Level 2 – Resource allocation:** Given the feasibility of integrating sensing/localization into an existing wireless system, the next level of integration is to efficiently optimize the utilization of wireless resources for different kinds of capabilities. To better serve the diverse requirements of users, radio resources once exclusively allocated to communication must now be redistributed to support multiple functionalities, including positioning, sensing, and communication. Thus, the wireless resource allocation in the ILSAC system needs to accommodate multiple purposes and minimize redundancy in resource utilization across transmissions, devices, and infrastructure. In addition, due to certain overlaps in waveform design and signal processing for sensing/localization and communication, the collaborative support of these three functionalities can significantly enhance resource utilization while ensuring service quality.
- **Level 3 – Value realization:** The ultimate objective of an integrated system is to customize solutions to meet the specific requirements of users, effectively fulfilling the diverse needs of individuals and industries, as illustrated in Fig. 1.2. In the next generation of wireless systems, addressing the highly stringent service requests of various applications requires considering the benefits of each connected user and the overall system. This means that the value of integration goes beyond the addition of multiple functions; it lies in effectively utilizing limited resources and maximizing satisfaction for diverse users, ultimately optimizing the long-term gains for the entire system. Taking smart

manufacturing as an example, intelligent devices with varying hardware capabilities are assigned different tasks with varying levels of urgency. The radio resource allocation strategy will directly impact the efficiency of task completion. Thus, the value-oriented integrated system design will be focused on achieving individualized service provisioning at low operation costs for end-users, while ensuring the high resource allocation efficiency for the entire network. The ILSAC system will be an integrated framework that encompasses various service requests, spatiotemporal available resources, and device hardware capabilities, among other aspects.

Despite the promise of ILSAC systems, the integration of these three functionalities introduces new challenges that are not yet addressed.

1.2 Challenges Faced by ILSAC Systems

ILSAC has been envisioned as a crucial booster for next-generation wireless systems to support emerging applications with diverse service demands. However, as application scenarios become increasingly complex, numerous technical challenges inevitably hinder the development of the integrated system. To unlock the full potential of the ILSAC system, critical challenges must be addressed which are summarized in three categories.

- **Efficient ILSAC system mechanism to support applications:** Existing wireless systems usually feature stringent resource conditions to fulfill various functionalities, presenting significant challenges in meeting the rapidly growing service demands of emerging vertical applications. To overcome these limitations, an integrated system needs to efficiently utilize available resources and equipment to comprehensively optimize the system's potential value. This includes not only supporting broader service requests but also enhancing service provisioning efficiency while maintaining service quality. To achieve these goals, the following two trade-offs need to be considered.
 - *The trade-off between users:* In future intelligent IoT scenarios, the connected users within the network will demonstrate a high degree of heterogeneity. Consequently, these users not only present diverse service requirements but also exhibit varying

hardware capabilities, leading to a mismatch between their capabilities and needs. Some users or devices with limited capabilities may have exceedingly high service requests that demand substantial resources, which are beyond the hardware capabilities of the device. Conversely, other devices may not have high-priority service requests but possess better hardware capabilities. Hence, efficiently managing heterogeneous users in the network and allocating resources to meet individual service requests for realizing the system's value is an urgent challenge that needs to be tackled.

- *The trade-off between resources and needs:* In a multi-user integrated system, the concurrent but diverse service requests in terms of localization/sensing accuracy and communication performance from a particular application impose further requirements on wireless resource allocation. On the one hand, the needs of users are often random and unpredictable, which leads to resource contention among service requests at any given moment. On the other hand, within a particular service request, localization/sensing services also compete with communication services for stringent radio resources. Hence, resource allocation guided by a unified goal is essential for the ILSAC system.
- **Robust metric to guide the ILSAC system design:** To achieve integrated system operation, a critical objective is to reach and maintain a common goal among different functionalities and users. Thus, the state-of-the-art objective in integrated multifunctional systems (for example, ISAC) is to optimize the trade-off between sensing and communication performance while considering the multiple constraints of the system. However, to support heterogeneous QoS provisioning from diverse users in the ILSAC system, such evaluation metric design is outdated and limited. On the one hand, from the user's perspective, the wide variety of service requests combining sensing and communication reduces the effectiveness of existing resource allocation based on maximizing traditional QoS, which results in difficulty in ensuring an optimal service experience. On the other hand, from the perspective of the ILSAC system operation, improving either individual sensing accuracy or communication data rate separately doesn't necessarily maximize

the system's overall service value. Thus, the value of an integrated system should be able to adaptively adjust based on different users' needs and resource conditions.

- **Flexible and timely system orchestration to optimize resource utilization:** To achieve robust, on-demand and real-time service provisioning and ultimately achieve system-level value maximization, collaboratively management of resources, and devices under dynamic situations is critical and challenging. On the one hand, in the ILSAC system, the diverse service requests from heterogeneous applications propose beyond communication requirements to the wireless system. Optimally allocating available resources to fulfill hybrid and application-specific service requests becomes a new design challenge. Generally, localization, sensing and data transmission cannot be performed at the same time at the same RF front end. This means three capabilities are competing resources for their own performance improvement. Without a flexible and efficient multi-dimensional resource utilization strategy, three independent goals would lead to a one-sided emphasis on localization/sensing accuracy or communication data rate, which deteriorates the overall system performance. On the other hand, adapting to real-time service requests in a dynamic environment is another challenge that needs to be addressed. The dynamic topology of the environment and the stochastic density of the users result in fast varying channel conditions, which cause a major obstacle for radio resource allocation to guarantee the system's performance.

1.3 Research Objective of Thesis

To overcome the aforementioned challenges under heterogeneous intelligent application scenarios, our ultimate objective is to maximize the value of service (VoS) provisioning in an ILSAC system through multi-dimensional resource allocation. To achieve this objective, we first introduce a new evaluation metric, VoS to guide the ILSAC system design. Subsequently, we formulate distinct objective functions tailored for the ILSAC system to adapt to various application scenarios. As depicted in Fig. 1.1, different system configurations in diverse application scenarios are represented by the establishment of specific goals for maximizing their value. Three specific objectives are illustrated as follows.

- **High-accuracy 5G-enabled localization and sensing:** To optimize the orchestration of the ILSAC system, it is crucial to enhance localization and sensing accuracy to support stringent service requests. 5G-based positioning should not only fulfill the demands of emerging commercial and industrial location-based services but also enhance communication performance across different network layers in various aspects. For example, location-aided channel estimation, beam alignment, and network optimization. In conventional 5G mmWave-based localization, a device is modelled as a point target whose location is only defined by the 3D coordinates with three degrees of freedom while neglecting its orientations. The goal of environment sensing is to estimate the scatters (or reflection points) in the environment to improve the moving device localization accuracy only in the 2D scenario. However, to achieve accurate maneuvering for broader intelligent tasks like cargo transportation, robotic control and others, not only device position but also its orientations are required. To address these deficiencies, we propose a joint localization and environment sensing scheme of a rigid body with the assistance of 5G mmWave MIMO.
- **Value-oriented ILAC systems through joint resource allocation:** Within the ILAC system, diverse service requests with varying location accuracy and communication performance requirements pose additional challenges for wireless resource allocation. User requests in the ILAC system may encompass specific requirements based on the diverse applications. Effectively allocating available resources while meeting these hybrid and application-specific service requests emerges as a new design challenge for ILAC systems. Consequently, finding the right balance between localization and communication performance becomes crucial to address this challenge. However, this task proves to be complex due to the shared use of hardware platforms and radio resources for both communication and localization purposes. Previous research has proposed resource allocation strategies for ILAC/ISAC systems. However, these approaches fall short of demonstrating how to orchestrate and operate integrated systems to achieve the objectives and value realization of vertical applications. Therefore, we propose a value-oriented ILAC system that jointly allocates bandwidth and temporal resources. Furthermore, as dis-

cussed earlier, the provision of reliable real-time services in an integrated system is hindered by the dynamic environment and evolving service requests. Thus, a successive ISAC system operation is proposed to tackle the resource allocation problem under dynamic situations.

- **Value-oriented collaborative service provisioning in ISAC systems:** One of the main challenges encountered by the ISAC system is the resource-hungry nature of sensing processes, coupled with competing demands from coexisting users, which poses the fundamental challenge of effective and fair resource allocation among users. This challenge arises from the inadequacy of traditional QoS in guiding resource allocation and the mismatch between users' needs and their hardware capabilities. To address this challenge, we propose a VoS-oriented resource allocation scheme for heterogeneous service provisioning in multi-user collaborative sensing processes within a wireless network. A performance indicator VoS is utilized to achieve system-wide effective resource allocation while guaranteeing fairness for each individual user.

1.4 Contributions of the Thesis

The main contributions of the thesis are summarized as follows.

- In numerous intelligent applications, there is a requirement for acquiring not only the location and orientation of devices but also information about the surrounding environment. To support such applications with high localization and environment sensing service requests, the mm-wave MIMO-assisted rigid body active localization and environment sensing scheme is proposed. In the considered 3D scenario, the six degrees of freedom of the rigid body are successfully resolved with only one base station equipped with a uniform rectangular array (URA). Three different cases are investigated: with only line-of-sight (LOS), with both LOS and non-line-of-sight (NLOS), and with only the NLOS. Moreover, when there's NLOS, the position of reflection points in the environment is also estimated. Both the rigid body localization and reflection point estimation are achieved at the rigid body end with the one-way signals. To guarantee high rigid

body/reflection points localization accuracy, a new strategy of the multi-step hierarchical design is developed.

- To fulfill various users' needs with limited available resources, a service-oriented joint resource allocation scheme for the ILAC system is introduced. A comprehensive metric, named Value of Service (VoS), is proposed to evaluate the unified system performance. Our goal is to maximize VoS by jointly allocating multi-dimensional resources. Specifically, a new mechanism of integrating localization and communication processes is proposed by jointly allocating the shared radio and temporal resources to meet the needs of diverse applications. To share the limited resources among concurrent service requests with different priorities, a new performance metric, VoS, is proposed in this paper to guide the ILAC system design. With VoS maximization as the objective, a joint radio and temporal resource allocation algorithm is proposed. The optimization of multi-dimensional resource allocation is formulated as a mixed-integer nonlinear problem. A joint resource allocation (JRA) strategy is developed to decompose the overall problem into two sub-problems. Firstly, the bandwidth resource is optimized with a Kelly mechanism-based continuous allocation method followed by discretization. Secondly, the temporal resource is assigned with the aid of an adaptive particle swarm optimization (PSO)- based approach.
- Predictively offering integrated services poses a significant challenge due to the dynamic nature of service requests, resources, and environments. To further adaptively meet real-time service requests in a dynamic environment, a joint radio and power resources allocation scheme for successive ISAC systems is proposed. A successive ISAC system mechanism is proposed by adaptively allocating the bandwidth and power to meet the real-time integrated sensing and communication service requests under a dynamic environment. A deep-reinforcement learning (DRL) based algorithm is developed to maximize the long-term ISAC system gain. To adaptively orchestrate the allocation strategy, the changeable environments and service requests are embedded into the DRL scheme.
- Ensuring precise sensing service provisioning is challenging, given the resource-intensive nature of the process, particularly for users with hardware limitations. To improve the

sensing efficiency in a large-scale ISAC system, a value of service (VoS)-oriented resource allocation scheme for heterogeneous service provisioning in multi-user collaborative sensing processes within a wireless network is proposed. A performance indicator VoS is utilized to achieve system-wide effective resource allocation while guaranteeing fairness for each individual user. Specifically, we formulate the multi-user resource allocation problem as a bargaining game-based model and tackle it with an iterative algorithm to attain the Nash equilibrium. In each iteration, power and bandwidth resources are optimized by solving the Lagrangian dual problem.

1.5 Thesis Outlines

The remainder of this thesis is organized as follows.

In Chapter 2, a comprehensive study of integrated localization, sensing and communication systems is conducted. An overview of the development of ILSAC is given first, followed by the current challenges and progress in the ILSAC system, including the system structure and evaluation metric design as well as the resource allocation strategy. Finally, a survey on the resource allocation method used in multi-dimensional resource allocation is given.

In Chapter 3, the 3D active rigid body localization and environmental sensing enabled by 5G mm-wave MIMO is proposed to support various applications. Specifically, the position and orientation of the rigid body are solved through a two-step hierarchical compressive sensing algorithm followed by a PSO-based approach. Meantime, the reflection points in the surrounding environment are unravelled with the assistance of multiple paths. Moreover, the Cramér-Rao lower bound (CRLB) is derived to analyze the theoretical performance limits. Finally, comprehensive simulations are carried out in MATLAB to illustrate the effectiveness of the proposed scheme in terms of localization accuracy even under obstructed line-of-sight (OLOS) conditions, providing a basis for the integration of localization and communication.

In Chapter 4, a value-oriented, need-driven integrated localization and communication (ILAC) system is proposed to achieve the value of service (VoS) maximization through joint resource allocation. A novel concept, termed VoS, is established to characterize the satisfaction degree of users in the ILAC system. Specifically, as a unified performance metric, the

VoS of the system is formulated as the weighted sum of diverse service provisioning including localization accuracy and communication data rate. With the aim of VoS maximization, the bandwidth and time allocation are achieved through an iterative joint resource allocation approach. The simulation results demonstrated the effectiveness of VoS metric and JRA method in the ILAC system under limited resources.

In Chapter 5, a successive ISAC scheme is proposed to maximize VoS with limited resources, to meet real-time concurrent localization and communication service requests. The bandwidth and power allocation are rationally investigated via a deep-reinforcement learning (DRL) based algorithm. The dynamic service provisioning is elaborated to maximize the long-term ISAC system gain. Specifically, both channel variation and service request changes are coined into the updating scheme. Comprehensive simulation results illustrate the robustness and adaptiveness of our proposed resource allocation scheme under dynamic environments.

In Chapter 6, a multi-user cooperative ISAC system is proposed with the game theory-based resource allocation. Based on the principle of data fusion, cooperative sensing is enabled to enhance the sensing efficiency. The bandwidth and power resources are optimized to maximize the user-specific VoS with fairness through the game theory. Finally, numerical simulations are performed under varying resource conditions, service demands, and channel states. The results demonstrate the superiority of the proposed scheme over non-collaborative alternatives and the other two benchmark schemes.

Finally, all the contributions are summarized in Chapter 7, with the identification of future research directions.

Chapter 2

Challenges and Existing Solutions of Resource Allocation in ILSAC Systems

In this chapter, we first introduce the background of the ILSAC system, including the advanced wireless localization and sensing techniques, as well as the development of integrated localization/sensing and communication. Integrating multiple services into a single wireless system brings significant challenges in resource allocation to fulfill diverse user's needs. Thus, we subsequently introduce existing resource allocation objectives and solutions in integrated systems and applications. It is worth noting that there is ongoing research in the academic community related to the different terms of ILAC, JCR, and ISAC to describe the integrated system. ILAC focuses on the integration of device-based positioning and communication, JCR refers to the fusion of wireless communication and radar positioning, while ISAC emphasizes the detection, positioning, and tracking of objects in a device-free environment. However, in terms of design objectives and methodologies, these three directions share significant similarities. Therefore, we encompass all of these directions within our discussion of system design, evaluation and resource allocations.

2.1 Background of ILSAC Systems

2.1.1 Wireless Localization and Sensing Technologies

5G-based wireless localization aims to utilize the capabilities of 5G networks, such as beamforming, massive MIMO, and network slicing, to provide high-precision and real-time location information for devices. It enables a wide range of applications, including target tracking, navigation, smart management, and industrial automation. The wireless positioning technologies including received signal strength (RSS) [8], time of arrival (TOA) [9], time difference of arrival (TDOA) [10], and angle of arrival (AOA) [11] combine multiple localization methods as shown in Fig. 2.1. Last decades, researchers proposed diverse algorithms and methods to enhance localization accuracy and performance. For example, [11] proposed a cooperative AOA-based localization method, and the localization accuracy can approach the CRLBs even under high noise contaminations. Apart from the traditional wireless localization method, the authors in [12] proposed a deep reinforcement learning (DRL) based method, which introduced the possibility of implementing localization without geometrical modelling and parameterization of the environment. However, state-of-the-art cellular localization technologies are mostly implemented in a device-based manner, where a signalling device is attached to the object to be located. Therefore, it is challenging to generalize to broader scenarios which require the sensing of device-free objects [4].

Traditionally, wireless sensing is mainly applied in wireless sensor networks, where the sensing process is to collect data from sensors distributed in the environment or attached to objects. For instance, [13] gave a comprehensive survey of IoT sensing applications using wireless sensor networks, including sports-leisure, healthcare, localization and tracking etc. With the development of 5G, wireless sensing can be performed concurrently with data transmission [4, 14–16]. [4] introduced the possibility of MIMO and mmWave-based sensing and proposed the concept of sensing QoS. Generally, wireless sensing can be classified into two types: bi-static and mono-static sensing as shown in Fig. 2.2. In the bi-static sensing, the Rx and Tx are not deployed in one device while in the mono-static sensing, the Rx and Tx are co-located at one wireless end (*e.g.* BS). Both the mono-static and bi-static sensing have been incorporated into different scenarios of the ISAC system [17]. However, it can be costly

to deploy a wireless sensing system and set up the required infrastructure. Furthermore, it remains a challenge to achieve high localization and sensing accuracy in complex 3D environments, such as urban areas and indoor spaces. In recent two years, [14] investigated the fingerprint-based 3D localization for MIMO systems. [15] proposed a multi-stage algorithm for the 3D position and orientation estimation of the reconfigurable intelligent surfaces and 3D position of users. [16] utilized the TDOA and RSS measurements to achieve rigid body localization under NLOS environments. Factors like multipath propagation, signal interference, and non-line-of-sight conditions would greatly impact sensing accuracy.

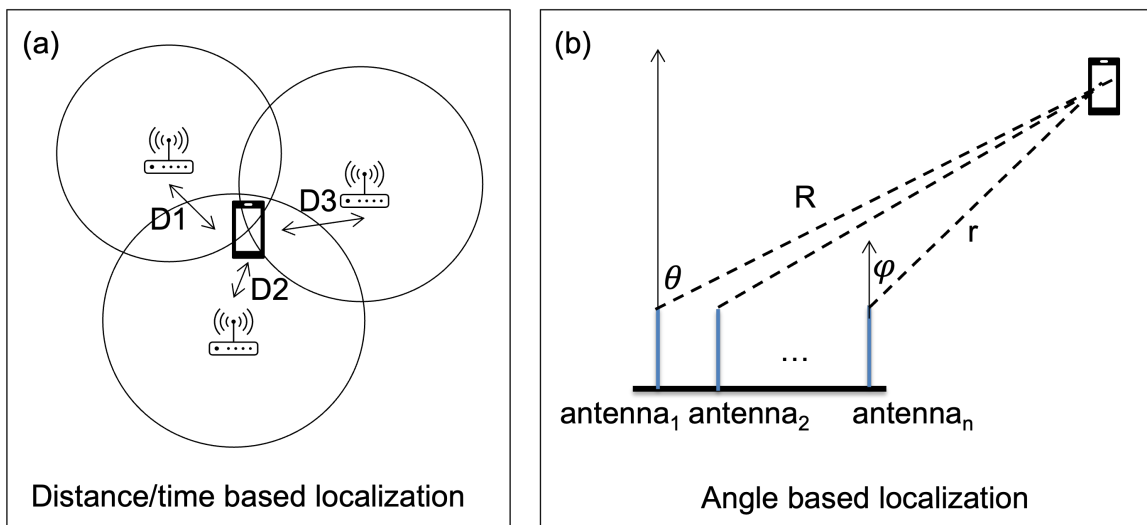


Figure 2.1. Examples of two types of wireless-based localization methods. (a) Localization method based on RSS or TOA, and (b) localization method using angular estimation (AOA/AOD).

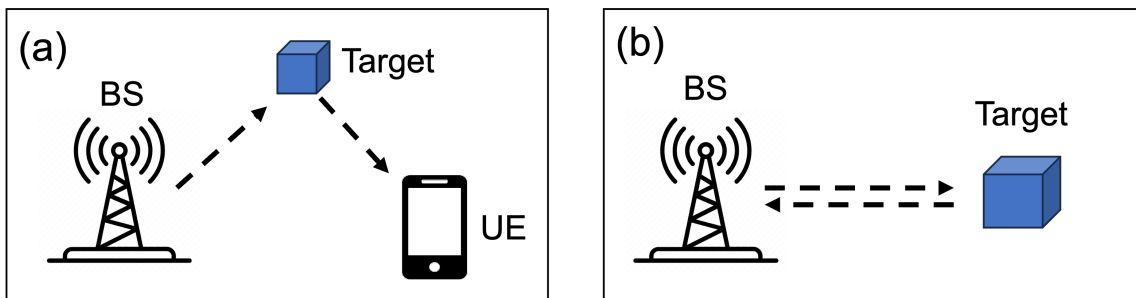


Figure 2.2. Schematic illustration of (a) bi-static and (b) mono-static wireless sensing. The Tx and Rx are located at different devices in bi-static sensing. The Tx and Rx are co-located at BS in mono-static sensing.

2.1.2 Integrated Localization, Sensing and Communication

The idea of integrating localization, sensing and communication into one system has been proposed years ago in many different areas, such as navigation [18], robotics [19] and so on. In recent years, with the development of mmWave and MIMO technologies, this concept has been redefined because localization/sensing and communication functionalities can be integrated and designed from signal level [2]. Indeed, radio localization and communication systems are both evolving towards higher frequency bands, larger antenna arrays, and miniaturization, thereby becoming increasingly similar in terms of hardware architectures, channel characteristics, and signal processing [1]. For example, beamforming optimizes signal transmission and reception in a specific direction, minimizing interference from other directions. This not only strengthens the received signal but also enhances sensing accuracy while reducing interference. Against these backgrounds, the community has recognized that ILSAC will become a key technology in future wireless systems, allowing for the exploitation of dense cell infrastructures to construct a perceptive network [1, 20]. In recent years, there have been more and more studies on ILSAC [21–24]. The major research directions can be summarized as several aspects: the application of ISAC, framework design, waveform design and performance analysis.

- **Applications:** The applications of ISAC are discussed in many areas for the industrial IoT [25, 26]. As investigated in [25], ISAC-enabled IoT devices can be used in many applications, such as smart home, vehicle-to-everything (V2X) [27] and environmental monitoring [28]. In [29], the authors gave the ISAC-enabled transportation scenarios, introduced the unique characteristics of the vehicular environment and demonstrated the necessity and readiness of ISAC in vehicular scenarios. [30] discussed the raw sensing data sharing among connected and automated vehicles (CAVs). In addition, [31] explored the capacity of intelligent reflecting surfaces (IRS) to enable concurrent multi-user communication and localization with the same time-frequency resources.
- **Framework design:** Since ISAC systems often include the integration of various technologies such as wireless communication, radar sensing, and intelligent reflecting surfaces, a well-designed framework provides a structured approach to integrate these technologies seamlessly. In [32], a spatially-spread orthogonal time frequency space (SS-

OTFS)-enabled ISAC system framework was proposed. In [33], the authors introduced a framework known as semi-ISAC, offering increased flexibility by enabling the dedicated allocation of a portion of the bandwidth to either wireless communication or radar detection, while reserving the remainder for ISAC signal transmission.

- **Waveform design:** As mentioned before, ISAC systems often serve multiple functions. Tailoring waveforms for these different modalities enables the system to switch between modes efficiently while ensuring optimal performance for each function. Furthermore, [34] claimed that the ISAC technique has the potential of sharing the same waveform, which means the cost of hardware implementation can be greatly reduced and the efficiency of spectrum resource utilization can be improved. Thus, the waveform design for the ISAC system is critical and necessary. In [35], an OFDM SDR testbed was designed to validate the possibility of the dual-functional model in ISAC systems. The results demonstrate that the dual-function approach can achieve BER performance comparable to that of a purely communication-based solution while simultaneously providing precise sensing functionality. In [36], an innovative full-duplex (FD) ISAC scheme was introduced that leverages the idle periods of conventional pulsed radars for transmitting communication signals.
- **Performance analysis:** In an ISAC system, one of the most critical issues is how to balance the resource allocation between sensing and communication to fulfill the needs of users. For example, in [37], a boundary named CRB-rate region boundary was designed to describe the relationship between Shannon theory to Fisher information. However, as mentioned in [20], the unified theoretical frameworks, the fundamental performance limits and the optimal ISAC schemes are still open issues. Last two or three years, a lot of researchers have focused on resource allocation and performance analysis in ISAC systems and the details are summarized in Table 2.1. Nevertheless, from a user perspective, the variety of multiple service request combinations leads to the existing performance analysis design being inadequate for ensuring an optimal service experience. Moreover, from an integrated system design perspective, existing performance analysis designs are still hard to provide timely adjustable resource allocation and meet a variety of dynamic

service requests.

TABLE 2.1 Resource allocation strategies in ISAC systems.

Citation	Evaluation Metric	Resources	Method
[24]	Maximization of radar total mutual information (MI) with the communication channel capacity as a constraint.	Time	Non-cooperative game theory
[38]	Maximization of weighted average sensing performance with rate constraints.	Bandwidth	KKT-condition
[39]	Maximization of detection rate as performance metric.	Devised beam-forming vectors	Gradient decent method
[40]	Optimization of the outage probabilities (OPs).	Power	Lagrangian method
[41]	Maximization of the system sum secrecy rate.	Snapshot duration	BCD-based method
[42]	Minimization the total transmit power while guaranteeing the minimal SINR.	Power, beam-forming vector	Successive convex approximation

2.2 Existing Solutions of Resource Allocation and Their Challenges in ILSAC systems

2.2.1 System Mechanism and Evaluation Metric

To develop and design a resource allocation strategy for an ILSAC system, a comprehensive evaluation metric is critical for individual and system value realization. However, the traditional quality of service (QoS) evaluation indices is inadequate especially when confronted with diverse and unique service requests from users. In a conventional network dedicated to either communication or sensing, the QoS is typically employed to evaluate the effectiveness of the respective functionalities. For example, sensing QoS requires low detection/estimation error while communication QoS aims for high bite rate and low bite error. However, the current separated evaluation metric design is outdated to support the heterogeneous requirements of diverse users in the ILSAC system. Thus, in the current multifunctional systems design including ISAC, ILAC and JCR, novel evaluation metrics have been introduced.

In ILAC and JCR, the resource allocation mechanisms are mostly focused on location-aided or location-aware communication [43, 44], which aims to utilize the accurate location information of devices or targets for resource allocation to improve communication performance. In this area, the localization and communication systems are designed separately, and the resources and hardware are not shared between the two systems. From the localization and communication co-design perspective, the studies mainly are focused on joint communication and radar (JCR) [7, 45] system, where the JCR base station has to be full-duplex. For example, [2] was to maximize the average SNR, signal-to-clutter-plus-noise-ratio (SCNR) of the radar system with data rate requirement as a constraint. Besides, beamforming optimization is another important direction in previous works [46–48]. For example, in [46], a beamforming and power allocation strategy was proposed in mmWave networks. For the evaluation metric design, [49] proposed the preference levels of different tasks and users in communication systems. However, the concurrent requests of both communication and localization have rarely been exploited. In [50], the term VoS was proposed to assess the benefits perceived by users in mobile computing systems. However, the concept has not been customized to adapt to the ILAC system. In [2], three ILAC architectures were proposed, where the trade-off between localization and communication performance was derived. In [51], the authors studied the co-design of localization and communication in mm-wave systems. Specifically, location features which can be used in mmWave communication were discussed. Although the general overview of ILAC was introduced in [2] and [51], the specific system design mechanism to support applications by joint resource allocation schemes is hardly discussed therein. A user-driven value-oriented evaluation metric to guide the long-term resource allocation in the ILAC system is still untapped.

In ISAC, some of the works aim to maximize sensing performance while using communication data rate as a constraint. For example, in [24], the goal was to enhance the network's sensing performance, while simultaneously ensuring a specified sum rate for communication quality of service. [51] aimed to optimize the sensing performance of the network in terms of the weighted average range resolution, and simultaneously guarantee the communications QoS sum rate. Some research introduces mechanisms aimed at concurrently optimizing sensing and communication performance. For instance, in [40], the power allocation problem was formu-

lated as a pair of problems of maximizing the receive signal-to-interference-plus-noise ratio of the sensing signal and maximizing the sum rate of communication. The objective in a recent study [52] was to maximize the averaged communication throughput, computation delay and sensing mutual information by radio resource allocation. Additionally, certain works aim to maximize data rates while ensuring an acceptable level of achievable sensing performance [41]. For instance, [20] aimed at maximizing the system sum secrecy rate over M snapshots within the scanning period while ensuring the average achievable rate of each legitimate user is above a pre-defined threshold. Furthermore, to reveal the trade-off between multi-functionalities in one wireless system, [53] considered dividing the time budget into sensing and communication cycles. In [54, 55], different metrics to measure “sensing capability” were explored to achieve the maximum integrated gain. Li. *et al.* [56] proposed the human activity recognition (HAR) system in ISAC, focusing on the connections between the physical-layer system parameters and HAR performance metrics. However, the constraints of sensing and communication performance do not directly reflect users’ needs. Since users’ needs and requirements and the relative importance of sensing and communication services can vary, using average or minimum constraints to evaluate the service performance has its limitations.

2.2.2 Resource Allocation Technologies

Resource allocation is crucial for ILSAC systems and it will directly impact the operation efficiency of the system and the completeness degree of service requests. Multi-dimensional resource allocation has been widely studied in wireless communication systems. For example, in [57], the time-, power- and spatial-domain resource allocation scheme was designed for maximizing the users’ uplink sum throughput. To support different types of applications in wireless communication and ILSAC systems, various algorithms have been developed. Herein, the state-of-art resource allocations including the convex optimization, heuristic methods and learning-based methods are summarized. In addition, the challenges of utilizing these technologies in the ILSAC system are discussed.

- **Convex optimization:** Resource allocation in wireless systems has been the subject of extensive research [58–60]. Many resource allocation problems include the minimization

of a convex and differentiable objective function over a convex set. For convex optimization problems, the local optimal solution is also a global optimal solution. The primal optimization problem can be converted into its dual problem with the Lagrangian dual variables, where the optimal solutions can be obtained with Karush-Kuhn-Tucker (KKT) conditions [61]. In general, the explicit solutions of the KKT condition are difficult to derive. Thus, the most common techniques to solve the KKT condition are through the use of a line search procedure, *e.g.*, sub-gradient methods. However, many of the resource allocation problems are non-convex, making convex optimization fail to apply.

- **Heuristic methods:** Another approach to solving the resource allocation problem is utilizing the heuristic algorithms. Recently, this technique has gained considerable interest from researchers. Heuristic algorithms prioritize the attainment of an optimal solution without the need to explore the entire solution space. One of the most famous heuristic algorithms to deal with resource allocation problems is the particle swarm algorithm (PSO) [62]. For instance, in [63], the author demonstrated the effectiveness of the PSO algorithm in multi-dimensional resource allocation problems, especially for non-convex global optimization. Specifically, a channel-time allocation based on the PSO algorithm was introduced to meet the throughput and delay constraints in multimedia applications. However, for the ILSAC system, how to sufficiently incorporate the heuristic algorithms to adaptively allocate multi-dimensional resources has not yet been exploited.
- **Learning-based methods:** To effectively solve the resource allocation-related issues and adaptively maximize the system performance in many uncertain environments, the machine learning-based methods have been increasingly studied and applied in conventional communication and ISAC systems [64, 65]. Since the receiver may have prior knowledge of channel conditions and integrated signals, it is possible to leverage these features to enhance the localization accuracy and communication data rate. For example, [65] proposed a deep learning approach to a class of active sensing problems in wireless communications to gather information to perform a sensing or actuation task for maximizing utility function. [64] designed an efficient learning-based algorithm which can adaptively choose appropriate parameters according to the sensing of the environ-

ment. [66,67] used deep reinforcement learning techniques to learn an optimal resource allocation policy from data. Authors in [68] proposed to use of a deep reinforcement learning-based resource allocation method to ensure the long-term performance of a 5G ultra-dense network. Authors in [69] review the roles of machine learning in resource allocation of ISAC systems. [70] introduced a deep learning-based scheme to maximize the weighted sum of the normalized sensing rate and normalized communication rate in the uplink ISAC system. [71] proposed a deep learning-based beam allocation and user association approach for ISAC systems. However, these methods only work if there is enough training time and properly selected training parameters. Moreover, the exploitation of a machine learning method for such integrated tasks makes the resource allocation between localization and communication challenging, given that the relationship between the accuracy rate and the amount of allocated wireless resources could be mathematically intractable for deep reinforcement learning-based recognition tasks.

2.3 Chapter Summary

As one of the most important enablers in future wireless systems, integrated localization, sensing and communication allow for the exploitation of dense cell infrastructures to construct a perceptive network to fulfill the needs of diverse users from vertical applications. In this chapter, a detailed summary of state-of-the-art technologies in the ILSAC system is given. Specifically, we introduce the advanced technologies of wireless localization and wireless sensing. Then we provide the development and research directions in ILSAC systems. Finally, the resource allocation objectives and solutions for existing applications and research within the integrated system are discussed.

Chapter 3

5G mmWave based Joint Localization and Environment Sensing

3.1 Introduction

The rapid proliferation of localization-enabled applications including warehouse management, asset tracking and factory automation are significantly boosting the need for high-accuracy target positioning under challenging conditions [72]. Albeit there have been many investigations into real-time localization for many years, this area is attracting growing research interest due to new harsh localization environments and stringent accuracy requirements from many emerging applications. Traditionally, a target is modelled as a point target whose location is only defined by the 3D coordinates with three degrees of freedom while neglecting its orientations [73]. However, to achieve accurate maneuvering for tasks like cargo transportation, robotic control and others, not only the target's position but also its orientations are required. For this purpose, a target has to be modelled as a rigid body, which always maintains its shape and size. Apart from the 3D coordinates, a rigid body has the other three degrees of freedom including three Euler angles.

As a result, the rigid body localization (RBL) problem has been studied recently to determine a rigid body's centre position and orientation. In general, the rigid body localization problem for outdoor scenarios relies on the combined use of global navigation satellite systems (GNSS) and inertial measurement unit (IMU). However, GNSS suffers from limited sig-

nal coverage and poor position accuracy in indoor environment, while IMU requires frequent calibration, which rules out most localization-based indoor applications. Meanwhile, some alternative indoor rigid body localization technologies, using radar [74], laser [75], infrared light (IR) [76], ultrasound [77] and cameras [78], are either very sensitive to environmental changes or dependent on expensive hardware.

Recently, the rapid advancements of 5G technologies such as MIMO and mmWave have brought enormous improvements in network throughput and energy efficiency, as well as their potential for localization [79,80]. Such technological advancements could be exploited to enhance localization performance. In particular, operating at carrier frequencies beyond 30 GHz with ultra-wide bandwidths, mmWave-based 5G MIMO systems provide extremely high data rates through dense spatial multiplexing by using a large number of antennas [81]. The high spatial resolution and large bandwidth provided by these 5G technologies are expected to bring in revolutionary impact on wireless localization [79]. However, the 5G technology usually requires a minimum bandwidth of 100 MHz, hundreds of antennas, and ultra-densely deployed base stations. These characteristics indicate that applying Nyquist's sampling theorem to 5G techniques may pose unprecedented challenges, including very large overheads, computational complexity, and power consumption due to the substantial number of samplings. In such cases, compressive sensing provides a sub-Nyquist sampling approach for efficiently reconstructing sparse signals in an under-determined linear system with high computational efficiency. In addition, 5G mmWave MIMO not only enables the active localization of the rigid body but also provides the opportunity of positioning the surrounding physical objects serving as reflection points simultaneously to achieve environment sensing. It has been proved that the non-light-of-sight (NLOS) components in the channel estimation results can be turned into benefits to assist the radio map construction [82]. The precise rigid body posture and reflection points location information also in turn contribute to the design, operation and optimization of future 5G beyond and 6G wireless networks. For instance, location information of rigid body and reflection points can be utilized to construct location-specific channel state information (CSI), which can boost the spatial spectrum efficiency of future networks. Motivated by these considerations, joint localization and environment sensing of a rigid 5G mobile terminal equipped with MIMO has become one of the promising research directions.

While 5G mm-wave MIMO assisted rigid body localization and environment sensing have many advantages, several challenges of previous studies have yet to be overcome. On one hand, existing studies on angle information of a target only consider one [83] or two rotation angles [84] in 2D or 3D scenarios, which neglects part of rotation due to the inherent complexity. Solving the translation vector and rotation information of a rigid body from signals transmitted by fixed anchor nodes is a complicated nonlinear optimization problem. For rigid body localization, [85] proposed a range measurement method in a sensor network, in which four anchor nodes and five wireless sensors mounted on the rigid body are used. Jiang *et al.* [86, 87] presented a refined positioning algorithm using the range measurements between the anchors and several sensors in both 2D and 3D cases. In [88], an angle of arrival (AOA) based method is introduced by utilizing only one base station and four wireless sensors in the rigid body localization problem. However, the aforementioned methods need to guarantee that the topology of how the sensors are mounted on the rigid body is known and the LOS exists. In addition, these methods are based on passive localization which gathers the measurements from an incoming signal transmitted/reflected by sensors mounted on the rigid body and the robustness of distance estimation to the environment noises/shadowing is limited due to the fluctuations of practical path conditions. Therefore, active localization performed at the rigid body with received signals from only one anchor node is more controllable and efficient.

On the other hand, the derivation of NLOS components for reflection points localization has also been studied for years [89–93]. The reflection points localization problem can be solved by exploiting the AOA and angle of departure (AOD) with the sparsity of channel information. Among several popular algorithms, the distributed compressed sensing-simultaneous orthogonal matching pursuit (DCS-SOMP) [94–96] and its modifications like CoSaMP/OMP are useful tools by manipulating sparsity of mm-wave channels. [81] demonstrated a three-stage improved DCS-SOMP algorithm by linear antenna arrays with AOA and AOD to estimate the scatters (or reflection points) to improve the moving target localization accuracy only in the 2D scenario. However, the reflection points localization in the 3D scenario has not been investigated and its implementation at the rigid body end is yet to be studied. Thus, an integrated rigid body localization and environment sensing technique with accurate and robust performance in 3D is quite challenging yet demanding.

In this chapter, the mm-wave MIMO assisted rigid body active localization and environment sensing scheme is proposed to tackle the aforementioned challenges. In the considered 3D scenario, the six degrees of freedom of rigid body are successfully resolved with only one base station equipped with uniform rectangular array (URA). Three different cases are investigated: with only line-of-sight (LOS), with both LOS and non-line-of-sight (NLOS), and with only the NLOS. Moreover, when there's NLOS, the position of reflection points in the environment is also estimated. Both the rigid body localization and reflection point estimation are achieved at the rigid body end with the one-way signals. To guarantee high rigid body/reflection points localization accuracy, a new strategy of the multi-step hierarchical design is developed. Specifically, the primary contributions of this chapter comprise the following three aspects.

- (1) A novel rigid body active localization and environment sensing strategy is proposed with the assistance of one anchor node. To the best of our knowledge, there are no developed solutions for joint rigid body and reflection points localization estimation under 3D scenarios. Although some works were reported to detect the 2D reflection points, an optimal reflection points localization solution to deal with the 3D situation has never been studied using the mm-wave MIMO at the rigid body end. Our proposed strategy achieves the rigid body location estimation accuracy to the centimetre level and orientation estimation accuracy to 0.02 rad and improves the reflection points localization accuracy to decimeter level with reasonable computational complexity.
- (2) A novel hierarchical DCS-SOMP algorithm incorporated with iterative maximum likelihood (IML) is presented to resolve the channel information from received signals. In particular, by using the sparsity of the mm-wave channel in the angle domain, the AOA/AOD estimation accuracy is increased to 0.01 rad and distance estimation accuracy to the centimetre level. Compared with the original DCS-SOMP, the estimation precision is enhanced greatly.
- (3) The theoretical CRLBs of angular, rigid body posture and reflection points location estimation are derived to evaluate the effectiveness and robustness of the proposed algorithms. Simulations demonstrate that our proposed joint rigid body and reflection points

localization method approaches the theoretical bounds while the signal-to-noise ratio (SNR) is not less than 0 dB.

The rest of the chapter is organized as follows. The system models including the environments, rigid body localization and reflection points localization are formulated in Section 3.2. The novel compressive sensing method for channel parameter estimation is investigated in Section 3.3.1. The PSO-based joint rigid body and reflection points localization strategy are proposed in Section 3.3.2. The fundamental bounds are derived in Section 3.4. Section 3.5 presents the simulation results. Finally, Section 3.6 summarizes and concludes the chapter.

3.2 System Model

3.2.1 Environment Model

We consider a 3D indoor environment with an anchor node AN located at $\mathbf{s} = [s_x, s_y, s_z]^T \in \mathbb{R}^3$ and a rigid body with posture $[\mathbf{p}; \mathbf{q}] \in \mathbb{R}^6$. Note that $\mathbf{p} = [p_x, p_y, p_z]^T \in \mathbb{R}^3$ is the position and $\mathbf{q} = [q_1, q_2, q_3]^T \in \mathbb{R}^3$, $q_1, q_3 \in [0, 2\pi)$ and $q_2 \in [0, \pi]$, represents the orientation of rigid body. The objects in the environment are characterized by $L - 1$ reflection points located at $\boldsymbol{\kappa}_l = [\kappa_{l,x}, \kappa_{l,y}, \kappa_{l,z}]^T \in \mathbb{R}^3$, $l = 1, 2, \dots, L - 1$. It is assumed that the anchor node as signal transmitter carries a uniform rectangular array (URA) consisting of N_T ($N_{Tx} \times N_{Ty}$) antennas while rigid body as receiver carries URA with N_R ($N_{Rx} \times N_{Ry}$) antennas. The value of \mathbf{s} is assumed to be known, while $[\mathbf{p}; \mathbf{q}]$ and $\boldsymbol{\kappa}_l$ are unknown.

3.2.2 Joint Rigid Body and Reflection Points Localization Model

Fig. 3.1 illustrates the rigid body and reflection points localization scenario. In our considered mmWave wireless system, the signal transmitted by AN is orthogonal frequency division multiplexing (OFDM) signal [81]. The mmWave network operates at carrier frequency f_c and bandwidth B . In particular, G signals are transmitted sequentially for each subcarrier. The g -th signal is denoted as $\mathbf{x}^{(g)}[n] \in \mathbb{C}^{N_s \times 1}$ for n -th subcarrier $n = 0, 1, 2, \dots, N - 1$, where N_s is the number of transmitted symbols. $\mathbf{F}[n] = \mathbf{F}_{RF} \mathbf{F}_{BB}[n] \in \mathbb{C}^{N_T \times N_s}$ is the beamforming matrix where $\mathbf{F}_{RF} \in \mathbb{C}^{N_T \times N_T^{RF}}$ is analog precoding matrix and $\mathbf{F}_{BB} \in \mathbb{C}^{N_T^{RF} \times N_s}$ is the digital beamformer. N_T^{RF}

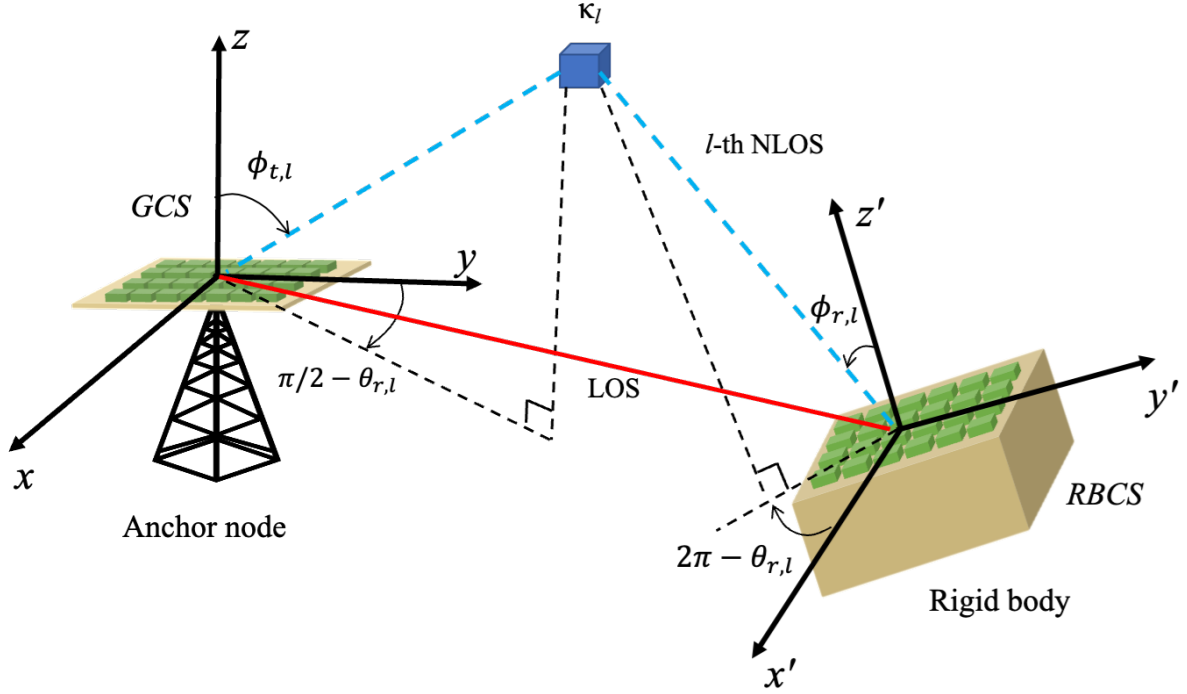


Figure 3.1. Schematic illustration of signal transmission between anchor node and rigid body.

is the number of RF chains at the transmitter. The transmitted power is denoted as P_T and satisfies $\sum_{n=0}^{N-1} \|\mathbf{F}[n]\|_F^2 = P_T$. In this work, without loss of generality, we don't designate the specific expression of $\mathbf{F}[n]$ but keep the general form during derivation. It is assumed there are L paths in the channel, where path index $l = 0$ is the LOS while the remaining paths are NLOS ($l = 1, 2, \dots, L-1$) corresponding to $L-1$ reflection points. Each reflection point is assumed to provide one propagation path between AN and the rigid body. Under this model, the $N_R \times N_T$ channel matrix associated with n -th subcarrier is modeled as

$$\mathbf{H}[n] = \mathbf{A}_R[n] \mathbf{\Gamma}[n] \mathbf{A}_T^H[n], \quad (3.1)$$

where

$$\mathbf{\Gamma}[n] = \sqrt{N_R N_T} \text{diag} \left\{ \frac{h_0}{\sqrt{\rho_0}} e^{-\frac{j2\pi n \tau_0}{N T_s}}, \dots, \frac{h_{L-1}}{\sqrt{\rho_{L-1}}} e^{-\frac{j2\pi n \tau_{L-1}}{N T_s}} \right\}. \quad (3.2)$$

In (3.2), h_l is complex channel gain and ρ_l here is the path loss of the l -th channel ($l = 0, 1, 2, \dots, L-1$). $T_s = 1/B$ denotes the sampling period. The transmission time τ_0 at LOS is obtained by $\tau_0 = |\mathbf{p} - \mathbf{s}|/c$ (c is the speed of light) while τ_l ($l = 1, 2, \dots, L-1$) is calculated by

$\tau_l = (|\mathbf{p} - \boldsymbol{\kappa}_l| + |\boldsymbol{\kappa}_l - \mathbf{s}|)/c$. The response vectors at transmitter and receiver can be represented as

$$\begin{aligned} \mathbf{A}_T[n] &= [\mathbf{a}_{t,n}(\theta_{t,0}, \phi_{t,0}), \dots, \mathbf{a}_{t,n}(\theta_{t,L-1}, \phi_{t,L-1})]^T, \\ \mathbf{A}_R[n] &= [\mathbf{a}_{r,n}(\theta_{r,0}, \phi_{r,0}), \dots, \mathbf{a}_{r,n}(\theta_{r,L-1}, \phi_{r,L-1})]^T, \end{aligned} \quad (3.3)$$

where the sub-vector $\mathbf{a}_{t,n}(\theta_{t,l}, \phi_{t,l}) = \boldsymbol{\chi}_x(\theta_{t,l}, \phi_{t,l}) \otimes \boldsymbol{\chi}_y(\theta_{t,l}, \phi_{t,l})$. And there are

$$\boldsymbol{\chi}_x(\theta_{t,l}, \phi_{t,l}) = \frac{1}{\sqrt{N_{Tx}}} [e^{-j\frac{N_{Tx}-1}{2} \frac{2\pi}{\lambda_n} d_o \cos(\theta_{t,l}) \sin(\phi_{t,l})}, \dots, e^{j\frac{N_{Tx}-1}{2} \frac{2\pi}{\lambda_n} d_o \cos(\theta_{t,l}) \sin(\phi_{t,l})}], \quad (3.4)$$

$$\boldsymbol{\chi}_y(\theta_{t,l}, \phi_{t,l}) = \frac{1}{\sqrt{N_{Ty}}} [e^{-j\frac{N_{Ty}-1}{2} \frac{2\pi}{\lambda_n} d_o \sin(\theta_{t,l}) \sin(\phi_{t,l})}, \dots, e^{j\frac{N_{Ty}-1}{2} \frac{2\pi}{\lambda_n} d_o \sin(\theta_{t,l}) \sin(\phi_{t,l})}], \quad (3.5)$$

where $[\theta_{t,l}, \phi_{t,l}]^T$ denotes the azimuth and elevation angles of AOD of l -th path at the anchor node side. $\lambda_n = c/(n/(NT_s) + f_c)$ is the signal wavelength at the n -th subcarrier and d_o denotes the distance between the antenna elements. The sub-vector $\mathbf{a}_{r,n}(\theta_{r,l}, \phi_{r,l})$ can also be derived with similar equations. $\theta_{r,l}$ and $\phi_{r,l}$ are azimuth and elevation angles of AOA of l -th path.

In this chapter, the origin of the global coordinate system (GCS) is the position of the gravity center of URA antennas on the anchor node, and the z-axis of GCS is parallel to the antenna (as shown in Fig. 3.1). All of our calculations are under GCS. However, since the posture of URA antennas on the rigid body changes as the rigid body moves, $\phi_{r,l}$ and $\theta_{r,l}$ are measured at the rigid body coordinate system (RBCS). Thus, we need to calculate the transformation relationship from RBCS to GCS as shown in

$$\begin{aligned} &[\cos(\theta_{r,l})\sin(\phi_{r,l}), \sin(\theta_{r,l})\sin(\phi_{r,l}), \cos(\phi_{r,l})]^T = \\ &\mathbf{R} \cdot [\cos(\theta_{r,l,g})\sin(\phi_{r,l,g}), \sin(\theta_{r,l,g})\sin(\phi_{r,l,g}), \cos(\phi_{r,l,g})]^T, l = 0, 1, 2, \dots, L-1. \end{aligned} \quad (3.6)$$

In (3.6), \mathbf{R} is the rotation matrix related to the rigid body orientation \mathbf{q} . We use $\phi_{r,l,g}$ and $\theta_{r,l,g}$ to represent the elevation and azimuth angles of AOA at path l under the global coordinate system as

$$\begin{aligned} \phi_{r,l,g} &= \arccos\left(\frac{\kappa_{l,z} - p_z}{|\boldsymbol{\kappa}_l - \mathbf{p}|}\right), \\ \theta_{r,l,g} &= \arctan\left(\frac{\kappa_{l,y} - p_y}{\kappa_{l,x} - p_x}\right), \end{aligned} \quad (3.7)$$

$$\mathbf{R} = \begin{bmatrix} c_3 c_2 & -s_3 c_1 + c_3 s_2 s_1 & s_3 s_1 + c_3 s_2 c_1 \\ s_3 c_2 & c_3 c_1 + s_3 s_2 s_1 & -c_3 s_1 + s_3 s_2 c_1 \\ -s_2 & c_2 s_1 & c_2 c_1 \end{bmatrix}, \quad (3.8)$$

where $c_i = \cos(q_i)$ and $s_i = \sin(q_i)$, $i = 1, 2, 3$ for simplicity.

Therefore, the received signal at n -th subcarrier and g -th transmission can be expressed as

$$\mathbf{y}^{(g)}[n] = \mathbf{H}[n]\mathbf{F}^{(g)}[n]\mathbf{x}^{(g)}[n] + \mathbf{n}^{(g)}[n], \quad (3.9)$$

where $\mathbf{n}^{(g)}[n] \in \mathbb{C}^{N_R}$ is a Gaussian noise vector with zero mean and variance $N_0/2$. $\mathbf{x}^{(g)}[n] = [x_1[n], \dots, x_{N_s}[n]]^T$ is the g -th transmission. Our goal is to estimate rigid body posture $[\mathbf{p}; \mathbf{q}]$ and reflection points position κ_i from \mathbf{y} .

3.3 Proposed Joint Rigid Body and Reflection Points Localization Scheme

In this section, a joint rigid body posture estimation and reflection points location estimation scheme is introduced. Firstly, channel parameters including AOD, AOA and transmission time are estimated by exploiting the sparsity of the mm-wave MIMO channel. Secondly, to recover the rigid body posture and reflection points location in both NLOS and OLOS scenarios, we use different expressions of the location of reflection points to build a minimization problem and solve it with the heuristic algorithm.

3.3.1 Channel Parameters Estimation

Since the AOA and AOD estimation accuracy are limited to the size of the grid by using the original DCS-SOMP algorithm, we propose a novel two-step channel estimation algorithm. The coarse estimation is based on an improved DCS-SOMP algorithm called hierarchical DCS-SOMP (H-DCS-SOMP) while the further fine estimation is achieved by an iterative maximum likelihood (IML) method.

3.3.1.1 H-DCS-SOMP

In the coarse reflection points location estimation, assuming the received signal \mathbf{y} from the anchor node is the compressive measurement, the reflection points localization can be formulated as compressive sensing (CS) problem. The angle, transmission time measurements and channel gain are solvable by constructing a hierarchical sensing dictionary.

Firstly, the mm-wave MIMO channel model is transformed into beamspace to reduce the complexity due to the sparsity of mm-wave signals in the angular domain [97]. In the 3D environment, we introduce the $N_T \times N_T$ transformation matrix, uniformly sampling the virtual spatial angles of AOD, shown as

$$\mathbf{U}_T = \mathbf{U}_{T_x} \otimes \mathbf{U}_{T_y}, \quad (3.10)$$

$$\mathbf{U}_{T_x} \triangleq [\mathbf{u}_{T_x}(-(N_{T_x} - 1)/2), \dots, \mathbf{u}_{T_x}((N_{T_x} - 1)/2)], \quad (3.11)$$

$$\mathbf{U}_{T_y} \triangleq [\mathbf{u}_{T_y}(-(N_{T_y} - 1)/2), \dots, \mathbf{u}_{T_y}((N_{T_y} - 1)/2)],$$

where

$$\begin{aligned} \mathbf{u}_{T_x}(b) &\triangleq [e^{-j2\pi \frac{N_{T_x}-1}{2} \frac{b}{N_{T_x}}}, \dots, e^{j2\pi \frac{N_{T_x}-1}{2} \frac{b}{N_{T_x}}}]^T, \\ \mathbf{u}_{T_y}(b) &\triangleq [e^{-j2\pi \frac{N_{T_y}-1}{2} \frac{b}{N_{T_y}}}, \dots, e^{j2\pi \frac{N_{T_y}-1}{2} \frac{b}{N_{T_y}}}]^T, \end{aligned} \quad (3.12)$$

where $-(N_{T_x} - 1)/2 \leq b \leq (N_{T_x} - 1)/2$. Similarly, we can define the $N_R \times N_R$ transformation matrix \mathbf{U}_R with the same rule. The virtual representation of the channel concerning the angular domain and the received signal is expressed as

$$\tilde{\mathbf{H}}[n] = \mathbf{U}_R^H \mathbf{H}[n] \mathbf{U}_T, \quad (3.13)$$

$$\tilde{\mathbf{y}}[n] = \mathbf{\Omega}[n] \tilde{\mathbf{h}}[n] + \tilde{\mathbf{n}}[n], \quad (3.14)$$

where

$$\mathbf{\Omega}[n] = \begin{bmatrix} \mathbf{\Omega}^{(1)}[n] \\ \vdots \\ \mathbf{\Omega}^{(G)}[n] \end{bmatrix}, \quad (3.15)$$

$$\mathbf{\Omega}^{(g)}[n] = (\mathbf{U}_T^H \mathbf{F}^{(g)}[n] \mathbf{x}^{(g)}[n])^T \otimes \mathbf{U}_R, \quad (3.16)$$

$$\tilde{\mathbf{h}}[n] = \text{vec}(\tilde{\mathbf{H}}[n]). \quad (3.17)$$

In principle, this is a 3D CS problem, where $\mathbf{\Omega}[n]$ denotes the sparse dictionary (sensing matrix) and $\tilde{\mathbf{h}}[n] \in \mathbb{C}^{N_R N_T \times 1}$ is the vectorization of $\tilde{\mathbf{H}}[n]$ that corresponds to the coarse estimation of the AOA/AOD.

To provide a brief overview of CS theory, consider a sparse variable $\tilde{\mathbf{h}}[n] \in \mathbb{C}^{N_R N_T \times 1}$ with a sparsity level of k (i.e., $\tilde{\mathbf{h}}[n]$ contains only $k \ll N_R N_T$ non-zero elements). In CS theory, the primary challenge lies in recovering $\tilde{\mathbf{h}}[n]$ by solving the under-determined set of equations $\tilde{\mathbf{y}}[n] = \mathbf{\Omega}[n] \tilde{\mathbf{h}}[n]$, given $\tilde{\mathbf{y}}[n]$ and $\mathbf{\Omega}[n]$.

With the received signal $\tilde{\mathbf{y}}[n]$, $\mathbf{\Omega}[n]$ and the number of NLOS paths as input, the steps of DCS-SOMP to solve this problem can be summarized as

- For $n = 0, 1, \dots, N - 1$, initialize the residual vectors to $\mathbf{r}_{-1}[n] = 0$ and $\mathbf{r}_0[n] = \mathbf{y}_o[n]$. k is the iteration number and $\omega_m[n]$ denotes the m -th column of measurement matrix.
- Find the largest projection of $\mathbf{r}_{k-1}[n]$ on the columns by

$$\hat{n}_k = \arg \max_m \sum_{n=0}^{N-1} \frac{|\omega_m^H[n] \mathbf{r}_{k-1}[n]|}{\|\omega_m[n]\|_2}. \quad (3.18)$$

- Update indices according to (3.18).
- Calculate the k -th orthogonalized basis vector $\boldsymbol{\rho}_k[n]$ with Gram–Schmidt process using (3.19). When $k = 0$, $\boldsymbol{\rho}_0[n] = \omega_0^H[n]$.

$$\boldsymbol{\rho}_k[n] = \omega_k^H[n] - \sum_{k'=0}^{k-1} \frac{\omega_k^H[n] \boldsymbol{\rho}_{k'}[n]}{\|\boldsymbol{\rho}_{k'}[n]\|_2^2} \boldsymbol{\rho}_{k'}[n]. \quad (3.19)$$

- Update the residual vector $\mathbf{r}_k[n]$.
- Repeat until all the L indices are found.

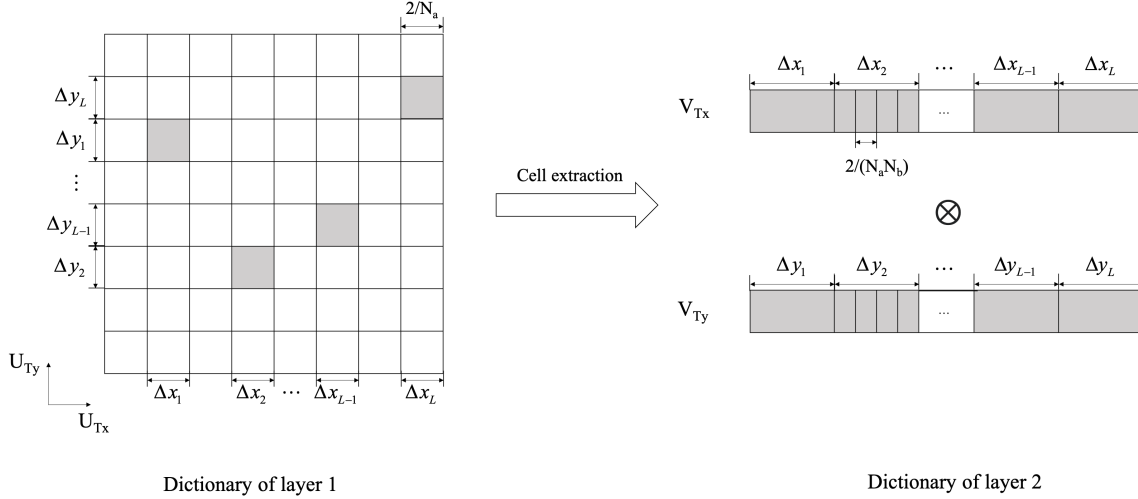


Figure 3.2. Dictionary construction in H-DCS-SOMP procedure.

It is noted that the size of $\Omega[n]$ will limit the upper bound on estimation accuracy. However, to improve the accuracy of parameter estimation, the size of the dictionary and the amount of computation will increase exponentially. In this chapter, the channel parameter estimation is refined through a hierarchical procedure, which is initialized by the original DCS-SOMP. The structure of the dictionary matrix in H-DCS-SOMP is shown in Fig. 3.2. A new dictionary is constructed based on the subdivision of the L angular cells in DCS-SOMP. Since the dictionary resolution in DCS-SOMP depends on N_{Tx} and N_{Ty} , to make the second layer dictionary resolution the same in two dimensions, we set $N_a = \min\{N_{Tx}, N_{Ty}\}$ and consider the width between the adjacent virtual angle index as $2/N_a$ in both dimension of U_{Tx} and U_{Ty} for simplicity. Assume the indexes of L angular cells are $(\Delta x_1, \Delta y_1), \dots, (\Delta x_L, \Delta y_L)$ in the first layer, the $(N_b \times L) \times (N_b \times L)$ transformation matrix V_T can be rebuilt, uniformly sampling the virtual spatial angles of multipath. In the other words, N_b depicts the sampling density of the second layer of the dictionary. In principle, the two-dimensional AOA/AOD estimation performance degrades greatly by using the original single layer DCS-SOMP due to the sparsity of antenna numbers. However, by using H-DCS-SOMP, increasing N_b will contribute to a higher upper bound on parameter estimation accuracy. We'll demonstrate the effectiveness of the hierarchical process in Section 3.4.1. For the second layer of the dictionary, we have

$$V_T = V_{Tx} \otimes V_{Ty}, \quad (3.20)$$

$$\begin{aligned} \mathbf{V}_{Tx}(\Delta x) &\triangleq [\mathbf{v}_{Tx}(\Delta x_{1,c} - 1/N_a), \dots, \mathbf{v}_{Tx}(\Delta x_{L,c} + 1/N_a)], \\ \mathbf{V}_{Ty}(\Delta y) &\triangleq [\mathbf{v}_{Ty}(\Delta y_{1,c} - 1/N_a), \dots, \mathbf{v}_{Ty}(\Delta y_{L,c} + 1/N_a)], \end{aligned} \quad (3.21)$$

where $\Delta x_{l,c}$ represents the center of Δx_l and the sampling interval is $2/(N_a N_b)$ as demonstrated in Fig. 3.2. The construction of $\mathbf{v}_{Tx}(b)$ and $\mathbf{v}_{Ty}(b)$ are similar to (3.12). Also, we define the $N_R \times N_R$ matrix \mathbf{V}_R in the same way. After conducting the DCS-SOMP algorithm again, indices with better precision can be obtained. If there are more than two layers, the construction rule is similar.

With the estimated $\hat{\mathbf{h}}, \hat{\mathbf{\Omega}}$, we can rewrite (3.14) as

$$\hat{\mathbf{y}}[n] = \Theta + \tilde{\mathbf{n}}[n], \quad (3.22)$$

where Θ can be separated into the multiplication of channel gain as

$$\Theta = \text{diag}\{h_0, h_1, \dots, h_{L-1}\} \cdot f_1(\tau_0, \tau_1, \dots, \tau_{L-1}) \cdot f_2(\boldsymbol{\theta}, \boldsymbol{\phi}), \quad (3.23)$$

and f_1, f_2 are determined by (3.1) and (3.2) [81]. $\boldsymbol{\theta}$ and $\boldsymbol{\phi}$ are azimuth angles and elevation angles of all paths.

Therefore, h_l and τ_l can be resolved by minimizing the following least squares problem. For path l , there is

$$\underset{\tau_l, h_l}{\text{argmin}} \sum_n \|\hat{\mathbf{y}}[n] - \Theta\|. \quad (3.24)$$

3.3.1.2 Fine Estimation

In the following environment sensing process, the 3D position estimation error of reflection points is proportional to the square of AOA or AOD estimation. Therefore, to ensure satisfied angular estimation accuracy in applications as well as reduce the computation cost, an iterative approach is developed to further improve the channel estimation performance based on the maximum likelihood principle. The iterative procedure to refine the channel parameter estimation is initialized by the coarse estimation and the search for optimal angles is subject to $\pm\delta$ around the coarse estimation values.

Let $\boldsymbol{\eta} = [\boldsymbol{\eta}_0, \boldsymbol{\eta}_1, \dots, \boldsymbol{\eta}_{L-1}]^T$ be the vector of the parameters under estimation.

$\boldsymbol{\eta}_l = [\theta_{t,l}, \phi_{t,l}, \theta_{r,l}, \phi_{r,l}, \tau_l, h_l]^T \in \mathbb{R}^6$ consists of the angle parameters, channel gain and transmission time for the l -th path. The likelihood function of the random vector \mathbf{y} conditioned on $\boldsymbol{\eta}$ can be written as [98]

$$f(\mathbf{y}|\boldsymbol{\eta}) \propto \exp\left\{\frac{2}{N_0} \sum_{n=0}^{N-1} \Re\{\boldsymbol{\mu}^H[n]\mathbf{y}[n]\} - \frac{1}{N_0} \sum_{n=0}^{N-1} \|\boldsymbol{\mu}[n]\|^2\right\}, \quad (3.25)$$

where $\boldsymbol{\mu}[n] = \mathbf{H}[n]\mathbf{F}[n]\mathbf{x}[n]$ and \Re means taking the real part in $\{\cdot\}$.

Generally, the maximum of $f(\mathbf{y}|\boldsymbol{\eta})$ can be calculated directly using its Jacobian and Hesse matrix. However, due to the multi-dimensional ($\boldsymbol{\eta} \in \mathbb{R}^{6L}$) maximization of our problem, the complexity of using the analytical methods is high. The regularly utilized searching approach for ML estimator is not feasible well. Therefore, in this chapter, a simplified method is employed by utilizing an iterative algorithm to update the variables one by one. Since there are L paths, we consider beginning the iteration with the LOS followed by the NLOS paths. For instance, considering the l -th path, we firstly update one of the angles by gradient descent algorithm with the remaining parameters fixed to maximize $f(\mathbf{y}|\boldsymbol{\eta})$, which stops when the variation of $f(\mathbf{y}|\boldsymbol{\eta})$ gets smaller than or equal to the threshold α . Since the estimation error of transmission time of H-DCS-SOMP is relatively small, in the fine estimation, we consider the refinement of angular parameters. Firstly, the four angles (AOA/AOD azimuth and elevation) in l -th path are updated iteratively until the variation of $f(\mathbf{y}|\boldsymbol{\eta})$ reaches threshold α . Then the L paths are updated in the loop to ensure the convergence of all the angular variables. The steps are summarized as follows.

- Initialize all the angles using the AOA/AOD measurements obtained from the coarse estimation.
- Calculate the likelihood function $f(\mathbf{y}|\boldsymbol{\eta})$ with only one angle as a variable while keeping all other angles fixed.
- Update the angle by using the gradient descent algorithm until the $f(\mathbf{y}|\boldsymbol{\eta})$ reaches the local maximum.

- Repeat the steps above for all the remaining angles until the variation of the likelihood function is less than or equal to threshold α .

During the iteration, there's no priority difference among the angular variables since the estimation precision of them cannot be distinguished theoretically. For instance, the iteration of l -th path is carried by using

$$\begin{aligned}
\theta''_{r,l} &= \operatorname{argmax}_{\theta_{r,l}} \left\{ f(\mathbf{y}|\boldsymbol{\eta})|_{\theta_{r,l}, \theta'_{t,l}, \phi'_{t,l}, \phi'_{r,l}} \right\}, \\
\theta''_{t,l} &= \operatorname{argmax}_{\theta_{t,l}} \left\{ f(\mathbf{y}|\boldsymbol{\eta})|_{\theta'_{r,l}, \theta_{t,l}, \phi'_{t,l}, \phi'_{r,l}} \right\}, \\
\phi''_{t,l} &= \operatorname{argmax}_{\phi_{t,l}} \left\{ f(\mathbf{y}|\boldsymbol{\eta})|_{\theta'_{r,l}, \theta'_{t,l}, \phi_{t,l}, \phi'_{r,l}} \right\}, \\
\phi''_{r,l} &= \operatorname{argmax}_{\phi_{r,l}} \left\{ f(\mathbf{y}|\boldsymbol{\eta})|_{\theta'_{r,l}, \theta'_{t,l}, \phi'_{t,l}, \phi_{r,l}} \right\},
\end{aligned} \tag{3.26}$$

where the results $\theta''_{r,l}$, $\theta''_{t,l}$, $\phi''_{t,l}$, $\phi''_{r,l}$ are calculated from the iteration results of last step $\theta'_{r,l}$, $\theta'_{t,l}$, $\phi'_{t,l}$, $\phi'_{r,l}$.

Here, the gradient descent method is used to obtain each maximum within a certain searching angular range. Taking the $\theta''_{r,l}$ as an example, with $\theta'_{r,l}$ as the original value, the steps are shown as follows.

- (1) Set $0 < \alpha < 1$ as the error bound and iteration number $k = 0$.
- (2) Calculate $\varphi^{(k)} = \nabla f(\mathbf{y}|\boldsymbol{\eta})|_{\theta_{r,l}^{(k)}, \theta'_{t,l}, \phi'_{t,l}, \phi'_{r,l}}$.
- (3) If $\|\varphi^{(k)}\| < \alpha$, break the iteration, return $\theta''_{r,l} = \theta_{r,l}^{(k)}$.
- (4) Find the value of $\varrho > 0$ from $\theta_{r,l}^{(k)}$ to get the $\operatorname{argmax}_{\varrho} f(\mathbf{y}|\boldsymbol{\eta})|_{\theta_{r,l}^{(k)} + \varrho \times \varphi^{(k)}, \theta'_{t,l}, \phi'_{t,l}, \phi'_{r,l}}$.
- (5) Make $\theta_{r,l}^{(k+1)} = \theta_{r,l}^{(k)} + \varrho \times \varphi^{(k)}$ and go to (2).

3.3.2 Joint Rigid Body and Reflection Points Localization

In this subsection, based on the estimation results of AOAs/AODs/transmission times, we demonstrate that the posture of the rigid body and the position of reflection points can be recovered from the parameters. Both two scenarios with and without LOS are discussed.

The case with LOS is first investigated. As shown in Fig. 3.1, the distances between AN and rigid body, AN and reflection point l , reflection point l and rigid body is denoted by d_0 ,

$d_{l,1}$ and $d_{l,2}$ ($l = 1, 2, \dots, L - 1$), respectively. Their estimated values can be expressed with transmission times as

$$\begin{aligned}\hat{d}_0 &= c \cdot \hat{\tau}_0, \\ \hat{d}_{l,1} + \hat{d}_{l,2} &= c \cdot \hat{\tau}_l.\end{aligned}\tag{3.27}$$

Then, the rigid body position can be directly estimated with the AOD of LOS and \hat{d}_0 as

$$\hat{\mathbf{p}} = \mathbf{s} + \hat{d}_0 \cdot [\sin\hat{\phi}_{t,0}\cos\hat{\theta}_{t,0}, \sin\hat{\phi}_{t,0}\sin\hat{\theta}_{t,0}, \cos\hat{\phi}_{t,0}]^T.\tag{3.28}$$

However, the orientation and reflection points cannot be resolved directly from channel parameters. Thus, we formulated it as an optimization problem with the following steps. As can be seen in Fig. 3.1, the position of reflection point κ_l calculated by $\theta_{t,l}$, $\phi_{t,l}$ and $d_{l,1}$ as

$$\kappa'_l = \mathbf{s} + d_{l,1} \cdot [\sin\hat{\phi}_{t,l}\cos\hat{\theta}_{t,l}, \sin\hat{\phi}_{t,l}\sin\hat{\theta}_{t,l}, \cos\hat{\phi}_{t,l}]^T,\tag{3.29}$$

and it can also be derived by $\theta_{r,l,g}$, $\phi_{r,l,g}$ and $d_{l,2}$ as

$$\kappa''_l = \hat{\mathbf{p}} + d_{l,2} \cdot [\sin\hat{\phi}_{r,l,g}\cos\hat{\theta}_{r,l,g}, \sin\hat{\phi}_{r,l,g}\sin\hat{\theta}_{r,l,g}, \cos\hat{\phi}_{r,l,g}]^T.\tag{3.30}$$

$\hat{\theta}_{r,l,g}$, $\hat{\phi}_{r,l,g}$ is expressed by $\hat{\theta}_{r,l}$, $\hat{\phi}_{r,l}$ and \mathbf{q} as introduced in (3.6) and (3.8).

Hence, the problem is reformulated as the estimation of \mathbf{q} and $d_{l,1}$, which is to minimize the difference between κ'_l and κ''_l subject to certain constraints as is shown in P .

$$P : \min_{\mathbf{q}, d_{l,1}} \sum_{l=1}^{L-1} \|\kappa'_l - \kappa''_l\|,\tag{3.31}$$

s.t.

$$0 < d_{l,1} < d_l,\tag{31a}$$

$$0 \leq q_1, q_3 < 2\pi,\tag{31b}$$

$$0 \leq q_2 \leq \pi,\tag{31c}$$

$$d_l = d_{l,1} + d_{l,2}.\tag{31d}$$

To solve P , we propose to use the particle swarm algorithm (PSO) based approach [99]. PSO is a kind of population-based search algorithm. The advantage of PSO is that it can quickly find the optimal solution without searching the entire solution space, and it has low complexity to execute. In [100], the effectiveness of the PSO algorithm, especially for non-convex global optimization has been proved. Generally, it simulates the social behaviour of birds/fishes in nature. During the execution, the individuals' positions are changing with the social tendency of the group. In PSO, each individual, called a particle, benefits from the historical experience of its own and that of the other members when searching for food. In particular, each particle i records the best position it has experienced so far as $pbest_i$, and the best position of its neighbours or the global community as $gbest$. With the iteration, the particle i can update its velocity v_{ij} and position ϖ_{ij} (j -th dimension of optimization vector) through the personal best position and swarm's best position. In problem P , the position of particle i is denoted as $\varpi_i = [q_1, q_2, q_3, d_{1,1}, d_{2,1}, \dots, d_{L-1,1}] \in \mathbb{R}^{L+2}$. In Algorithm 1, w is the inertia weight, c_1 and c_2 are learning factors while $rand_1$ and $rand_2$ are random numbers between 0 and 1. The iteration is stopped when the $gbest$ is convergent or the maximum iteration number is reached.

Under the OLOS scenario, i.e., the LOS is not available due to obstruction, \hat{d}_0 cannot be obtained since (3.27) is not valid. In this case, we further revise Algorithm 1 to estimate the $\tilde{\mathbf{x}}_i = [p_1, p_2, p_3, q_1, q_2, q_3, d_{1,1}, d_{2,1}, \dots, d_{L-1,1}] \in \mathbb{R}^{L+5}$ with NLOS information.

3.3.3 Complexity Analysis

In this subsection, we analyze the complexity of the channel parameter estimation algorithm and joint rigid body and reflection points localization algorithm.

3.3.3.1 Channel Parameter Estimation

The complexity in performing (3.18) is on the order of $O(N_R^2 N_T^2 GN)$ as same as [81]. During the coarse estimation, the coefficients derived from the second layer dictionary approximately take $O(N_b^2 GN)$. (3.24) requires $O(NL)$ operations. Consequently, the maximum complexity for H-DCS-SOMP is $L \times O(N_R^2 N_T^2 N_b^2 GN)$. In fine estimation, the complexity is mainly caused by iterations of the gradient descent algorithm. Since the gradient descent algorithm is an iterative

process, the complexity is subject to initial values and step size factor ϱ , threshold α . Assume dimension of optimized vector is \mathcal{N}_1 , the maximum complexity from fine estimation will be $\mathcal{N}_1 \log(1/\alpha)/\varrho$.

3.3.3.2 Joint Position Estimation

The calculation of rigid body location in the LOS case is easy to implement since it involves only some basic operations. For rigid body posture estimation and reflection points position estimation, the complexity is mainly from the PSO algorithm. Assume the PSO algorithm iterates \mathcal{N}_2 times and in each iteration of the algorithm \mathcal{N}_3 particles are updated. The (3.31) is invoked \mathcal{N}_4 times in each iteration. Hence the overall time complexity of the joint position estimation algorithm is $O(\mathcal{N}_2 \mathcal{N}_3 \mathcal{N}_4)$.

Algorithm 1: Joint rigid body and reflection points localization

Input : $L, \mathbf{s}, \hat{\tau}_l, \hat{\theta}_{t,l}, \hat{\phi}_{t,l}, \hat{\theta}_{r,l}, \hat{\phi}_{r,l}$

Output: $\mathbf{p}, \mathbf{q}, \kappa_l$

1 **Initializaiton**:

2 Calculate the rigid body position $\hat{\mathbf{p}}$ and d_l .

3 Generate particles $\mathcal{P}_1, \dots, \mathcal{P}_S \in \mathbb{R}^{L+2}$.

4 Generate velocities of each particle $\mathbf{v}_{i,j}$.

5 **Loop**

6 Calculate the fitness score of each particle fit_i .

7 Determine the $pbest_i$ and $gbest$ through the fitness score evaluation of the original swarm.

8 Update swarm at iteration number k with

9 (1) $\nu_{ij}(k+1) = w\nu_{ij}(k) + c_1 rand_1(pbest_{ij}(k) - \varpi_{ij}(k)) + c_2 rand_2(gbest_{ij}(k) - \varpi_{ij}(k))$

10 (2) $\varpi_{ij}(k+1) = \varpi_{ij}(k) + \nu_{ij}(k+1)$.

11 Update the new fitness for each particle.

12 Update the $gbest$ through the fitness score evaluation.

13 **End loop**

3.4 Fundamental bounds

In this section, we first derive the Cramér-Rao lower bound (CRLB) of the channel parameters. Then the theoretical lower bounds of rigid body position, orientation, and reflection points position are calculated.

CRLB determines the lower limit of the variance of any unbiased estimator in the parameter estimation problems. The variance of the estimator can only approach the CRLB indefinitely, but cannot be less than it. Therefore, it provides important information for the performance evaluation of algorithms. Here, we derive the fisher information matrix (FIM) and the CRLB for the channel parameters and apply them to investigate rigid body posture and reflection points estimation bounds. To simplify the notation without loss of generality, we consider the case of $G = 1$ which means only one OFDM signal is transmitted. First, we discuss the situation where both LOS and NLOS exist in the channel.

Defining $\hat{\boldsymbol{\eta}} = [\boldsymbol{\eta}_0, \boldsymbol{\eta}_1, \dots, \boldsymbol{\eta}_{L-1}]^T$ as the unbiased estimation of $\boldsymbol{\eta}_l = [\theta_{t,l}, \theta_{r,l}, \phi_{t,l}, \phi_{r,l}, h_l, \tau_l]^T \in \mathbb{R}^6$ ($l = 0, 1, 2, \dots, L-1$), the mean squared error (MSE) is bounded as

$$E_{y|\boldsymbol{\eta}}[(\hat{\boldsymbol{\eta}} - \boldsymbol{\eta})(\hat{\boldsymbol{\eta}} - \boldsymbol{\eta})^T] \geq \mathbf{J}_{\boldsymbol{\eta}}^{-1}, \quad (3.32)$$

where $E[\cdot]$ represents the expectation of $[\cdot]$ and $6L \times 6L$ FIM $\mathbf{J}_{\boldsymbol{\eta}}$ is defined as

$$\mathbf{J}_{\boldsymbol{\eta}} = E_{y|\boldsymbol{\eta}}\left[-\frac{\partial \ln f(\mathbf{y}|\boldsymbol{\eta})}{\partial \boldsymbol{\eta} \partial \boldsymbol{\eta}^T}\right]. \quad (3.33)$$

In (3.33), $f(\mathbf{y}|\boldsymbol{\eta})$ is the likelihood function of the vector \mathbf{y} which is expressed as (3.25). Regarding each paths in the channel model, the FIM can be rewritten as (3.34) and the operator is defined as

$$\mathbf{J}_{\boldsymbol{\eta}} = \begin{bmatrix} \boldsymbol{\Psi}(\boldsymbol{\eta}_0, \boldsymbol{\eta}_0) & \cdots & \boldsymbol{\Psi}(\boldsymbol{\eta}_0, \boldsymbol{\eta}_{L-1}) \\ \vdots & \ddots & \vdots \\ \boldsymbol{\Psi}(\boldsymbol{\eta}_{L-1}, \boldsymbol{\eta}_0) & \cdots & \boldsymbol{\Psi}(\boldsymbol{\eta}_{L-1}, \boldsymbol{\eta}_{L-1}) \end{bmatrix}, \quad (3.34)$$

$$\boldsymbol{\Psi}(\boldsymbol{\eta}_{l_1}, \boldsymbol{\eta}_{l_2}) = E_{y|\boldsymbol{\eta}}\left[-\frac{\partial^2 \ln f(\mathbf{y}|\boldsymbol{\eta})}{\partial \boldsymbol{\eta}_{l_1} \partial \boldsymbol{\eta}_{l_2}^T}\right]. \quad (3.35)$$

In particular, the sub-matrix in \mathbf{J}_η is the sum of $\psi_n(\boldsymbol{\eta}_{l_1}, \boldsymbol{\eta}_{l_2}) \in \mathbb{C}^{6 \times 6}$ across all the subcarriers and

$$\boldsymbol{\Psi}(\boldsymbol{\eta}_{l_1}, \boldsymbol{\eta}_{l_2}) = \sum_{n=0}^{N-1} \psi_n(\boldsymbol{\eta}_{l_1}, \boldsymbol{\eta}_{l_2}), \quad (3.36)$$

$$\psi_n(\boldsymbol{\eta}_{l_1}, \boldsymbol{\eta}_{l_2}) = \psi_n \begin{bmatrix} (\theta_{t,l_1}, \theta_{t,l_2}) & (\theta_{t,l_1}, \theta_{r,l_2}) & \dots & (\theta_{t,l_1}, \tau_{l_2}) \\ (\theta_{r,l_1}, \theta_{t,l_2}) & (\theta_{r,l_1}, \theta_{r,l_2}) & \dots & (\theta_{r,l_1}, \tau_{l_2}) \\ \dots & \dots & \dots & \dots \\ (\tau_{l_1}, \theta_{t,l_2}) & (\tau_{l_1}, \theta_{r,l_2}) & \dots & (\tau_{l_1}, \tau_{l_2}) \end{bmatrix}. \quad (3.37)$$

Taking $\mathbf{y}[n] = \mathbf{H}[n]\mathbf{F}[n]\mathbf{x}[n] + \mathbf{n}[n]$ into \mathbf{J}_η (note $E_{y|\eta}[\mathbf{n}[n]] = 0$), the scalar operator $\psi(x_{l_1}, x_{l_2})$ can be derived as

$$\psi(x_{l_1}, x_{l_2}) = \frac{2}{N_0} \Re \left\{ \frac{\partial \boldsymbol{\mu}^H[n]}{\partial x_{l_1}} \frac{\partial \boldsymbol{\mu}[n]}{\partial x_{l_2}} \right\}, \quad (3.38)$$

where $\boldsymbol{\mu}[n] = \mathbf{H}[n]\mathbf{F}[n]\mathbf{x}[n]$, $x_{l_1}, x_{l_2} \in \{\theta_{t,l}, \theta_{r,l}, \phi_{t,l}, \phi_{r,l}, h_l, \tau_l, l = l_1, l_2\}$. A more detailed derivation and expression of all elements in (3.38) can be found in APPENDIX A.1. With the FIM, the CRLB of channel parameters in LOS can be calculated by

$$\begin{aligned} \text{CRLB}(\hat{\theta}_{t,0}) &= \sqrt{[\mathbf{J}_\eta^{-1}]_1}, \\ \text{CRLB}(\hat{\theta}_{r,0}) &= \sqrt{[\mathbf{J}_\eta^{-1}]_2}, \\ \text{CRLB}(\hat{\phi}_{t,0}) &= \sqrt{[\mathbf{J}_\eta^{-1}]_3}, \\ \text{CRLB}(\hat{\phi}_{r,0}) &= \sqrt{[\mathbf{J}_\eta^{-1}]_4}. \end{aligned} \quad (3.39)$$

The averages of the CRLBs of AOD/AOA in NLOS are derived in (3.40) where $\text{diag}[\mathbf{J}]_{e_1, e_2, \dots, e_{l_3}}$ denotes the diagonal matrix comprising of the e_1, e_2, \dots, e_{l_3} -th diagonal elements in \mathbf{J} . The

CRLB of \hat{h}_l and $\hat{\tau}_l$ can be deduced similarly as

$$\begin{aligned}
\text{CRLB}(\hat{\theta}_{t,l}) &= \sqrt{\text{tr} \left\{ \text{diag} \left[\mathbf{J}_{\boldsymbol{\eta}}^{-1} \right]_{7,13,\dots,6L-5} \right\} / (L-1)}, \\
\text{CRLB}(\hat{\theta}_{r,l}) &= \sqrt{\text{tr} \left\{ \text{diag} \left[\mathbf{J}_{\boldsymbol{\eta}}^{-1} \right]_{8,14,\dots,6L-4} \right\} / (L-1)}, \\
\text{CRLB}(\hat{\phi}_{t,l}) &= \sqrt{\text{tr} \left\{ \text{diag} \left[\mathbf{J}_{\boldsymbol{\eta}}^{-1} \right]_{9,15,\dots,6L-3} \right\} / (L-1)}, \\
\text{CRLB}(\hat{\phi}_{r,l}) &= \sqrt{\text{tr} \left\{ \text{diag} \left[\mathbf{J}_{\boldsymbol{\eta}}^{-1} \right]_{10,16,\dots,6L-2} \right\} / (L-1)}.
\end{aligned} \tag{3.40}$$

With the FIM of channel parameters, the CRLB of rigid body position ($\hat{\mathbf{p}}$), orientation ($\hat{\mathbf{q}}$) and reflection point position ($\hat{\boldsymbol{\kappa}}_l$) can be derived through the variable transformation tensor \mathbf{T} from $\boldsymbol{\eta}$ to $\boldsymbol{\xi} = [\mathbf{p}, \mathbf{q}, \boldsymbol{\kappa}_1, \boldsymbol{\kappa}_2, \dots, \boldsymbol{\kappa}_{L-1}]^T$. Then the FIM of $\boldsymbol{\xi}$ can be expressed as $\mathbf{J}_{\boldsymbol{\xi}} = \mathbf{T} \mathbf{J}_{\boldsymbol{\eta}} \mathbf{T}^T$. The transformation matrix \mathbf{T} is calculated with $\mathbf{T} = \frac{\partial \boldsymbol{\eta}^T}{\partial \boldsymbol{\xi}}$. The elements of \mathbf{T} are calculated by using the geometric relationships as

$$\begin{aligned}
\tau_0 &= |\mathbf{p} - \mathbf{s}|/c, \tau_l = (|\mathbf{p} - \boldsymbol{\kappa}_l| + |\boldsymbol{\kappa}_l - \mathbf{s}|)/c, \\
\phi_{t,0} &= \arccos[(p_z - s_z)/|\mathbf{p} - \mathbf{s}|], \\
\theta_{t,0} &= \arctan[(p_y - s_y)/(p_x - s_x)], \\
\phi_{t,l} &= \arccos[(\kappa_{3,l} - s_z)/|\boldsymbol{\kappa}_l - \mathbf{s}|], \\
\theta_{t,l} &= \arctan[(\kappa_{2,l} - s_y)/(\kappa_{1,l} - s_x)].
\end{aligned} \tag{3.41}$$

Here, we structured \mathbf{T} analog to (3.34) by considering each path in the channel model ($[\mathbf{p}, \mathbf{q}] \subseteq \boldsymbol{\xi}$ is treated as path 0) as

$$\mathbf{T} = \begin{bmatrix} \mathbf{T}_{1,0} & \cdots & \mathbf{T}_{0,L-1} \\ \vdots & \ddots & \vdots \\ \mathbf{T}_{L-1,0} & \cdots & \mathbf{T}_{L-1,L-1} \end{bmatrix}, \tag{3.42}$$

$$\mathbf{T}_{w,v} = \frac{\partial \boldsymbol{\eta}_w}{\partial \boldsymbol{\xi}_v}. \tag{3.43}$$

With the Jacobian matrix notation, it's clear that $\mathbf{T} \in \mathbb{C}^{(3L+3) \times 6L}$, and the elements in $\mathbf{T}_{w,v}$

can be abbreviated as shown as

$$\begin{aligned}\mathbf{T}_{w,0} &= \frac{\partial(\theta_{l,w}, \theta_{r,w}, \phi_{l,w}, \phi_{r,w}, h_w, \tau_w)}{\partial(p_x, p_y, p_z, q_1, q_2, q_3)}, \\ \mathbf{T}_{w,v,v \neq 0} &= \frac{\partial(\theta_{l,w}, \theta_{r,w}, \phi_{l,w}, \phi_{r,w}, h_w, \tau_w)}{\partial(\kappa_{1l}, \kappa_{2l}, \kappa_{3l})}.\end{aligned}\quad (3.44)$$

Consequently, the entries for the transmission time and AOD are derived as

$$\begin{aligned}\partial\tau_0/\partial p_i &= (p_i - s_i)/(c|\mathbf{p} - \mathbf{s}|), \quad i = x, y, z, \\ \partial\phi_{t,0}/\partial p_i &= (p_i - s_i)(p_z - s_z)|\mathbf{p} - \mathbf{s}|^{-3}/|\sin\phi_{t,0}|, \quad i = x, y, \\ \partial\phi_{t,0}/\partial p_z &= [(p_z - s_z)^2|\mathbf{p} - \mathbf{s}|^{-3} - |\mathbf{p} - \mathbf{s}|^{-1}]/|\sin\phi_{t,0}|, \\ \partial\theta_{t,0}/\partial p_x &= (p_y - s_y)/[(p_x - s_x)^2(1 + \tan^2\theta_{t,0})], \\ \partial\theta_{t,0}/\partial p_y &= [(p_x - s_x)(1 + \tan^2\theta_{t,0})]^{-1},\end{aligned}\quad (3.45)$$

for LOS terms and

$$\begin{aligned}\partial\tau_l/\partial p_i &= (p_i - \kappa_{l,i})/(c|\mathbf{p} - \boldsymbol{\kappa}_l|), \quad i = x, y, z, \\ \partial\tau_l/\partial \kappa_{l,i} &= -\partial\tau_l/\partial p_i, \quad i = x, y, z, \\ \partial\phi_{t,l}/\partial \kappa_{l,i} &= (\kappa_{l,i} - s_i)(\kappa_{l,z} - s_z)|\boldsymbol{\kappa}_l - \mathbf{s}|^{-3}/|\sin\phi_{t,l}|, \quad i = x, y, \\ \partial\phi_{t,l}/\partial \kappa_{l,z} &= [(\kappa_{l,z} - s_z)^2|\boldsymbol{\kappa}_l - \mathbf{s}|^{-3} - |\boldsymbol{\kappa}_l - \mathbf{s}|^{-1}]/|\sin\phi_{t,l}|, \\ \partial\theta_{t,l}/\partial \kappa_{l,x} &= (\kappa_{l,y} - s_y)/[(\kappa_{l,x} - s_x)^2(1 + \tan^2\theta_{t,l})], \\ \partial\theta_{t,l}/\partial \kappa_{l,y} &= [(\kappa_{l,x} - s_x)(1 + \tan^2\theta_{t,l})]^{-1},\end{aligned}\quad (3.46)$$

for NLOS entries ($l \neq 0$) while the rest elements of matrix \mathbf{T} related to AOD and transmission time are zero.

Moreover, the entries regarding the AOA are more complex since the AOA is measured in RBCS. The expression of the same vector at RBCS and GCS is connected by rotation matrix \mathbf{R} .

Therefore, we introduce the notation $\boldsymbol{\zeta}_l(\mathbf{p}, \mathbf{s}, \boldsymbol{\kappa}_l) = [\cos(\theta_{r,l,g})\sin(\phi_{r,l,g}), \sin(\theta_{r,l,g})\sin(\phi_{r,l,g}), \cos(\phi_{r,l,g})]^T$,

and there is

$$\begin{aligned}\phi_{r,l} &= \arccos(\mathbf{R}(3, :) \cdot \zeta_l(\mathbf{p}, \mathbf{s}, \boldsymbol{\kappa}_l)), \\ \theta_{r,l} &= \arctan\left(\frac{\mathbf{R}(2, :) \cdot \zeta_l(\mathbf{p}, \mathbf{s}, \boldsymbol{\kappa}_l)}{\mathbf{R}(1, :) \cdot \zeta_l(\mathbf{p}, \mathbf{s}, \boldsymbol{\kappa}_l)}\right).\end{aligned}\quad (3.47)$$

The remaining entries in \mathbf{T} containing AOA terms can be deduced by (3.48) (details of the final results are in APPENDIX A.2) while the rests entries in \mathbf{T} are zero.

$$\begin{aligned}\partial\theta_{r,0}/\partial p_i &= (\mathbf{R}(3, :) \cdot \partial\zeta_0/\partial p_i) / |\sin\theta_{r,0}|, \\ \partial\theta_{r,l}/\partial q_i &= \frac{\partial\mathbf{R}(3, :)}{\partial q_i} \cdot \frac{\zeta_l}{|\sin\theta_{r,l}|}, \\ \partial\theta_{r,l}/\partial\kappa_{l,i} &= (\mathbf{R}(3, :) \cdot \partial\zeta_l/\partial\kappa_{l,i}) / |\sin\theta_{r,l}|, \\ \partial\phi_{r,0}/\partial p_i &= \frac{\partial [\mathbf{R}(2, :) \cdot \zeta_0 / \mathbf{R}(1, :) \cdot \zeta_0]}{(1 + \tan^2\phi_{r,0})\partial p_i}, \\ \partial\phi_{r,l}/\partial\kappa_{l,i} &= \frac{\partial [\mathbf{R}(2, :) \cdot \zeta_l / \mathbf{R}(1, :) \cdot \zeta_l]}{(1 + \tan^2\phi_{r,l})\partial\kappa_{l,i}}, \\ \partial\phi_{r,l}/\partial q_i &= \frac{\partial [\mathbf{R}(2, :) \cdot \zeta_l / \mathbf{R}(1, :) \cdot \zeta_l]}{(1 + \tan^2\phi_{r,l})\partial q_i}.\end{aligned}\quad (3.48)$$

Using the FIM $\mathbf{J}_\xi \in \mathbb{C}^{(3L+3) \times (3L+3)}$, the CRLB of rigid body position and orientation estimation can be obtained as

$$\begin{aligned}\text{CRLB}(\hat{\mathbf{p}}) &= \sqrt{\text{tr}\{[\mathbf{J}_\xi^{-1}]_{1:3,1:3}\}}, \\ \text{CRLB}(\hat{\boldsymbol{\eta}}) &= \sqrt{\text{tr}\{[\mathbf{J}_\xi^{-1}]_{4:6,4:6}\}},\end{aligned}\quad (3.49)$$

where $[\cdot]_{e_1:e_2, e_3:e_4}$, means the selection of the $(e_2 - e_1 + 1) \times (e_4 - e_3 + 1)$ submatrix and tr is the trace of the matrix. For the CRLB of reflection points estimation, the average bound of all the NLOS paths is taken as

$$\text{CRLB}(\hat{\boldsymbol{\kappa}}_l) = \sqrt{\text{tr}\{[\mathbf{J}_\xi^{-1}]_{7:3L+3, 7:3L+3}\}}.\quad (3.50)$$

In the case of OLOS, there is no AOA/AOD for LOS to be detected. Hence, the estimation of the channel becomes $\tilde{\boldsymbol{\eta}} = [\boldsymbol{\eta}_1, \dots, \boldsymbol{\eta}_{L-1}]^T$ while the $\tilde{\boldsymbol{\xi}} = \boldsymbol{\xi}$ since the NLOS channel model is still related to all components in $\boldsymbol{\xi}$. The following derivation under OLOS is similar to LOS.

3.5 Simulation Results

In this section, simulation results of the proposed 5G mm-wave rigid body active localization and environment sensing methods are discussed. First, the environmental setup and performance metric are introduced. Second, we present simulation results of the rigid body posture estimation for both NLOS and OLOS situations. Third, the reflection points localization results are presented including the performance comparison of different algorithms. The CRLB as the theoretical optimal solution is also investigated.

3.5.1 Simulation Setup

We consider a 3D indoor scenario with the size of $5 \times 5 \times 5 \text{ m}^3$ in MATLAB 2020b. The location of AN is $s = [0, 0, 0]^T$. To simplify the problem without loss of generality, we randomly set the real position and orientation of rigid body within far-field regime $\mathbf{p} = [5, 5, 3]^T$ and $\mathbf{q} = [\pi/6, 2\pi/5, \pi/5]^T$. Reflection points can be located anywhere in the cube indoor environment except the positions on the extension line between AN and the rigid body. The URAs with half-wavelength antennas inter-element spacing on both AN and the rigid body consists of $N_T = N_{Tx} \times N_{Ty} = N_R = N_{Rx} \times N_{Ry} = 8 \times 4$ antennas. We set $L = 5, N = 10, c = 0.3 \text{ m/ns}, B = 100 \text{ MHz}, f_c = 60 \text{ GHz}$. The number of beams sent is 10 and the average reflection loss for the first order reflection is -10 dB similar to [81] introduced. The SNR represents the signal-to-noise ratio of the signal from s . It is related to the channel information and can be defined as

$$SNR \triangleq \sum_{n=1}^N \frac{\|\mathbf{H}[n]\mathbf{F}[n]\mathbf{x}[n]\|_2^2}{\|\mathbf{n}[n]\|_2^2}. \quad (3.51)$$

The root mean square error (RMSE) of Ξ is used to evaluate the estimation accuracy of the joint rigid body and reflection points localization algorithm. Suppose $\hat{\Xi}_i$ is the estimation of true value Ξ_i in the i -th simulation, there is

$$RMSE_{\Xi} = \sqrt{\frac{1}{M} \sum_{i=1}^M |\Xi_i - \hat{\Xi}_i|^2}. \quad (3.52)$$

The effectiveness of the embedded PSO algorithm is impacted by the size of the swarm. If there are too few particles, the algorithm may become stuck in local optima, whereas too many

particles slow down the algorithm's speed. As the dimensionality of the problem increases, the size of the swarm needs to be increased. In the reflection point estimation problem, the dimension of the particle is $L + 2$. Considering there are three main NLOS paths, an initial population is set to 300 to balance the global optima searching effectiveness and efficiency. Selecting the inertial weight is crucial for balancing exploration and exploitation. A value of inertial weight closer to 1.0 emphasizes exploration, while a value closer to 0.0 emphasizes exploitation. Common choices are between 0.4 and 0.9 [101]. An inertia weight of 0.8 is applied throughout to promote exploration while preventing the algorithm from being trapped in local optima. Selecting the learning factor in the PSO algorithm is essential for balancing the influence of personal best and global best positions on particle movement. In this section, both the self-learning factor and group learning factor are set to be 0.5 for an equal emphasis on both personal best and global best positions. The total iteration number is set to 50 to ensure convergence of iterations.

3.5.2 Rigid Body Posture Estimation

Firstly, we evaluate the CDF (Cumulative Distribution Function) of rigid body position and orientation estimation against different compressive sensing methods. Both the rigid body position and posture are denoted by the three dimension vector. The \mathbf{E}_i in (3.52) is the three components of the vector with $\mathcal{M} = 3$. The algorithms are repeated 200 times as is shown in Fig. 3.3. Here, the DCS-SOMP algorithm is taken from paper [102]. In Fig. 3.3, we set $SNR = 20$ dB and $N_b = 4$. It can be observed that our proposed modified H-DCS-SOMP algorithm has narrower distribution width for both position and orientation estimation compared with the other two algorithms. Moreover, for rigid body position estimation in Fig. 3.3a, the DCS-SOMP algorithm can achieve around 0.65 m RMSE with 90% probability, and with the same condition, H-DCS-SOMP can achieve around 0.25 m RMSE and our proposed method can achieve around 0.08 m RMSE. Thus, the performance of the DCS-SOMP algorithm is much more restricted compared with our method. In addition, for rigid body orientation estimation in Fig. 3.3b, our proposed method achieves 0.1 rad RMSE with 90% probability, which is higher than the DCS-SOMP method.

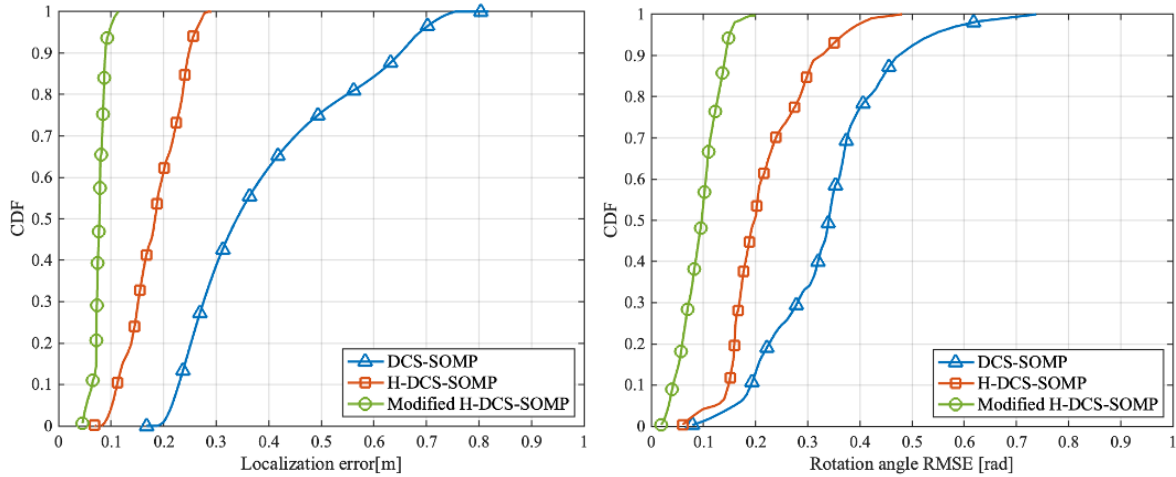


Figure 3.3. The CDF of rigid body localization RMSE (left) and rigid body rotation angle RMSE (right) of three methods when SNR is 20 dB.

In addition, the localization and posture error are investigated when SNR is 0 dB, indicating a low-to-medium SNR case. The CDF is shown in Fig. 3.4. When SNR is lower, the localization performance using the three algorithms degrades due to the increased noise level. However, it can be observed that the performance degradation of modified H-DCS-SOMP is much smaller than the other two methods. The average error of position and posture decreases less than 0.1 m and 0.1 rad, with distributions less than 0.1 m and 0.25 rad, respectively. This demonstrates the great robustness of proposed method in rigid body posture estimation.

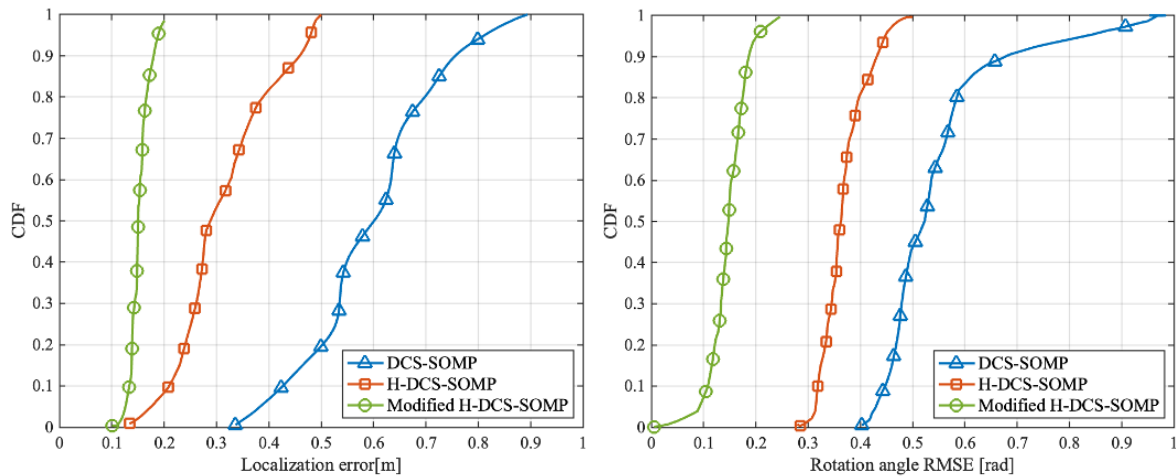


Figure 3.4. The CDF of rigid body localization RMSE (left) and rigid body rotation angle RMSE (right) of of three methods when SNR is 0 dB.

To further demonstrate the influence of SNR, we compare the variation of rigid body position and orientation RMSE of the three algorithms under different SNRs from -20 dB to 20 dB with an interval of 10 dB, i.e., the SNR of adjacent point are related by a factor of ten, as shown in Fig. 3.5. Instead of using the CDF, all the performance is the average value of 200 simulations except for the CRLB. As can be seen in Fig. 3.5a, when $SNR = 0$ dB our proposed method reaches the corresponding theoretical bound. When $SNR = 10$ dB, the RMSE of the rigid body position is less than 0.1 m. Similar to position estimation results, in Fig. 3.5b, the orientation RMSE of our method reaches the corresponding theoretical bound when $SNR = 0$ dB. When $SNR = 20$ dB, our proposed algorithm's location and orientation precision could reach 0.04 m and 0.027 rad while the other two algorithms can only achieve 0.072 m and 0.035 rad, and 0.15 m and 0.107 rad. Both the position and orientation results show the effectiveness of our proposed method.

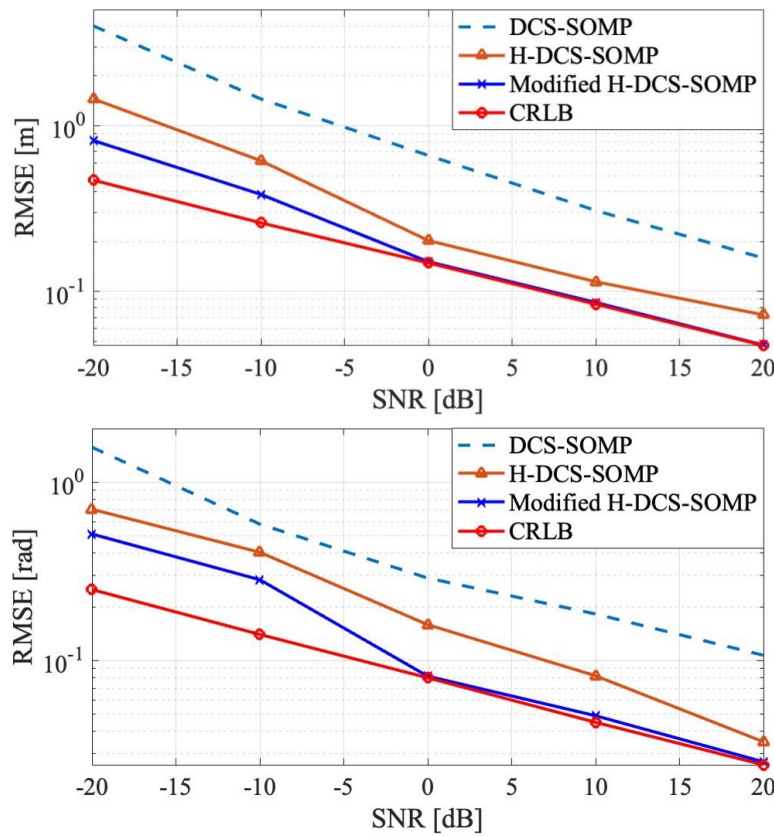


Figure 3.5. The rigid body localization RMSE (top) and rigid body rotation angle RMSE (bottom) of DCS-SOMP, H-DCS-SOMP, modified H-DCS-SOMP and corresponding theoretical bound vs different SNRs.

In addition, we also evaluate the performance of our proposed method when there is no LOS path (OLOS situation). It can be observed from Fig. 3.6, that when $SNR = -10$ dB, position estimation RMSE reaches the corresponding theoretical bound and when $SNR = 0$ dB, orientation estimation RMSE reaches the corresponding theoretical bound. It is also noted that when the LOS is blocked, the theoretical bound of location and orientation estimation is worse than the previous situation due to the less effective information acquisition. In the absence of LOS, only angle and distance information from NLOS can be used to assist rigid body posture estimation. However, the information provided by NLOS has a relatively large error due to the influence of the path loss, which leads to the deterioration of the positioning performance. Compared with Fig. 3.5, the position and orientation estimation error are doubled. Even though, when the $SNR = 10$ dB, the rigid body localization and orientation estimation can reach decimeter level and 0.1 rad, respectively.

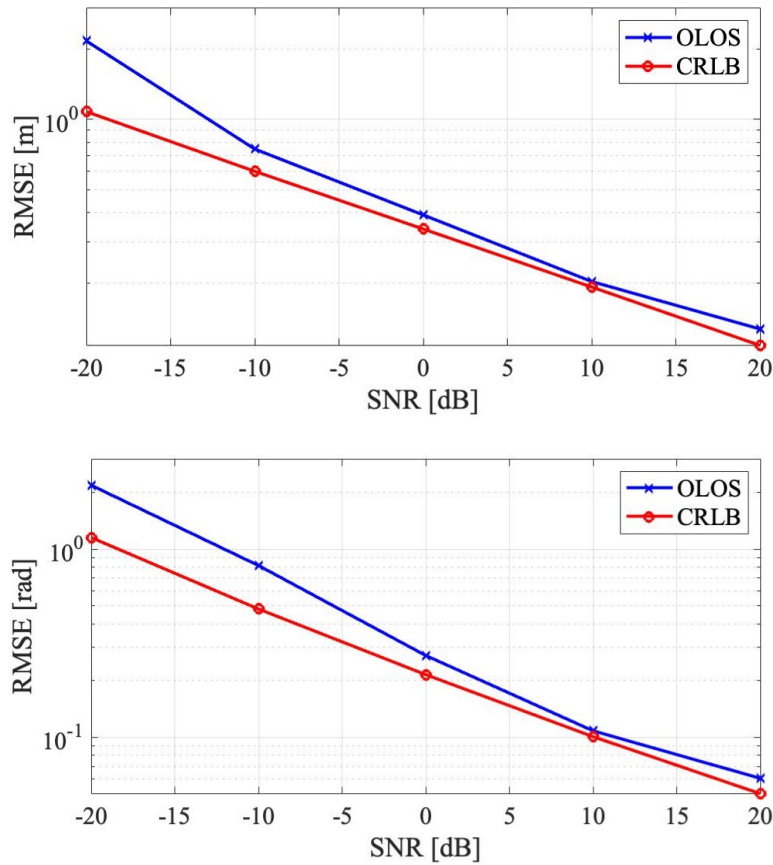


Figure 3.6. In the OLOS situation, the rigid body localization RMSE (top) and rigid body rotation angle RMSE (bottom) of modified H-DCS-SOMP and corresponding theoretical bound vs different SNRs.

3.5.3 Reflection Points Location Estimation

In this subsection, we evaluate the performance of our proposed reflection points location estimation method. As introduced in Section 3.2.2, the position of reflection points is estimated from the angle and distance of NLOS using Algorithm 1. Thus, the NLOS channel parameter estimation results are first evaluated. Each NLOS path has four angle parameters (AOA/AOD azimuth and AOA/AOD elevation, $[\theta_{t,l}, \theta_{r,l}, \phi_{t,l}, \phi_{r,l}]^T$) and there are $L - 1$ NLOS paths. We calculate the average RMSE and CRLB of each angle among different NLOS paths, respectively. Fig. 3.7 illustrates the average azimuth angle estimation RMSE of AODs and AOAs of NLOS paths. And the average CRLB is labelled with red lines. It is observed that the RMSE of both elevation angles and azimuth angles reach 0.1 rad accuracy when SNR is above 0 dB. While the SNR is large than -10 dB, the angular estimation converges to the theoretical bounds. The results demonstrate the validation of the proposed algorithm to resolve the NLOS channel for the following reflection points localization.

The theoretical lower bound and simulation results of RMSE for the different reflection points localization algorithms under various SNRs are shown in Fig. 3.8. The well-known genetic algorithm (GA) [103] has also been widely used for optimization problems. Thus, (3.31) can be potentially solved with the classic GA. Herein, if the optimal solution of (3.31) is obtained with GA, we denote it as Modified H-DCS-SOMP (GA-based). The cyan dash line is the RMSE of DCS-SOMP algorithm with the PSO algorithm, the orange line with a triangular symbol represents the RMSE of the modified H-DCS-SOMP algorithm with GA while the blue line with a cross symbol is the RMSE of the modified H-DCS-SOMP algorithm with PSO algorithm. The crossover rate and mutation rate are 0.5 and 0.1, respectively in the GA algorithm with an initial population of 500 and a maximal generation of 100. It is observed that in our optimization problem, under the same conditions, the PSO algorithm has better performance than GA and can converge faster to the theoretical lower bound. The performance of the PSO method is improved up to 40% compared with GA. The explanation is that, for the global optimization of continuous variables, the memory parameters g_{best} and p_{best}_i of PSO make it easier to find the optimal solution while the GA-based method doesn't track the optimal solutions in the generations. Moreover, under restricted iteration number/generations,

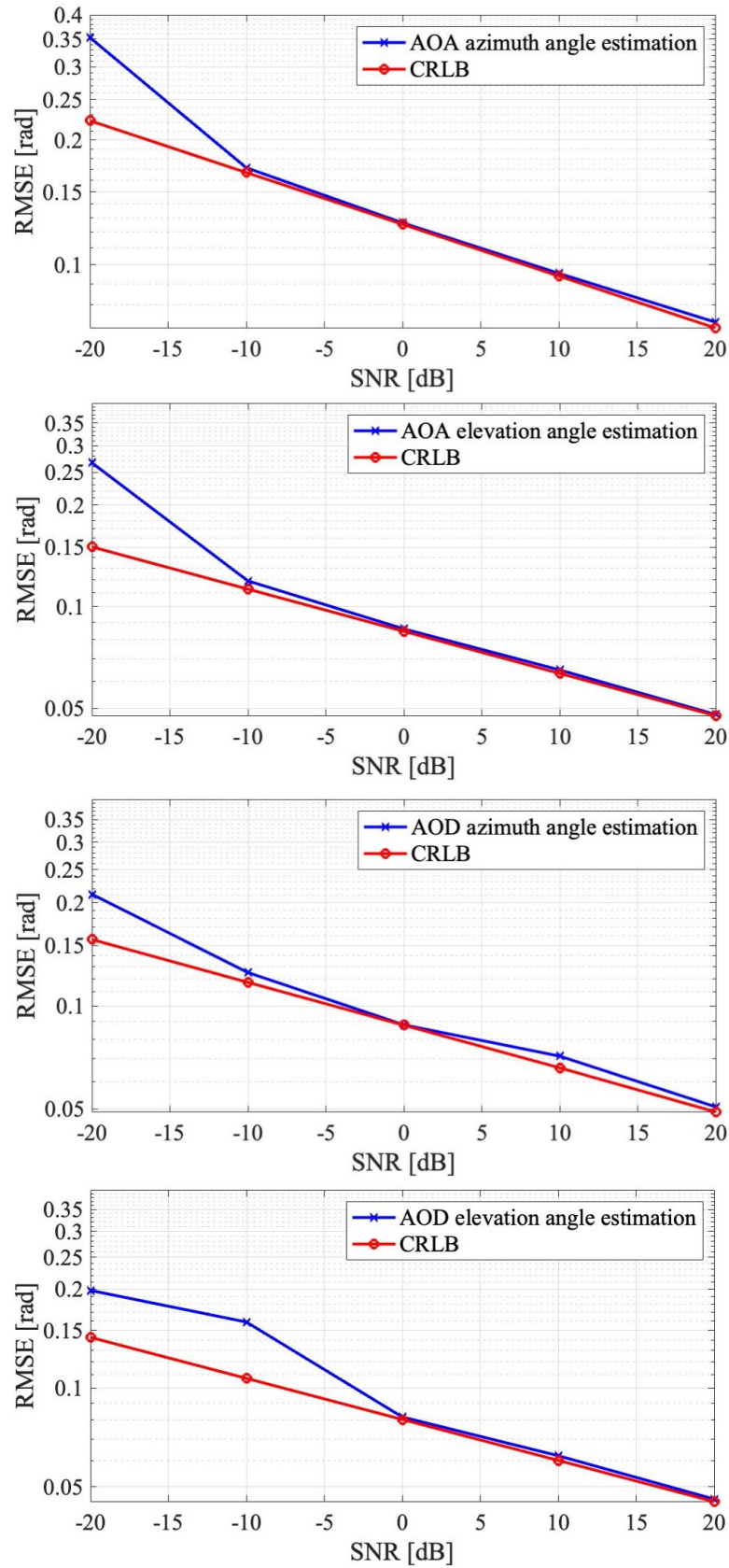


Figure 3.7. The average AOA/AOD RMSE of the NLOS paths and their corresponding theoretical bounds under different SNRs.

the PSO method costs less than the GA-based method to get converged. Thus, the PSO-based Algorithm 1 is much more preferred when the time resource is limited.

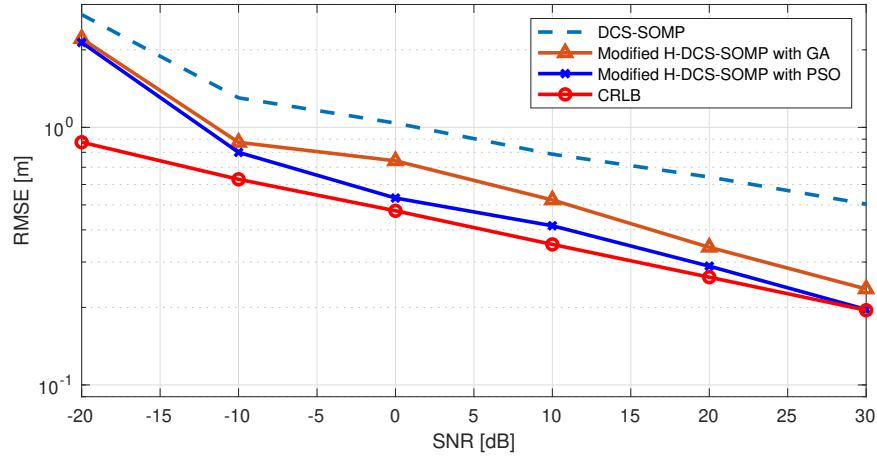


Figure 3.8. The reflection points localization RMSE of DCS-SOMP, modified H-DCS-SOMP with GA method, modified H-DCS-SOMP with PSO method and corresponding theoretical bound vs different SNRs.

3.6 Chapter Summary

In this chapter, a rigid body active localization and environment sensing scheme with the assistance of 5G mm-wave MIMO is proposed. A novel hierarchical compressive sensing algorithm refined by an iterative maximum likelihood step for channel angle and distance estimation is presented. Furthermore, we joint consider the rigid body and reflection points localization problem and a PSO-based optimization algorithm is used to estimate the posture of the rigid body and position of reflection points. We also calculate the theoretical bounds (CRLB) on the rigid body posture, NLOS angular and reflection points position estimate uncertainties. Compared to the traditional rigid body localization approaches, our proposed method using only one anchor node can achieve centimeter-level rigid body posture estimation accuracy under both NLOS and OLOS situations. Simulation results reveal that the rigid body posture and reflection points position estimation of our proposed algorithm approach the corresponding bounds with an increase in SNR value. The results also demonstrate that the proposed scheme can achieve high performance for both rigid body localization and reflection points estimation when SNR reaches 20 dB.

The localization method presented in this chapter can be extended to the scenarios when the reflection points are known. In such cases, the anchor node transmits a reference signal to the known reflection points and then the reflected signal received by the rigid body is used to assist the rigid body localization. The wireless signal bouncing off the reflection points is treated as a signal originating from virtual transmitters (VT). Then the rigid body localization can be achieved with the assistance of multipath propagations. One way is the determination of rigid body position using the maximum likelihood estimation method of both LOS and NLOS signals. Another way is to use the Bayesian filters. The LOS-based localization techniques can be utilized to estimate the position of the rigid body. The NLOS measurements are then introduced as additional observations. Using LOS-based localization as a prior, incorporating NLOS measurements enables the derivation of the posterior distribution, which involves updating and refining the estimation of the target's position.

Chapter 4

Value of Service Maximization in ILAC System through Joint Resource Allocation

4.1 Introduction

With the ongoing deployment of the fifth generation (5G) networks, a significantly growing number of smart devices and intelligent machines including autonomous vehicles and robots, have been connected to the communication infrastructures, leading to a networked society enabled by the Internet of everything [104]. In the next ten years, a wide variety of emerging applications are expected to bring tremendous data traffic growth due to the massive connectivity provided by 5G and beyond [7, 105]. However, conventional design objectives for wireless communication systems including data rate, spectrum efficiency and reliability have proven to be insufficient to meet the diverse requirements of many emerging applications [106, 107]. New vertical applications, e.g. smart factory and intelligent transportation, require concurrent accurate localization and high data rate communication services under challenging environments where global positioning system (GPS) signals are not available. While there are many technologies have been developed for wireless locationing, the separated design of wireless communication and localization leads to redundant, costly and low efficient solutions.

Thus, new wireless paradigms with multiple functions, including integrated localization and communication (ILAC), have been proposed to enhance resource utilization efficiency for simultaneous localization and communication services [108–110]. The ILAC paradigm can

be regarded as a typical device-based integrated sensing and communication (ISAC) [1]. The benefits of the ILAC system are two-fold. Firstly, the hardware cost and power consumption can be reduced by embedding the localization functionality into the current existing communication infrastructure [111]. The combination of millimeter wave (mmWave) frequency band and highly directional large antenna arrays has proven to be sufficient to provide high accuracy localization service [51, 112], which offers the possibility of shared use of one common radio frequency (RF) front end for localization and communication. Instead of multiple RF front end, the shared one makes the system free from frequent switching between different receivers. Secondly, reduced bandwidth and temporal resource consumption can be achieved by jointly designing the waveform for localization and communication. The ILAC system provides the possibilities of joint resource management, rather than optimization of two separate systems, which will greatly reduce the preamble overhead and the corresponding resource consumption. This partially benefits from the fact that localization can be performed together with channel estimation during the communication pilot transmission period [46]. Therefore, through the synergistic design of localization and communication, newly integrated service provisioning can be effectively developed over two isolated systems.

In the ILAC system, the concurrent but diverse service requests in terms of locationing accuracy and communication performance from a particular application impose further requirements on wireless resource allocation. An ILAC user request could consist of application-specific and hybrid requirements. How to optimally allocate the available resources while fulfilling the hybrid and application-specific service requests becomes the new design challenge of ILAC systems. Conventionally, the resource allocation for localization and communication systems is designed separately. The design goal of localization is mainly to maximize accuracy, while the communication systems focus on maximizing the reliable data transmission rate [2]. However, such outdated design objectives are not useful in overcoming the ILAC challenges, as the two performance indicators are often contradictory to each other and cannot always be optimized at the same time.

Therefore, achieving the trade-off between localization and communication performance in the ILAC system is with the key to solving the above problem. However, this turns out to be a difficult task due to the shared use of hardware platforms and radio resources during commu-

nication and localization. Generally, the localization process and data transmission cannot be performed at the same time at the RF front end. This means localization and communication are competing resources for their own performance improvement. Without a unified design objective, two independent resource allocation goals would lead to a one-sided emphasis on localization accuracy or communication data rate that deteriorates the overall system performance. For instance, if more pilot signals are transmitted for better positioning accuracy [113], the reduced channel utilization for data symbols will introduce more communication delay. Thus, a comprehensive evaluation metric is urgent to balance the resource for localization and communication based on different user requests.

Resource allocation in many integrated systems [4, 20, 25, 52] aims to maximize the averaged indicators of different capabilities through competition for resources. For example, the objective in a recent study [52] is to maximize the averaged communication throughput, computation delay and sensing mutual information by radio resource allocation. However, directly using the numerical averaging indicator as performance metric to optimize resource allocation has two drawbacks. Firstly, from the user's perspective, the performance indicator of service is not the higher the better. For instance, it is resource-wasting to provide decimeter-level localization accuracy for navigation applications that require meter-level locationing. To this end, the value of service provisioning should be reflected in the supporting applications. Secondly, for different merged applications, the importance of localization and communication services varies and the performances of services cannot be simply evaluated by their average. Using mobile robotics as an example, when performing navigation tasks, real-time updated positioning services are often required, so the evaluation of positioning performance is more important. However, when performing interactive tasks, it is necessary to continuously send and receive information, which makes communication functionality more important. Thus, the evaluation metric of resource allocation should be able to adaptively adjust based on different users' needs [47]. In summary, another challenge faced by the ILAC system is how to quantify the value of service provisioning and maximize the value when the available resources are limited.

In addition, to coping with heterogeneous demands in the presence of varied performance constraints, the third challenge faced by ILAC system is multi-dimensional resource management. Since localization and communication are sharing the hardware infrastructure, both time

and bandwidth resources should be properly allocated. However, the growth of service requests might be exponential and the number of users is unprecedented in ILAC system, which poses greater difficulties for joint resource allocation. The multi-dimensional resource allocation including the bandwidth and time of traditional communication systems has been proven to be NP-hard in previous studies [114, 115]. Thus, multi-dimensional resource management in ILAC system can be extremely complicated.

Regarding the challenges discussed above, in this chapter, a service-oriented joint resource allocation scheme for the ILAC system is introduced. Inspired by [50], a comprehensive metric, named Value of Service (VoS), is proposed to evaluate the unified system performance. Our goal is to maximize VoS by jointly allocating multi-dimensional resources. The main contributions are summarized as follows.

- (1) A new mechanism of integrating localization and communication processes is proposed by jointly allocating the shared bandwidth and temporal resources for meeting the needs of diverse applications. For the first time, we develop a new integrated resource allocation technique in ILAC system based on the concurrent location and communication needs of users. Specifically, we identify the difficulties of the separated resource allocation in existing designs and develop a new integrated resource allocation scheme with the goal of maximizing the value provisioning for services provided by the ILAC. Besides, the proposed joint resource allocation in ILAC will be adaptively adjusted according to various and hybrid service requests from users.
- (2) To share the limited resources among concurrent service requests with different priorities, a new performance metric, VoS, is proposed in this chapter to guide the ILAC system design. The VoS metric is designed specifically based on the unique characteristics of the ILAC system with the aim to evaluate the capability of meeting the needs of users with limited resources. To achieve this goal, the trade-off between the service requests from users and available resources is properly modelled. Simulation results not only showed the high robustness and generalizability of the proposed VoS metric but also demonstrated consistency between the system performance and resource allocation by using VoS as the evaluation metric.

- (3) With VoS maximization as the objective, a joint bandwidth and temporal resource allocation algorithm is proposed. The optimization of multi-dimensional resource allocation is formulated as a mixed-integer nonlinear problem. A joint resource allocation (JRA) strategy is developed to decompose the overall problem into two sub-problems. Firstly, the static bandwidth resource allocation under fixed temporal resource distribution is solved with continuous optimization based on Kelly's theory followed by discretization. Secondly, an adaptive Particle Swarm Optimization (PSO)-based algorithm is adopted to achieve temporal resource allocation. The proposed strategy achieves a suboptimal solution with limited resources. Simulation results showed that the proposed JRA algorithm can guarantee the highest VoS with a different number of service requests under limited resource conditions compared with the other two classic resource allocation methods.

The remainder of this chapter is organized as follows. Section 4.2 presents the system model. The proposed methodology of joint resource allocation for VoS maximization is implemented in Section 4.3. Simulation and discussion are given in Section 4.4, followed by the chapter summary in Section 4.5.

4.2 System Model

In this section, we first present the resource allocation architecture of the ILAC system in Section 4.2.1. Since localization and communication are two key components in the scenario, elaboration of localization and communication models are introduced in Section 4.2.2 and 4.2.3, separately. Finally, the system objective of VoS maximization is given in Section 4.2.4.

4.2.1 Architecture of ILAC System

As shown in Fig. 4.1, the joint design of localization and communication is mainly reflected in the shared use of resources and physical platform to achieve a common goal of supporting different applications. In our considered system model, each intelligent application is independently associated with a device [52] and each device corresponds to one service request at one time slot. Assuming there are M service requests entering the ILAC system and the set of all

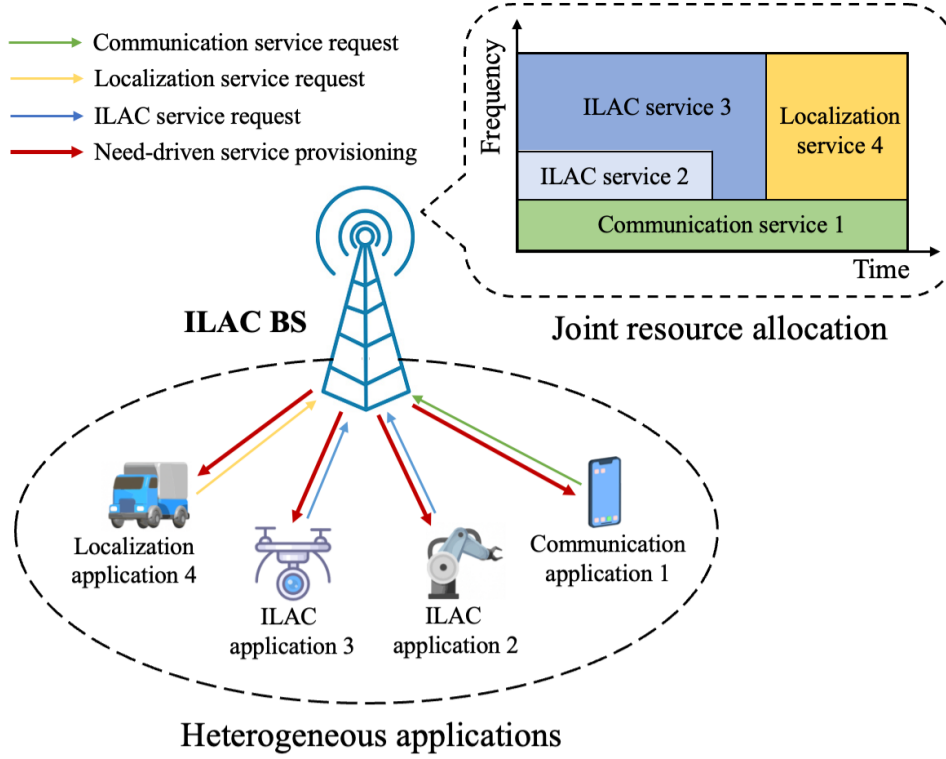


Figure 4.1. Illustration of joint resource allocation in ILAC system for tailored service provisioning.

service requests is $\mathcal{S} = \{S_1, S_2, \dots, S_M\}$ (S_m is used to denote the m -th service request). The parameterized service requests are denoted as $s = [s_1^T, s_2^T, \dots, s_M^T]^T$. Each service request can be defined as a vector $s_m = [\gamma_m, \tau_m, s_{m,c}^T, s_{m,l}^T]^T$, $m = 1, 2, \dots, M$, where γ_m is the normalized priority of S_m ($\sum_{m=1}^M \gamma_m = 1, 0 \leq \gamma_m \leq 1$) and τ_m is service life time. The communication and localization requests are denoted as $s_{m,c}$ and $s_{m,l}$, respectively. The communication request is given by $s_{m,c} = [w^{(m,c)}, d_{m,c}, \varpi_{m,c}, r_{m,c}]^T$, where $w^{(m,c)}$ is the communication weight and $d_{m,c}$ is denoted as the bits of packets for transmission. Herein, the binary $\varpi_{m,c}$ is used to describe the type of communication, where $\varpi_{m,c} = 1$ is real-time and $\varpi_{m,c} = 0$ is the delay-tolerant communication requirements. Moreover, the utility parameters of communication are denoted as $r_{m,c}$ and detailed expression is covered in section 4.3.2. The localization request, $s_{m,l} = [w^{(m,l)}, \sigma_m, k_{m,l}]^T$, consists of the localization weight $w^{(m,l)}$, localization accuracy requirements σ_m and localization utility parameter $k_{m,l}$. The $k_{m,l}$ is the parameter in the utility function of localization, describing the relation between the VoS of localization and achievable localization accuracy. Further details can be found in section 4.3.3 (Equ. 4.15). Note that for m -th service request,

there's $w^{(m,c)} + w^{(m,l)} = 1, 0 \leq w^{(m,c)} \leq 1, 0 \leq w^{(m,l)} \leq 1$. Depending on different localization/communication weights due to various applications, S_m can be communication-centric, localization-centric or integrated localization and communication requests.

In our proposed ILAC system, base station (BS) is responsible for gathering the requests and assigning the available resources to maximize the fulfillment of requests. The signal transmitted between the base station and device is orthogonal frequency division multiplexing (OFDM) signal. We assume there are total N orthogonal subcarriers in the frequency domain and T service time in the time domain to serve M services. It's supposed the total power is equally allocated for each service. To better leverage the frequency and time resources simultaneously, the physical resource block (PRB) as the minimum allocation unit is used. Each PRB includes N_0 subcarriers (e.g., in LTE network, $N_0 = 12$) with subcarrier spacing Δf and one time slot (each time slot spans T_0 with s_0 OFDM symbols in the time domain). Therefore, there are $K_f K_t$ PRBs in total, where K_f and K_t are the numbers of PRBs mapped into frequency ($N = K_f N_0$) and time domain ($T = K_t T_0$), respectively. Here, \mathcal{P}_{ij} is used to denote the PRB at the i -th ($1 \leq i \leq K_f$) subcarrier block and j -th ($1 \leq j \leq K_t$) time slot. We use the binary variables $u_{i,j}^{(m,c)}$ and $u_{i,j}^{(m,l)}$ to represent the assignment of PRBs to service m , which are defined as

$$u_{i,j}^{(m,c)} = \begin{cases} 1 & \text{if } \mathcal{P}_{ij} \text{ is assigned to } S_m \text{ for communication} \\ 0 & \text{otherwise,} \end{cases} \quad (4.1)$$

$$u_{i,j}^{(m,l)} = \begin{cases} 1 & \text{if } \mathcal{P}_{ij} \text{ is assigned to } S_m \text{ for localization} \\ 0 & \text{otherwise.} \end{cases} \quad (4.2)$$

Note that $u_{i,j}^{(m,c)}$ and $u_{i,j}^{(m,l)}$ cannot be equal to one at the same time. With given service requests, the details of VoS of communication and localization w.r.t. the PRBs are elaborated.

4.2.2 VoS of Communication

In wireless communication, the application utility functions (i.e., fulfillment percentage) are widely utilized to characterize the satisfaction of data rate [116]. According to Shannon's

theory, the upper limit of data rate at the j -th time slot can be written as

$$C_j^{(m,c)} = \sum_{i=1}^{K_f} u_{ij}^{(m,c)} B_{ij}^{(m,c)} \log_2(1 + \Gamma_{ij}^{(m,c)}), \quad (4.3)$$

where $B_{ij}^{(m,c)}$ is the effective bandwidth of \mathcal{P}_{ij} which is proportional to the signal bandwidth ($(B_{ij}^{(m,c)})^2 = \frac{\pi^2}{3} (N_0 \Delta f)^2$) [117–119]. $\Gamma_{ij}^{(m,c)}$ denotes the signal to noise ratio for S_m on \mathcal{P}_{ij} , given as $\Gamma_{ij}^{(m,c)} = P_0 \gamma_{ij}^{(m,c)}$ where P_0 is the power for each PRB. The power channel gain to noise power ratio is written as $\gamma_{ij}^{(m,c)} = h_{ij}^{(m,c)} / \epsilon^2$, where $h_{ij}^{(m,c)}$ is the power channel gain and ϵ^2 is the additive white Gaussian noise (AWGN) power.

With given upper limit $C_j^{(m,c)}$, the utility function is usually studied separately based on real-time and non-real-time applications. Several types of utility functions are widely investigated in the literature [120, 121] on wireless communication and networking due to the distinct properties of different applications. In this work, without loss of generality, the real-time and delay-tolerant services are modelled as sigmoidal and logarithmic utility functions, respectively [120, 122–127] as

$$U_j^{(m,c)} = \begin{cases} c_m \left(\frac{1}{1 + e^{-a_m(C_j^{(m,c)} - b_m)}} - \frac{1}{1 + e^{a_m b_m}} \right) & \text{if } \varpi_m = 1 \\ \frac{\log(1 + k_{m,c} C_j^{(m,c)})}{\log(1 + k_{m,c} C^{m,max})} & \text{if } \varpi_m = 0, \end{cases} \quad (4.4)$$

where $c_m = \frac{1 + e^{a_m b_m}}{e^{a_m b_m}}$ is the parameter for normalization. The sigmoidal-like utility function is a good approximation for real-time applications (e.g., video streams [126, 127]). It can be easily verified from two aspects. Firstly, the inflection point of the sigmoidal function is b_m . The parameter a_m indicates the slope of the utility function. Secondly, larger a_m means a steeper slope and vice versa. Thus, in such case, the utility parameter of communication is written as $\mathbf{r}_{1,m,c} = [a_m, b_m]^T$. As for the delay-tolerant service, we use the logarithmic utility function. The logarithmic utility function, as a strictly concave, increases not as dramatically as the sigmoidal function used in real-time cases. $C^{m,max}$ represents the required data rate for 100% satisfaction. $k_{m,c} > 0$ is the parameter describing the slope of the utility function. Therefore, the data rate request is $\mathbf{r}_{0,m,c} = [k_{m,c}, C^{m,max}]^T$. Furthermore, our proposed framework can be easily extended with other utility functions as long as they fulfill specific criteria. (i) The utility function is

a differentiable and continuous function with the allocated physical resource blocks. (ii) The utility is bounded within $[0, 1]$, and non-decreasing. (iii) $\lim_{x \rightarrow 0} U(x) = 0$, $\lim_{x \rightarrow \infty} U(x) = 1$. Note that both real-time and delay-tolerant applications can have either high-rate or low-rate requirements.

With $U_j^{(m,c)}$, the utility function of data rate in the total communication time slots of S_m is

$$U^{(m,c)} = \frac{\sum_{j=1}^{K_t} U_j^{(m,c)}}{\sum_{j=1}^{K_t} \tilde{u}_j^{(m,c)}}, \quad (4.5)$$

where $\tilde{u}_j^{(m,c)} = \left\| \sum_{i=1}^{K_f} u_{ij}^{(m,c)} \right\|_0$ is the binary variable to represent whether j -th time slot is used for communication. Specifically, the data rate at j -th time slot is non-zero when $\tilde{u}_j^{(m,c)} \neq 0$.

In addition to the data rate satisfaction, the transmission amount of packets should be considered. The reason is that even if the satisfaction of the data rate is high, the required transmission bits cannot be guaranteed without enough transmission time. The constraints regarding the required transmission bits are described as

$$\sum_{j=1}^{K_t} C_j^{(m,c)} T_0 \geq d_{m,c}. \quad (4.6)$$

In this work, we incorporate constraint (4.6) into the VoS of communication as a penalty factor $\beta^{(m)}$ instead of hard constraint, by considering the completeness degree of packet transmission in communication. That is to say, when constraint (4.6) can be satisfied, the penalty $\beta^{(m)} = 1$, whereas in other cases is between 0 and 1, which is defined as

$$\beta^{(m)} = \begin{cases} \frac{\sum_{j=1}^{K_t} C_j^{(m,c)} T_0}{d_{m,c}} & \text{if } d_{m,c} > \sum_{j=1}^{K_t} C_j^{(m,c)} T_0 \\ 1 & \text{if } d_{m,c} \leq \sum_{j=1}^{K_t} C_j^{(m,c)} T_0. \end{cases} \quad (4.7)$$

Synthesizing the satisfaction of data rate and completeness of transmission data amount, the VoS of communication is summarized as

$$V^{(m,c)} = \beta^{(m)} U^{(m,c)}. \quad (4.8)$$

By adopting the expression of (4.8), not only is the rate utility $U^{(m,c)}$ included, time fairness is also taken into consideration, which is more appropriate than only using the data rate metric.

4.2.3 VoS of Localization

In the localization model, we assume that the BS receives wideband OFDM reference signals to achieve one-way localization. The wireless localization is performed via range and angular estimation. Herein, the range estimation is achieved with time of arrival (TOA) and angles are estimated with the angle of arrival (AOA) [128] and angle of departure (AOD). And the localization performance is benchmarked by the fundamental limits of localization accuracy, called position error bound (PEB), which are derived from the Fisher information matrix (FIM, $\mathbf{J}(\mathbf{p})$) as

$$\mathbb{E}(\|\widehat{\mathbf{p}} - \mathbf{p}\|^2) \geq \text{tr}\{\mathbf{J}^{-1}(\mathbf{p})\}, \quad (4.9)$$

where $\widehat{\mathbf{p}}$ and \mathbf{p} are the estimation and true value of device location, respectively. $\mathbb{E}(\cdot)$ denotes the expectation and $\text{tr}\{\cdot\}$ is the trace of matrix.

The PEB based on TOA and AOA/AOD w.r.t. allocated bandwidth is investigated in [117–119]. The estimation of TOA and AOA/AOD can be resolved from received reference signals. Thus, the resource spent on sending localization reference signals influences localization accuracy greatly, as the channel estimation accuracy highly depends on the number of measurements. Following the derivation in [113] and the fact that channel parameter error and PEB are connected with the linear transformation matrix [129], the PEB is inversely proportional to the number of PRB across time spanning.

Consider PRBs spanning successively from j -th to $(j + N_j^{(m,l)})$ -th time slots (denoted as time slot set \mathcal{N}_j) is used for localization of S_m , the achievable PEB can be derived as

$$\tilde{\sigma}_j^{(m)} = \frac{\xi^{(m)}}{\sum_{j \in \mathcal{N}_j} \{g_j^{(m)} P_0 (\sum_{i=1}^{K_f} u_{ij}^{(m,l)} B_{ij}^{(m,l)})^2\}}, \quad (4.10)$$

where $g_j^{(m)}$ represents the effective channel gain, $B_{ij}^{(m,l)}$ is the effective bandwidth of \mathcal{P}_{ij} for localization and $\xi^{(m)}$ indicates the proportional coefficients relating to device state. For the effective bandwidth $B_{ij}^{(m,l)}$, the localization in ILAC system is performed via communication

waveform. Thus, the $B_{ij}^{(m,l)}$ can be approximated with the bandwidth of transmitted signals, following $(B_{ij}^{(m,l)})^2 = \frac{\pi^2}{3} (N_0 \Delta f)^2$. The *Proof* of (4.10) is given below.

As is proved in [130], the inverse of the squared ranging error bound, i.e., range information (RI), with the time of arrival, is given by

$$\lambda_j = \frac{8\pi^2 \tilde{B}_j^2}{c^2} (1 - \chi_j) SNR_j, \quad (4.11)$$

where \tilde{B}_j is the effective bandwidth of the signal, χ_j represents the path-overlap coefficient (POC) depicting the multipath propagation, c is the velocity of light and SNR_j is the signal-to-noise ratio as

$$SNR_j = \frac{E_j}{\epsilon^2} \propto \frac{P_j^{(m,l)} |g_j|^2}{\epsilon^2}, \quad (4.12)$$

where $P_j^{(m,l)}$ is the transmit power of the base station, g_j is the effective channel gain amplitude of the line-of-sight path and ϵ^2 denotes the noise power.

Then, the range information during the $N_j^{(m,l)}$ slots is written as

$$\lambda_{total} = \sum_j \lambda_j. \quad (4.13)$$

The transformation of range information into the FIM of position is via the transformation matrix \mathbf{T} where $\mathbf{J}(\mathbf{p}) = \mathbf{T} \lambda_{total} \mathbf{T}^T$, which is derived from $\mathbf{T} = \frac{\partial \tau_0}{\partial \mathbf{p}}$ and $\tau_0 = \|\mathbf{p} - \mathbf{q}\|_2 / c$. \mathbf{p} and \mathbf{q} is the position of the target and base station, respectively. By taking the first derivative, there is $\mathbf{T} = \frac{[\cos\theta, \sin\theta]^T}{c}$ where θ is the angle from base station to target. The PEB can be derived as

$$(\sigma_j^m)^2 = tr \left\{ \left(\sum_j \frac{8\pi^2 \tilde{B}_j^2}{c^2} (1 - \chi_j) \frac{E_j}{\epsilon^2} \mathbf{T} \mathbf{T}^T \right)^{-1} \right\} = \frac{\xi^{(m)}}{\sum_{j \in \mathcal{N}_j} \left\{ g_j^{(m)} P_j^{(m,l)} (\sum_{i=1}^{K_f} u_{ij}^{(m,l)} B_{ij}^{(m,l)})^2 \right\}}. \quad (4.14)$$

Remark 1: Generally, the localization is considered independent among the different time slots in \mathcal{N}_j . In such cases, the location is solved through a maximum likelihood estimator (MLE), where the theoretical estimation lower bound is limited by the PEB. Nonetheless, if the localization process is seen as a successive procedure, the employment of priori information for channel estimation could perform lower than the PEB. In principle, by using the Bayesian method [113], the estimation accuracy can achieve as higher as desired, as long as adequate

prior information is provided. Such cases are beyond the scope of this chapter.

To the best of our knowledge, there's lacking the utility function of localization at the service level. Herein, for the first time, we incorporate the exponential function to depict the VoS of localization in the ILAC system. Similar to communication, the utility function of localization is the function of completeness of localization accuracy as

$$U_j^{(m,l)} = \begin{cases} \frac{1}{1 - e^{-k_{m,l}}} [1 - e^{-k_{m,l}(\frac{\sigma_m}{\tilde{\sigma}_j^m})}] & \text{if } \tilde{\sigma}_j^m > \sigma_m \\ 1 & \text{if } \tilde{\sigma}_j^m \leq \sigma_m, \end{cases} \quad (4.15)$$

where $k_{m,l} \in \mathbb{R}$. It can be easily verified that (4.15) satisfies, (a) an increasing function of $\tilde{\sigma}_j^{(m)}$; (b) twice continuously differentiable; (c) when $\tilde{\sigma}_j^{(m)} = \infty$, i.e., the localization fails, the $U_j^{(m,l)} = 0$.

The quantity $U_j^{(m,l)}$ reflects the fitness and satisfaction of S_m . The benefits of employing the exponential utility function are obvious. With only one additional parameter $k_{m,l}$, it's able to express the different types of risk profiles by adjusting $k_{m,l}$ with positive, negative and zero. In comparison to economics, a larger value of $k_{m,l}$ indicates that the decision-maker is less averse to taking risks. In (4.15), as the $k_{m,l}$ increase to more positive, the function becomes more convex, indicating a localization accuracy-tolerant application. The curved function becomes more concave when the $k_{m,l}$ decreases to more negative, indicating a high location required application. When $k_{m,l} = 0$, the VoS of localization is proportional to the $\sigma_m/\tilde{\sigma}_j^m$. Therefore, we use $U_j^{(m,l)}$ to represent the utility of the localization accuracy.

With $U_j^{(m,l)}$, the VoS of localization during the total localization time slots of S_m is

$$V^{(m,l)} = \frac{\sum_{j=1}^{K_l} U_j^{(m,l)}}{N^{(m,l)}}. \quad (4.16)$$

In (4.16), $N^{(m,l)}$ is the total localization slots for S_m , which is written as

$$N^{(m,l)} = \sum_{j=1}^{K_l} \tilde{u}_j^{(m,l)}, \quad (4.17)$$

where $\tilde{u}_j^{(m,l)} = \left\| \sum_{i=1}^{K_f} u_{ij}^{(m,l)} \right\|_0$ is the binary variable to represent the assigned bandwidth state.

4.2.4 Problem Formulation

With given VoS of communication $V^{(m,c)}$, VoS of localization $V^{(m,l)}$, and weight factors $w^{(m,c)}$ and $w^{(m,l)}$ (the definitions of $w^{(m,c)}$ and $w^{(m,l)}$ are given in Section 4.2.1), the value of S_m is defined as the weighted sum of $V^{(m,c)}$ and $V^{(m,l)}$, shown as

$$V^{(m)} = w^{(m,c)}V^{(m,c)} + w^{(m,l)}V^{(m,l)}. \quad (4.18)$$

In this chapter, our problem is to maximize the weighted sum of VoS from all service requests through the optimization of PRB assignments $(u_{ij}^{(m,c)}, u_{ij}^{(m,l)})$ with the bandwidth and time constraints. The resource allocation problem in ILAC system is formulated as

$$P : \max_{u_{ij}^{(m,c)}, u_{ij}^{(m,l)}} \sum_{m=1}^M \gamma_m V^{(m)}, \quad (4.19)$$

$$s.t. \quad u_{ij}^{(m,c)}, u_{ij}^{(m,l)} \in \{0, 1\}, \quad (19a)$$

$$\sum_{i=1}^{K_f} (u_{ij}^{(m,c)} + u_{ij}^{(m,l)}) \leq K_f, \forall 1 \leq j \leq K_t, \quad (19b)$$

$$\sum_{j=1}^{K_t} (u_{ij}^{(m,c)} + u_{ij}^{(m,l)}) \leq K_t, \forall 1 \leq i \leq K_f, \quad (19c)$$

$$\sum_{i=1}^{K_f} u_{ij}^{(m,c)} \leq K_f^{(m)}, \forall 1 \leq j \leq K_t, \quad (19d)$$

$$\sum_{i=1}^{K_f} u_{ij}^{(m,l)} \leq K_f^{(m)}, \forall 1 \leq j \leq K_t, \quad (19e)$$

$$\sum_{j=1}^{K_t} u_{ij}^{(m,c)} \leq K_t^{(m)}, \forall 1 \leq i \leq K_f, \quad (19f)$$

$$\sum_{j=1}^{K_t} u_{ij}^{(m,l)} \leq K_t^{(m)}, \forall 1 \leq i \leq K_f, \quad (19g)$$

where (19b) and (19c) are the restrictions of total available resources ($K_f \times K_t$), and constraints (19d) and (19e) imply that the bandwidth resources are limited for communication and localization in each service. Constraints (19f) and (19g) impose that the time slot number of communication and localization in each service has upper bounds. The VoS that can be achieved

by an ILAC system is primarily influenced by three key factors: the service requirements of users, the wireless environment in which the system operates, and the strategy employed for allocating system resources. Also, the definition and concept of VoS can be readily expanded to encompass other integrated systems, such as ISAC system.

4.3 Proposed Resource Allocation Scheme

In this section, we give the solution of P by using a joint resource allocation scheme. Note that the optimization problem P is a mixed-integer nonlinear optimization problem because the bandwidth resource is discretized while the service time slots are large (i.e., $K_t \gg 1$) enough to be treated as quasi-continuous variables. Thus, P could not be directly solved by analytic methods. We propose to decompose P into two subproblems to allocate bandwidth and time slots separately. Then, an iterative joint resource allocation scheme is proposed to iteratively update the allocated bandwidth and time resources for each service.

4.3.1 Bandwidth Allocation

Firstly, we consider the bandwidth allocation at j -th time slot. Let $r_j^{(m,q)} = \sum_{i=1}^{K_f} u_{ij}^{(m,q)}$ be the bandwidth allocated to S_m at j -th time slot, where binary $q \in \{l, c\}$ represents localization or communication, respectively. To simplify the notation, we use $V_j^{(m,q)}$ to denote the VoS of S_m at j -th time slot, which can be written as

$$V_j^{(m,q)} = \begin{cases} \frac{C_j^{(m,c)} T_0}{d_{m,c}} U_j^{(m,c)} & \text{if } q = c \\ U_j^{(m,l)} & \text{if } q = l, \end{cases} \quad (4.20)$$

where the data rate can be rewritten as

$$C_j^{(m,c)} = r_j^{(m,c)} B_j^{(m,c)} \log_2(1 + \bar{\Gamma}_j^{(m,c)}). \quad (4.21)$$

$\bar{\Gamma}_j^{(m,c)} = (\sum_i \Gamma_{ij}^{(m,c)}) / \tilde{u}_j^{(m,c)}$ is the average signal to noise ratio of S_m at time slot j . Then, the bandwidth resource allocation problem can be formulated as P_1 , which is an optimization

problem of the mapping between the bandwidth resource and services.

$$P_1 : \max_{r_j^{(m,q)}} \sum_{m=1}^M \gamma_m W^{(m,q)} V_j^{(m,q)} \quad (4.22)$$

$$s.t. \quad \sum_{m=1}^M r_j^{(m,q)} \leq K_f, \quad (22a)$$

$$r_j^{(m,q)} \in N, \quad (22b)$$

$$q \in \{l, c\}, \quad (22c)$$

$$r_j^{(m,q)} \leq K_f^{(m)}. \quad (22d)$$

To solve P_1 , we propose a two-step strategy. Firstly, condition (22b) is relaxed to continuous variables and the continuous bandwidth allocation is solved based on Kelly's mechanism [61, 131] in Section 4.3.1.1. Secondly, the continuous bandwidth allocation is discretized in Section 4.3.1.2.

4.3.1.1 Continuous Bandwidth Allocation

The service requests are competing with the limited bandwidth resource to maximize the overall system VoS. Thus, inspired by Kelly's theory, the continuous bandwidth resource allocation scheme can be depicted in the following steps.

- (i) The devices request services S_m and original bids $b_j^{(m,q)}$ (either for localization or communication) to BS.
- (ii) BS calculates the assigned bandwidth from (4.23) and shadow prices p_j from (4.24) to each service.
- (iii) The devices evaluate the assignments and update their new bids.

With given bids, from the proportional fairness allocation [125], the $r_j^{(m,q)}$ can be written as

$$r_j^{(m,q)} = \frac{b_j^{(m,q)}}{\sum_m b_j^{(m,q)}} K_f. \quad (4.23)$$

The shadow price p_j is defined as the average of the total received bids from devices on the available PRB numbers in the frequency domain (K_f). It can be noted that the bids of each service request can largely influence p_j while p_j also affects the optimal bidding strategies. With p_j , the $r_j^{(m,q)}$ can be rewritten as

$$r_j^{(m,q)} = \frac{b_j^{(m,q)}}{p_j}, \quad (4.24)$$

where $p_j = \frac{\sum_m b_j^{(m,q)}}{K_f}$.

The bidding strategy for each service request in step (iii) is derived by solving P_1 with the Lagrangian methods due to the convexity property of sigmoidal and logarithmic functions in $U_j^{(m,c)}$ [125] and exponential function in $U_j^{(m,l)}$. Therefore, the optimal solution can be derived through Lagrangian duality

$$P'_1 : \min_{\lambda} \max_{r_j^{(m,q)}} L(r_j^{(m,q)}, \lambda), \quad (4.25)$$

where λ is the Lagrangian multiplier ($\lambda \geq 0$). Herein, the Lagrangian of (4.22) is written as

$$L(r_j^{(m,q)}, \lambda) = \sum_{m=1}^M \gamma_m w^{(m,q)} V_j^{(m,q)} - \lambda \left(\sum_{m=1}^M r_j^{(m,q)} - K_f \right). \quad (4.26)$$

From Kelly's mechanism, the optimal Lagrangian multiplier is the stationary shadow price. To solve P'_1 , we use the iterative strategy to update the $r_j^{(m,q)}$ and p_j until convergence. From the perspective of interactions between BS and devices, the iteration includes the updating of $b_j^{(m,q)}$ (or $r_j^{(m,q)}$) at device in step (iii) and p_j at BS in step (ii). Specifically, with the p_j from initialization or last step, the $r_j^{(m)}$ is calculated according to

$$r_j^{(m,q)} = \operatorname{argmax} f(r_j^{(m,q)}), \quad (4.27)$$

subject to (22d), where

$$f(r_j^{(m,q)}) = \gamma_m w^{(m,q)} V_j^{(m,q)} - p_j (r_j^{(m,q)} - K_f^{(m)}). \quad (4.28)$$

This optimization is readily solved by the well-known damped Newton's method. Then, the

optimal bids $b_j^{(m,q)}$ for S_m can be calculated via the $b_j^{(m,q)} = p_j r_j^{(m,q)}$. The iteration breaks when the shadow price reaches the stationary value. The process of continuous bandwidth resource allocation is summarized in Algorithm 2.

Algorithm 2: Continuous bandwidth resource allocation algorithm

Input : Bandwidth resources K_f , service request s , threshold δ , incremental step κ .

Output: Bandwidth resource allocation results $r_{m,q}$.

- 1 **Initialization:** iteration number $s = 0$, $b_j^{(m)}(0) = 1$ for each service.
 - 2 **Loop**
 - 3 Calculate the $p_j(s)$ and $r_j^{(m,q)}(s)$ with (4.28).
 - 4 Update the $b_j^{(m,q)}(s)$ for each service with $b_j^{(m,q)}(s) = p_j(s) \cdot r_j^{(m,q)}(s)$.
 - 5 **if** $|b_j^{(m,q)}(s) - b_j^{(m,q)}(s-1)| > \delta$ **then**
 - 6 $b_j^{(m,q)}(s+1) = b_j^{(m,q)}(s) + \text{sign}(b_j^{(m,q)}(s+1) - b_j^{(m,q)}(s)) \cdot \kappa$;
 - 7 Update $p_j(s)$;
 - 8 **end**
 - 9 **if** $|b_j^{(m,q)}(s) - b_j^{(m,q)}(s-1)| \leq \delta$ **then**
 - 10 Calculate $r_j^{(m,q)*} = \frac{b_j^{(m,q)}(s)}{p_j(s)}$;
 - 11 Update $p_j(s)$;
 - 12 **Break**;
 - 13 **end**
 - 14 **End loop**
-

4.3.1.2 Discretization

After finding the continuously allocated bandwidth in (4.25), the next step is discretization. The discrete optimization is solved by extracting a sequence of feasible candidates from the optimal continuous resources. The detailed steps of discretization are shown below.

- (i) Suppose vector $[r_j^{(1)*}, r_j^{(2)*}, \dots, r_j^{(m)*}]$ is the continuous optimal resource from Algorithm 2. To reduce the complexity, the neighbours of the continuous optimal $r_j^{(m)*}$ are focused. Specifically, the lower (floor function) integer points less than $r_j^{(m)*}$ and the upper (ceiling function) integer points higher than $r_j^{(m)*}$ are chosen. The continuous rates smaller than one should be mapped to one to avoid zero resource allocation results. The candidate dis-

crete PRB allocation is the M dimensional vectors which yield in 2^M feasible allocation vectors.

- (ii) To further restrict the search space, the constraint (22a) is considered. The vectors which are not satisfied will be filtered out.
- (iii) The VoS of the qualified vectors is calculated and compared. And the allocation vector with the largest VoS with the least PRBs is stored.

4.3.2 Time Slot Allocation

Different from the bandwidth allocation, the service time slots can be very large (i.e., $K_t \gg 1$). Moreover, the allocation of time slots for service requests depends on its assigned bandwidth, which further hinders its analytic solution. In this subsection, the time slot allocation of each service in the ILAC system with fixed allocated bandwidth is discussed.

With given PRB number $r_j^{(m,q)}$ for service request S_m , the time slots for localization and communication of S_m are denoted as

$$\begin{aligned}\tau^{(m,l)} &= \sum_{j=1}^{K_t} u_{ij}^{(m,l)}, \\ \tau^{(m,c)} &= \sum_{j=1}^{K_t} u_{ij}^{(m,c)}.\end{aligned}\tag{4.29}$$

Then, the time slot allocation is formulated as

$$P_2 : \max_{\tau^{(m,l)}, \tau^{(m,c)}} \sum_{m=1}^M \gamma_m [w^{(m,l)} V^{(m,l)}(\tau^{(m,l)}) + w^{(m,c)} V^{(m,c)}(\tau^{(m,c)})]\tag{4.30}$$

$$s.t. \quad \sum_{m=1}^M (\tau^{(m,l)} + \tau^{(m,c)}) \leq K_t,\tag{30a}$$

$$\tau^{(m,l)} \leq K_t^{(m)},\tag{30b}$$

$$\tau^{(m,c)} \leq K_t^{(m)}.\tag{30c}$$

In P_2 , the expressions of the functions $V^{(m,l)}(\tau^{(m,l)})$ and $V^{(m,c)}(\tau^{(m,c)})$ can be derived by taking by taking (4.29) into (4.20), shown as

$$\begin{aligned} V^{(m,c)}(\tau^{(m,c)}) &= \frac{\left(\sum_{j=1}^{K_t} C_j^{(m,c)} T_0\right) \left(\sum_{j=1}^{K_t} U_j^{(m,c)}\right)}{d_{m,c} \tau^{(m,c)}}, \\ V^{(m,l)}(\tau^{(m,l)}) &= \frac{\sum_{j=1}^{K_t} U_j^{(m,l)}}{\tau^{(m,l)}}. \end{aligned} \quad (4.31)$$

With the multiple constraints, the traditional optimization methods are difficult to solve P_2 . As mentioned in Chapter 2, the PSO-based algorithm is a kind of population-based search algorithm, and it is easy to execute and has good global optimization performance. Generally, it simulates the social behaviour of birds/fishes in nature. During the execution, the individuals' positions are changing with the social tendency of the group. In PSO, each individual, called a particle, benefits from the historical experience of its own and that of the other members when searching for food. In particular, each particle μ records the best position it has experienced so far as $pbest_\mu$, and the best position of its neighbours or the global community as $gbest$. The objective function in P_2 is called the fitness score of each particle. With the iteration, the particle μ can update its velocity $v_{\mu\nu}$ and position $x_{\mu\nu}$ (ν -th dimension of optimization vector) through the personal best position and swarm's best position following two equations

$$v_{\mu\nu}(s+1) = \rho v_{\mu\nu}(s) + c_1 rand_1(pbest_{\mu\nu}(s) - x_{\mu\nu}(s)) + c_2 rand_2(gbest_{\mu\nu}(s) - x_{\mu\nu}(s)), \quad (4.32)$$

$$x_{\mu\nu}(s+1) = x_{\mu\nu}(s) + v_{\mu\nu}(s+1), \quad (4.33)$$

where s is the iteration number, $v_{\mu\nu}(s+1)$ and $x_{\mu\nu}(s+1)$ are velocity and position of the μ -th particle, and ρ is the inertia weight. c_1 and c_2 are learning factors while $rand_1$ and $rand_2$ are random numbers between 0 and 1. To balance the exploration and exploitation characteristics in PSO, the inertia is updated adaptively with the iteration number as

$$\rho(s) = (\rho_{max} - \rho_{min}) \Omega_s(s) + \rho_{min}, \quad (4.34)$$

where $[\rho_{min}, \rho_{max}]$ is the range of the inertia weight and $\Omega_s(s) = \frac{\sum_{\mu=1}^{N_{particles}} \zeta(\mu,s)}{N_{particles}}$ is the success

values of the particles where

$$\zeta(\mu, s) = \begin{cases} 1 & \text{if } \text{fitness}(pbest_\mu(s)) < \text{fitness}(pbest_\mu(s-1)) \\ 0 & \text{if } \text{fitness}(pbest_\mu(s)) = \text{fitness}(pbest_\mu(s-1)). \end{cases} \quad (4.35)$$

In the temporal allocation subproblem, there are multiple constraints to be included in the classic PSO algorithm. It is important but challenging to balance the multiple constraints. Thus, we introduce the weighted penalty factor to deal with the constraints encountered in P_2 . When a particle does not satisfy the constraints, a penalty term will be added to the objective function (fitness function). Then the subproblem is converted to

$$P'_2 : \max_{\tau^{(m,l)}, \tau^{(m,c)}} \sum_{m=1}^M \gamma_m [w^{(m,l)} V^{(m,l)}(\tau^{(m,l)}) + w^{(m,c)} V^{(m,c)}(\tau^{(m,c)})] + \varepsilon Q(\tau^{(m,l)}, \tau^{(m,c)}), \quad (4.36)$$

where ε is the penalty factor $\varepsilon = s / \sqrt{s}$ and Q is the penalty term following

$$\begin{aligned} Q(\tau^{(m,l)}, \tau^{(m,c)}) &= \sum_j \phi_j e_j(\tau^{(m,l)}, \tau^{(m,c)}), \\ \phi_j &= \frac{e_j}{\sum_j e_j}, \\ e_j &= \max(0, -g_j(\tau^{(m,l)}, \tau^{(m,c)})). \end{aligned} \quad (4.37)$$

The term ϕ_j is introduced to balance the weight of different constraints ($\sum_j \phi_j = 1$). And g_j represents the j -th inequality constraint in (4.30). For instance, for (4.30), $g_j = \sum_m (\tau^{(m,l)} + \tau^{(m,c)}) - K_t$. Similar rules can be applied to other constraints. The convergence analysis of PSO algorithm was theoretically investigated in [132] and the performance is demonstrated in simulation section.

Although the constrained problem can be converted into an unconstrained problem for an iterative solution, it is still possible that the solution of the problem does not meet the constraints. Therefore, some other rules need to be included to make sure that the solutions are satisfying the multiple constraints. Herein, the following rules are considered in the algorithm. (1) If generated particle exceeds the upper and lower limits, the position will be changed to any one of the upper and lower limits. (2) If both solutions are feasible, the particle with the higher

fitness value will be chosen. The scheme for the PSO-based time slot allocation is shown in Algorithm 3.

Algorithm 3: PSO-based time slot allocation algorithm

Input : Total time slot number K_t , service request s , bandwidth assignment $r_j^{(m,q)}$.

Output: Time slot allocation results $\tau^{(m,l)}$ and $\tau^{(m,c)}$.

- 1 **Initialization:** Generate particles $x_1, \dots, x_S \in R^{2M}$,
 - 2 Generate velocities of each particle $v_{\mu,\nu}$.
 - 3 **Loop**
 - 4 Calculate fitness score of each particles $fitness_{\mu}$.
 - 5 Determine the $pbest_{\mu}$ and $gbest$ through the fitness evaluation.
 - 6 Update the new position for each particle.
 - 7 **End loop**
-

4.3.3 Joint Resource Allocation Scheme

Till now, the allocations of the bandwidth and time slots are considered individually. However, the two kinds of resources are highly dependent to affect the total value of the service. Thus, it is demanding to integrate them cooperatively to achieve long-term VoS maximization. To guarantee the maximization of VoS in the ILAC system, herein, we proposed the joint resource allocation (JRA) scheme. The bandwidth and time allocation are updated with an iterative manner. During each iteration, the bandwidth allocation utilizes the time assignment from the previous step, which is then followed by the time slot allocation that updates with the allocated bandwidth as input. The detailed steps of the JRA are designed as follows and the specific process is summarized in Algorithm 4. The time stamp t is employed to track the time slot utilization during the allocation. The joint scheme can be detailed as the following steps.

- (i) *Initialization:* With given available resources, the bandwidth allocation $r_j^{(m,q)}$ ($q = l, c$) at j -th time slot for m -th service request is performed by solving P_1 , with equally time slot allocation for localization and communication in each service as initial input. Then, with $r_j^{(m,q)}$ as input, the time slot allocation $\tau^{(m,l)}$ and $\tau^{(m,c)}$ is updated by solving P_2 .

Algorithm 4: Joint resource allocation algorithm**Input :** Total PRB number $K_f \times K_t$, service request s , iteration number K , threshold δ .**Output:** Bandwidth allocation results $r_j^{(m)}$, temporal resource allocation results $\tau^{(m,c)}, \tau^{(m,l)}$.1 **Initialization:**2 Time stamp $t = 0$;3 **for** $k \leq K$ **do**4 Assign bandwidth to the M services with the bandwidth allocation algorithm (Algorithm 2) followed by discretization.

5 Apply the PSO-based method (Algorithm 3) to optimize the localization and communication time of each service.

6 **if** $VoS = 1$ **then**7 **break**8 **end**9 **end**10 **Loop**11 **if** $t = \min\{\tau_{m,c} + \tau_{m,l}\}$ **then**

12 Reallocate the remaining resources through

13 **for** $k \leq K$ **do**

14 Assign available bandwidth with Algorithm 2.

15 Apply Algorithm 3 to allocate time slots.

16 **if** $VoS = 1$ **then**17 **break**18 **end**19 **end**20 **end**21 **if** $VoS = 1$ or all time are used up **then**

22 Report the total value of service.

23 **end**24 **End loop**

- (ii) *Iteration:* The $r_j^{(m,q)}$ and $\tau^{(m,q)}$ ($q = l, c$) are updated by solving P_1 and P_2 in an iterative manner till reach the stopping condition. The stopping condition consists of two parts. Firstly, the iteration ends when the iteration number reaches K . Secondly, if the variation

of objective functions in P_1 and P_2 is convergent, the iteration will stop.

- (iii) *Reallocation mechanism*: The VoS of each service with given resources are calculated and the services that meet the VoS threshold (δ_1) will be filtered out. The corresponding optimal allocated resources, namely $r_j^{(m,q)}$, $\tau^{(m,l)}$ and $\tau^{(m,c)}$ are calculated. The minimum of $\tau^{(m,l)} + \tau^{(m,c)}$ of all these service requests is obtained. Next, the available resources are updated by subtracting the allocated resources from the original available resources, and the new service request set is updated by removing the services that already meet the VoS threshold. Then the resource reallocation is triggered and return to (i). Note that this reallocation mechanism can also be extended to meet the changeable service requests. When the variation of service request is larger than a certain threshold, the reallocation is triggered.
- (iv) *Stopping criterion*: The resource allocation process will terminate when the total service value reaches the threshold (δ_2) or when the temporal resources are exhausted. At this point, a VoS report will be generated, which includes the resource allocation results of each service, VoS of each service and VoS of the whole system.

4.3.4 Complexity Analysis

The algorithm complexity in the JRA (Algorithm 4) mainly depends on bandwidth resource allocation and PSO-based algorithms. In bandwidth resource allocation, the major complexity comes from the discretization of continuous values. It can be found that not all 2^M possible combinations of the lower and upper bounds will meet the constraints of the available resources. Filtering out the discrete combinations which cannot satisfy the constraints can reduce the complexity. Thus, suppose the bandwidth resource allocation is invoked \mathcal{N}_1 times, the computational complexity for M service requests is at most $O(2^M \cdot \mathcal{N}_1)$. In time slot allocation, the complexity is mainly from the PSO algorithm. Assume the PSO algorithm iterates \mathcal{N}_2 times and in each iteration of the algorithm \mathcal{N}_3 particles are updated. Algorithm 3 is invoked \mathcal{N}_4 times in Algorithm 4. Hence the complexity of temporal allocation is $O(\mathcal{N}_2 \mathcal{N}_3 \mathcal{N}_4)$. The total computation complexity is $O(2^M \mathcal{N}_1 \mathcal{N}_2 \mathcal{N}_3 \mathcal{N}_4)$.

4.4 Simulation Results

In this section, the simulation results are provided from three aspects. Firstly, we compared our proposed VoS metric with two conventional used integrated system evaluation metrics to show the robustness of VoS metric. Secondly, to illustrate the effectiveness of the proposed joint resource allocation scheme, we compared our JRA algorithm with the other two resource allocation methods. Thirdly, we also discuss the impact of localization weights on resource allocation results.

All simulations are performed in MATLAB 2020b, operating on a macOS Monterey laptop with 8GB memory and Apple M1 chip. The service request parameters are generated following the ranges given in Table. 4.1. Specifically, to illustrate the robustness of the proposed scheme, the respective weighting factors of each service request in Sections 4.4.1 and 4.4.2 are generated randomly. For the parameters in Algorithm 3, the initial population is set to 50 and the speed limit is 1. The inertia weight is 0.8, and the self-learning factor and group-learning factor are 0.5. The maximum iterative number is set to 100.

TABLE 4.1 System parameters in chapter 4.

Parameters	Descriptions	Values
K_f	Total PRB in frequency dimension	$[1, 500] \in \mathbb{N}^+$
K_t	Total time slot	$[1, 200] \in \mathbb{N}^+$
γ_m	Weight of each service	$[0, 1] \in \mathbb{R}$
$w_{(m,l)}$	Weight of localization in S_m	$[0, 1] \in \mathbb{R}$
$w_{(m,c)}$	Weight of communication in S_m	$[0, 1] \in \mathbb{R}$
$\sigma^{(m)}$	Localization accuracy request	$[0.01, 10] \in \mathbb{R}$
$d_{(m,c)}$	Data amount	$[1, 1000] \in \mathbb{N}^+$
$K_{f,max}^{(m)}$	Maximum PRB	50
$K_{f,min}^{(m)}$	Minimum PRB	0
$K_{t,max}^{(m)}$	Maximum time slot	20
$K_{t,min}^{(m)}$	Minimum time slot	1
K	Iterative number	80

4.4.1 Evaluation of Metrics

To evaluate the effectiveness of VoS metric, we compare it with two other metrics under limited bandwidth and time resources.

- **Metric 1:** the weighted sum rate maximization under accuracy constraints as is used in [133]. In this metric, localization accuracy is treated as a constraint.
- **Metric 2:** the averaged multi-objective metric same as the definition in [52].

In metric 1, the objective is to maximize the throughput while keeping the localization as a constraint. Suppose the allocation strategy is π , the throughput is C and localization accuracy is σ . The objective can be expressed as: $\max_{\pi} C(\pi)$ subject to $\sigma(\pi) \leq \sigma_0$ and other constraints in P .

In metric 2, averaged multi-objective metric is employed as objective function to optimize the resource allocation results. Specifically, we set the weight factor of localization and communication to 0.5, i.e., $\max_{\pi} \sum_m \gamma_m \left(\frac{1}{2} V^{(m,c)} + \frac{1}{2} V^{(m,l)} \right)$ subject to constraints in P .

Under limited resource conditions, our goal is to fulfill the service requests from users. Therefore, the achieved localization accuracy and communication data need to be as close to the requests as possible. We introduce the averaged localization accuracy and communication data rate deviation from the required performance indicators as

$$\begin{aligned} \check{\sigma} &= \sum_{m=1}^M \frac{|\sigma^{(m)} - \check{\sigma}^{(m)}|}{M}, \\ \check{C} &= \sum_{m=1}^M \frac{|C^{(m)} - \check{C}^{(m)}|}{M}. \end{aligned} \tag{4.38}$$

The simulation results are shown in Fig. 4.2. Using the proposed VoS as the evaluation metric, both the localization accuracy and data rate are close to the targeted service requests. However, using metrics 1 and metric 2, the deviations are away from the required values. Specifically, for metric 1, due to the strict constraint of localization accuracy, localization satisfaction is the priority. Thus, the maximized communication data rate is larger than the required ones, leading to a waste of resources, especially when there are fewer service requests. For metric 2, both the communication and localization performance are away from the service request. This results from the uniform maximization of two functionalities, neglecting that it's not always better for larger indicators. Both metric 1 and metric 2 can be regarded as a special case of the VoS metric and put fixed emphasis on either functionality. The simulation results

demonstrate the robustness of our proposed VoS metric for a service-oriented ILAC system.

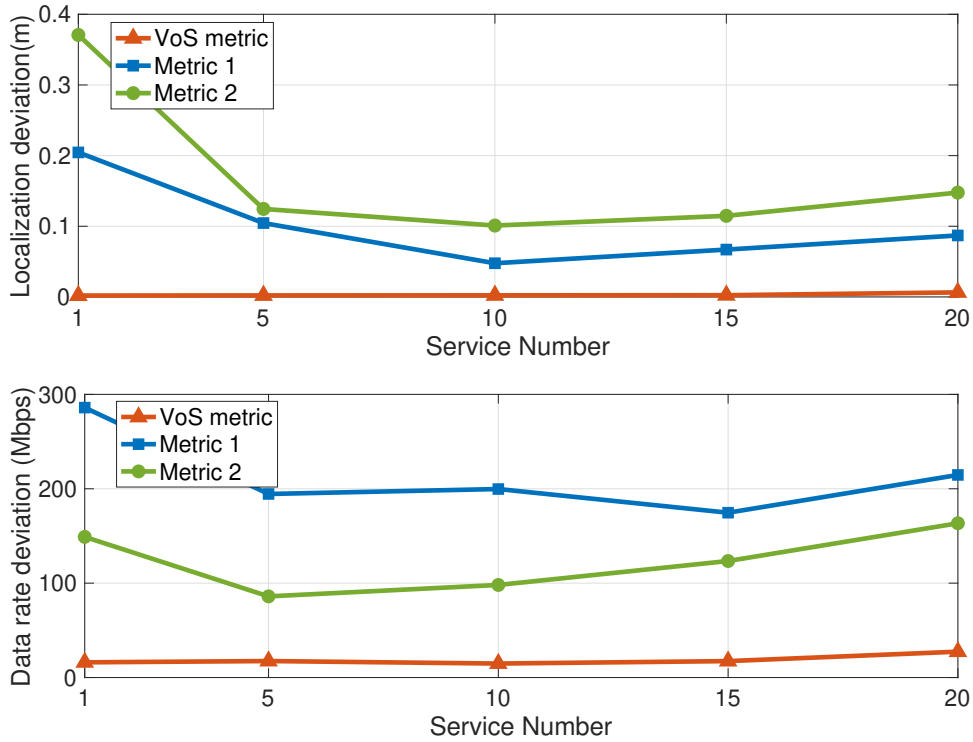


Figure 4.2. The localization accuracy (top) and communication data rate (bottom) deviation with the three metrics as the objective function.

4.4.2 Evaluation of Resource Allocation

Herein, we compared the performance of the proposed JRA with the following two approaches.

- **Non-joint resource allocation (NJRA):** The bandwidths are optimized with a continuous allocation method followed by discretization while the time slots are considered as the constraints. This approach doesn't involve the joint resource allocation process.
- **Random resource allocation (RRA):** The bandwidth and time slot are assigned to the service requests randomly while keeping the constraints satisfied.

The performance of our proposed resource allocation scheme will be evaluated from two aspects, the impact of service number on VoS, and the relationship between available bandwidth and time resources with VoS. Finally, the computation of the involved methods is analyzed.

4.4.2.1 Influence of Service Number

Firstly, we evaluate the robustness of the proposed scheme with different service numbers in the ILAC system. To support amounts of hierarchical applications, the number of service requests is uncertain or even has great changes in a short period, which puts forward higher requirements on the robustness of resource allocation. Therefore, we compare the performance of JRA and NJRA schemes under different service numbers. We vary the number of service number from available MDs from 1 to 20. The number of available bandwidth resource blocks and time slots are set to 150 and 300, and the service number is changed from 1 to 30. Besides VoS, VoS of communication and VoS of localization are also presented in Fig. 4.3. When the service number is increasing with limited bandwidth and time resources, i.e., the relative work loading is increasing if the resources are fixed. Hence, the overall lower rates and localization accuracy are lowered. When the service request number is limited (e.g. less than 5), both the JRA and NJRA show high VoS. However, when the service number is larger than 10, the NJRA exhibits a significant degradation of VoS. When the service number is above 25, the VoS of the NJRA strategy decreases to less than 0.7 while the JRA strategy can retain 0.9. It's demonstrated that the JRA method has better robustness as the service number increases. Similar trends are also observed for the VoS of communication and localization. The robustness of the JRA scheme is attributed to the management and efficient utilization of resources. On the contrary, when using NJRA, the allocation of the time slot is based on the assignment of bandwidth, which is not always the globally optimized solution. The performance of the RRA strategy decreases dramatically since it doesn't take the integrated service request (e.g., service priority) into consideration.

Another well-known heuristic algorithm, genetic algorithm (GA) based resource allocation [134] is also tested in the time slot allocation, in comparison to the PSO algorithm. The parameters of the GA used in this subsection are set as followings. The initial population is 1000 and spatial dimension is $2 * M + 1$. The maximal generation is 10 and the iterative number is 1000. As shown in Fig. 4.3, with the JRA strategy, the VoS of the system is very close by using PSO-based and GA-based time slot allocation. However, as the number of services increases from 1 to 20, the time consumption of the PSO-based algorithm increases linearly

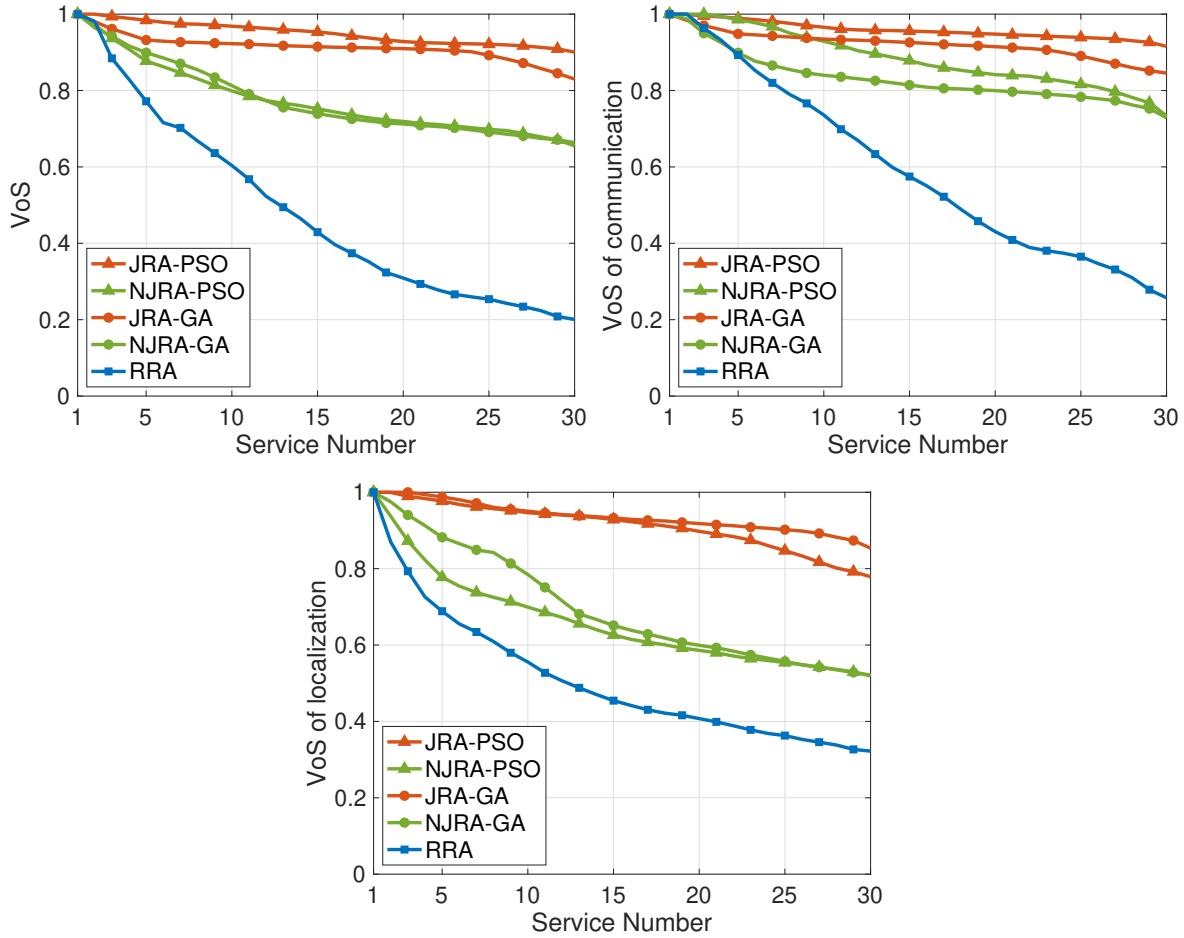


Figure 4.3. The VoS (top left), VoS of communication (top right), VoS of localization (bottom) of JRA, NJRA and RRA under different service numbers.

while the GA-based algorithm increases exponentially as shown in Fig. 4.4. For the global optimization, the memory parameters g_{best} and p_{best} of PSO make it easier to find the optimal solution. In contrast, the GA-based algorithm requires more initial populations and an evolution process to get convergent optimization results. Therefore, the following discussions are based on the JRA scheme incorporated with PSO-based time slot allocation.

Next, we evaluate the VoS against different resource conditions in the ILAC system. In this subsection, we set $M = 20$ as moderate service traffic. Considering the repeatability of allocations, we compare the statistical performance of three schemes by cumulative distribution function (CDF). The algorithms are repeated 1000 times to obtain the CDF as is shown in Fig. 4.5. Here, we consider two different resource levels. When $K_f = 100, K_t = 150$, the resources are scarce for 20 service requests, denoted as a low resource scenario. While $K_f = 150, K_t =$

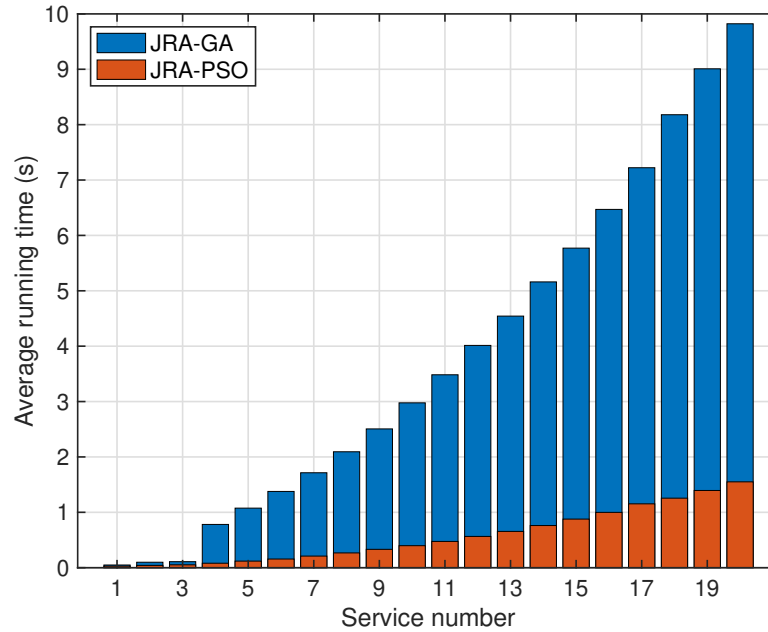


Figure 4.4. The comparison of JRA-GA algorithm and JRA-PSO algorithm vs average running time under different service numbers.

250, it is supposed that the resources are still tight to some extent, but through a reasonable allocation strategy, a satisfactory VoS can be achieved.

4.4.2.2 Influence of Resources

As can be seen from Fig. 4.5, the JRA has narrower distribution width under different resource conditions. Taking the low resource scenario as an example, the distribution width of the NJRA strategy is 0.3 while the proposed JRA is only 0.16, which is more stable than NJRA strategy. Moreover, in this case, the NJRA can achieve around 0.4 VoS with 90% probability and with the same condition, JRA can achieve more than 0.7. When it comes to the higher available resources, where the JRA scheme gives VoS of nearly 0.9, the NJRA only reaches an average of 0.5. This means that the NJRA scheme has smaller VoS per unit resources than the JRA scheme. To this end, the performance of the NJRA scheme is much more restricted and sensitive to temporal and bandwidth resources while the JRA method can still retain much value even when the resources are very limited. Moreover, it is noted that, the VoS of communication is generally higher than the VoS of localization. This could be attributed to the weight of communication being higher than localization on average among the service requests. For

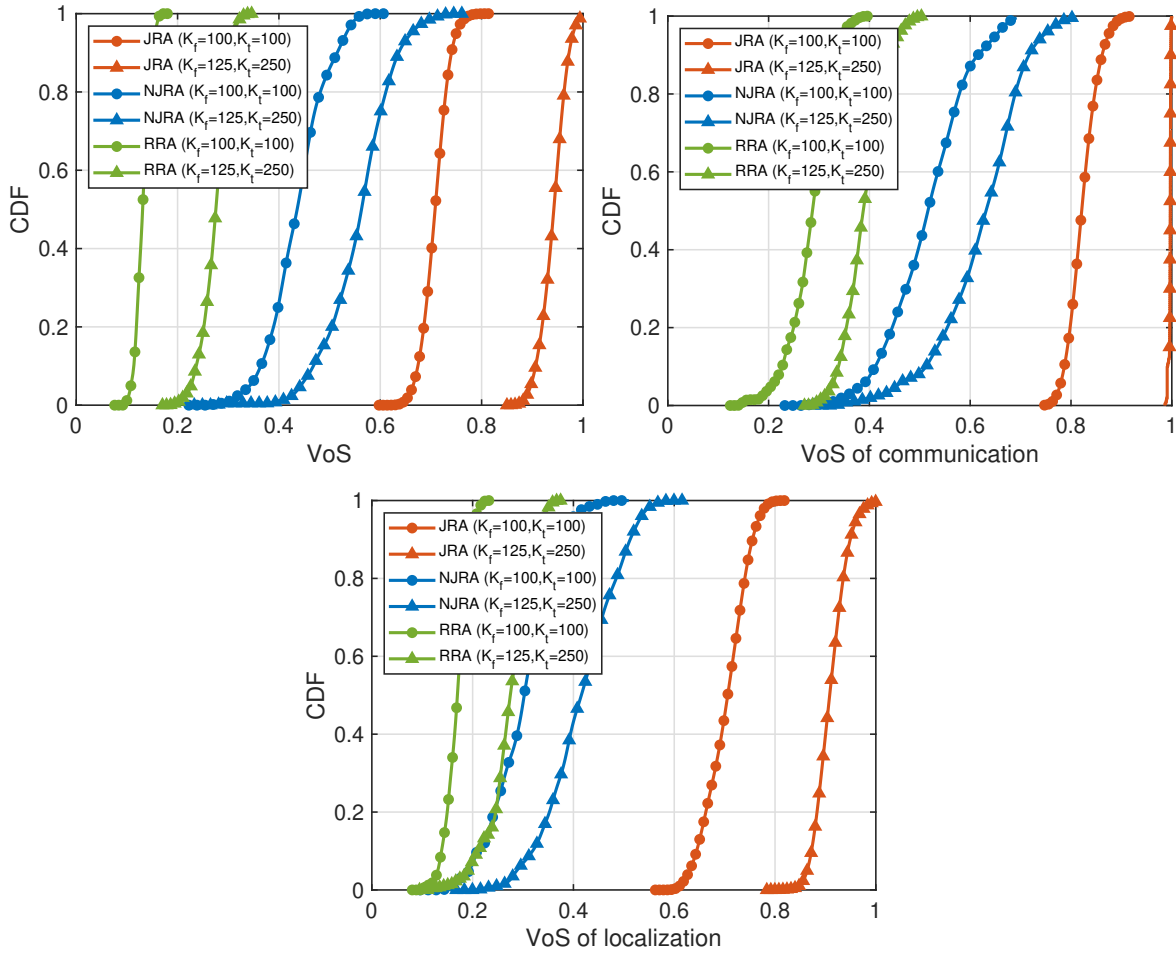


Figure 4.5. The CDF of VoS (top left), VoS of communication (top right), VoS of localization (bottom) with JRA, NJRA and RRA under different resource conditions.

the RRA scheme, the achievable VoS is much lower than the other two strategies. This can be attributed to the negligence of specific service requirements from various devices.

To further demonstrate the influence of available resources in detail, we compare the variation of VoS of the three schemes with varied time slots under different bandwidth resources. In Fig. 4.6, we mainly considered three different levels of bandwidth ($K_f = 50, 150, 300$ respectively) with continuously increasing time slots (K_t) from 50 to 500. As can be seen in Fig. 4.6, under limited time slots, increasing bandwidth cannot enhance the value of service, demonstrating the significance of allocating time as resources in the ILAC system. In such cases, the VoS of communication is more sensitive to bandwidth resources. The explanation is that bandwidth resources can make up for the time slots in communication better than local-

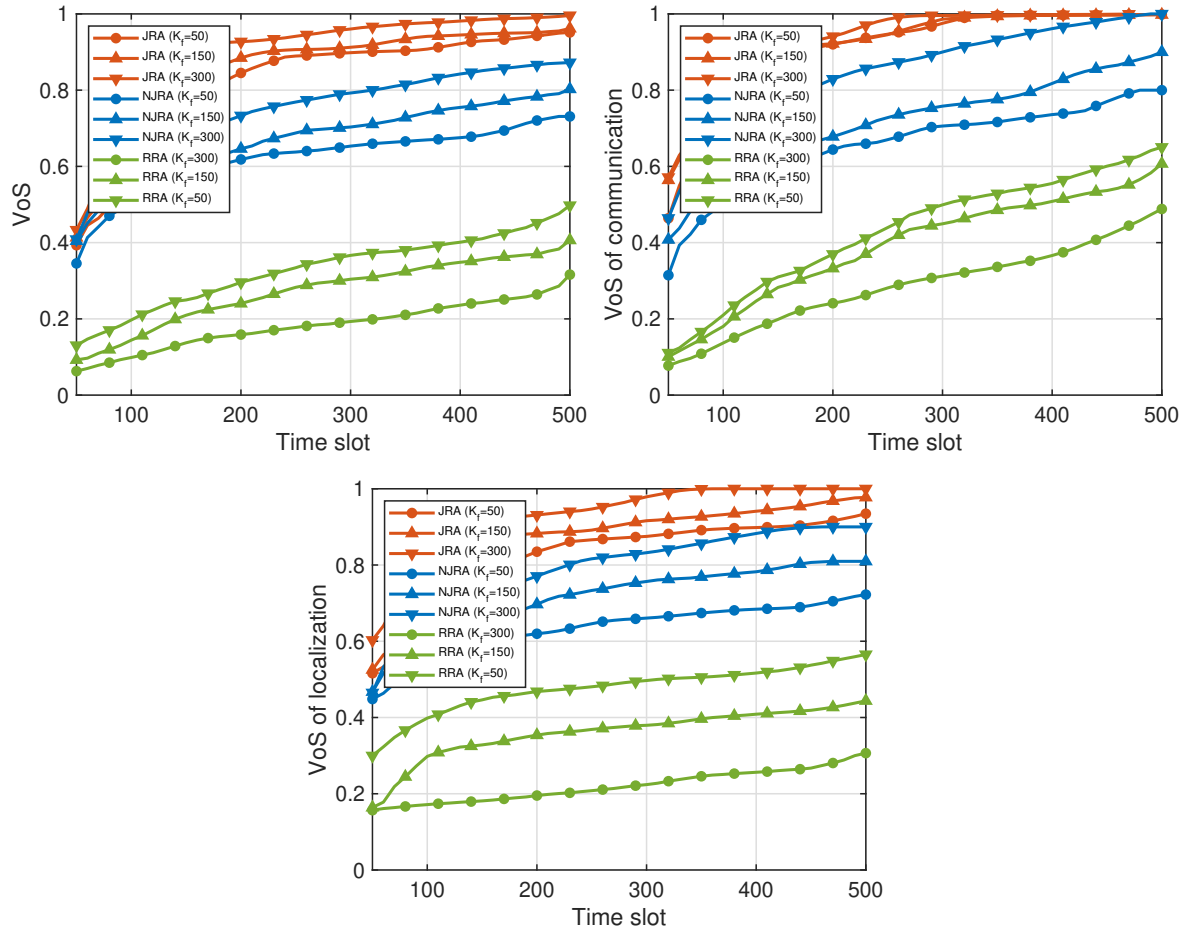


Figure 4.6. The VoS (top left), VoS of communication (top right), VoS of localization (bottom) with JRA, NJRA and RRA under varied temporal resource conditions.

ization. When the number of time slots is high (e.g., > 300), the bandwidth resource impacts the VoS of NJRA larger than the JRA. In such scenarios, the JRA scheme has come to the saturated performance to not be sensitive to resource variations. Moreover, we can observe from Fig. 4.6, that when both the time slot and bandwidth resource are adequate, both the JRA and NJRA method can reach a VoS of 0.9. But JRA requires much fewer time slots to reach the same level of value under fixed bandwidth resources. For the RRA scheme, when the time slot is abundant, the VoS of RRA can only achieve from 0.4 to 0.5. This can be attributed to the fact that there are real-time restrictions (e.g., data rate) from adaptive bandwidth assignment, even though time slots can make up for some utility in the service.

4.4.2.3 Complexity Analysis

The complexity analysis of the JRA-PSO can be found in Section 4.3.4. The complexity of the other two methods (JRA-GA and NJRA) is shown as below.

- **JRA-GA:** The JRA-GA has the same bandwidth resource allocation procedure with JRA-PSO algorithm. Thus, the high bound of computational complexity of bandwidth resource allocation is $O(2^M \mathcal{N}_1)$. The complexity of temporal resource allocation by using GA methods are affected by many parameters (e.g., the generation numbers and chromosome design). Generally, the complexity is proportional to the number of dimensions, the number of generations and the computation time per generation. Given the service number is M , the complexity can be expressed as $O((2M + 1)\mathcal{N}_g(\mathcal{N}_{mutation} + \mathcal{N}_{crossover}))$ where $\mathcal{N}_{mutation}$, $\mathcal{N}_{mutation}$ and \mathcal{N}_g are number of mutations, number of crossovers per generation, and number of generations, respectively. The total computation complexity of JRA-GA algorithm is $O(2^M \mathcal{N}_1(2M + 1)\mathcal{N}_g(\mathcal{N}_{mutation} + \mathcal{N}_{crossover}))$.
- **NJRA:** In the NJRA scheme, Algorithm 2 and Algorithm 3 are invoked only once. Thus, this can be treated as a special case of JRA-PSO algorithm when $\mathcal{N}_1 = \mathcal{N}_4 = 1$. Thus, for the NJRA-PSO, the complexity is $O(2^M \mathcal{N}_2 \mathcal{N}_3)$.

4.4.3 Influence of Localization Weight

The overall objective of the proposed resource allocation method is to maximize the total VoS of the service requests. For each service, the VoS is defined as the weighted sum of VoS of localization and communication, which are determined by the different users depending on the requirements of the applications. To evaluate the impact of the localization weights on the VoS and resource allocation, the service request with different localization weights should be evaluated. The total service number is 9 and the localization weight is varied from 0.1 to 0.9 at step of 0.1. Fig. 4.7 show the total PRB numbers for localization and the total VoS for different weights with fixed resource conditions ($K_f = 100$, $K_t = 300$, $\sigma^{(m)} = 0.5$, $C^{(m,l)} = 250$). The PRB numbers for localization are increased with the rise of localization weight, using either JRA or NJRA. The larger localization weight means the high importance of localization

in the service request. Thus, to achieve high VoS, more PRB numbers need to be allocated for localization with limited resources. It can be noted that the JRA scheme achieves higher VoS than the NJRA. This is attributed to the effective temporal allocation in JRA method, which adaptively assigns the time slots. Therefore, the higher utilization of temporal resources enables the JRA to allocate the PRBs more adaptively and effectively to maximize the VoS of ILAC system.

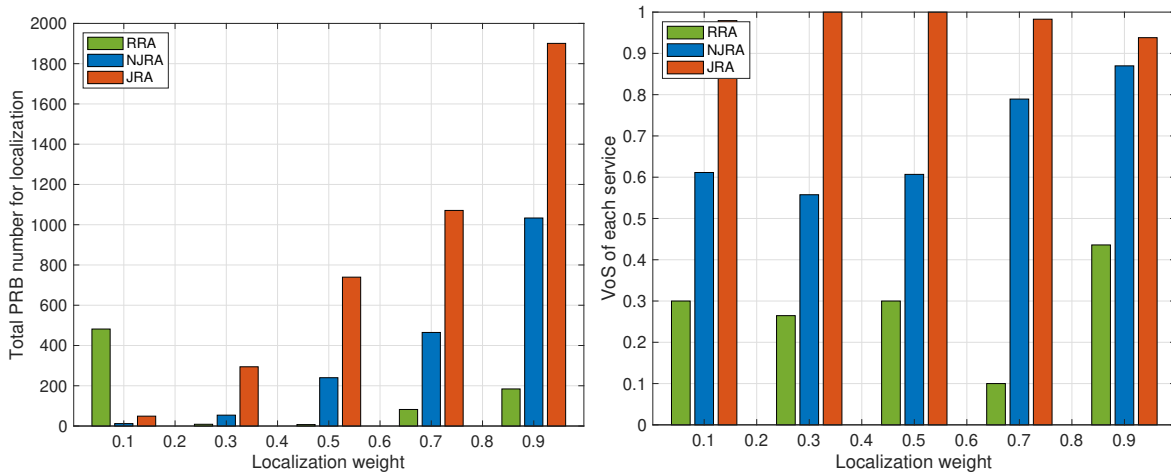


Figure 4.7. The allocated PRB number for localization (left) and VoS (right) with JRA, NJRA and RRA under different required localization weights.

4.5 Chapter Summary

To support diverse merging applications, in this chapter, a joint resource allocation scheme in the ILAC system is proposed. To evaluate the ILAC system comprehensively, a value of service (VoS) metric is introduced consisting of the value from localization and communication components. A novel JRA scheme of both bandwidth and time resources is proposed to maximize the VoS of the ILAC system. The bandwidth resource is allocated by the continuous optimization algorithm followed by discretization. And the temporal resource is assigned with a PSO-based algorithm. From the simulation results, the effectiveness of our redefined ILAC system evaluation metric VoS is confirmed, and the high VoS can be obtained by using the proposed JRA scheme. In addition, our proposed method is more robust and has significantly improved VoS compared with other two resource allocation schemes.

Chapter 5

Successive Resource Allocation in Multi-User ISAC System through Deep Reinforcement Learning

5.1 Introduction

The rapid proliferation of intelligent devices, further driven by emerging next-generation vertical applications, including augmented reality (AR), smart factories, and autonomous robotics, has brought explosively growing demands for concurrent sensing and communication services. To meet such service requirements, the concept of integrated sensing and communication (ISAC) system [25, 108] along with various resource allocation schemes [4, 135–138] has been proposed in recent years. One integrative design goal of the ISAC system is to share both constrained radio resources and the wireless hardware platform to dynamically fulfill users' sensing and communication needs while enhancing cost and operational efficiencies. To effectively achieve this goal, a unified performance metric for both communication and sensing is essential to guide shared resource allocation among concurrent services. For this purpose, a new performance indicator named Value of Service (VoS) was proposed in our previous work to evaluate the ISAC operational effectiveness under static environments [139] when the channel conditions, target locations and service requests are invariant. Given the dynamic needs of

concurrent users and varying resource conditions, it is therefore extremely important to further adapt the definition of VoS as a time-dependent evaluation metric to support dynamic resource allocation according to the varying demands of multiple ISAC users.

However, meeting the changing requirements of sensing and communication through adaptive resource allocation is challenging in dynamic environments with multiple users. On the one hand, the dynamic topology of wireless networks and the stochastic density of the users could result in both fast-varying channel conditions and radio resource availability, which creates many uncertainties for ISAC operation. On the other hand, different ISAC users could have varying sensing and communication demands at different time intervals, which makes the resource allocation even more complicated and challenging. Consequently, it is critical to design successive resource allocation strategies to optimally meet users' needs and demands in the long term under dynamic scenarios.

Specifically, the high complexity of the resource allocation in multi-user ISAC is mainly due to the challenge of effectively modelling and matching the independent varying patterns of network resources and multi-user requests. As a result, new approaches beyond conventional model-based approaches are needed to solve this problem. Deep reinforcement learning (DRL) has been demonstrated as an efficient model-free approach to realize dynamic system operation [140, 141]. In dynamic ISAC, both sensing accuracy and communication data rate could be enhanced with DRL by utilizing the features extracted from integrated signals and priori historical information. For instance, [142] proposed a DRL-based method in a reconfigurable intelligent surface-aided ISAC system, demonstrating an improved data rate over other benchmark approaches. The authors in [143] presented a DRL-based method to address the power allocation problem within an ISAC UAV network, which illustrates the effectiveness of employing DRL in a dynamic ISAC system. However, there is an urgent requirement for the efficient integration of DRL into a successive ISAC system, taking into consideration users' needs and evolving environmental conditions.

Motivated by these observations, this chapter proposes a successive resource allocation strategy in multi-user ISAC systems driven by DRL. We particularly tackle a VoS maximization problem subject to dynamically varying conditions, *i.e.*, changing environment, concurrent service requests and resource constraints. A customized DRL framework is proposed to extract

the optimal allocation of bandwidth and power, where the problem is formulated in a mixed integer optimization form. The service fidelity of our proposed scheme is demonstrated in terms of VoS gain, as per numerical simulations under dynamic network scenarios.

Notations: In this chapter, we use lowercase bold letters and uppercase bold letters to denote vectors and matrices, respectively. $(\cdot)^T$ and $(\cdot)^H$ represent the transposition and Hermitian transposition of a vector or matrix. The imaginary number is denoted with $j = \sqrt{-1}$. The $\|\mathbf{a}\|_F$ is the Frobenius norm and $\Re\{\cdot\}$ is the real component of complex variable $\{\cdot\}$.

The remainder of this chapter is organized as follows. Section 5.2 presents the system model and problem formulation. The proposed DRL-based resource allocation scheme is introduced in Section 5.3. Simulations are given in Section 5.4, followed by the conclusion in Section 5.5.

5.2 System Model

5.2.1 Architecture of Successive ISAC System

We consider an ISAC system composed of M users and one base station (BS) operating at mmWave with ISAC ability shown in Fig. 5.1. The BS is equipped with N_T transmitting uniform linear antennas (ULA) at a known position and each user is equipped with N_R receiving ULA antennas at an unknown position. We incorporate multiple antenna arrays at the user side due to their dual benefits: enhancing position coordinate accuracy and facilitating real-time target position updates with Doppler frequency offset [144]. The users with a single antenna are treated as a special case ($N_R = 1$, e.g., when there is no sensing service request from the user).

Each user corresponds to one ISAC service request denoted as SR_m ($1 \leq m \leq M$). The time-dependent SR_m of m -th user at t -th channel coherence time is denoted as $\mathbf{R}_m(t) = [R_{m,s}(t), R_{m,c}(t)]^T$. Herein, the sensing request $R_{m,s}(t)$ [20] is the sensing accuracy to localize the user's position (device-based sensing). The communication request $R_{m,c}(t)$ is the data rate from BS to the user. The available radio spectrum is divided into N subchannels denoted as $\mathcal{N} = \{1, 2, \dots, N\}$, utilizing Orthogonal Frequency Division Multiplexing (OFDM). The bandwidth of each subchannel

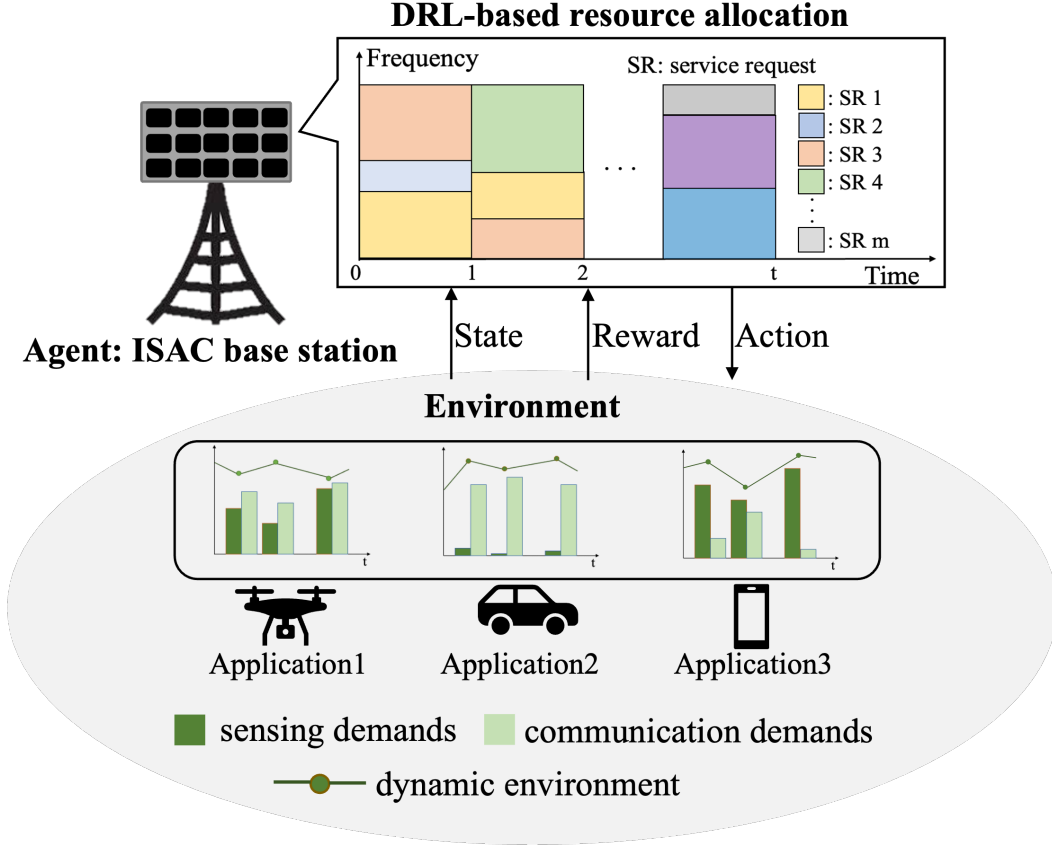


Figure 5.1. Illustration of successive resource allocation in multi-user ISAC system for tailored service provisioning.

is B_0 . At t -th channel coherence time, the number of subchannels allocated for the sensing and communication of SR_m are $N_{m,s}(t)$, $N_{m,c}(t)$, respectively. Each coherence time includes two phases. In phase I, the BS transmits N_s sensing reference symbols with power $P_{m,s}(t)$. In phase II, N_d data symbols with power $P_{m,c}(t)$ are transmitted for communication.

5.2.2 Sensing Model

In this subsection, we introduce the signal model for sensing. During the t -th coherence time, $\mathbf{s}_{ref,k}^{(m,n)}(t)$ is used to denote the transmitted k -th ($1 \leq k \leq N_s$) reference signal symbol to m -th user at n -th subchannel ($1 \leq n \leq N_{m,s}(t)$). It is supposed inaccurate location of users is known for beamforming [46]. Let $\mathbf{F}_s^{(m,n)}(t) \in \mathbb{C}^{N_T \times N_s}$ denote the beamforming matrix, satisfying $\sum_{n=1}^{N_{m,s}(t)} \|\mathbf{F}_s^{(m,n)}(t)\|_F^2 = P_{m,s}(t)$. Herein, we assume perfect beamforming with unity beamforming gain. The impact of imperfect beamforming can be described with fractional gain for different

expressions of $\mathbf{F}_s^{(m,n)}(t)$, as is in [4]. The design of $\mathbf{F}_s^{(m,n)}(t)$ for ISAC system [118] is out of scope for this work.

In the sensing channel model, assume there are L reflection points in the scenario. Let $\theta_{m,T,l}$, $\theta_{m,R,l}$, and $\tau_{m,l}$ denote the AOD, AOA and transmission time from BS to m -th user via l -th path, where $l = 0$ is the line-of-sight (LOS) path and $1 \leq l \leq L$ are non-line-of-sight (NLOS) path. Then, the channel matrix $\mathbf{H}^{(m,n)}(t) \in \mathbb{C}^{N_R \times N_T}$ is given by

$$\mathbf{H}^{(m,n)}(t) = \mathbf{A}_R^{(m,n)} \mathbf{\Gamma}^{(m,n)}(t) \mathbf{A}_T^{(m,n)H}, \quad (5.1)$$

$$\mathbf{\Gamma}^{(m,n)}(t) = \sqrt{N_T N_R} \text{diag}[h_0^{(m)}(t) e^{-j2\pi \frac{n}{N_{m,s}(t)T_s} \tau_{m,0}}, \dots, h_L^{(m)}(t) e^{-j2\pi \frac{n}{N_{m,s}(t)T_s} \tau_{m,L}}]. \quad (5.2)$$

where $h_l^{(m)}(t)$ is the complex channel gain. In (5.1), $\mathbf{A}_T^{(m,n)}$ and $\mathbf{A}_R^{(m,n)}$ are the steering matrix at the BS and response matrix at the user, written as

$$\mathbf{A}_T^{(m,n)} = [\mathbf{a}_T(\theta_{m,T,0}), \mathbf{a}_T(\theta_{m,T,1}), \dots, \mathbf{a}_T(\theta_{m,T,L})]^T, \quad (5.3)$$

where the vector $\mathbf{a}_T(\theta_{m,T,l})$ is

$$\mathbf{a}_T(\theta_{m,T,l}) = \frac{1}{\sqrt{N_T}} [e^{-j \frac{d_T 2\pi \sin \theta_{m,T,l}}{\lambda_n} (1-1)}, \dots, e^{-j \frac{d_T 2\pi \sin \theta_{m,T,l}}{\lambda_n} (N_T-1)}]^T. \quad (5.4)$$

In (5.4), λ_n is the signal wavelength and d_T denotes the distance between the antenna elements ($d_T = \lambda_n/2$). The response matrix $\mathbf{A}_R^{(m,n)}$ can be defined similarly.

Let $\mathbf{z}_k^{(m,n)}(t)$ denote the received k -th reference signal symbol at the receiver after cyclic prefix (CP) removal and fast Fourier transform (FFT), which can be expressed as

$$\mathbf{z}_k^{(m,n)}(t) = \mathbf{W}^{(m,n)H}(t) \mathbf{H}^{(m,n)}(t) \mathbf{F}_s^{(m,n)}(t) \mathbf{s}_{ref,k}^{(m,n)}(t) + \mathbf{n}^{(m,n)}(t), \quad (5.5)$$

where $\mathbf{n}^{(m,n)}(t) \sim \sigma_e^2 \mathcal{C}(0, \mathbf{I})$ is white Gaussian noise vector and $\mathbf{W}^{(m,n)}(t) \in \mathbb{C}^{N_R \times N_s}$ is the combiner matrix at receiver.

Let $\tilde{\mathbf{z}}^m(t)$ be the received sensing signal of m -th user among all subchannels, expressed as

(the time stamp t is omitted for clarification from (5.6) to (5.11))

$$\tilde{\mathbf{z}}^{(m)} = \underbrace{[\mathbf{z}_1^{(m,1)}, \dots, \mathbf{z}_1^{(m,N_{m,s})}]_{1^{\text{st}} \text{ sensing symbol}}}, \dots, \underbrace{[\mathbf{z}_{N_s}^{(m,1)}, \dots, \mathbf{z}_{N_s}^{(m,N_{m,s})}]_{N_s^{\text{th}} \text{ sensing symbol}}}]^T, \quad (5.6)$$

and can be rewritten as

$$\tilde{\mathbf{z}}^{(m)} = \tilde{\mathbf{\Omega}}^{(m)} \tilde{\mathbf{h}}^{(m)} + \mathbf{n}^{(m)}, \quad (5.7)$$

$$\tilde{\mathbf{\Omega}}^{(m)} = [\mathbf{\Omega}_1^{(m,1)}, \dots, \mathbf{\Omega}_1^{(m,N_{m,s})}, \mathbf{\Omega}_{N_s}^{(m,1)}, \dots, \mathbf{\Omega}_{N_s}^{(m,N_{m,s})}]^T, \quad (5.8)$$

$$\mathbf{\Omega}_k^{(m,n)} = \left(\mathbf{F}_s^{(m,n)} \mathbf{s}_{ref,k}^{(m,n)} \right)^T \otimes \mathbf{W}^{(m,n)H}, \quad (5.9)$$

$$\tilde{\mathbf{h}}^{(m)} = [\mathbf{h}_1^{(m,1)}, \dots, \mathbf{h}_1^{(m,N_{m,s})}, \mathbf{h}_{N_s}^{(m,1)}, \dots, \mathbf{h}_{N_s}^{(m,N_{m,s})}]^T, \quad (5.10)$$

$$\mathbf{h}_k^{(m,n)} = \text{vec}(\mathbf{H}^{(m,n)}). \quad (5.11)$$

From (5.9), it can be seen that $\tilde{\mathbf{\Omega}}^{(m)}$ is independent with the AOA, AOD and transmission time. The channel vector $\tilde{\mathbf{h}}^{(m)}$ is dependent on the hyperparameter defined as $\xi^{(m,n)}(t) = [\xi_0^{(m,n)}(t), \dots, \xi_L^{(m,n)}(t)]^T \in \mathbb{R}^{5(L+1)}$ with

$$\xi_l^{(m,n)}(t) = \underbrace{[\theta_{m,T,l}, \theta_{m,R,l}, \tau_{m,l}]_{\text{sensing parameters}}}_{\text{sensing parameters}}, \underbrace{[h_{l,R}^{(m)}(t), h_{l,I}^{(m)}(t)]}_{\text{channel gain}}, \quad (5.12)$$

where the complex channel response can be written as $h_l^{(m)}(t) = h_{l,R}^{(m)}(t) + jh_{l,I}^{(m)}(t)$. The first three components of $\xi_l^{(m,n)}(t)$ is dependent on the user position $\mathbf{x}^{(m)}(t)$ and reflection point position $\kappa_l^{(m)}(t)$. The geometrical relation between the $\theta_{m,T,l}, \theta_{m,R,l}, \tau_{m,l}$ and $\mathbf{x}^{(m)}(t), \kappa_l^{(m)}(t)$ can be found in [145].

The channel vector $\tilde{\mathbf{h}}^{(m)}$ can be expressed with $\boldsymbol{\eta}^{(m,n)}(t) = [\mathbf{x}^{(m)}(t), \kappa_l^{(m)}(t), h_{l,R}^{(m,n)}(t), h_{l,I}^{(m)}(t)]_{l=1:L}$.

Let $\hat{\mathbf{x}}^{(m)}(t)$ denote the estimated position of m -th user. The sensing mean squared error (MSE) is bounded with

$$\mathbb{E} \left\{ \left\| \hat{\mathbf{x}}^{(m)}(t) - \mathbf{x}^{(m)}(t) \right\|^2 \right\} \geq \text{tr} \left\{ \mathbf{J}_{[1:2,1:2]}^{-1}(\boldsymbol{\eta}^{(m)}(t)) \right\}. \quad (5.13)$$

where $\mathbf{J}(\boldsymbol{\eta}^{(m)}(t))$ is the Fisher information matrix (FIM).

The (i, j) element of $\mathbf{J}(\boldsymbol{\eta}^{(m)}(t))$ from measurement is calculated with [98]

$$\mathbf{J}_{i,j}(\boldsymbol{\eta}^{(m)}(t)) = \frac{2}{\sigma_e^2} \sum_{k=1}^{N_s} \sum_{n=1}^{N_{m,s}(t)} \Re \left\{ \left(\frac{\partial \boldsymbol{\mu}_k^{(m,n)}}{\partial \boldsymbol{\eta}_i} \right)^H \left(\frac{\partial \boldsymbol{\mu}_k^{(m,n)}}{\partial \boldsymbol{\eta}_j} \right) \right\}, \quad (5.14)$$

where $\boldsymbol{\mu}_k^{(m,n)} = \boldsymbol{\Omega}_k^{(m,n)} \mathbf{h}_k^{(m,n)}$.

In the successive process, the temporal correlation of $h_l^{(m)}(t)$ is modeled as the first order autoregressive model

$$h_l^{(m)}(t) = \rho_t h_l^{(m)}(t-1) + \sqrt{1 - \rho_t^2} u(t), \quad (5.15)$$

where $u(t)$ is the complex Gaussian noise and the ρ_t is the time correlation coefficient, which follows Jakes' model [146]. The FIM with priori information is recursively written as

$$\tilde{\mathbf{J}}(t) = (|\rho_t|^2 \tilde{\mathbf{J}}(t-1) + (1 - |\rho_t|^2) \mathbf{R}_u) + \mathbf{J}(\boldsymbol{\eta}^{(m)}(t)), \quad (5.16)$$

where the \mathbf{R}_u is the covariance matrix of Gaussian noise $u(t)$. Therefore, the Cramér–Rao lower bound (CRLB) of sensing with priori information is expressed with

$$\text{CRLB}(\hat{\mathbf{x}}^{(m)}(t)) = \sum_{i=1}^2 \{ \tilde{\mathbf{J}}^{-1}(t) \}_{i,i}. \quad (5.17)$$

The VoS of sensing $V_{m,s}(t)$ is defined as the completeness degree of sensing request [139]

$$V_{m,s}(t) = \begin{cases} \frac{R_{m,s}(t)}{\text{CRLB}(\hat{\mathbf{x}}^{(m)}(t))} & \text{if } \text{CRLB}(\hat{\mathbf{x}}^{(m)}(t)) > R_{m,s}(t) \\ 1 & \text{if } \text{CRLB}(\hat{\mathbf{x}}^{(m)}(t)) < R_{m,s}(t) \end{cases}. \quad (5.18)$$

5.2.3 Communication Model

In the ISAC system, both the sensing and communication share the same front-end. Thus, the Rx at UE with multiple antenna arrays for sensing signal also serves as communication Rx.

In communication model, let $\mathbf{s}_{d,k}^{(m,n)}(t)$ and $\mathbf{y}_k^{(m,n)}(t)$ denote the transmitted and received k -th data symbol, respectively

$$\mathbf{y}_k^{(m,n)}(t) = \mathbf{W}_d^{(m,n)H}(t) \mathbf{H}^{(m,n)}(t) \mathbf{F}_d^{(m,n)}(t) \mathbf{s}_{d,k}^{(m,n)}(t) + \mathbf{n}^{(m,n)}(t). \quad (5.19)$$

It is supposed the channel remains unchanged during one coherence time frame t . Thus, the signal-to-noise ratio (SNR) $\gamma^{(m)}(t)$ is

$$\gamma^{(m)}(t) = \frac{P_{m,c}(t) |h_0^{(m)}(t)|^2}{\sigma_e^2(t)}, \quad (5.20)$$

We assume non-overlapping subcarriers in the system, and the achievable data rate of SR_m is

$$\tilde{R}^{(m)}(t) = (1 - \alpha) B_0 N_{m,c}(t) \log_2 \left(1 + \gamma^{(m)}(t) \right), \quad (5.21)$$

where α is the time ratio of frame t used for sensing expressed as $\alpha = \frac{N_s}{N_s + N_c}$.

The VoS of communication is formulated as the completeness of communication request [139]

$$V_{m,c}(t) = \begin{cases} \frac{\tilde{R}^{(m)}(t)}{R_{m,c}(t)} & \text{if } \tilde{R}^{(m)}(t) \leq R_{m,c}(t) \\ 1 & \text{if } \tilde{R}^{(m)}(t) > R_{m,c}(t) \end{cases}. \quad (5.22)$$

5.2.4 Problem Formulation

Considering the different priorities of service requests, the VoS of the ISAC system is defined as the weighted sum of VoS from each service, shown as

$$V(t) = \sum_m \omega_m V_m(t), \quad (5.23)$$

$$V_m(t) = \omega_{m,c} V_{m,c}(t) + \omega_{m,s} V_{m,s}(t), \quad (5.24)$$

where $0 < \omega_m < 1$ is the priority of the SR_m . $\omega_{m,c}$ and $\omega_{m,s}$ are the weight of communication and sensing for SR_m ($0 \leq \omega_{m,c} \leq 1, 0 \leq \omega_{m,s} \leq 1, \omega_{m,c} + \omega_{m,s} = 1$), respectively.

The objective function is defined as maximizing the weighted sum of the VoS over a period T . Herein, the joint bandwidth and power allocation ($\mathbf{N}_m(t) = [N_{m,s}(t), N_{m,c}(t)]$, $\mathbf{P}_m(t) =$

$[P_{m,c}(t), P_{m,s}(t)]$ problem is formulated as

$$P : \max_{\mathbf{P}_m(t), \mathbf{N}_m(t)} \sum_{t=1}^T \gamma_0^t V(t) \quad (5.25)$$

$$s.t. \quad \sum_{m=1}^M P_{m,s}(t) \leq P_{T,max} \quad (25a)$$

$$\sum_{m=1}^M P_{m,c}(t) \leq P_{T,max} \quad (25b)$$

$$0 < P_{m,s}(t), P_{m,c}(t) \leq P_{m,max} \quad (25c)$$

$$\sum_{m=1}^M N_{m,s}(t) \leq N \quad (25d)$$

$$\sum_{m=1}^M N_{m,c}(t) \leq N \quad (25e)$$

$$N_{m,s}(t), N_{m,c}(t) \in N^+ \quad (25f)$$

where $\gamma_0 \in [0, 1)$ is the discount rate of the VoS. Constraints (25a)-(25c) give the maximum power limit, where $P_{T,max}$ is the transmission power limit of BS and $P_{m,max}$ is the receiving power limit of m -th user. (25d)-(25e) is the maximum bandwidth number limit. Due to the complexity of the mixed integer optimization problem, it is challenging to find the global optimal solution of P . Therefore, we utilize a DRL-based method to solve P .

5.3 Resource Allocation with DRL

5.3.1 Deep Reinforcement Learning

In our system, the BS as the single agent determines the resource allocation of all users. At coherence time step t , the agent observes the state s_t , and takes action a_t according to a policy $\pi(s | a)$. Here, $\pi(s | a)$ is the probability of taking action a under state s , satisfying $\int_{a \in \mathcal{A}} \pi(s | a) = 1$. When the agent takes action a_t , the state transits from s_t to s_{t+1} due to the random variation of channel conditions and service requests. And the agent obtains the immediate reward r_t . Meantime, the agent stores the experience $\{s_t, a_t, r_t, a_{t+1}\}$, describing one interaction

with environment. The three key components of MDP in our problem are elaborated as follows.

5.3.1.1 State space

The organization of hyper-parameters to construct the state vector is based on systematic and intuitive principles, as in [147]. The state of the agent at t is described with three feature groups. The first group includes five elements of the users' service requests with $[R_{m,s}(t), R_{m,c}(t), \omega_m(t), \omega_{m,c}(t), \omega_{m,s}(t)]$. These features are necessary since they are user-specific and indicate the service-oriented principle of the design. The second group includes the complex channel gain and noise power $[h_l^{(m)}(t), \sigma_e(t)]_{l=0:L}$. These features describe the environments with which users interact. Additionally, channel state features introduce Markov properties between time slots. Intuitively, the reward of the action is directly related to the VoS of sensing and the VoS of communication. Thus, we choose to include the VoS of sensing $V_{m,s}(t-1)$ and communication $V_{m,c}(t-1)$ of the last time step, which will help the agent to make better decisions.

Therefore, the state vector can be defined as

$$\mathbf{s}_t = [\mathbf{s}_1(t), \mathbf{s}_2(t), \dots, \mathbf{s}_M(t)], \quad (5.26)$$

where the subvector is

$$\mathbf{s}_m(t) = [R_{m,s}(t), R_{m,c}(t), \omega_m(t), \omega_{m,c}(t), \omega_{m,s}(t), h_l^{(m)}, \sigma_e^{(m)}(t), V_{m,s}(t-1), V_{m,c}(t-1)]. \quad (5.27)$$

It is noted that all the components in \mathbf{s}_t are continuous variables, where the probability at specific state is zero. Thus, the probability of transition from \mathbf{s}_t to \mathbf{s}_{t+1} by taking action \mathbf{a}_t is expressed as

$$\Pr(\mathbf{s}_{t+1} | \mathbf{s}_t, \mathbf{a}_t) = \int_{S(t)} f(\mathbf{s}_t, \mathbf{a}_t, s') ds', \quad (5.28)$$

where s' is the all actions in the action space and the $f(\cdot)$ is the state transition function.

5.3.1.2 Action space

In our problem, the BS determines the resource allocation strategy, including the power and number of subchannels allocated for sensing/communication. Thus, the action space \mathcal{A} con-

tains

$$\mathbf{a}(t) = [\mathbf{a}_1(t), \mathbf{a}_2(t) \dots \mathbf{a}_M(t)], \quad (5.29)$$

where $\mathbf{a}_m(t) = [N_{m,c}(t), N_{m,s}(t), P_{m,c}(t), P_{m,s}(t)]$. The variables in action $\mathbf{a}(t) \in \mathcal{A}$ include two types of action. The power is a continuous variable while the subchannel number is discrete. One option to deal with the continuous action is to discretize it into finite levels as in [148]. However, the discretization of the continuous variable may lead to a great increase of action space size and training overhead. Thus, we relax the discrete constraint of subchannel number, followed by the post-discretization process.

5.3.1.3 Reward space

The agent receives the immediate reward after taking action. The reward is designed to evaluate the performance of the action. We introduce the VoS defined in (5.23) as the immediate reward function $r_t = V(t)$.

5.3.2 DRL-based Resource Allocation

In this work, we adopt an actor-critic based DRL scheme [149] to solve P as illustrated in Fig. 5.2. The structure of AC-based DRL can be found in [149]. The actor is employed to determine the action policy π , which maps the state \mathcal{S} to the action space \mathcal{A} . The critic is utilized to evaluate the policy by estimating the value function, enabling subsequent updates to the policy parameters in the actor. By adopting the actor-critic architecture, convergence of the system can be well guaranteed.

The actor employs the policy gradient approach. Suppose the parameters in the policy $\pi(a | s)$ are denoted as $\boldsymbol{\phi} = [\phi_1, \phi_2, \dots, \phi_n]$. We adopt the fully connected neural network in actor network with the input layer, hidden layer and output layer. The local maximum of the gradient function can be obtained with the policy ascending, where the action-value function (i.e., Q -function [150]) is defined as

$$Q_{\pi}(s, a) = \mathbb{E}_{\pi} \left[\sum_{t=1}^{\infty} \gamma^t r_t \mid s = s_t, a = a_t \right]. \quad (5.30)$$

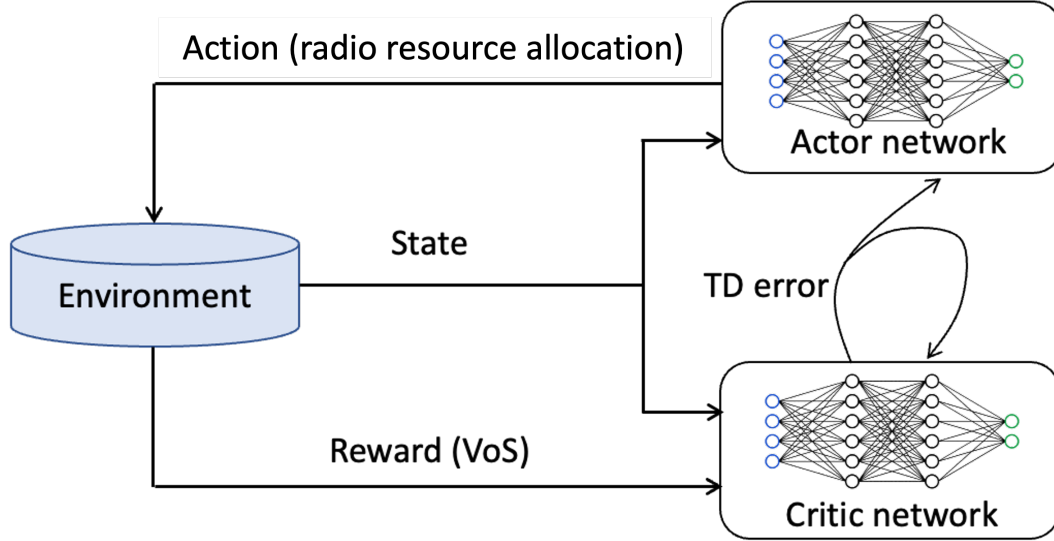


Figure 5.2. Illustration of the interaction between actor and critic network.

Q function is used as a metric to evaluate the effectiveness of action a_t at state s_t , so as to optimize the policy. The optimal Q function can be expressed in the form of Bellman optimality equation as

$$Q_{\pi}(s, a) = E_{\pi} [r_t + \gamma_0 Q_{\pi}(s, a) \mid s = s_{t+1}, a = a_{t+1}]. \quad (5.31)$$

According to (5.31), the Q function can be updated through a recursive approach to obtain the optimal Q value. In order to maximize the reward by considering the continuous action space, the policy objective function is given as

$$J_{\pi} = E [Q_{\pi}(s, a)] = \int_S d^{\pi} s \int_{\mathcal{A}} \pi(a \mid s) Q_{\pi}(s, a) ds, \quad (5.32)$$

where the $d^{\pi} s$ denotes the state distribution under policy π . Then, the gradient of the objective function is calculated with

$$\nabla_{\phi} J_{\pi} = \frac{\partial J}{\partial \pi_{\phi}} \frac{\partial \pi_{\phi}}{\partial \phi}. \quad (5.33)$$

The variation of arguments is expressed as

$$\Delta \phi = \alpha_{a,t} \nabla_{\phi} J_{\pi}, \quad (5.34)$$

where $\alpha_{a,t} > 0$ is the learning rate of the actor. Then, the gradient of the policy is rewritten as

$$\nabla_{\phi} J_{\pi} = \int_{\mathcal{S}} d^{\pi} s \int_{\mathcal{A}} \nabla_{\phi} \pi Q_{\pi}(s, a) ds. \quad (5.35)$$

The Gaussian probability distribution is utilized to model the random policy to select the action. So the parameterized strategy is expressed as

$$\pi_{\phi}(s, a) = \frac{1}{\sqrt{2\pi}\sigma_0} \exp\left[-\frac{(a - \zeta)^2}{2\sigma_0^2}\right], \quad (5.36)$$

where ζ is the mean of the actions and σ_0 is the standard deviation of all actions.

The critic process is utilized to evaluate the policies. We use a Q network $Q_{\varpi}(s, a)$ with parameter ϖ to approximate the $Q^{\pi}(s, a)$. When the action a_t is chosen by the actor, the agent will execute it in the environment and send the current observation s_t along with the feedback from the environment to the critic. Given the tuple $\{s_t, a_t, r_{t+1}, s_{t+1}, a_{t+1}\}$, the critic can calculate the temporal difference (TD) error. The TD error represents the error between the approximated value and real value at a state, expressed as

$$\delta_t = r_{t+1} + \gamma_0 Q_{\varpi}(s_{t+1}, a_{t+1}) - Q_{\varpi}(s_t, a_t). \quad (5.37)$$

After the actor receives the rewards, it will update the policy accordingly. During the policy update process, the agent introduces noise to the target action, thereby reducing the possibility of exploiting actions that yield high Q -value estimates. Suppose that policy gradient is denoted by $\nabla_{\phi} J_{\pi}$. The gradient function can be formulated as the statistical average of the rewards. There are several policy function parameters updating strategies. In this work, we used TD-based updating with

$$\varpi \leftarrow \varpi + \alpha_{c,t} \nabla_{\varpi} \log \pi_{\varpi}(s_t, a_t) \delta_t. \quad (5.38)$$

where $\alpha_{c,t} > 0$ denotes the learning rate.

Algorithm 5: Resource allocation with DRL

Input : initial state s_1 , Gaussian policy $\pi_\phi(s, a)$ and its gradient, learning rates $\alpha_{s,t}, \alpha_{c,t}$
and discount factor γ_0 .

Output: The optimal action of each time step.

- 1 **Initialization:**
 - 2 Initialize the initial state vectors.
 - 3 Initialize the policy and action-value function with random weight.
 - 4 **while** $t \leq T_{max}$ **do**
 - 5 Choose action a_t following policy $\pi_\phi(s | a)$.
 - 6 Update the immediate reward R_t and the state
 - 7 evolves to s_{t+1} .
 - 8 **Actor process**
 - 9 Update the state feature vector.
 - 10 Calculate the policy gradient $\nabla_\phi J_\pi$ with (5.35).
 - 11 Update the policy parameter ϕ .
 - 12 **Critic process**
 - 13 Calculate the TD error according to (5.37).
 - 14 Update the eligibility traces with (5.39).
 - 15 Update the critic parameter ϖ with (5.40).
 - 16 **End**
-

Herein, we introduce the eligibility traces at time step t to improve the RL efficiency, as

$$\chi_t = \nabla_\varpi Q_\varpi(s_t, a_t) + \gamma_0 \chi_{t-1} \vartheta. \quad (5.39)$$

where the $\vartheta \in [0, 1)$ denotes the trace-decay rate. Then, the ϖ can be updated with TD error and eligibility using

$$\varpi \leftarrow \varpi + \alpha_{c,t} \chi_t \delta_t. \quad (5.40)$$

While finding the power $P_{m,s}(t), P_{m,c}(t)$ and the subchannel number $N_{m,s}(t), N_{m,c}(t)$ with continuous variables, the discrete optimization is solved by extracting a sequence of feasible candidates from the optimal continuous resources as

- (i) Suppose vector $[N_{m,c}^*(t), N_{m,s}^*(t)]^T$ ($m = 1, \dots, M$) is the continuous optimal subchannel from DRL. The lower (floor function) integer number less than $[N_{m,c}^*(t), N_{m,s}^*(t)]^T$ and the upper (ceiling function) integer points higher than $[N_{m,c}^*(t), N_{m,s}^*(t)]^T$ are selected. The subchannel number smaller than one is mapped to one to avoid zero resource allocation. The candidate of discrete subchannel allocation is the $2M$ dimensional vectors which yield in 2^{2M} feasible allocation vectors.
- (ii) To further restrict the search space, vectors that do not satisfy constraints (5.25d) and (5.25e) will be filtered out.
- (iii) The VoS of the qualified vectors is calculated and compared. The allocation vector with the largest VoS and/or with the least subchannel numbers is stored.

The proposed DRL-based resource allocation algorithm is in Algorithm 5. During training, the agent dynamically updates the actor and critic components at every time step. It utilizes a circular experience buffer to retain past experiences and selects mini-batches of experiences randomly from this buffer to update the actor and critic networks. Furthermore, the agent introduces stochastic noise to the selected action according to a noise model, perturbing it during each training iteration.

Complexity analysis: For the actor-critic network, suppose the number of layers of the actor network and critic network is N_{actor} and N_{critic} , respectively. The computation complexity is expressed as

$$O\left(T\left(M\sum_{i=1}^{N_{\text{actor}}}u_a^{(i)}u_a^{(i+1)}+2M\sum_{j=1}^{N_{\text{critic}}}u_c^{(j)}u_c^{(j+1)}\right)\right), \quad (5.41)$$

where T is the maximum episode number, M is the number of users, and $u_a^{(i)}, u_c^{(j)}$ are the number of neurons in i -th layer of actor and j -th layer critic networks, respectively.

5.4 Simulation Results

All simulations are performed in MATLAB 2022a on a Lambda deep learning workstation with an Intel Core CPU at 3.90 GHz, 256 GB RAM memory and NVIDIA RTX A6000 GPU. In the DRL model, the discount factor is 0.99 and the experience buffer length is 10^6 . The actor

and critic learning rate is both 0.01. The target smooth factor is set to 0.001. The training episode threshold is 0.8 with a maximum episode of 10^4 . A larger batch size leads to more stable updates and reduced variance in the learning process but requires more memory and computational resources, while a smaller batch size can be more memory-efficient but may result in noisier updates and slower convergence. The experience replay batch size is set to 128 to achieve a balance between stability, convergence speed, and resource efficiency. The actor and critic network of the DRL scheme are both set as a fully connected network with 3 hidden layers. We begin with 64 neurons in each hidden layer and gradually increase them until we determine that 256 neurons produce stable value realization. During the training process, the agent employs a Gaussian noise model to smooth the target network policy with a noise variance of $\alpha = 1e^{-4}$ to increase the exploration capabilities. The total service number is within [1, 30]. In all simulations, the weights and priorities of service requests are randomly generated, ensuring a fair and comprehensive representation of various types of service requests. The power restriction P_{max} is set to 45 dBm and the maximum bandwidth is 12 MHz divided into 100 subchannels. Herein, we compared the performance of the proposed DRL-based method with three approaches: particle swarm optimization (PSO), average and random allocation methods.

- Heuristic approach (PSO):** The PSO (particle swarm optimization), as a representative heuristic algorithm, simulates the social behaviour of birds within a flock [62, 151]. The subchannel number and power are allocated at the beginning of each frame. During the execution, the individuals' positions are changing with the social tendency of the group. In PSO, each individual, called a particle, benefits from the historical experience of its own and that of the other members when searching for food. In particular, each particle μ records the best position it has experienced so far as $pbest_{\mu}$, and the best position of its neighbours or the global community as $gbest$. The object function (immediate reward in our problem) is called the fitness score of each particle. With the iteration, the particle μ can update its velocity $v_{\mu\nu}$ and position $x_{\mu\nu}$ (ν -th dimension of optimization vector)

through the personal best position and swarm's best position following two equations

$$v_{\mu\nu}(s+1) = \rho v_{\mu\nu}(s) + c_1 \text{rand}_1(pbest_{\mu\nu}(s) - x_{\mu\nu}(s)) + c_2 \text{rand}_2(gbest_{\mu\nu}(s) - x_{\mu\nu}(s)), \quad (5.42)$$

$$x_{\mu\nu}(s+1) = x_{\mu\nu}(s) + v_{\mu\nu}(s+1), \quad (5.43)$$

where s is the iteration number, $v_{\mu\nu}(s+1)$ and $x_{\mu\nu}(s+1)$ are velocity and position of the μ -th particle, and ρ is the inertia weight. c_1 and c_2 are learning factors while rand_1 and rand_2 are random numbers between 0 and 1. In our problem, the channel state at time step t is unknown during the optimization to be taken from the last frame.

- **Average resource allocation:** The bandwidth in each frame is average allocated to localization and communication. The power is evenly assigned to each user all the time.
- **Random resource allocation:** Both the bandwidth and power are allocated randomly while keeping the constraints satisfied.

5.4.1 Parameter Setting of DRL

The selection of the network parameters decides the learning convergence performance, especially the actor learning rate. The learning rate of optimizers should be selected carefully because it controls the rate or speed at which the model learns. It can be seen that different learning rates have different effects on the performance of the DRL algorithm. The learning process with three different learning rates is investigated in Fig. 5.3. It can be observed that the total reward increases as the number of episodes increases until it reaches a relatively stable value in three cases. This demonstrates that the proposed DRL-based algorithm is convergent. Specifically, as observed from Fig. 5.3, the oscillations for the large learning rate (of $\alpha = 0.05$), and its reward are lower than that of $\alpha = 0.01$. This indicates that a larger learning rate will result in local optimum instead of global optimum solutions. Also, if we set the small learning rate of $\alpha = 0.001$, it requires a relatively short time to achieve the convergence, but the reward is very low. Hence, we select a suitable learning rate of 0.01 for the following simulations, if not specified.

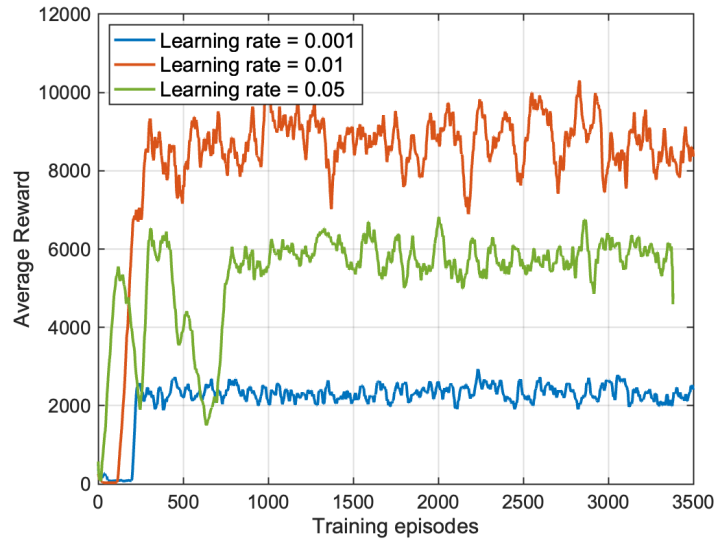


Figure 5.3. Average reward performance versus episodes under different learning rates.

5.4.2 Effect of Available Resources

In this subsection, we set the maximum service numbers to 10. The parameters in sensing request and communication requests are generated randomly and the results are averaged within 100 episodes. As can be seen from Fig. 5.4, the VoS changes are more sensitive to bandwidth resources. Even with more resources (*e.g.*, maximum power > 30 dBm, number of subchannels > 60), the average allocation cannot reach very high VoS without considering the user-specific needs and changeable environments. Compared with the heuristic approach, the DRL-based method has higher VoS under the same power and bandwidth situations. This improvement can be attributed to the dynamic allocation of bandwidth and power, taking into account changing environments and service requests. The VoS of sensing and communication is also presented in Fig.5.4. When using the DRL method, the VoS of communication is higher than the VoS of sensing under the same conditions, indicating the resource-hungry nature of sensing tasks in the integrated system. The VoS of communication with proposed DRL is *ca.* 0.2 higher than that of heuristic methods, showcasing the effective utilization of constrained bandwidth and power resources. This demonstrates the advantage of using the channel correlation in the time domain. It can also be observed that communication is more sensitive to subchannel variations compared to power variations.

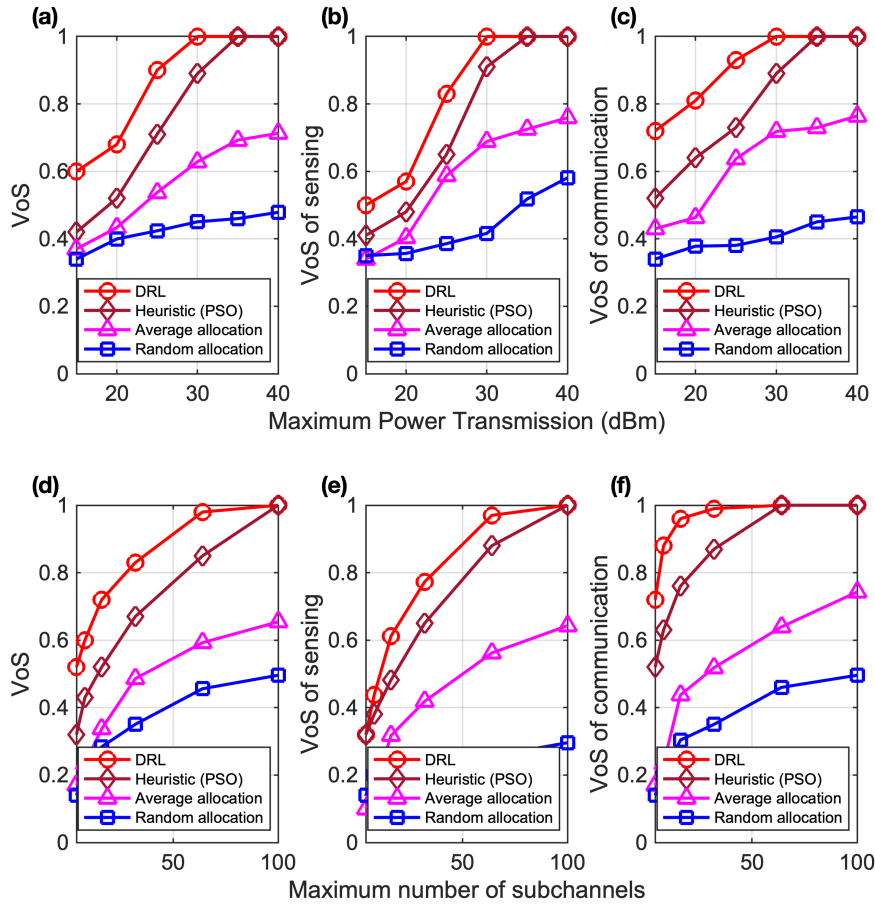


Figure 5.4. The VoS versus different resource conditions: different power constraints (left) and bandwidth constraints (right) with four different methods.

5.4.3 Effect of Service Request Number

We vary the maximum service request number from 1 to 20 to study the robustness of the algorithm. The increase in service requests indicates the increase in sensing reflection points and communication data. The total transmission power is set to 30 dBm and the maximum subchannel number is set to 64. Each result is the averaged VoS over 100 randomly generated environment settings, including the sensing/communication requests and channel states. The VoS v.s. different service request number using the proposed DRL algorithm and three other non-learning-based approaches is shown in Fig. 5.5. Due to the limited resources, it can be observed that the VoS decreases with increased service numbers in all cases. Compared with the heuristic method, the DRL method retains higher VoS. When the number of service requests exceeds 15, the DRL-based method can keep VoS above 0.9. This is because it adjusts

the allocation strategy and predicts the trends of changing environments and service requests, ultimately enhancing resource efficiency.

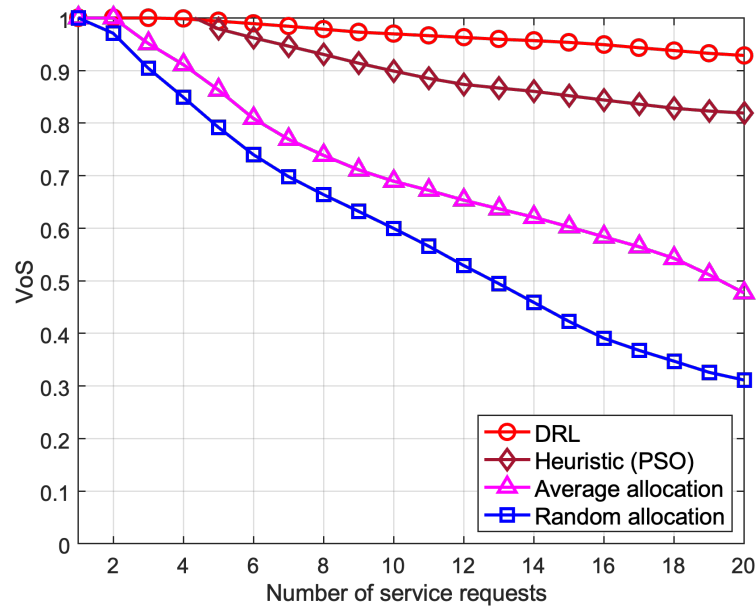


Figure 5.5. The VoS versus service request number with four different resource allocation methods.

5.4.4 Effect of Dynamic Situation

In this subsection, we evaluate the adaptiveness of the proposed scheme under dynamic situations involving different resource conditions. Five resource levels are examined as shown in Fig. 5.6. The CDF is obtained from 300 successive time steps. It can be observed that with increased power or bandwidth, the VoS becomes larger with a narrower distribution, indicating higher stability of the DRL method. Specifically, when the medium resource condition is satisfied (total subchannel number limit is 40 and power limit is 25 dBm), the variation of VoS during the successive process is less than 0.1. This demonstrates the situation-awareness service provisioning of the proposed resource allocation scheme.

From these results, it is demonstrated that the proposed scheme ensures consistent user-specific VoS performance in dynamic scenarios. Unlike baseline schemes, such as heuristic and average allocation, which rely solely on the information of the most recent time step for resource assignment, our proposed scheme leverages Markov properties over large time scales

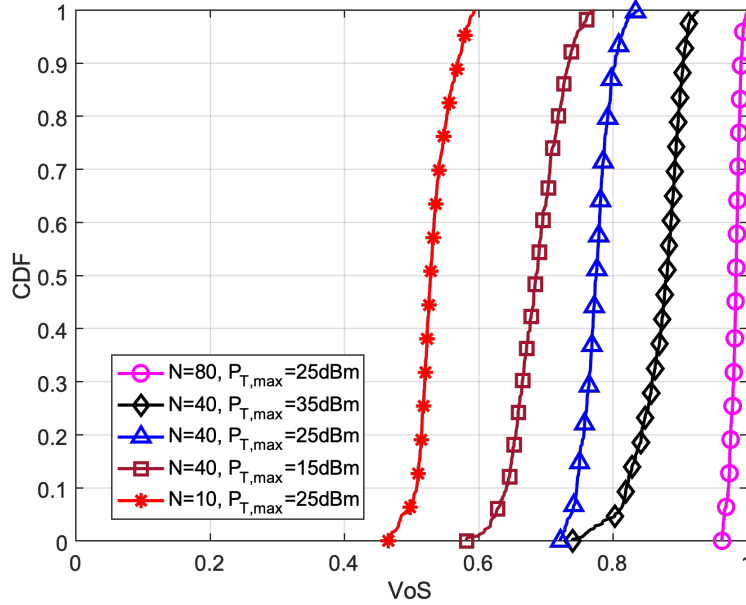


Figure 5.6. The CDF of VoS under different resource conditions with DRL method.

to predict state vectors. Moreover, the proposed scheme exhibits intelligent management of subchannel and power resources, adeptly addressing diverse service requests.

5.5 Chapter Summary

In this Chapter, we proposed a DRL-based successive resource allocation scheme to maximize the VoS in multi-user ISAC systems. An ISAC system mechanism was proposed to ensure adaptive resource allocation under dynamic environments and varying service requests. The bandwidth and power resource allocation problem was formulated as a mixed integer optimization problem and solved by a customized DRL framework. The numerical simulation results verified the adaptiveness and effectiveness of our proposed resource allocation scheme under dynamic environments.

Chapter 6

Value of Service Maximization in Multi-User ISAC Systems through Collaborative Resource Allocation

6.1 Introduction

6.1.1 Motivations

The unprecedented proliferation of wireless infrastructures and their ongoing convergence with diverse industrial applications brings new requirements for future wireless networks to provide situation-awareness functionalities. To achieve this goal, the integrated sensing and communication (ISAC) system [1, 4, 20, 108, 152] has been proposed, allowing for the concurrent exchange of data and sensing information on a unified wireless platform. By enabling dynamic sharing of the spectrum, hardware and signal processing procedures [1], ISAC unlocks the potential for application-specific service provisioning, especially in environment-aware scenarios including but not limited to automatic factory operations, intelligent robotics, and vehicle-to-everything communication.

Despite the promising potentials of ISAC, there are significant challenges that still need to be addressed, particularly in meeting stringent diverse application requirements and operation under highly constrained radio resource conditions [3]. These challenges arise from the inade-

quacy of traditional quality of service (QoS) evaluation indices in guiding resource allocation when confronted with heterogeneous service requests from coexisting users.

From the user's perspective, the wide variety of service requests combining sensing and communication reduces the effectiveness of existing resource allocation based on maximizing traditional QoS, which results in difficulty in ensuring an optimal service experience. Specifically, traditional QoS metrics focus on maximizing individual indicators and fail to consider the impact of user-specific needs and hardware capabilities on services. Given the heterogeneity in users' hardware capabilities and their corresponding requirements, the resource cost to achieve comparable levels of sensing/communication performance varies. Moreover, once a user's requests have been fulfilled, the value of allocating additional resources for achieving higher data rates or sensing accuracy decreases significantly. Thus, it is essential to develop a customized evaluation metric tailored to the specific service demands and capabilities at the user's end.

From the perspective of ISAC system operation, improving either individual sensing accuracy or communication data rate separately doesn't necessarily maximize the system's overall service value. This is because integrated systems aim to meet all user requests with shared resource constraints. Unlike individual goals, the system evaluation metric should prioritize both fairness of resource allocation among users and the overall resource utilization efficiency. For instance, allocating all available resources exclusively to a single user's urgent request is unwise, as it would render other users with no benefits. Hence, a fairness-guaranteed evaluation metric is critical in guiding the multi-user ISAC system design.

Another challenge in ISAC systems is the resource-hungry and environment-dependent nature of the sensing process, which leads to imbalanced and inefficient resource allocation. Device-free sensing is a resource-consuming process that requires multiple reference signals as measurements to reduce sensing errors. If a user has restricted hardware capabilities and high sensing requirements, its achievable sensing performance will be significantly limited. In addition, the sensing tasks for static or inanimate objects in the environment are generally less demanding compared to those involving important or sensitive targets [4]. Consequently, how to balance the multiple objectives of heterogeneous users while considering the trade-off between sensing and communication performance is a critical problem that must be tackled.

6.1.2 Related Work

ISAC systems design and evaluation have been widely studied in the literature [21–23, 153], aiming to optimize the resource allocation efficiency. Meanwhile, there is a growing research focus on collaborative wireless system design and modelling, driven by the increasing users' demands in sensing and communication.

To address the resource trade-off between sensing and communication, various resource allocation strategies and evaluation metrics have been proposed [24, 38, 40, 41]. The majority of works aimed to maximize sensing performance while using communication data rate as a constraint. For example, in [38], the objective was to improve the network's sensing accuracy while maintaining a specified sum rate for communication QoS. [24] aimed to maximize radar mutual information (MI) while constraining the communication channel's capacity for multiple connected automated vehicles (CAVs). [4] evaluated the detection QoS, localization QoS and tracking QoS with communication data rate as constraints. Certain works aimed to maximize data rates while ensuring an acceptable level of achievable sensing performance, as exemplified by [41]. Furthermore, some studies introduced mechanisms aiming at concurrently optimizing both sensing and communication performance. For instance, in [40], the power allocation problem was formulated to maximize the receive signal-to-interference-plus-noise ratio of the sensing signal and maximize the sum rate of communication. Nevertheless, given the diversity of service requests and stringent resource conditions, existing performance indicators often struggle to precisely demonstrate the effectiveness of user-tailored service provisioning.

To reduce the wireless system operation cost, collaborative resource allocation schemes were separately studied in wireless sensing [58], localization [60, 66] and communication systems [67]. Inspired by the cost-efficiency property of the collaborative scheme, collaborative ISAC systems were proposed in a number of recent studies [40, 154]. Using the collaboration scheme in ISAC mainly benefits in two ways. On one hand, collaborative strategies can enhance sensing efficiency by enabling multiple users to cooperate and improve the accuracy and reliability of sensing services [155]. On the other hand, collaborative strategies can guarantee a balanced resource allocation among heterogeneous users while ensuring efficient utilization of limited resources. Nevertheless, how to model multi-user collaborative sensing with the goal

of value of service maximization has not been discussed.

6.1.3 Contributions

Motivated by these considerations, this chapter aims to design a multi-user collaboration scheme to efficiently and fairly utilize the resources and maximize the value of service provisioning in an ISAC system. Recognizing the resource-intensive property of sensing operation, we consider collaborative sensing among users with a common region of interest (ROI). The base station (BS) allocates bandwidth and power resources to each user based on their specific service requests and sensing ROI. And the multiple users with a common ROI can collaboratively sense the targets and share the results. However, even with multi-user collaboration, resource competition remains as individual users seek to maximize their personal benefits. Thus, we utilize a bargaining game-based model to ensure fair resource allocation when formulating our optimization problem. The main contributions of the chapter are summarized as follows.

- (1) A multi-user collaborative mechanism in the ISAC system is proposed to improve service provisioning efficiency in resource-constrained scenarios. Several user-specified attributes, including the user's sensing/communication request, priority of service request and hardware capability, are incorporated to achieve heterogeneous service provisioning. A collaborative sensing strategy among users sharing the same ROI is introduced to improve the efficiency of power and bandwidth resource allocation. Through collaboration, even under stringent resource conditions, high complexity and resource-consuming sensing service requests of users can be achieved.
- (2) A two-level evaluation metric named VoS is utilized to guide the power and bandwidth resource allocation. The system-level VoS metric aims to enhance overall system resource allocation efficiency while guaranteeing fairness among users. The individual-level VoS metric is to maximize each user's sensing/communication service fulfillment with minimum resource consumption. Different from the existing designs and chapter 4 [139], this chapter's focus is on multi-user collaboration in ISAC systems, with the objective of maximizing VoS while ensuring fairness. To achieve this goal, three factors are considered in the VoS design, including users' specific service requests, sensing

ROI and individual service completeness. Simulation results show the effectiveness and adaptiveness of the proposed evaluation metric under stringent resource conditions.

- (3) A collaborative game-based resource allocation problem is modelled and the Nash bargaining solution is obtained with an iterative algorithm. In each iteration, the optimal bandwidth and power allocation for both communication and collaborative sensing are derived using the Lagrangian optimization method. Moreover, the designed scheme is evaluated by numerical simulations with different resource conditions, service requirements and channel states. The results demonstrate that the proposed collaborative resource allocation scheme outperforms the scheme without cooperation and the other two benchmark schemes.

Notations: In this chapter, lowercase bold letters and uppercase bold letters represent vectors and matrices, respectively. $(\cdot)^T$ and $(\cdot)^H$ represent the transposition and Hermitian transposition of a vector/matrix, respectively. $j = \sqrt{-1}$ is the imaginary number. $\|\mathbf{a}\|_2$ is the Euclidean norm. $\{\cdot\}^{Re}$ is the real component of complex variable $\{\cdot\}$.

The rest of this chapter is organized as follows. The system model and problem formulation of the proposed VoS-oriented multi-user collaborative ISAC system are established in Section 6.2. In Section 6.3, we model our problem as a bargaining game-based optimization problem and solve it by using an iteration algorithm. The numerical simulation results and performance analysis are provided in Section 6.4, followed by the conclusion in Section 6.5.

6.2 System Model

As depicted in Fig. 6.1, we consider an ISAC system with one BS, M' users and Q' sensing targets. The BS with a known position is equipped with a transmitter (Tx) antenna array comprising N_t elements. Each user, whose precise position is unknown, is associated with one device equipped with a receiver (Rx) antenna array consisting of N_r elements. Tx and Rx are both uniform linear arrays (ULA). The orthogonal frequency division multiplexing (OFDM) signals at the mm-wave band are used for communication and/or sensing service provisioning. In this chapter, both device-free and device-based sensing are considered. When the sensing

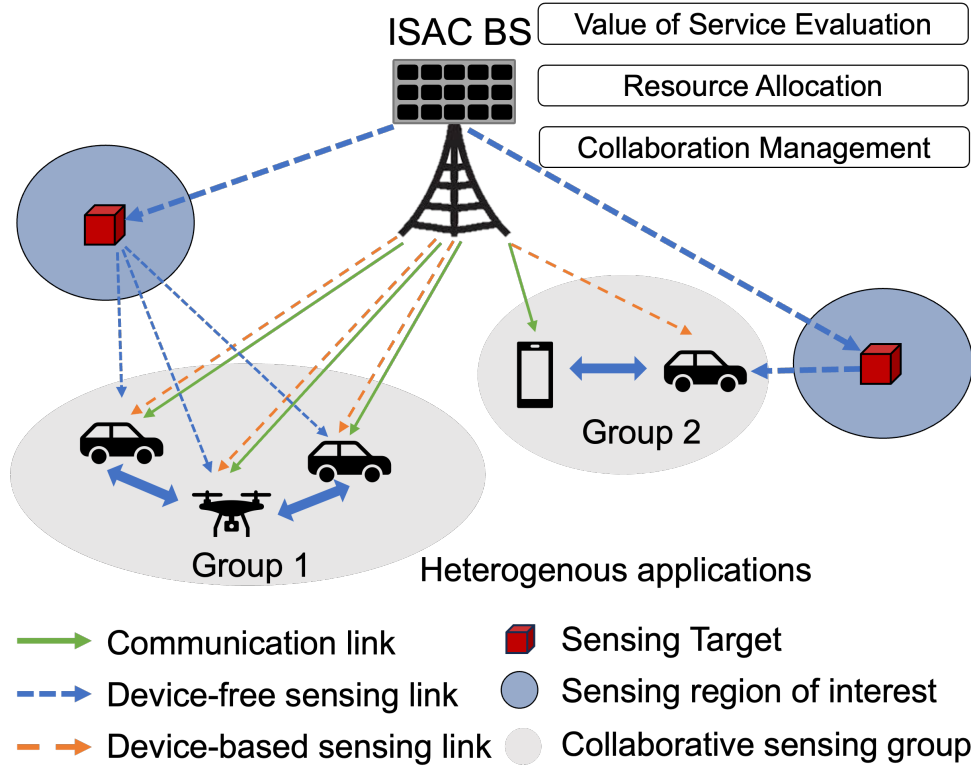


Figure 6.1. Illustration of collaborative sensing service provisioning in a multi-user ISAC system. Users within a group can collaborate in sensing and sharing the results.

targets are objects without carrying electronic devices, it's device-free sensing [156]. Otherwise, when the sensing target is the user itself, it's device-based sensing [144].

In the collaborative ISAC scheme, the total M' users are clustered into K collaborative sensing groups ($\sum_{k=1}^K M_k = M'$, M_k is the number of users in k -th cluster, $k = 1, 2, \dots, K$), according to the collaborative protocols [80]. The feature of users within the same cluster should exhibit a high correlation while having less correlation with users in other clusters. The relative positions and channel conditions are usually selected as similarity measurements. In this work, the similarity of users should be estimated from the position of users and sensing targets. The clustering process can be achieved with populated algorithms, e.g., K -means algorithm. Note that when one user doesn't belong to any cluster, it forms a group of one without including collaborative sensing process.

Let $\mathbf{SR}_{k,m} = [R_{k,m,req}, S_{k,m,req}]^T$ denote the service request for m -th user in k -th cluster. $R_{k,m,req}$ represents the data rate requirements (bit/s) and $1/S_{k,m,req}$ is the sensing accuracy re-

quirements ($[m]$) for its sensing target $Q_{k,m}$. Note that $Q_{k,m}$ can be individually sensed by its service requestor (*i.e.*, m -th user) or collaboratively sensed by other users within the k -th cluster. We assume that users in the same cluster share the sensing measurements. Note that the collaborative sensing is managed by the ISAC BS (Fig. 6.1) and primarily determined by sensing requests and resource availability. In resource-rich networks with low demands for sensing accuracy, sensing tasks are preferably allocated for local execution to avoid collaborative overheads. However, in situations where sensing tasks are challenging or impossible for the service requestor (SR) to complete, collaborative sensing is implemented. For instance, in target tracking scenarios, if the sensed target moves out of range from the SR, resulting in a significant drop in signal reception, other users close to the target are assigned to engage in collaborative sensing to meet the SR's sensing requirements.

The total bandwidth of ISAC system is B , which is divided into N subchannels denoted as $\mathcal{N} = \{1, 2, \dots, N\}$. Each subchannel has the same bandwidth B_0 . We introduce binary set $a_{k,m,n}, b_{k,m,n,m'} \in \{0, 1\}$ to denote the subchannel allocation. $a_{k,m,n} = 1$ means subchannel n is allocated to m -th user in k -th cluster for communication and $b_{k,m,n,m'} = 1$ means subchannel n is assigned to m -th user in k -th cluster for the sensing of target $Q_{k,m'}$. Here, we assume that the sensing targets move slowly, and the channel environment experienced by the signals from the BS to targets remains approximately time-invariant.

6.2.1 Communication Model

In the communication model, it is assumed that m -th user ($1 \leq m \leq M_k$) in k -th cluster associated with n -th subchannel ($1 \leq n \leq N$). The downlink transmitted symbols is $\mathbf{s}_n = [s_{n,1}, s_{n,2}, \dots, s_{n,N_s}]^T \in \mathbb{C}^{N_s \times 1}$, where N_s is the number of symbols. Let $\mathbf{F}_{k,m,n} = \mathbf{F}_{RF,k,m,n} \mathbf{F}_{BB,k,m,n} \in \mathbb{C}^{N_t \times N_s}$ denote the beamforming matrix, where $\mathbf{F}_{RF,k,m,n} \in \mathbb{C}^{N_t \times N_t^{RF}}$ is analog precoding matrix and $\mathbf{F}_{BB} \in \mathbb{C}^{N_t^{RF} \times N_s}$ is the digital beamformer matrix. N_t^{RF} is the number of radio frequency (RF) chains at the transmitter. The combiner at the receiver is denoted as $\mathbf{W}_{k,m,n}$. We assume that inaccurate location information of users is available at BS, which can be used for beamforming schemes [46]. It's assumed that both the communication channels and sensing channels are exclusively comprised of Line-of-Sight (LoS) paths, as Non-Line-of-Sight (NLoS) paths

experience attenuation at mmWave frequencies, as is considered in [1, 4, 154, 157, 158]. This assumption would lead to overestimated data rate performance due to the unavoidable NLoS effect. Then, the received communication signal $\mathbf{y}_{k,m,n}^{(c)}$ is

$$\mathbf{y}_{k,m,n}^{(c)} = \mathbf{W}_{k,m,n}^H \mathbf{H}_{k,m,n} \mathbf{F}_{k,m,n} \mathbf{s}_n + \mathbf{W}_{k,m,n}^H \mathbf{n}_{k,m,n}, \quad (6.1)$$

where the channel matrix $\mathbf{H}_{k,m,n} \in \mathbb{C}^{N_r \times N_t}$ is expressed as

$$\mathbf{H}_{k,m,n} = \sqrt{N_t N_r p_{k,m,n}} \times \frac{h_{k,m,n}}{\sqrt{\rho_{k,m,n}}} e^{-j2\pi \frac{n\tau_{k,m}}{NT_s}} \mathbf{A}_{k,m,r} \mathbf{A}_{k,m,t}^H. \quad (6.2)$$

In (6.2), $p_{k,m,n}$, $h_{k,m,n}$, $\rho_{k,m,n}$, T_s , $\tau_{k,m}$ denote the transmission power, complex channel gain, path loss, sampling period and the time-delay, respectively. The steering vector $\mathbf{A}_{k,m,t}$ and response vector $\mathbf{A}_{k,m,r}$ with ULA are written as

$$\mathbf{A}_{k,m,t}(\theta_{k,m}) = \frac{1}{\sqrt{N_t}} \times [e^{-j\frac{N_t-1}{2} \frac{2\pi}{\lambda_n} d \sin(\theta_{k,m})}, \dots, e^{j\frac{N_t-1}{2} \frac{2\pi}{\lambda_n} d \sin(\theta_{k,m})}]^T, \quad (6.3)$$

$$\mathbf{A}_{k,m,r}(\theta_{k,m}) = \frac{1}{\sqrt{N_r}} \times [e^{-j\frac{N_r-1}{2} \frac{2\pi}{\lambda_n} d \sin(\theta_{k,m})}, \dots, e^{j\frac{N_r-1}{2} \frac{2\pi}{\lambda_n} d \sin(\theta_{k,m})}]^T, \quad (6.4)$$

where $\theta_{k,m}$ is angle of departure (AOD), d is the distance between antenna elements ($d = \lambda_n/2$), and λ_n is the signal wavelength. $\mathbf{n}_{k,m,n}$ is the zero-mean additive white Gaussian noise (AWGN) with power σ_c^2 . It is assumed that the BS and user are synchronized to compensate for the Doppler effect and time delay. Based on Shannon's capacity formula, the achievable data rate of m -th user at subchannel n is

$$R_{k,m,n} = B_0 \log_2 (1 + \text{SNR}_{k,m,n}). \quad (6.5)$$

The interference between different users is omitted at receivers [4] and the signal-to-noise ratio is calculated with

$$\text{SNR}_{k,m,n} = p_{k,m,n} \xi_{k,m,n}, \quad (6.6)$$

where

$$\xi_{k,m,n} = \frac{N_r N_t h_{k,m,n} |\mathbf{W}_{k,m,n}^H \mathbf{A}_{k,m,r} \mathbf{A}_{k,m,t}^H \mathbf{F}_{k,m,n}|^2}{\rho_{k,m,n} \sigma_c^2}, \quad (6.7)$$

is the communication channel gain divided by the noise power. The achievable data rate is

$$R_{k,m}^{(c)} = \sum_{n=1}^N a_{k,m,n} R_{k,m,n}. \quad (6.8)$$

Let $\mathcal{N}_{k,m}^{(c)} = \{i_{k,m}^{(c)}, i_{k,m}^{(c)} + 1, \dots, i_{k,m}^{(c)} + N_{k,m}^{(c)}\}$ denote the set of allocated subchannels to m -th user in k -th cluster for communication, where $i_{k,m}^{(c)}$ is the initial index of subchannel and $N_{k,m}^{(c)}$ is the number of subchannels. Let $P_{k,m}^{(c)}$ denote the total power of $\mathcal{N}_{k,m}^{(c)}$ for user m in k -cluster. The optimal power assignment for each subchannel is $P_{k,m}^{(c)}/N_{k,m}^{(c)}$, which can be readily approved with inequality of arithmetic and geometric means (AM-GM inequality). Assume the complex channel gain and noise power are the same in $\mathcal{N}_{k,m}^{(c)}$, the achievable data rate can be further derived as

$$R_{k,m}^{(c)} = N_{k,m}^{(c)} B_0 \log_2 \left(1 + \frac{P_{k,m}^{(c)} \xi_{k,m}}{N_{k,m}^{(c)}} \right). \quad (6.9)$$

Denote $B_{k,m}^{(c)} = N_{k,m}^{(c)} B_0$, the achievable data rate can be expressed with $B_{k,m}^{(c)}$ and $P_{k,m}^{(c)}$, expressed as

$$R_{k,m}^{(c)} = B_{k,m}^{(c)} \log_2 \left(1 + \frac{B_0 P_{k,m}^{(c)} \xi_{k,m}}{B_{k,m}^{(c)}} \right). \quad (6.10)$$

To describe the communication fulfillment of individual users, we define the user-specific VoS of communication as [139]

$$V_{k,m}^{(c)} = \begin{cases} \frac{R_{k,m}^{(c)}}{R_{k,m,req}^{(c)}} & \text{if } R_{k,m}^{(c)} < R_{k,m,req}^{(c)} \\ 1 & \text{if } R_{k,m}^{(c)} \geq R_{k,m,req}^{(c)}. \end{cases} \quad (6.11)$$

If the achieved data rate meets or exceeds the specified requirement from user ($R_{k,m}^{(c)} \geq R_{k,m,req}^{(c)}$), the VoS of this communication service remains constant. Otherwise, the VoS of communication is proportional to the achievable data rate.

6.2.2 Sensing Model

Note that the general concept of sensing includes detection, localization and tracking. We only consider the localization of sensing targets in this work. In a bi-static sensing model, the BS transmits sensing reference signals to targets, and the user can resolve the target positions through the signal processing of reflected signals. We assume that the inaccurate position of the target in the range of interest is known [159]. The signal received by the m -th UE of k -th cluster in the time domain, assuming perfect time-frequency synchronization, can be expressed as

$$\mathbf{y}_{k,m,n} = \mathbf{y}_{k,m}^{(c)} + \sum_{m'} \mathbf{y}_{k,m,n,m'}^{(s)}. \quad (6.12)$$

Device-free sensing. In device-free sensing, the sensing target of user m can be any object, excluding itself. Suppose user m in k -th cluster localize $Q_{k,m'}$ with subchannel n . The signal received by m -th user from BS reflected by target $Q_{k,m'}$ is expressed as

$$\begin{aligned} \mathbf{y}_{k,m,n,m'}^{(s)} &= \sqrt{N_t N_r p_{k,m,n,m'}} \frac{h_{k,m,n,m'}}{\sqrt{\rho_{k,m,n,m'}}} e^{-\frac{j2\pi n \tau_{k,m,m'}}{NT_s}} \times \mathbf{W}_{k,m,n}^H \mathbf{A}_{k,m,r}(\phi_{k,m,m'}^{(s)}) \mathbf{A}_{k,m,t}^H(\theta_{k,m,m'}^{(s)}) \mathbf{F}_{k,m,n} \\ &\times \mathbf{s}_{ref} + \mathbf{W}_{k,m,n}^H \mathbf{w}_{k,m,m',n}, \end{aligned} \quad (6.13)$$

where $p_{k,m,n,m'}$, $h_{k,m,n,m'}$, $\rho_{k,m,n,m'}$ are the transmission power, complex channel gain, path loss, respectively. $\mathbf{w}_{k,m,m',n}$ is the AWGN with power σ_s^2 , and \mathbf{s}_{ref} is the transmitted sensing reference signal. $\tau_{k,m,m'}$ is the transmission time from BS to m -th user reflected by $Q_{k,m'}$, expressed as

$$\tau_{k,m,m'} = \frac{d_{BS,k,m'} + d_{k,m',m}}{c}, \quad (6.14)$$

$$d_{BS,k,m'} = \sqrt{(x_{BS} - x_{k,m'}^{(q)})^2 + (y_{BS} - y_{k,m'}^{(q)})^2}, \quad (6.15)$$

$$d_{k,m',m} = \sqrt{(x_{k,m} - x_{k,m'}^{(q)})^2 + (y_{k,m} - y_{k,m'}^{(q)})^2}. \quad (6.16)$$

In (6.14), c is the speed of light, $d_{BS,k,m'}$ is the distance between BS and $Q_{k,m'}$ while $d_{k,m',m}$ is the distance between $Q_{k,m'}$ and m -th user. The position of user m , BS, sensing target $Q_{k,m'}$ is denoted as $\mathbf{x}_{k,m} = [x_{k,m}, y_{k,m}]^T$, $\mathbf{x}_{BS} = [x_{BS}, y_{BS}]^T$, $\mathbf{x}_{k,m'}^{(q)} = [x_{k,m'}^{(q)}, y_{k,m'}^{(q)}]^T$, respectively. The steering and response vector function is same as (6.3, 6.4) where $\theta_{k,m,m'}^{(s)}$ is the AOD from BS to

$Q_{k,m'}$ and $\phi_{k,m,m'}^{(s)}$ is the AOA from $Q_{k,m'}$ to m -th user, in form of

$$\theta_{k,m,m'}^{(s)} = \arccos\left(\frac{x_{BS} - x_{k,m}}{\|\mathbf{x}_{k,m'}^{(q)} - \mathbf{x}_{BS}\|_2}\right), \phi_{k,m,m'}^{(s)} = \pi - \arccos\left(\frac{x_{k,m'}^{(q)} - x_{k,m}}{\|\mathbf{x}_{k,m'}^{(q)} - \mathbf{x}_{k,m}\|_2}\right). \quad (6.17)$$

Device-based sensing. When the sensing target $Q_{k,m'}$ is user m itself, the expression of received signal model by user m is similar to (6.13), by replacing both the angles $\theta_{k,m,m'}^{(s)}$, $\phi_{k,m,m'}^{(s)}$ with $\theta_{k,m}$. $\theta_{k,m}$ represents the AOD/AOA from BS to user m .

A commonly used wireless sensing metric is the Position Error Bound (PEB) of the sensing target, derived from the Fisher information matrix (FIM, $\mathbf{J}(\mathbf{x}_{k,m'}^{(q)})$) as

$$\mathbb{E}\left(\|\widehat{\mathbf{x}}_{k,m'}^{(q)} - \mathbf{x}_{k,m'}^{(q)}\|^2\right) \geq \text{tr}\{\mathbf{J}^{-1}(\mathbf{x}_{k,m'}^{(q)})\}, \quad (6.18)$$

where $\widehat{\mathbf{x}}_{k,m'}^{(q)}$ and $\mathbf{x}_{k,m'}^{(q)}$ are the estimation and true location of sensing target $Q_{k,m'}$. $\mathbb{E}(\cdot)$ denotes the expectation and $\text{tr}\{\cdot\}$ is the trace of matrix.

Instead of deriving the PEB directly, a more practical approach is to solve the Cramér–Rao low bound (CRLB) of $\tau_{k,m,m'}$, $\theta_{k,m,m'}^{(s)}$, $\phi_{k,m,m'}^{(s)}$ (or $\tau_{k,m}$, $\theta_{k,m}$ for device-based sensing). Denote $\boldsymbol{\eta}_{k,m,m'} = [\tau_{k,m,m'}, \theta_{k,m,m'}^{(s)}, \phi_{k,m,m'}^{(s)}]^T$, the FIM of $\boldsymbol{\eta}_{k,m,m'}$ is calculated by

$$\mathbf{J}_{\boldsymbol{\eta}_{k,m,m'}} = \mathbb{E}_{\boldsymbol{\eta}_{k,m,m'}} \left[-\frac{\partial^2 \ln f(\mathbf{y}_{k,m,m'}^{(s)} | \boldsymbol{\eta}_{k,m,m'})}{\partial \boldsymbol{\eta}_{k,m,m'} \partial \boldsymbol{\eta}_{k,m,m'}^T} \right], \quad (6.19)$$

where $f(\mathbf{y}_{k,m,m'}^{(s)} | \boldsymbol{\eta}_{k,m,m'})$ is the likelihood function of $\mathbf{y}_{k,m,m'}^{(s)}$ on $\boldsymbol{\eta}_{k,m,m'}$, as

$$f(\mathbf{y}_{k,m,m'}^{(s)} | \boldsymbol{\eta}_{k,m,m'}) = \frac{1}{(2\pi\sigma_s^2)^{N_{k,m,m'}^{(s)}}} \exp \left\{ \sum_n \text{Re} \left[\frac{1}{2\sigma_s^2} (\mathbf{H}_{k,m,n,m'}^{(s)} \mathbf{F}_{k,m,n} \mathbf{s}_{ref})^H \mathbf{y}_{k,m,n,m'}^{(s)} - \frac{1}{\sigma_s^2} |\mathbf{H}_{k,m,n,m'}^{(s)} \mathbf{F}_{k,m,n} \mathbf{s}_{ref}|^2 \right] \right\}, \quad (6.20)$$

$$\mathbf{H}_{k,m,n,m'}^{(s)} = \sqrt{N_t N_r p_{k,m,n,m'}} \frac{h_{k,m,n,m'}}{\sqrt{\rho_{k,m,n,m'}}} e^{-\frac{j2\pi n \tau_{k,m,m'}}{NT_s}} \mathbf{A}_{k,m,r}(\phi_{k,m,m'}^{(s)}) \mathbf{A}_{k,m,t}^H(\theta_{k,m,m'}^{(s)}). \quad (6.21)$$

Let $\mathcal{N}_{k,m,m'}^{(s)} = \{i_{k,m,m'}^{(s)}, \dots, i_{k,m,m'}^{(s)} + N_{k,m,m'}^{(s)}\}$ denote the set of allocated subchannels to m -th user

in k -th cluster for sensing task $Q_{k,m'}$, where $i_{k,m,m'}^{(s)}$ is the initial index of subchannel and $N_{k,m,m'}^{(s)}$ is the number of subchannels. Then the total bandwidth allocated to sensing is expressed as $B_{k,m,m'}^{(s)} = N_{k,m,m'}^{(s)} B_0$. In principle, both $B_{k,m}^{(c)}$ and $B_{k,m,m'}^{(s)}$ can only multiple times of B_0 . Herein, $B_{k,m}^{(c)}$ and $B_{k,m,m'}^{(s)}$ are relaxed to be continuous variables in the following discussions. After the optimization of continuous bandwidth, discretization can be performed to obtain the number of subchannels [139].

The derivation of $\mathbf{J}_{\eta_{k,m,m'}}$ with respect to $B_{k,m,m'}^{(s)}$ and total power for sensing $P_{k,m,m'}^{(s)}$ is shown in Appendix B.1. Then, the $\text{PEB}_{k,m,m'}$ can be approximated with

$$\text{PEB}_{k,m,m'} \approx \frac{\zeta_{k,m,m'}}{\sqrt{N_{k,m,m'}^{(s)} P_{k,m,m'}^{(s)}}}. \quad (6.22)$$

where the coefficient $\zeta_{k,m,m'}$ is related to bandwidth, antenna array, channel gain, noise power, and position of sensing targets and users (expression can be found in Appendix B.2). Without loss of generality, we introduce $0 \leq \alpha \leq 1$ and $0 \leq \beta \leq 1$ as power index to model the PEB as

$$\frac{1}{\text{PEB}_{k,m,m'}} \approx \kappa_{k,m,m'} P_{k,m,m'}^{(s)\alpha} B_{k,m,m'}^{(s)\beta}, \quad (6.23)$$

where $\kappa_{k,m,m'} = \vartheta_{k,m} / \zeta_{k,m,m'}$ and $0 \leq \vartheta_{k,m} \leq 1$ are the relative sensing capability of the device. The coefficient involves the constants related to the system configuration, signal designs, imperfect beamforming gain, filtering gain and the signal processing algorithms.

In the collaborative sensing scheme, the PEB on $Q_{k,m'}$ can be expressed as the geometrical sum of $\text{PEB}_{k,m,m'}$ as

$$\frac{1}{\text{PEB}_{k,m'}} = \underbrace{\frac{1}{\text{PEB}_{k,m',m'}}}_{\text{Non-collaborative term}} + \underbrace{\sum_{m=1, m \neq m'}^{M_k} \frac{1}{\text{PEB}_{k,m,m'}}}_{\text{Collaborative term}}, \quad (6.24)$$

where the non-collaborative term represents the sensing performance the m' -th user can get by itself, and the collaborative term is the performance improvement with the assistance of other collaborators, as illustrated in Fig. 6.2.

Similar to the communication model, the individual VoS of sensing $V_{k,m}^{(s)}$ is calculated

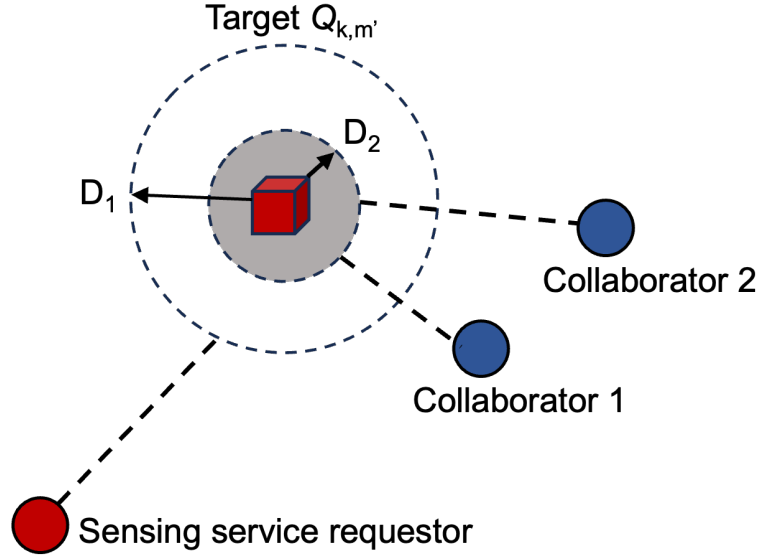


Figure 6.2. Illustration of position error bounds with collaborative and non-collaborative sensing scheme (D_1 : Sensing PEB without collaboration; D_2 : Sensing PEB with collaboration).

by the requested sensing accuracy over achievable sensing accuracy. Introducing $V_{k,m}^{\prime(s)} = \sum_{i=1}^{M_k} \frac{K_{k,i,m} P_{k,i,m}^{(s)\alpha} B_{k,i,m}^{(s)\beta}}{S_{k,m,req}}$, the $V_{k,m}^{(s)}$ is represented as

$$V_{k,m}^{(s)} = \begin{cases} \sum_{i=1}^{M_k} \frac{K_{k,i,m} P_{k,i,m}^{(s)\alpha} B_{k,i,m}^{(s)\beta}}{S_{k,m,req}} & \text{if } V_{k,m}^{\prime(s)} < 1 \\ 1 & \text{otherwise.} \end{cases} \quad (6.25)$$

6.2.3 Problem Formulation

The VoS of each user can be written as the weighted sum of VoS of communication and sensing

$$V_{k,m} = w_{k,m}^{(c)} V_{k,m}^{(c)} + w_{k,m}^{(s)} V_{k,m}^{(s)}. \quad (6.26)$$

where $w_{k,m}^{(c)}$ and $w_{k,m}^{(s)}$ are the weight of communication and sensing for m -th user in k -th cluster. With different $w_{k,m}^{(c)}$ and $w_{k,m}^{(s)}$ ($w_{k,m}^{(c)} + w_{k,m}^{(s)} = 1, 0 \leq w_{k,m}^{(c)} \leq 1, 0 \leq w_{k,m}^{(s)} \leq 1$), the service can be communication-centric, sensing-centric or integrated sensing and communication requests.

Then the total VoS of the ISAC system is expressed as

$$V = \prod_{k=1}^K \prod_{m=1}^{M_k} V_{k,m}. \quad (6.27)$$

When collaborative sensing is included, there is collaborative overhead with sensing coordination, information exchange, etc., which are mainly determined by the number of users involved in the collaboration. For k -th cluster, the overhead increases monotonically to the number of non-zero entries in $[B_{k,m,m'}^{(s)}]_{m=1:M_k, m'=1:M_k}$. In this work, we consider the overhead condition with all collaboration established, which gives fixed overhead and eliminated in the objective function, for simplicity.

In this chapter, our goal is to maximize the VoS of an ISAC system through allocating the available resources $\mathbf{P} = [P_{k,m}^{(c)}, P_{k,m,m'}^{(s)}]_{k=1:K, m=1:M_k, m'=1:M_k}$, $\mathbf{B} = [B_{k,m}^{(c)}, B_{k,m,m'}^{(s)}]_{k=1:K, m=1:M_k, m'=1:M_k}$, with respect to $V_{k,m}$ while guaranteeing fairness among multiple users within each group, formulated as P

$$\begin{aligned}
 & \mathbf{P} : \max_{\mathbf{P}, \mathbf{B}} U(V_{k,m}) & (6.28) \\
 s.t. \quad & C1 : \sum_{k=1}^K \left(\sum_{m=1}^{M_k} P_{k,m}^{(c)} + \sum_{i=1}^{M_k} \sum_{j=1}^{M_k} P_{k,i,j}^{(s)} \right) \leq P_{max}, \\
 & C2 : \sum_{k=1}^K \left(\sum_{m=1}^{M_k} B_{k,m}^{(c)} + \sum_{i=1}^{M_k} \sum_{j=1}^{M_k} B_{k,i,j}^{(s)} \right) \leq B_{max}, \\
 & C3 : \sum_{j=1}^{M_k} P_{k,m,j}^{(s)} + P_{k,m}^{(c)} \leq P_{k,m,max}, \forall k, m, \\
 & C4 : \sum_{j=1}^{M_k} B_{k,m,j}^{(s)} + B_{k,m}^{(c)} \leq B_{k,m,max}, \forall k, m, \\
 & C5 : \sum_{k=1}^K \sum_{i=1}^{M_k} \sum_{j=1}^{M_k} P_{k,i,j}^{(s)} \leq P_{s,max}, \\
 & C6 : \sum_{k=1}^K \sum_{i=1}^{M_k} \sum_{j=1}^{M_k} B_{k,i,j}^{(s)} \leq B_{s,max},
 \end{aligned}$$

where $U(V_{k,m})$ is the utility function of the ISAC system to describe the fulfillment of users' service requests, determined by the VoS of each user. Constraint C1 indicates that the limit of total power for total users is smaller than P_{max} , while C2 is the total bandwidth resource limitation. Constraints C3 and C4 are the limits of the transmission power and bandwidth to m -th user in k -th cluster. C5 and C6 are the maximum power and bandwidth constraints of sensing for all users. C5 and C6 are introduced as resource budgets for sensing, which

reflects the property of the ISAC system covering sensing-centric, communication-centric or joint types.

6.3 Methodology

In this section, we begin by presenting the bargaining game model in a multi-user ISAC system. Subsequently, the resource allocation problem is formulated using VoS as the utility function. Finally, an iterative algorithm is developed for bargaining-based resource allocation.

6.3.1 Collaborative Resource Allocation Game Formulation

In our considered scenario, the players in the game are the ISAC users. The resources include the power and bandwidth (\mathbf{P}, \mathbf{B}). If there exists the Nash Equilibrium (NE), it indicates that none of the users can benefit more by changing its own resource allocation unilaterally. The NE serves as the stable solution for a non-collaborative game, assuming its existence and uniqueness. However, in non-collaborative strategy, all the users in a game with conflicting interests will act selfishly to maximize their own value functions, which may not result in the Pareto optimal solution.

Therefore, the collaborative Nash bargaining resource allocation game (NBPAG) is modelled. In a multi-player game, there exists an unbounded set of Pareto optimal points. Thus, it is crucial to establish a criterion to identify the optimal Pareto point of the system. One criterion is to allocate the resources considering the user fairness [160]. Under this criterion, the Nash bargaining solution (NBS) not only ensures the uniqueness of the Pareto optimal point but also guarantees its fairness, when satisfying axioms delineated in [66].

Existence of NBS. There is at least one NBS existing of the NBPAG in P when two criteria are satisfied. (i) $\forall i$, the resource vector x_i is a non-empty, convex, and compact subset of Euclidean space; (ii) $\forall i$, the utility functions $f_m(\mathcal{X}_m, \mathcal{X}_{m', m' \neq m})$ are continuous and quasi-concave in \mathcal{X}_m .

Proof. See [161].

Uniqueness of NBS. The NBS to NBPAG is unique.

Proof. See [161–163].

With NBS [66, 164], we define the utility function U in \mathbf{P} as

$$U(V_{k,m}, V_{k,m,\min}) = \prod_{k=1}^K \prod_{m=1}^{M_k} (V_{k,m} - V_{k,m,\min}), \quad (6.29)$$

where $V_{k,m,\min}$ is the minimum VoS requirements of user m in cluster k . Note that when $V_{k,m,\min} = 0$, $U(V_{k,m}, V_{k,m,\min}) = V$. Then, the problem \mathbf{P} can be reformulated as

$$\begin{aligned} \mathbf{P}_1 : \max_{\mathbf{P}, \mathbf{B}} & \sum_{k=1}^K \sum_{m=1}^{M_k} \ln(V_{k,m} - V_{k,m,\min}) \\ & s.t. \text{ C1} - \text{C6}. \end{aligned} \quad (6.30)$$

Proposition 1. The problem \mathbf{P}_1 is convex over a convex set and there is a unique optimal NBS when $0 < \alpha \leq 1, 0 < \beta \leq 1$.

Proof. See Appendix B.3.

Proposition 2. The utility function $U(V_{k,m}, V_{k,m,\min})$ presented in equation (6.29) conforms to the principles outlined in the Nash Bargaining theorem and satisfies the criterion of proportional fairness.

Proof. See Appendix B.4.

The primal problem \mathbf{P}_1 can be converted into the dual domain with the Lagrangian function. Note that we have relaxed the number of subchannels to be continuous. This actually approximates the nonconvex problem to be convex. The duality gap of a nonconvex optimization problem tends towards zero in multichannel systems with a sufficiently large number of subchannels [165]. In practical systems, this often translates to a typical configuration of more than 50 resource blocks (RBs) for 5G and beyond. The dual problem for P_1 can be written as

$$\begin{aligned} \min_{\mathbf{P}, \mathbf{B}, \lambda} & \mathcal{L}(\mathbf{P}, \mathbf{B}, \lambda). \\ & s.t. \text{ C1} - \text{C6}, \\ & \lambda \geq 0. \end{aligned} \quad (6.31)$$

where $\lambda = [\lambda_p, \lambda_b, \lambda_{p,s}, \lambda_{b,s}, \lambda_{p,k,m}, \lambda_{b,k,m}]$ are a set of Lagrangian multipliers related to the power

and bandwidth constraints. The expression of the Lagrangian function is shown in (6.32). From the definition of VoS in Equ. (6.11,6.25), the Lagrangian function is a piecewise function depending on the resource conditions and service numbers. The discussion of the following subsections considers the resource-deficient scenarios. During the updates of bandwidth and power, if the VoS of communication/sensing reaches 1, the allocated bandwidth and power are restricted with the value at VoS of 1. Then the dual problem can be solved iteratively using the corresponding Karush-Kuhn-Tucker (KKT) [166] solutions in each iteration.

$$\begin{aligned}
\mathcal{L}(\mathbf{P}, \mathbf{B}, \boldsymbol{\lambda}) = & \sum_{k=1}^K \sum_{m=1}^M \ln(V_{k,m} - V_{k,m,\min}) + \lambda_p \left(P_{\max} - \sum_{k=1}^K \left(\sum_{m=1}^{M_k} P_{k,m}^{(c)} + \sum_{i=1}^{M_k} \sum_{j=1}^{M_k} P_{k,i,j}^{(s)} \right) \right) + \lambda_b \left\{ B_{\max} - \right. \\
& \left. \sum_{k=1}^K \left(\sum_{m=1}^{M_k} B_{k,m}^{(c)} + \sum_{i=1}^{M_k} \sum_{j=1}^{M_k} B_{k,i,j}^{(s)} \right) \right\} + \sum_{k=1}^K \sum_{m=1}^{M_k} \lambda_{p,k,m} \left(P_{k,m,\max} - \sum_{j=1}^{M_k} P_{k,m,j}^{(s)} + P_{k,m}^{(c)} \right) + \sum_{k=1}^K \sum_{m=1}^{M_k} \lambda_{b,k,m} \left\{ B_{k,m,\max} \right. \\
& \left. - \sum_{j=1}^{M_k} B_{k,m,j}^{(s)} + B_{k,m}^{(c)} \right\} + \lambda_{p,s} \left(P_{s,\max} - \sum_{k=1}^K \sum_{i=1}^{M_k} \sum_{j=1}^{M_k} P_{k,i,j}^{(s)} \right) + \lambda_{b,s} \left(B_{s,\max} - \sum_{k=1}^K \sum_{i=1}^{M_k} \sum_{j=1}^{M_k} B_{k,i,j}^{(s)} \right).
\end{aligned} \tag{6.32}$$

6.3.2 Power Allocation Update

We first consider the optimal power allocation of communication and collaborative sensing with fixed bandwidth allocation. Based on the KKT conditions, the power allocation for communication of m -th user in k -th cluster can be obtained through taking the first derivative of \mathcal{L} with respect to $P_{k,m}^{(c)}$ as

$$\frac{\partial \mathcal{L}(\mathbf{P}, \mathbf{B}, \boldsymbol{\lambda})}{\partial P_{k,m}^{(c)}} = \frac{w_{k,m}^{(c)}}{R_{k,m,\text{req}}(V_{k,m} - V_{k,m,\min}) \ln 2} \times \frac{B_0 \xi_{k,m}}{B_{k,m}^{(c)} + P_{k,m}^{(c)} B_0 \xi_{k,m}} - \lambda_p - \lambda_{p,k,m}. \tag{6.33}$$

Here, we introduce

$$\tilde{P}_{k,m}^{(c)} = 1 + \frac{P_{k,m}^{(c)} \xi_{k,m} B_0}{B_{k,m}^{(c)}}. \tag{6.34}$$

Substitute (6.34) into (6.33) and use KKT condition, $\forall k, m$

$$\left[w_{k,m}^{(c)} B_{k,m}^{(c)} \ln \tilde{P}_{k,m}^{(c)} + R_{k,m,req} (w_{k,m}^{(s)} V_{k,m}^{(s)} - V_{k,m,min}) \ln 2 \right] \times (\lambda_p + \lambda_{p,k,m}) \tilde{P}_{k,m}^{(c)} - w_{k,m}^{(c)} B_{k,m}^{(c)} \xi_{k,m} B_0 = 0. \quad (6.35)$$

The (6.35) is a transcendental algebraic equation involving $B_{k,m}^{(c)}$. So this equation can be re-solved using iterative numerical techniques. With the Lambert-W function, the zero point $\tilde{P}_{k,m}^{(c)*}$ of (6.35) in terms of $\lambda_{m,c}$ can be derived as

$$\tilde{P}_{k,m}^{(c)*} = \exp \left[\frac{1}{a_{k,m}^{(1)}} W \left(b_{k,m}^{(1)} \cdot e^{\frac{c_{k,m}^{(1)}}{a_{k,m}^{(1)}}} \right) - \frac{1}{a_{k,m}^{(1)}} \right], \quad (6.36)$$

where

$$a_{k,m}^{(1)} = w_{k,m}^{(c)} B_{k,m}^{(c)}, b_{k,m}^{(1)} = \frac{w_{k,m}^{(c)} B_{k,m}^{(c)} \xi_{k,m} B_0}{\lambda_p + \lambda_{p,k,m}}, \quad (6.37)$$

$$c_{k,m}^{(1)} = R_{k,m,req} (w_{k,m}^{(s)} V_{k,m}^{(s)} - V_{k,m,min}) \ln 2. \quad (6.38)$$

Thus, with fixed bandwidth allocation and power allocation for sensing, the optimal power allocation for communication can be updated from (6.34) and (6.36).

Given the power allocation for communication, the power assignment $P_{k,i,m}^{(s)}$ of i -th user in k -th cluster for collaborative sensing of $Q_{k,m}$ need to be considered. By taking the first derivative of $\mathcal{L}(\mathbf{P}, \mathbf{B}, \lambda)$ with respect to $P_{k,i,m}^{(s)}$ and using KKT condition $\frac{\partial \mathcal{L}}{\partial P_{k,i,m}^{(s)}} = 0, \forall k, i, m$, there's

$$d_{k,i,m}^{(1)} P_{k,i,m}^{\alpha-1} = e_{k,i,m}^{(1)} + \sum_{i=1}^{M_k} \kappa_{k,i,m} P_{k,i,m}^{(s)\alpha} B_{k,i,m}^{(s)\beta}, \quad (6.39)$$

where

$$d_{k,i,m}^{(1)} = \frac{\kappa_{k,i,m} \alpha B_{k,i,m}^{(s)\beta}}{\lambda_p + \lambda_{p,s} + \lambda_{b,k,m}}, e_{k,i,m}^{(1)} = \frac{S_{k,m,req}}{w_{k,m}^{(s)}} (w_{k,m}^{(c)} V_{k,m}^{(c)} - V_{k,m,min}). \quad (6.40)$$

Note that (6.39) is a multivariable equation due to the second term on the right side. If k, m is

fixed, the second term will be the same. Thus, for (6.39) with k, i, m and k, i', m ($i \neq i'$), there is

$$\mathfrak{d}_{k,i,m}^{(1)} P_{k,i,m}^{\alpha-1} - e_{k,i,m}^{(1)} = \mathfrak{d}_{k,i',m}^{(1)} P_{k,i',m}^{\alpha-1} - e_{k,i',m}^{(1)}. \quad (6.41)$$

Denote $\tilde{P}_{k,i,m}^{(s)} = \mathfrak{d}_{k,i,m}^{(1)} P_{k,i,m}^{\alpha-1} - e_{k,i,m}^{(1)}$, there is

$$\tilde{P}_{k,i,m}^{(s)} = \sum_{i'=1}^{M_k} \kappa_{k,i',m} B_{k,i',m}^{(s)\beta} \left[\left(\tilde{P}_{k,i,m}^{(s)} + e_{k,i',m}^{(1)} \right) / \mathfrak{d}_{k,i',m}^{(1)} \right]^{\frac{\alpha}{\alpha-1}}. \quad (6.42)$$

There's no closed-form solution of (6.42). But we can have an approximation solution through the Taylor series. By expanding function $(x+b)^{\frac{\alpha}{\alpha-1}}$ to the first-order, there is

$$\tilde{P}_{k,i,m}^{(s)} \approx \sum_{i'=1}^{M_k} \frac{\kappa_{k,i',m} B_{k,i,m}^{(s)\beta}}{\mathfrak{d}_{k,i',m}^{(1)\frac{\alpha}{\alpha-1}}} \left(\frac{\alpha}{\alpha-1} e_{k,i',m}^{(1)\frac{1}{\alpha-1}} \tilde{P}_{k,i,m}^{(s)} + e_{k,i',m}^{(1)\frac{\alpha}{\alpha-1}} \right). \quad (6.43)$$

Note that high-order approximations up to three with quadratic or cubic equations can be derived in a similar manner. Thus, with given bandwidth allocation, the optimal power allocation $\tilde{P}_{k,i,m}^{(s)*}$ by solving equation (6.43) for collaborative sensing to first-order approximation is expressed as

$$\tilde{P}_{k,i,m}^{(s)*} \approx \sum_{i'=1}^{M_k} \frac{\kappa_{k,i',m} B_{k,i,m}^{(s)\beta} e_{k,i',m}^{(1)\frac{\alpha}{\alpha-1}}}{\mathfrak{d}_{k,i',m}^{(1)\frac{\alpha}{\alpha-1}}} / \left(1 - \sum_{i'=1}^{M_k} \frac{\kappa_{k,i',m} B_{k,i,m}^{(s)\beta}}{\mathfrak{d}_{k,i',m}^{(1)\frac{\alpha}{\alpha-1}}} \frac{\alpha}{\alpha-1} e_{k,i',m}^{(1)\frac{1}{\alpha-1}} \right). \quad (6.44)$$

6.3.3 Bandwidth Allocation Update

Then, we give the bandwidth allocation of communication and collaborative sensing with a fixed power level. For the bandwidth allocation of communication, the first-order derivative of \mathcal{L} with respect to $B_{m,c}$ is

$$\frac{\partial \mathcal{L}(\mathbf{P}, \mathbf{B}, \lambda)}{\partial B_{k,m}^{(c)}} = \frac{W_{k,m}^{(c)}}{R_{k,m,req}(V_{k,m} - V_{k,m,min}) \ln 2} \times \left[\ln \left(1 + \frac{P_{k,m}^{(c)} B_0 \xi_{k,m}}{B_{k,m}^{(c)}} \right) - \frac{P_{k,m}^{(c)} B_0 \xi_{k,m}}{B_{k,m}^{(c)} + P_{k,m}^{(c)} B_0 \xi_{k,m}} \right] - \lambda_b - \lambda_{b,k,m}. \quad (6.45)$$

With $\widetilde{B}_{k,m}^{(c)} = 1 + \frac{P_{k,m}^{(c)} B_0 \xi_{k,m}}{B_{k,m}^{(c)}}$ and KKT condition, there is

$$\alpha_{k,m}^{(2)} \left(\ln \widetilde{B}_{k,m}^{(c)} + \frac{1}{\widetilde{B}_{k,m}^{(c)}} - 1 \right) - \frac{\ln \widetilde{B}_{k,m}^{(c)}}{\widetilde{B}_{k,m}^{(c)} - 1} - \mathfrak{b}_{k,m}^{(2)} = 0, \quad (6.46)$$

where

$$\alpha_{k,m}^{(2)} = \frac{1}{P_{k,m}^{(c)} \xi_{k,m} B_0 (\lambda_b + \lambda_{b,k,m})}, \quad \mathfrak{b}_{k,m}^{(2)} = \frac{(w_{k,m}^{(s)} V_{k,m}^{(s)} - V_{k,m,\min}) R_{k,m,req} \ln 2}{w_{k,m}^{(c)} P_{k,m}^{(c)} \xi_{k,m} B_0}. \quad (6.47)$$

Then, (6.46) can be rewritten as

$$\left(\widetilde{B}_{k,m}^{(c)} - 1 - \frac{1}{\alpha_{k,m}^{(2)}} \right) \widetilde{B}_{k,m}^{(c)} \ln \widetilde{B}_{k,m}^{(c)} + (-\widetilde{B}_{k,m}^{(c)} + 1) \times \left[\left(\frac{\mathfrak{b}_{k,m}^{(2)}}{\alpha_{k,m}^{(2)}} - 1 \right) \widetilde{B}_{k,m}^{(c)} + 1 \right] = 0. \quad (6.48)$$

However, (6.48) doesn't have analytic solution, even with special functions. Thus, we cannot directly obtain the explicit expression. Let $g(t) = (t-1 - \frac{1}{\alpha_{k,m}^{(2)}})t \ln t + (-t+1) \left[\left(\frac{\mathfrak{b}_{k,m}^{(2)}}{\alpha_{k,m}^{(2)}} - 1 \right)t + 1 \right]$, $t > 1$. It is easy to verify that when $\lim_{t \rightarrow 1} g(t) = 0$ and $\lim_{t \rightarrow \infty} g(t) = +\infty$, $g'(1) = -\frac{1+\mathfrak{b}_{k,m}^{(2)}}{\alpha_{k,m}^{(2)}} < 0$. Therefore, there's at least one zero point in $\widetilde{B}_{k,m}^{(c)} > 1$ and can be found with the bisection method in $O(\log_2(\mathfrak{R} - 1))$, where \mathfrak{R} is the endpoint of the initial interval.

For the bandwidth allocation in collaborative sensing, the dual role of power and bandwidth in the expression with different power indexes α and β is considered. The derivation is similar to power allocation for sensing in Section 6.3.2,

$$\mathfrak{d}_{k,i,m}^{(2)} = \frac{\kappa_{k,i,m} \beta P_{k,i,m}^{(s)\alpha}}{\lambda_p + \lambda_{p,s} + \lambda_{b,k,m}}, \quad (6.49)$$

$$\mathfrak{e}_{k,i,m}^{(2)} = \frac{S_{k,m,req}}{w_{k,m}^{(s)}} (w_{k,m}^{(c)} V_{k,m}^{(c)} - V_{k,m,\min}). \quad (6.50)$$

The optimal bandwidth assignment for collaborative sensing is expressed as

$$\widetilde{B}_{k,i,m}^{(s)} = \sum_{i'=1}^{M_k} \kappa_{k,i',m} P_{k,i',m}^{(s)\alpha} \left[\left(\widetilde{B}_{k,i,m}^{(s)} + \mathfrak{e}_{k,i',m}^{(2)} \right) / \mathfrak{d}_{k,i',m}^{(2)} \right]^{\frac{\beta}{\beta-1}}, \quad (6.51)$$

where

$$\widetilde{B}_{k,i,m}^{(s)} = d_{k,i,m}^{(2)} B_{k,i,m}^{\alpha-1} - e_{k,i,m}^{(2)}. \quad (6.52)$$

Therefore, the optimal bandwidth allocation to first-order approximation is

$$\widetilde{B}_{k,i,m}^{(s)*} \approx \sum_{i'=1}^{M_k} \frac{\kappa_{k,i',m} P_{k,i,m}^{(s)\alpha} \mathcal{B}'_{k,i',m} \frac{\beta}{\beta-1}}{\mathcal{A}'_{k,i',m} \frac{\beta}{\beta-1}} / \left(1 - \sum_{i'=1}^{M_k} \frac{\kappa_{k,i',m} P_{k,i,m}^{(s)\alpha}}{\mathcal{A}'_{k,i',m} \frac{\beta}{\beta-1}} \frac{\beta}{\beta-1} \mathcal{B}'_{k,i',m} \frac{1}{\beta-1} \right). \quad (6.53)$$

6.3.4 Iterative Algorithm Design

Given the derivation of power and bandwidth allocation for communication and collaborative sensing services, the dual variables need to be updated iteratively [66]. Herein, we use $0 \leq j < J^{max}$ represents the iteration number, and $j \in N^+$. J^{max} is the maximum iteration number. In this work, the subgradient approach is utilized to update λ . In the $(j+1)$ -th iteration, there are

$$\lambda_p^{(j+1)} = \lambda_p^{(j)} - \gamma_1^{(j)} \left. \frac{\partial \mathcal{L}}{\partial \lambda_p} \right|_{\lambda_p^{(j)}}, \quad (6.54)$$

$$\lambda_b^{(j+1)} = \lambda_b^{(j)} - \gamma_2^{(j)} \left. \frac{\partial \mathcal{L}}{\partial \lambda_b} \right|_{\lambda_b^{(j)}}, \quad (6.55)$$

$$\lambda_{b,k,m}^{(j+1)} = \lambda_{b,k,m}^{(j)} - \gamma_3^{(j)} \left. \frac{\partial \mathcal{L}}{\partial \lambda_{b,k,m}} \right|_{\lambda_{b,k,m}^{(j)}}, \quad (6.56)$$

$$\lambda_{p,k,m}^{(j+1)} = \lambda_{p,k,m}^{(j)} - \gamma_4^{(j)} \left. \frac{\partial \mathcal{L}}{\partial \lambda_{p,k,m}} \right|_{\lambda_{p,k,m}^{(j)}}, \quad (6.57)$$

$$\lambda_{p,s}^{(j+1)} = \lambda_{p,s}^{(j)} - \gamma_5^{(j)} \left. \frac{\partial \mathcal{L}}{\partial \lambda_{p,s}} \right|_{\lambda_{p,s}^{(j)}}, \quad (6.58)$$

$$\lambda_{b,s}^{(j+1)} = \lambda_{b,s}^{(j)} - \gamma_6^{(j)} \left. \frac{\partial \mathcal{L}}{\partial \lambda_{b,s}} \right|_{\lambda_{b,s}^{(j)}}, \quad (6.59)$$

where $\gamma_i^{(j)}$ ($i = 1 - 6$) are the step sizes of iteration j .

Algorithm 6 is designed to iteratively updating $\mathbf{P}, \mathbf{B}, \lambda$ in k -th cluster. In each iteration, $\sum_{k=1}^K (4M_k^2 + 2M_k + 4)$ variables need to be updated. Note that the update of bandwidth and power variables is distributed within individual clusters analytically and the convergence is ensured by the subgradient updates of dual variables, which follows the order (6.54)-(6.59). Suppose Algorithm 6 needs ϵ iterations to converge. The computation complexity of solving (6.48) is

$O(\log_2(\mathfrak{N} - 1))$. The updates of λ needs operations $O(2M' + 4)$. Therefore, the complexity of Algorithm 6 is a polynomial function of $O(\epsilon(2M' + \log_2(\mathfrak{N} - 1) + 4))$.

6.4 Simulation Results

In this section, numerical simulations are performed from three perspectives to evaluate the proposed collaborative resource allocation schemes. First, we demonstrate its effectiveness by comparing it with three other methods across varying resource conditions. Second, we examine the VoS, data rate and sensing accuracy under different service numbers using different methods. Finally, the fairness and robustness of the proposed scheme are analyzed under different conditions. Herein, we note that the bandwidth and power allocation can be dynamically adjusted based on conditions such as channel state information and service requests. The proposed method remains flexible and adaptable, not limited to any particular resource conditions. In this work, we assume that the service request and channel state information remain static throughout the resource allocation process, resulting in static resource allocation.

Herein, we compared the proposed collaborative scheme collaborative resource allocation (CRA) with VoS metric (**CRA with VoS**) with three other schemes summarized as follows.

CRA with rate constraint: In this scheme, we adopt the objective function for evaluating sensing services from [4], which is maximizing the sensing QoS subject to the known communication data rate constraints as

$$P_2 : \max_{\mathbf{P}, \mathbf{B}} \text{Sensing QoS} \quad (6.60)$$

subject to $R(\mathbf{P}, \mathbf{B}) \geq R_{min}$.

The problem P_2 is solved by collaborative resource allocation in Algorithm 6 with $w_{k,m}^{(s)} = 1$. The computation complexity of this scheme is $O(\epsilon(2M' + \log_2(\mathfrak{N} - 1) + 4))$.

NCRA with VoS: In this scheme, the power and bandwidth are allocated with the objective in P_1 using a non-collaborative resource allocation strategy. This scheme doesn't involve the collaborative sensing process, and all the sensing service components can only be performed by the service requestor itself.

Algorithm 6: Collaborative bargaining-based resource allocation algorithm

Input : Service requests from M' users, available resources

$P_{max}, B_{max}, P_{k,m,max}, B_{k,m,max}$, hardware configuration N_r, N_t , channel state parameters σ_c, σ_s , maximum iteration number J^{max}

Output: Resource allocation results \mathbf{P}, \mathbf{B}

```

1 Initializaiton:
2 Initialize the bandwidth and power allocation for communication and sensing with
   uniform bandwidth and power distribution among  $M'$  users.
3 Initialize the dual variables  $\lambda$ .
4 Set iteration index  $j = 0$ .
5 Loop
6 for  $j = 0$  to  $J^{max}$  do
7   for  $k = 1$  to  $K$ 
8     for  $m = 1$  to  $M_k$  do
9       Update the power and bandwidth for communication with (6.36) and (6.48), respectively.
10    end for
11   for  $i = 1$  to  $M_k$ 
12     for  $m = 1$  to  $M_k$  do
13       Update the power and bandwidth allocation matrix for sensing with (6.44) and (6.53),
         respectively.
14     end for
15   end for
16 end for
17 Update the dual variables with (6.54-6.59).
18 if the  $\mathbf{P}, \mathbf{B}, \lambda$  converges
19   break
20 end if
21 End loop
22 end for
23 Report the individual and system VoS.

```

NCRA with VoS (matching approach): In this scheme, the resources are allocated with a matching-based algorithm, as is demonstrated in [136]. The branch and bound algorithms are utilized to allocate the subchannel and power for each user without considering the collabora-

tion among the users.

RRA: In this scheme, the bandwidth and power resources are assigned to each user randomly while keeping the constraints satisfied.

All simulations are performed in MATLAB 2022a operating on a macOS Monterey laptop with 8GB memory and an Apple M1 chip. In our simulation, the range of users is set to $[1, 30]$. N_t and N_r are 8. P_{max} is 10 dBW while B_{max} is 100 MHz. $w_{k,m}^{(s)}$ and $w_{k,m}^{(c)}$ are within $[0, 1]$. $S_{k,m,req}$ is in $[0.01, 10]$ while $R_{k,m,req}$ covers $[0, 100]$. The sensing request randomly generates targets for both device-free sensing and device-based sensing with equal likelihood. The parameters in objective function P are randomly generated to simulate the various service requests. We set the $B_0 = 180$ kHz, $\alpha = \beta = 0.8$. We obtain the performance indicator VoS by conducting 100 times repeated simulations, if not specified.

6.4.1 Influence of Resources

To demonstrate the influence of maximum available resources, we compare the VoS with four schemes, evaluated across different combinations of bandwidth and power. As depicted in Fig. 6.3, with fixed power/bandwidth conditions, increasing the bandwidth/power resource leads to an improved system VoS within both collaborative and non-collaborative schemes. However, our proposed collaborative scheme achieves high VoS with lower resource consumption. Moreover, it can be noted that even with substantial resources, the maximum achievable VoS for a non-collaborative scheme remains *ca.* 0.8. This limitation arises because sensing services demand high hardware capabilities. Without collaboration, each user must independently execute the sensing tasks, which is challenging for those with limited hardware capabilities to achieve satisfactory VoS. The performance of NCRA with VoS using the matching approach is slightly lower than the proposed algorithm in this work, which could be attributed to the fact that CRA with rate constraint the branch and bound algorithm tends to be stuck in local optima due to the complex search space.

In addition, CRA with VoS outperforms CRA with rate constraint due to the latter's treatment of communication QoS as a constraint. It means that the sensing service can only proceed when the communication service constraint is met. However, for users with urgent and high-

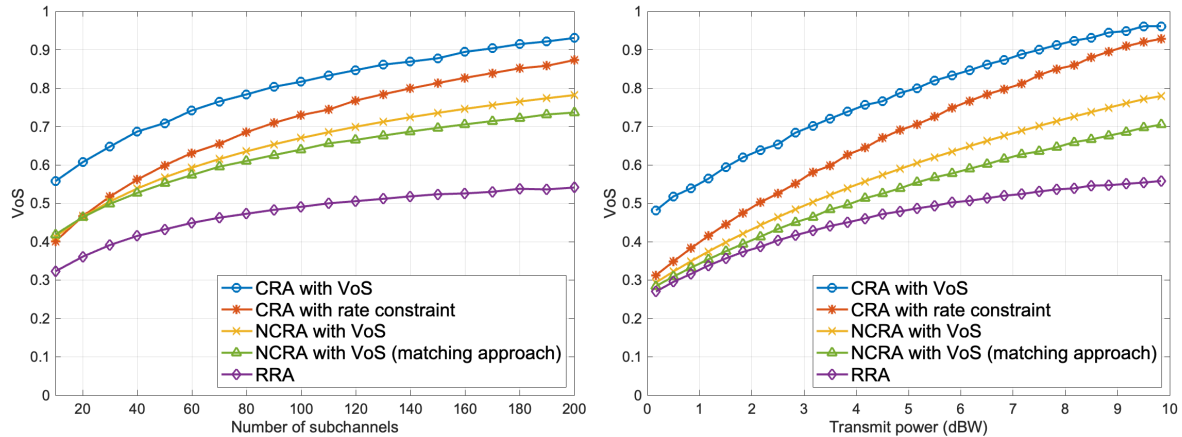


Figure 6.3. The VoS of four schemes under different bandwidth resources (left) and power resources (right).

priority sensing requests but low-priority data rate demands, allocating constrained resources primarily to communication services becomes inefficient, leading to inadequate resources for essential sensing services.

6.4.2 Influence of Service Number

To support heterogeneous applications, the unpredictable or rapidly changing nature of service requests places increased demands on the robustness of resource allocation. Therefore, we conduct a performance comparison between collaborative and non-collaborative schemes in scenarios with different numbers of service requests. We keep the number of available subchannels and power constant at 150 and 8 dBW, respectively, and vary the number of service requests from 1 to 15, as presented in Fig. 6.4 and Fig. 6.5. We first compared the variations in VoS of the four schemes with changes in the number of services. It can be observed from Fig. 6.4, when the service request number is limited, typically fewer than 4, both collaborative and non-collaborative schemes exhibit high VoS. However, when the service number exceeds 6, the non-collaborative scheme experiences a significant drop in VoS. With more than 10 service requests, the VoS of the non-collaborative strategy falls below 0.65, while the collaborative strategy maintains a VoS of 0.8. It's important to note that CRA with rate constraint performs less satisfaction than CRA with VoS, underscoring the superiority of the proposed VoS evaluation metric. The collaborative approach demonstrates increased robustness as the number of

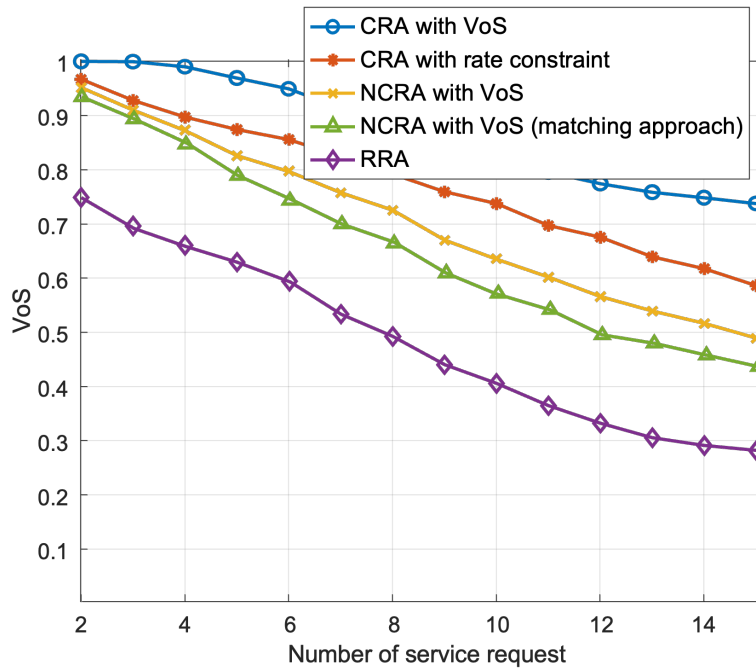


Figure 6.4. The VoS of four schemes under different service numbers.

service requests rises, due to its efficient resource utilization and collaborative strategy.

Furthermore, we simulate the variations in communication data rate and sensing accuracy with changes in the number of services. Fig. 6.5 illustrates that as the number of services increases, all four schemes exhibit a decrease in both average communication data rate and sensing accuracy. CRA with VoS demonstrates a slower rate of performance degradation as the number of services increases from 2 to 10. With a further increase from 10 to 15 services, the performance decline remains modest, benefiting from the VoS-guided collaborative approach. In contrast, CRA with rate constraint scheme can achieve a fair data rate but doesn't match the sensing performance of CRA with VoS. This demonstrates the effectiveness of the proposed algorithm in resource-constrained, multi-user scenarios.

6.4.3 Performance Analysis

6.4.3.1 Fairness Analysis

To evaluate the fairness of service provisioning among different users, we further investigate the individual VoS of five users with different service requests. As shown in Fig. 6.6, when

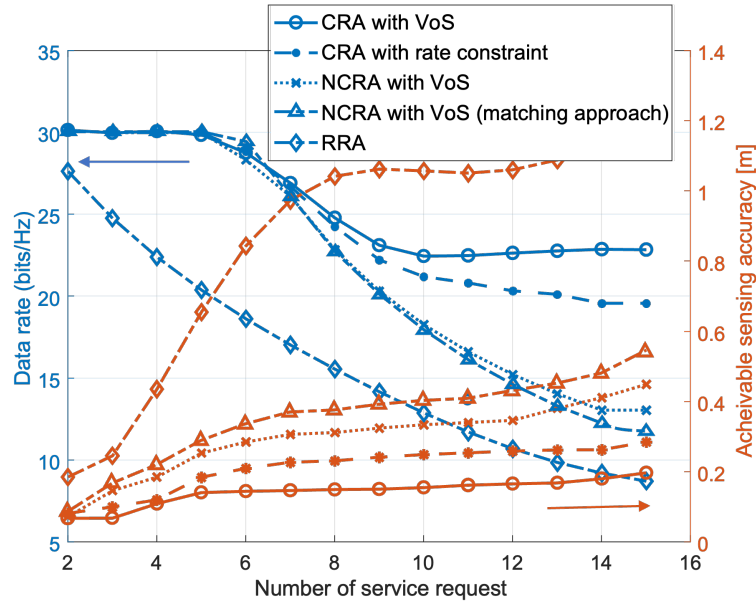


Figure 6.5. The data rate and achievable sensing accuracy of four schemes under different service numbers.

using the non-collaborative scheme, a considerable disparity in service completion is evident among various users. For instance, despite user 1 achieving a high VoS, it monopolizes a significant portion of resources, leaving limited resources for the remaining users, thereby impacting overall service quality. In contrast, the collaborative scheme, which prioritizes fairness among users, ensures that all users can maintain a reasonably high level of service quality. Note that the rate of increasing VoS of each user becomes slower as the bandwidth and power increase. Firstly, the data rate/sensing accuracy is not linearly dependent on the bandwidth and power. Secondly, the saturation effect can be partially attributed to the definition of VoS. the VoS is used to describe the fulfillment of users. When the service request is fulfilled, the VoS will not increase all the time, even more resources are assigned.

Furthermore, as observed in Fig. 6.7, in the non-collaborative scheme, each user's VoS is solely determined by their individual contributions, represented by the yellow bars (baseline). By using the collaborative scheme, over 50% of the VoS for each user comes from non-collaborative operations, namely, performed by the user itself. The remaining VoS, varying from 20% to 50%, is attributed to collaborative components, and this proportion depends on the user's capabilities and requests. The larger collaborative composition of user 1 indicates that its service request is difficult to fulfill by itself, owing to high sensing accuracy and/or low

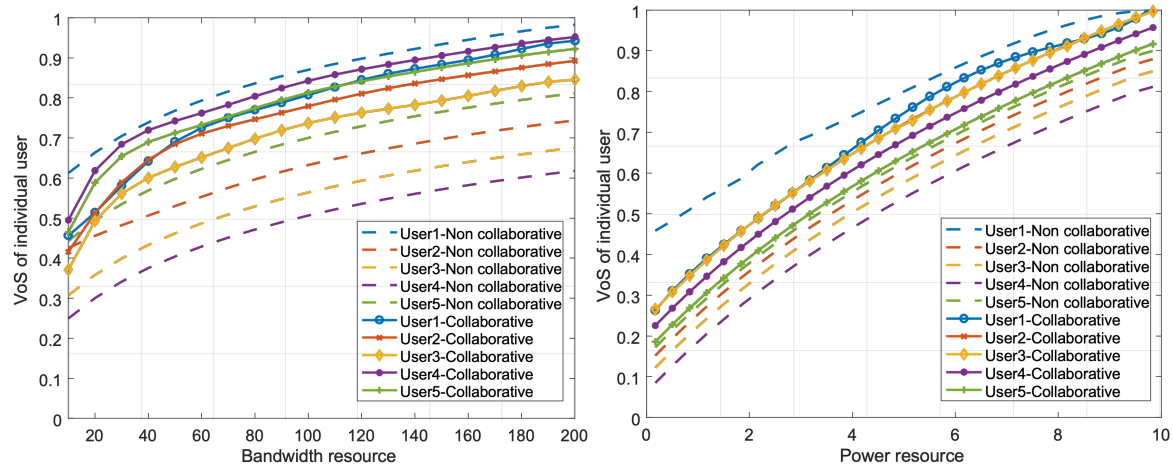


Figure 6.6. The individual VoS of each user with non-collaborative and collaborative schemes with respect to bandwidth (left) and power resources (right).

hardware capability. This can be seen from the VoS of user 1 using baseline is the smallest among the five users when the collaboration is not considered. This example showcases the trigger of the collaboration process in ISAC systems. Generally, collaborative resource allocation should be taken when the resources cannot satisfy the users' minimum needs without collaboration schemes. These findings demonstrate that through collaboration, we not only enhance the overall system's VoS but also maximize the VoS for each individual user by optimizing the efficient use of available resources.

6.4.3.2 Robustness Analysis

To further elaborate on the robustness of the proposed collaborative scheme, three simulations are performed. The first simulation entails a Cumulative Distribution Function (CDF) analysis of the VoS with randomly varying service requests, as shown in Fig. 6.8. The service requests are generated randomly to model the heterogenous services. The collaborative scheme exhibits a narrower distribution in comparison to the non-collaborative scheme. Specifically, the distribution width of the non-collaborative strategy exceeds 0.2, while the proposed collaborative scheme maintains a distribution width of less than 0.1, indicating greater stability than the non-collaborative approach. Furthermore, the non-collaborative scheme achieves a VoS of approximately 0.85 with an 80% probability, whereas the collaborative scheme, under the same conditions, achieves a VoS exceeding 0.95. For the random allocation scheme, the attainable

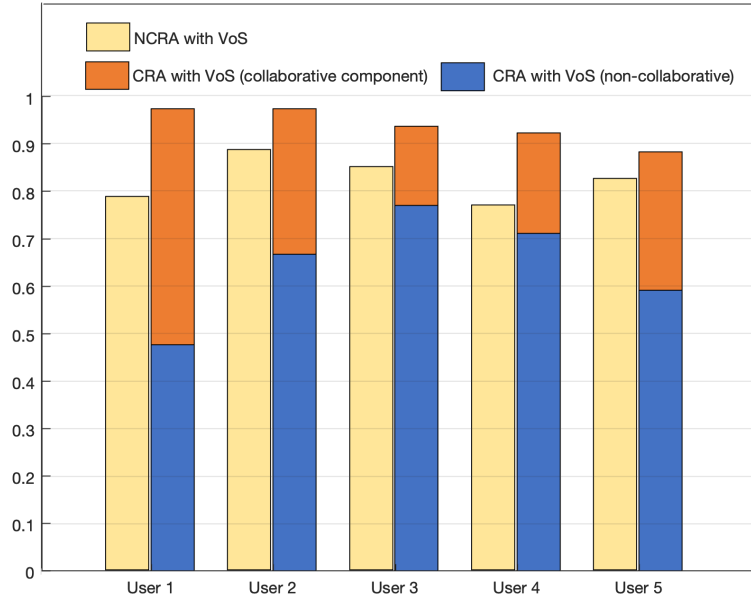


Figure 6.7. The individual VoS of each user with non-collaborative and collaborative scheme.

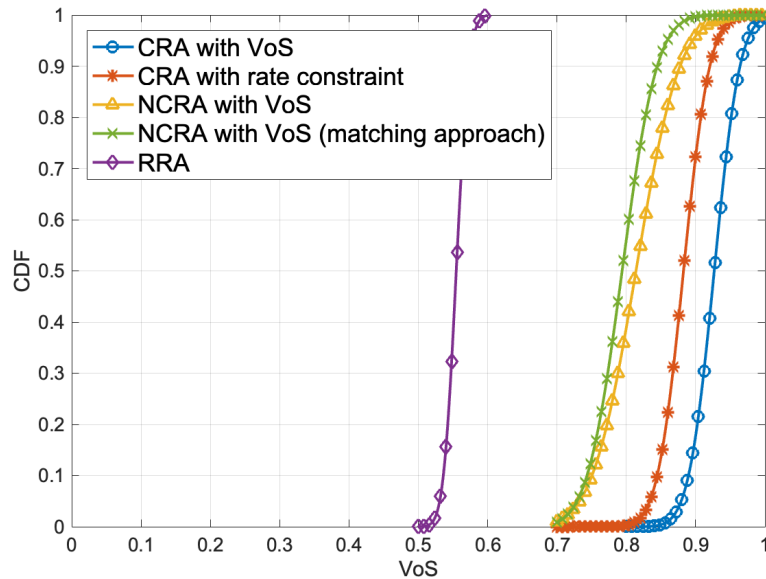


Figure 6.8. CDF of VoS with variable service requests.

VoS is notably lower than that of the other two schemes due to the neglect of specific service requirements from users.

The second simulation is achievable sensing accuracy versus average rate trade-off under the same resource conditions. Fig. 6.9 shows the Pareto boundaries by using different schemes. The trade-off analysis is based on the performance of multiple users in the ISAC system. It can be observed that our proposed algorithm achieves higher average data rates and sensing

accuracy. This is attributed to a more efficient resource allocation strategy and collaborative service execution among multiple users.

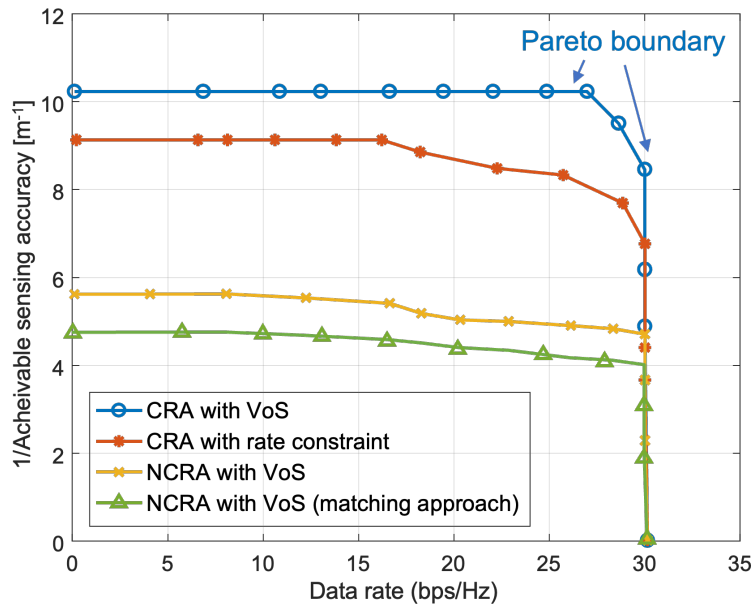


Figure 6.9. Achievable sensing accuracy vs. average rate trade-off using three different schemes.

The third simulation is the VoS versus different channel gains by changing the noise level. The VoS across Signal-to-Noise Ratios (SNR) ranging from -4 to 4 dB is presented in Fig. 6.10. Under fixed resource constraints, the collaborative allocation scheme consistently attains a VoS exceeding 0.9 as the SNR is larger than 0 dB. In contrast, under identical conditions, the non-collaborative scheme only achieves a VoS of less than 0.8. When using the CRA with rate constraint scheme, under high signal-to-noise levels, the VoS saturates at 0.9, which can be attributed to the collaborative scheme's limited consideration of user-specific sensing and communication requests. These simulation results demonstrate the feasibility of the proposed collaborative scheme in challenging, resource-constrained environments.

6.5 Chapter Summary

In this chapter, we propose a game theory-based method in collaborative integrated sensing and communication system, which aims at maximizing the user-specific and system value of ser-

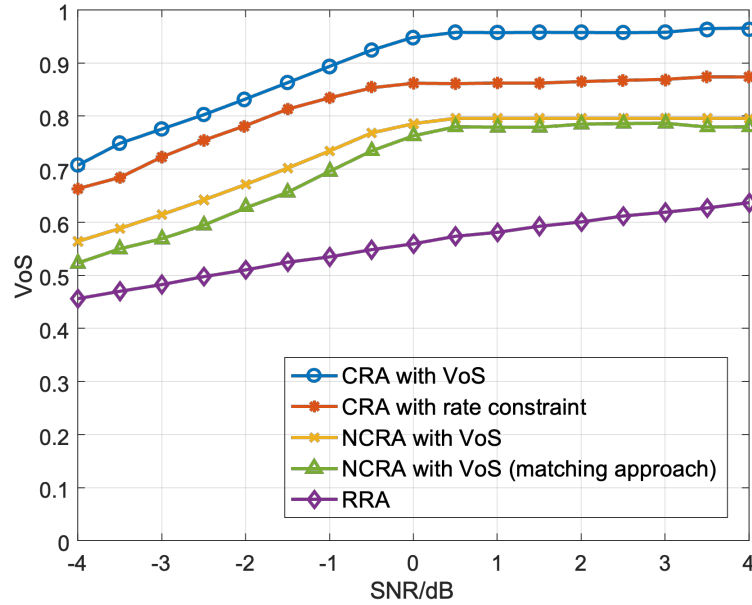


Figure 6.10. The VoS of three schemes under different SNR.

vice. Specifically, the proposed strategy consists of a joint allocation of bandwidth and power resources. The value-based performance metric (VoS) is introduced to adapt to the need-driven collaborative ISAC system. The tradeoff of sensing and communication is analyzed using the dependence on bandwidth and power allocation. Then, we propose to employ a game theory approach for the optimal bandwidth and power allocation to fulfill different service requests at a fine granularity. The joint resource allocation can be achieved through a proposed collaborative scheme. Extensive simulation results show that the proposed collaborative scheme has good robustness and achieves higher VoS as compared to the non-collaborative scheme and the baseline scheme by treating the communication requirements as a constraint.

Chapter 7

Conclusion and Future Works

7.1 Conclusion

With the extensive development of intelligent devices and applications, ILSAC are formed as one of the critical technologies of next generation wireless system. Through the integration of multiple services, ILSAC enables the concurrent exchange of data and localization/sensing information over the same wireless network. While establishing fundamental communication, ILSAC expands the boundary and scope of wireless network services. However, as application scenarios become increasingly complex, numerous technical challenges, including high accurate localization/sensing methods, efficient system design mechanism, and flexible and timely system orchestration to maximize resource utilization etc., inevitably hinder the development of the integrated system. Hence, this thesis developed a value-oriented mechanism to guide the ILSAC system design, resource allocation and localization/sensing state recovery. Firstly, a high accuracy rigid body joint localization and environment sensing scheme is proposed. Secondly, a VoS-guided ILAC system is presented to allocate radio resources for diverse service provisioning under both static and dynamic environments. Thirdly, we introduce a VoS-driven resource allocation scheme for cooperative service provisioning in a multi-user ISAC system.

The primary contributions of this thesis and the corresponding conclusions are summarized as follows.

In Chapter 2, a comprehensive review of localization/sensing method and resource allocation method in ILSAC systems has been conducted. As one of the most important enablers

in future wireless systems, ILSAC allows for the exploitation of dense cell infrastructures to construct a perceptive network to fulfill the needs of diverse users from vertical applications. In recent years, extensive literature reviews are conducted to investigate wireless localization and sensing technologies. However, the research on ILSAC are still at the beginning level. Thus, an introduction to ILSAC systems and a comprehensive survey of resource allocation methods and evaluation metrics of ILSAC are given in this chapter.

In Chapter 3, a rigid body active localization and environment sensing scheme with the assistance of 5G mm-wave MIMO is proposed. A novel hierarchical compressive sensing algorithm refined by an iterative maximum likelihood step for channel angle and distance estimation is presented. Furthermore, we joint consider the rigid body and reflection points localization problem and a PSO-based optimization algorithm is used to estimate the posture of the rigid body and position of reflection points. We also calculate the theoretical bounds (CRLB) on the rigid body posture, NLOS angular and reflection points position estimate uncertainties. Compared to the traditional rigid body localization approaches, our proposed method using only one anchor node can achieve centimeter-level rigid body posture estimation accuracy under both NLOS and OLOS situations. Simulation results reveal that the rigid body posture and reflection points position estimation of our proposed algorithm approach the corresponding bounds with an increase in SNR value. The results also demonstrate that the proposed scheme can achieve high performance for both rigid body localization and reflection points estimation when SNR reaches 20 dB.

In Chapter 4, a joint resource allocation scheme in the ILAC system is proposed to support diverse merging applications. To evaluate the ILAC system comprehensively, a value of service (VoS) metric is introduced consisting of the value from localization and communication components. A novel JRA scheme of both bandwidth and time resources is proposed to maximize the VoS of the ILAC system. The bandwidth resource is allocated by the continuous optimization algorithm followed by discretization. And the temporal resource is assigned with a PSO-based algorithm. From the simulation results, the effectiveness of our redefined ILAC system evaluation metric VoS is confirmed, and the high VoS can be obtained by using the proposed JRA scheme. In addition, our proposed method is more robust and has significantly improved VoS compared with other two resource allocation schemes.

In Chapter 5, we propose an integrated sensing and communication scheme under dynamic environments, which aims at maximizing the long-term VoS of the system. Specifically, the proposed strategy consists of a joint allocation of bandwidth and power resources in each time step. The value-based performance metric (VoS) is utilized to adapt to the need-driven successive ISAC system. The tradeoff of sensing and communication is analyzed using the dependence on bandwidth and power allocation. Then, based on MDP, we propose to employ an actor-critic DRL approach for learning the optimal bandwidth and power allocation strategy to fulfill different service requests at a fine granularity. Simulation results show that the proposed scheme has good robustness and achieves higher VoS as compared to the baseline scheme.

In Chapter 6, we propose a game theory-based method in a collaborative integrated sensing and communication system, which aims at maximizing the user-specific and system value of service. Specifically, the proposed strategy consists of a joint allocation of bandwidth and power resources. The value-based performance metric (VoS) is introduced to adapt to the need-driven collaborative ISAC system. The tradeoff of sensing and communication is analyzed using the dependence on bandwidth and power allocation. Then, we propose to employ a game theory approach for the optimal bandwidth and power allocation to fulfill different service requests at a fine granularity. The joint resource allocation can be achieved through a proposed collaborative scheme. Extensive simulation results show that the proposed collaborative scheme has good robustness and achieves higher VoS as compared to the non-collaborative scheme and the baseline scheme by treating the communication requirements as a constraint.

7.2 Future Works

The major technical issues to achieve efficient value-driven resource allocation in ILSAC systems have been resolved in this thesis. Many other challenges are still required to be investigated and addressed to further extend the scope and depth of service and resource management within ILSAC systems. The current research proposed in this thesis can be extended from several aspects, while some of the future research directions are identified and summarized in this section, including more flexible resource management, broader radio resource definition, opportunistic location/sensing awareness, and distributed integrated system design. Details of

these topics are given as follows:

- *Distributed Resource Management and Integrated System Design*: In practical environments, users are randomly and unevenly distributed within the coverage of the base station. On one hand, due to the non-uniform distribution of users and sensing objects, user-specific resource constraints in spatial domains are different, which restricts their sensing/communication performance with given spatial-related service requests. On the other hand, users' resource utilization costs and perceived distinctive value of integrated services are different, which increases the complexity of efficient resource allocation. Thus, the overall objective is to effectively meet distributed service requests within an ISAC system, considering the users' positions, spatial distributions, and their corresponding resource distributions to simultaneously minimize interference and maximize resource utilization efficiency.
- *Radio Resource Reuse*: In wireless communication systems, the allocation of radio resources, considering both temporal and spatial dimensions, is pivotal for efficient resource management. To improve radio resource utilization efficiency, several new multiple access techniques, particularly multiple-input multiple-output non-orthogonal multiple access (MIMO-NOMA) and rate-splitting multiple access (RSMA), have been proposed in wireless communication systems to explore additional degrees of freedom in spatial domains. For example, in massive MIMO-based beamforming, the subchannels can be reused according to the users' position and beam alignment. Inspired by this, the radio resource reuse can be extended to the ISAC system. Since sensing involves the detection and understanding of the physical environment, with spatial location information, resources can be allocated based on the spatial distribution of devices and their specific requirements. By knowing the spatial locations of users, network operators can adjust resource allocation strategies. When resources in the same frequency band do not interfere with each other in space, they can be reused at different locations simultaneously. Hence, if reference signal coverage areas do not overlap, then distributed users can use the same wireless frequency band simultaneously.
- *Opportunistic Location/Sensing Awareness*: In many intelligent IoT scenarios, the users'

sensing and communication demands are highly time-related. Following a first-come-first-served principle not only wastes time and power on frequent switching between communication and sensing functions but also results in the inability to complete certain urgent tasks. In practical environments, most objects are static, slow-moving or infrequently moving. Only a minority of objects move rapidly, requiring intensive resource consumption for real-time tracking and updates. Thus, at a given moment, if communication tasks have not reached their resource utilization peak and there are no ongoing sensing tasks, the remaining resources can be used for static object sensing. For dynamic objects, predictions can also be made based on historical location information and service requests. This inspires us to develop an opportunistic sensing mechanism for more resilient resource allocation in distributed ISAC systems.

Bibliography

- [1] F. Liu, Y. Cui, C. Masouros, J. Xu, T. X. Han, Y. C. Eldar, and S. Buzzi, “Integrated sensing and communications: Towards dual-functional wireless networks for 6G and beyond,” *IEEE j. Sel. Areas commun.*, 2022.
- [2] Z. Xiao and Y. Zeng, “An overview on integrated localization and communication towards 6G,” *Science China Inf. Sci.*, vol. 65, pp. 1–46, 2022.
- [3] X. Wang, J. Mei, S. Cui, C.-X. Wang, and X. S. Shen, “Realizing 6G: The operational goals, enabling technologies of future networks, and value-oriented intelligent multi-dimensional multiple access,” *IEEE Netw.*, vol. 37, no. 1, pp. 10–17, 2023.
- [4] F. Dong, F. Liu, Y. Cui, W. Wang, K. Han, and Z. Wang, “Sensing as a service in 6G perceptive networks: A unified framework for ISAC resource allocation,” *IEEE Trans. Wireless Commun.*, 2022.
- [5] J. G. Andrews, S. Buzzi, W. Choi, S. V. Hanly, A. Lozano, A. C. Soong, and J. C. Zhang, “What will 5G be?” *IEEE J. Sel. Areas Commun.*, vol. 32, no. 6, pp. 1065–1082, 2014.
- [6] T. S. Rappaport, S. Sun, R. Mayzus, H. Zhao, Y. Azar, K. Wang, G. N. Wong, J. K. Schulz, M. Samimi, and F. Gutierrez, “Millimeter wave mobile communications for 5G cellular: It will work!” *IEEE Access*, vol. 1, pp. 335–349, 2013.
- [7] F. Liu, C. Masouros, A. P. Petropulu, H. Griffiths, and L. Hanzo, “Joint radar and communication design: Applications, state-of-the-art, and the road ahead,” *IEEE Trans. Commun.*, vol. 68, no. 6, pp. 3834–3862, 2020.
- [8] A. Nasri, A. H. A. Bafghi, and M. Nasiri-Kenari, “Wireless localization in the presence of intelligent reflecting surface,” *IEEE Wireless Commun. Lett.*, vol. 11, no. 7, pp. 1315–1319, 2022.
- [9] X. Meng, Y. Li, Z. Wu, S. Hong, and S. Chang, “A semidefinite relaxation approach for mobile target localization based on TOA and doppler frequency shift measurements,” *IEEE Sensors J.*, 2023.
- [10] L. Wang, D. Su, M. Liu, and X. Du, “Modified zeroing neurodynamics models for range-based wsn localization from AOA and TDOA measurements,” *IEEE Sensors J.*, vol. 22, no. 13, pp. 13 716–13 726, 2022.

- [11] S. Wang, X. Jiang, and H. Wymeersch, “Cooperative localization in wireless sensor networks with AOA measurements,” *IEEE Trans. Wireless Commun.*, vol. 21, no. 8, pp. 6760–6773, 2022.
- [12] Y. Li, X. Hu, Y. Zhuang, Z. Gao, P. Zhang, and N. El-Sheimy, “Deep reinforcement learning (DRL): Another perspective for unsupervised wireless localization,” *IEEE Internet of Things J.*, vol. 7, no. 7, pp. 6279–6287, 2019.
- [13] K. Gulati, R. S. K. Boddu, D. Kapila, S. L. Bangare, N. Chandnani, and G. Saravanan, “A review paper on wireless sensor network techniques in Internet of Things (IoT),” *Materials Today: Proceedings*, vol. 51, pp. 161–165, 2022.
- [14] R. Liu, Z. Wan, J. Wang, H. Zhou, J. Li, D. Wang, and X. You, “Fingerprint-based 3d hierarchical localization for cell-free massive mimo systems,” *IEEE Trans. Veh. Technol.*, 2024.
- [15] R. Ghazalian, G. C. Alexandropoulos, G. Seco-Granados, H. Wymeersch, and R. Jäntti, “Joint 3d user and 6d hybrid reconfigurable intelligent surface localization,” *arXiv preprint arXiv:2401.03852*, 2024.
- [16] P. Wan, W. Li, J. Wei, and Y. Wen, “Joint rigid body localization and wireless signal transmission parameter estimation under nlos environment,” *IEEE Access*, vol. 11, pp. 128 514–128 525, 2023.
- [17] R. Li, Z. Xiao, and Y. Zeng, “Towards seamless sensing coverage for cellular multi-static integrated sensing and communication,” *IEEE Trans. Wireless Commun.*, pp. 1–1, 2023.
- [18] D. Avagnina, F. Dovis, A. Ghiglione, and P. Mulassano, “Wireless networks based on high-altitude platforms for the provision of integrated navigation/communication services,” *IEEE Commun. Mag.*, vol. 40, no. 2, pp. 119–125, 2002.
- [19] I. C. Rust and H. H. Asada, “A dual-use visible light approach to integrated communication and localization of underwater robots with application to non-destructive nuclear reactor inspection,” in *Proc. IEEE ICRA*. IEEE, 2012, pp. 2445–2450.
- [20] A. Liu, Z. Huang, M. Li, Y. Wan, W. Li, T. X. Han, C. Liu, R. Du, D. K. P. Tan, J. Lu *et al.*, “A survey on fundamental limits of integrated sensing and communication,” *IEEE Commun. Surveys Tuts.*, vol. 24, no. 2, pp. 994–1034, 2022.
- [21] T. Li, S. Leng, Z. Wang, K. Zhang, and L. Zhou, “Intelligent resource allocation schemes for UAV-swarm-based cooperative sensing,” *IEEE Internet Things J.*, vol. 9, no. 21, pp. 21 570–21 582, 2022.
- [22] Q. Zhao, A. Tang, and X. Wang, “Reference signal design and power optimization for energy-efficient 5G V2X integrated sensing and communications,” *IEEE Trans. Green Commun. Netw.*, 2023.

- [23] Y. Chen and X. Gu, "Time allocation for integrated bi-static radar and communication systems," *IEEE Commun. Lett.*, vol. 25, no. 3, pp. 1033–1036, 2020.
- [24] Q. Zhang, X. Wang, Z. Li, and Z. Wei, "Design and performance evaluation of joint sensing and communication integrated system for 5G mmWave enabled CAVs," *IEEE J. Sel. Top Signal Process.*, vol. 15, no. 6, pp. 1500–1514, 2021.
- [25] Y. Cui, F. Liu, X. Jing, and J. Mu, "Integrating sensing and communications for ubiquitous IoT: Applications, trends, and challenges," *IEEE Network*, vol. 35, no. 5, pp. 158–167, 2021.
- [26] Q. Huang, H. Chen, and Q. Zhang, "Joint design of sensing and communication systems for smart homes," *IEEE Network*, vol. 34, no. 6, pp. 191–197, 2020.
- [27] P. Kumari, J. Choi, N. González-Prelcic, and R. W. Heath, "IEEE 802.11 ad-based radar: An approach to joint vehicular communication-radar system," *IEEE Trans. Veh. Technol.*, vol. 67, no. 4, pp. 3012–3027, 2017.
- [28] H. Messer, A. Zinevich, and P. Alpert, "Environmental monitoring by wireless communication networks," *Science*, vol. 312, no. 5774, pp. 713–713, 2006.
- [29] X. Cheng, D. Duan, S. Gao, and L. Yang, "Integrated sensing and communications (ISAC) for vehicular communication networks (VCN)," *IEEE Internet of Things J.*, vol. 9, no. 23, pp. 23 441–23 451, 2022.
- [30] Q. Zhang, H. Sun, X. Gao, X. Wang, and Z. Feng, "Time-division ISAC enabled connected automated vehicles cooperation algorithm design and performance evaluation," *IEEE J. Sel. Areas Commun.*, vol. 40, no. 7, pp. 2206–2218, 2022.
- [31] Z. Yu, X. Hu, C. Liu, M. Peng, and C. Zhong, "Location sensing and beamforming design for IRS-enabled multi-user ISAC systems," *IEEE Trans. Signal Process.*, vol. 70, pp. 5178–5193, 2022.
- [32] S. Li, W. Yuan, C. Liu, Z. Wei, J. Yuan, B. Bai, and D. W. K. Ng, "A novel ISAC transmission framework based on spatially-spread orthogonal time frequency space modulation," *IEEE J. Sel. Areas Commun.*, vol. 40, no. 6, pp. 1854–1872, 2022.
- [33] C. Zhang, W. Yi, Y. Liu, and L. Hanzo, "Semi-integrated-sensing-and-communication (semi-ISaC): From OMA to NOMA," *IEEE Trans. Commun.*, 2023.
- [34] W. Zhou, R. Zhang, G. Chen, and W. Wu, "Integrated sensing and communication waveform design: A survey," *IEEE open j. Commun. Soc.*, vol. 3, pp. 1930–1949, 2022.
- [35] T. Xu, F. Liu, C. Masouros, and I. Darwazeh, "An experimental proof of concept for integrated sensing and communications waveform design," *IEEE open j. Commun. Soc.*, vol. 3, pp. 1643–1655, 2022.
- [36] Z. Xiao and Y. Zeng, "Waveform design and performance analysis for full-duplex integrated sensing and communication," *IEEE J. Sel. Areas Commun.*, vol. 40, no. 6, pp. 1823–1837, 2022.

- [37] Y. Xiong, F. Liu, Y. Cui, W. Yuan, and T. X. Han, “Flowing the information from Shannon to Fisher: Towards the fundamental tradeoff in ISAC,” in *IEEE GLOBECOM 2022*. IEEE, 2022, pp. 5601–5606.
- [38] Z. Wang, K. Han, X. Shen, W. Yuan, and F. Liu, “Achieving the performance bounds for sensing and communications in perceptive networks: Optimal bandwidth allocation,” *IEEE Wireless Commun. Lett.*, vol. 11, no. 9, pp. 1835–1839, 2022.
- [39] M. Ashraf, B. Tan, D. Moltchanov, J. S. Thompson, and M. Valkama, “Joint optimization of radar and communications performance in 6G cellular systems,” *IEEE Trans. Green Commun. Netw.*, 2023.
- [40] M. Liu, M. Yang, H. Li, K. Zeng, Z. Zhang, A. Nallanathan, G. Wang, and L. Hanzo, “Performance analysis and power allocation for cooperative ISAC networks,” *IEEE Internet Things J.*, 2022.
- [41] D. Xu, X. Yu, D. W. K. Ng, A. Schmeink, and R. Schober, “Robust and secure resource allocation for ISAC systems: A novel optimization framework for variable-length snapshots,” *IEEE Trans. Commun.*, vol. 70, no. 12, pp. 8196–8214, 2022.
- [42] Z. He, W. Xu, H. Shen, D. W. K. Ng, Y. C. Eldar, and X. You, “Full-duplex communication for ISAC: Joint beamforming and power optimization,” *IEEE J. Sel. Areas Commun.*, 2023.
- [43] G. Ghatak, R. Koirala, A. De Domenico, B. Denis, D. Dardari, B. Uguen, and M. Coupechoux, “Beamwidth optimization and resource partitioning scheme for localization assisted mm-wave communication,” *IEEE Trans. Commun.*, vol. 69, no. 2, pp. 1358–1374, 2020.
- [44] N. Varshney and S. De, “Optimum downlink beamwidth estimation in mmWave communications,” *IEEE Trans. Commun.*, vol. 69, no. 1, pp. 544–557, 2020.
- [45] Z. Ni, J. A. Zhang, K. Yang, X. Huang, and T. A. Tsiftsis, “Multi-metric waveform optimization for multiple-input single-output joint communication and radar sensing,” *IEEE Trans. Commun.*, vol. 70, no. 2, pp. 1276–1289, 2021.
- [46] G. Kwon, A. Conti, H. Park, and M. Z. Win, “Joint communication and localization in millimeter wave networks,” *IEEE J. Sel. Topics Signal Process.*, vol. 15, no. 6, pp. 1439–1454, 2021.
- [47] S. Jeong, O. Simeone, A. Haimovich, and J. Kang, “Beamforming design for joint localization and data transmission in distributed antenna system,” *IEEE Trans. Veh. Technol.*, vol. 64, no. 1, pp. 62–76, 2014.
- [48] W. Li, W. Yang, L. Yang, H. Xiong, and Y. Hui, “Bidirectional positioning assisted hybrid beamforming for massive MIMO systems,” *IEEE Trans. Commun.*, vol. 69, no. 5, pp. 3367–3378, 2021.

- [49] J. Zou, R. Liu, C. Wang, Y. Cui, Z. Zou, S. Sun, and K. Adachi, "Aiming in harsh environments: A new framework for flexible and adaptive resource management," *IEEE Network*, vol. 36, no. 4, pp. 70–77, 2022.
- [50] R. Chen and X. Wang, "Maximization of value of service for mobile collaborative computing through situation aware task offloading," *IEEE Trans. Mobile Comput.*, 2021.
- [51] J. Yang, J. Xu, X. Li, S. Jin, and B. Gao, "Integrated communication and localization in millimeter-wave systems," *Front. Inf. Technol. Electron. Eng.*, vol. 22, no. 4, pp. 457–470, 2021.
- [52] L. Zhao, D. Wu, L. Zhou, and Y. Qian, "Radio resource allocation for integrated sensing, communication, and computation networks," *IEEE Trans. Wireless Commun.*, vol. 21, no. 10, pp. 8675–8687, 2022.
- [53] G. Li, S. Wang, J. Li, R. Wang, F. Liu, M. Zhang, X. Peng, and T. Xiao Han, "Rethinking the tradeoff in integrated sensing and communication: Recognition accuracy versus communication rate," *arXiv e-prints*, pp. arXiv–2107, 2021.
- [54] J. Guerci, R. Guerci, A. Lackpour, and D. Moskowitz, "Joint design and operation of shared spectrum access for radar and communications," in *Proc. IEEE Radar Conf. (RadarCon)*. IEEE, 2015, pp. 0761–0766.
- [55] A. R. Chiriyath, B. Paul, G. M. Jacyna, and D. W. Bliss, "Inner bounds on performance of radar and communications co-existence," *IEEE Trans. Signal Process.*, vol. 64, no. 2, pp. 464–474, 2015.
- [56] X. Li, Y. Cui, J. A. Zhang, F. Liu, X. Jing, and O. A. Dobre, "Assisting living by wireless sensing: The role of integrated sensing and communications in 6G era," *arXiv preprint arXiv:2202.09522*, 2022.
- [57] J. Yang, J. Hu, K. Lv, Q. Yu, and K. Yang, "Multi-dimensional resource allocation for uplink throughput maximization in integrated data and energy communication networks," *IEEE Access*, vol. 6, pp. 47 163–47 180, 2018.
- [58] L. Xie, S. Song, Y. C. Eldar, and K. B. Letaief, "Collaborative sensing in perceptive mobile networks: Opportunities and challenges," *IEEE Wireless Commun.*, vol. 30, no. 1, pp. 16–23, 2023.
- [59] J. Chen, W. Dai, Y. Shen, V. K. Lau, and M. Z. Win, "Power management for cooperative localization: A game theoretical approach," *IEEE Trans. Signal Process.*, vol. 64, no. 24, pp. 6517–6532, 2016.
- [60] R. W. Ouyang, A. K.-S. Wong, and C.-T. Lea, "Received signal strength-based wireless localization via semidefinite programming: Noncooperative and cooperative schemes," *IEEE Trans. Veh. Technol.*, vol. 59, no. 3, pp. 1307–1318, 2010.

- [61] Y. K. Tun, N. H. Tran, D. T. Ngo, S. R. Pandey, Z. Han, and C. S. Hong, "Wireless network slicing: Generalized kelly mechanism-based resource allocation," *IEEE J. Sel. Areas Commun.*, vol. 37, no. 8, pp. 1794–1807, 2019.
- [62] J. Kennedy and R. Eberhart, "Particle swarm optimization," in *Proc. IEEE Int. Conf. Neural Net.*, vol. 4. IEEE, 1995, pp. 1942–1948.
- [63] S. Scott-Hayward and E. Garcia-Palacios, "Multimedia resource allocation in mmWave 5G networks," *IEEE Commun. Mag.*, vol. 53, no. 1, pp. 240–247, 2015.
- [64] J. Zhang and C. Masouros, "Beam drift in millimeter wave links: Beamwidth tradeoffs and learning based optimization," *IEEE Trans. Commun.*, vol. 69, no. 10, pp. 6661–6674, 2021.
- [65] F. Sohrabi, T. Jiang, W. Cui, and W. Yu, "Active sensing for communications by learning," *IEEE J. Sel. Areas Commun.*, vol. 40, no. 6, pp. 1780–1794, 2022.
- [66] H. Zhang, C. Jiang, N. C. Beaulieu, X. Chu, X. Wang, and T. Q. Quek, "Resource allocation for cognitive small cell networks: A cooperative bargaining game theoretic approach," *IEEE Trans. Wireless Commun.*, vol. 14, no. 6, pp. 3481–3493, 2015.
- [67] B. Mughal, Z. M. Fadlullah, M. M. Fouda, and S. Ikki, "Applying game theory to relay resource selection in hybrid-band wireless systems," *IEEE Sensors J.*, vol. 22, no. 23, pp. 23 552–23 564, 2022.
- [68] Z. Liu, X. Chen, Y. Chen, and Z. Li, "Deep reinforcement learning based dynamic resource allocation in 5G ultra-dense networks," in *Proc. IEEE Int. Conf. Smart Internet of Things (SmartIoT)*. IEEE, 2019, pp. 168–174.
- [69] U. Demirhan and A. Alkhateeb, "Integrated sensing and communication for 6g: Ten key machine learning roles," *IEEE Commun. Mag.*, 2023.
- [70] Q. Qi, X. Chen, C. Zhong, C. Yuen, and Z. Zhang, "Deep learning-based design of uplink integrated sensing and communication," *IEEE Trans. Wireless Commun.*, 2024.
- [71] L. Cazzella, M. Mizmizi, D. Tagliaferri, D. Badini, M. Matteucci, and U. Spagnolini, "Deep learning-based target-to-user association in integrated sensing and communication systems," *arXiv preprint arXiv:2401.12801*, 2024.
- [72] J. del Peral-Rosado, G. Granados, R. Raulefs, E. Leitinger, S. Grebien, T. Wilding, D. Dardari, E. Lohan, H. Wymeersch, J. Floch *et al.*, "Whitepaper on new localization methods for 5g wireless systems and the internet-of-things," in *White Paper of the COST Action CA15104 (IRACON)*. COST Action CA15104, IRACON, 2018, pp. 1–27.
- [73] Y. Wang, G. Wang, S. Chen, K. Ho, and L. Huang, "An investigation and solution of angle based rigid body localization," *IEEE Trans. Signal Process.*, vol. 68, pp. 5457–5472, 2020.

- [74] X. Shen, H. Zheng, and X. Feng, "A novel FMCW radar-based scheme for indoor localization and trajectory tracking," in *Proc. IEEE 6th Int. Conf. Comput. Commun.*, 2020, pp. 298–303.
- [75] J. Quenzel, M. Nieuwenhuisen, D. Droeschel, M. Beul, S. Houben, and S. Behnke, "Autonomous MAV-based indoor chimney inspection with 3D laser localization and textured surface reconstruction," *J. Intell. Robot. Syst.*, vol. 93, no. 1-2, pp. 317–335, 2019.
- [76] N. Q. Pham, K. Mekonnen, E. Tangdiongga, A. Mefleh, and T. Koonen, "User localization and upstream signaling for beam-steered infrared light communication system," *IEEE Photon. Technol. Lett.*, vol. 33, no. 11, pp. 545–548, 2021.
- [77] J. Wang, M. Zhang, Z. Wang, S. Sun, Y. Ning, X. Yang, and W. Pang, "An ultra-low power, small size and high precision indoor localization system based on MEMS ultrasonic transducer chips," *IEEE Trans. Ultrason., Ferroelect., Freq. Contr.*, vol. 69, no. 4, pp. 1469–1477, 2022.
- [78] G. Wang, W. Zhu, and N. Ansari, "Robust TDOA-based localization for IoT via joint source position and NLOS error estimation," *IEEE Internet Things J.*, vol. 6, no. 5, pp. 8529–8541, 2019.
- [79] Y. Wang, Y. Wu, and Y. Shen, "Joint spatiotemporal multipath mitigation in large-scale array localization," *IEEE Trans. Signal Process.*, vol. 67, no. 3, pp. 783–797, 2018.
- [80] F. Yin, Z. Lin, Q. Kong, Y. Xu, D. Li, S. Theodoridis, and S. R. Cui, "FedLoc: Federated learning framework for data-driven cooperative localization and location data processing," *IEEE Open J. Signal Process.*, vol. 1, pp. 187–215, 2020.
- [81] A. Shahmansoori, G. E. Garcia, G. Destino, G. Seco-Granados, and H. Wymeersch, "Position and orientation estimation through millimeter-wave MIMO in 5G systems," *IEEE Trans. Wireless Commun.*, vol. 17, no. 3, pp. 1822–1835, 2017.
- [82] K. Witrisal, P. Meissner, E. Leitinger, Y. Shen, C. Gustafson, F. Tufvesson, K. Haneda, D. Dardari, A. F. Molisch, A. Conti *et al.*, "High-accuracy localization for assisted living: 5G systems will turn multipath channels from foe to friend," *IEEE Signal Process. Mag.*, vol. 33, no. 2, pp. 59–70, 2016.
- [83] J. Talvitie, M. Valkama, G. Destino, and H. Wymeersch, "Novel algorithms for high-accuracy joint position and orientation estimation in 5G mmWave systems," in *Proc. IEEE Globecom Workshops (GC Wkshps)*. IEEE, 2017, pp. 1–7.
- [84] Z. Abu-Shaban, H. Wymeersch, T. Abhayapala, and G. Seco-Granados, "Single-anchor two-way localization bounds for 5G mmWave systems," *IEEE Trans. Veh. Technol.*, vol. 69, no. 6, pp. 6388–6400, 2020.
- [85] S. P. Chepuri, G. Leus, and A.-J. van der Veen, "Rigid body localization using sensor networks," *IEEE Trans. Signal Process.*, vol. 62, no. 18, pp. 4911–4924, 2014.

- [86] J. Jiang, G. Wang, and K. Ho, "Accurate rigid body localization via semidefinite relaxation using range measurements," *IEEE Signal Process. Lett.*, vol. 25, no. 3, pp. 378–382, 2017.
- [87] —, "Sensor network-based rigid body localization via semi-definite relaxation using arrival time and doppler measurements," *IEEE Trans. Wireless Commun.*, vol. 18, no. 2, pp. 1011–1025, 2019.
- [88] B. Zhou, M. Zhang, Y.-Q. Chen, N. Xiong, Y. Tian, and S. Ahmed, "Efficient AoA-based rigid body localization via single base station for internet of things applications," *IEEE Access*, vol. 7, pp. 171 140–171 152, 2019.
- [89] S. Chen, C. Seow, and S. Tan, "Elliptical lagrange-based NLOS tracking localization scheme," *IEEE Trans. Wireless Commun.*, vol. 15, no. 5, pp. 3212–3225, 2016.
- [90] A. A. Momtaz, F. Behnia, R. Amiri, and F. Marvasti, "NLOS identification in range-based source localization: Statistical approach," *IEEE Sensors J.*, vol. 18, no. 9, pp. 3745–3751, 2018.
- [91] Y. Wang, Q. Wu, M. Zhou, X. Yang, W. Nie, and L. Xie, "Single base station positioning based on multipath parameter clustering in NLOS environment," *EURASIP J. Adv. Signal Process.*, vol. 2021, no. 1, p. 20, 2021.
- [92] S. Al-Jazzar, J. Caffery, and H.-R. You, "Scattering-model-based methods for TOA location in NLOS environments," *IEEE Trans. Veh. Technol.*, vol. 56, no. 2, pp. 583–593, 2007.
- [93] H. Kim, K. Granström, L. Gao, G. Battistelli, S. Kim, and H. Wymeersch, "5G mmWave cooperative positioning and mapping using multi-model PHD filter and map fusion," *IEEE Trans. Wireless Commun.*, vol. 19, no. 6, pp. 3782–3795, 2020.
- [94] J. Talvitie, M. Koivisto, T. Levanen, M. Valkama, G. Destino, and H. Wymeersch, "High-accuracy joint position and orientation estimation in sparse 5G mmWave channel," in *Proc. IEEE Int. Conf. Commun. (ICC)*. IEEE, 2019, pp. 1–7.
- [95] D. Needell and J. A. Tropp, "CoSaMP: Iterative signal recovery from incomplete and inaccurate samples," *Appl. Comp. Harmonic Anal.*, vol. 26, no. 3, pp. 301–321, 2009.
- [96] C. K. Anjinappa, Y. Zhou, Y. Yapici, D. Baron, and I. Guvenc, "Channel estimation in mmWave hybrid MIMO system via off-grid Dirichlet kernels," in *Proc. IEEE Global Commun. Conf. (GLOBECOM)*. IEEE, 2019, pp. 1–6.
- [97] X. Lin, S. Wu, C. Jiang, L. Kuang, J. Yan, and L. Hanzo, "Estimation of broadband multiuser millimeter wave massive MIMO-OFDM channels by exploiting their sparse structure," *IEEE Trans. Wireless Commun.*, vol. 17, no. 6, pp. 3959–3973, 2018.
- [98] H. V. Poor, *An introduction to signal detection and estimation*. Springer Science & Business Media, 1998.

- [99] E. H. Houssein, A. G. Gad, K. Hussain, and P. N. Suganthan, "Major advances in particle swarm optimization: Theory, analysis, and application," *Swarm Evol. Comput.*, vol. 63, p. 100868, 2021.
- [100] S. Scott-Hayward and E. Garcia-Palacios, "Multimedia resource allocation in mmwave 5G networks," *IEEE Commun. Mag.*, vol. 53, no. 1, pp. 240–247, 2015.
- [101] A. Rezaee Jordehi and J. Jasni, "Parameter selection in particle swarm optimisation: a survey," *J. Exp. Theor. Artif. Intell.*, vol. 25, no. 4, pp. 527–542, 2013.
- [102] S. Sarvotham, D. Baron, M. Wakin, M. F. Duarte, and R. G. Baraniuk, "Distributed compressed sensing of jointly sparse signals," in *Proc. Asilomar Conf. Signals Syst. Comput.*, 2005, pp. 1537–1541.
- [103] S. Mirjalili and S. Mirjalili, "Genetic algorithm," *Evolutionary Algorithms and Neural Networks.*, pp. 43–55, 2019.
- [104] M. Vaezi, A. Azari, S. R. Khosravirad, M. Shirvanimoghaddam, M. M. Azari, D. Chasaki, and P. Popovski, "Cellular, wide-area, and non-terrestrial IoT: A survey on 5G advances and the road toward 6G," *IEEE Commun. Surveys Tuts.*, vol. 24, no. 2, pp. 1117–1174, 2022.
- [105] Y. Liu, X. Wang, J. Mei, G. Boudreau, H. Abou-Zeid, and A. B. Sediq, "Situation-aware resource allocation for multi-dimensional intelligent multiple access: A proactive deep learning framework," *IEEE J. Sel. Areas Commun.*, vol. 39, no. 1, pp. 116–130, 2020.
- [106] W. Jiang, B. Han, M. A. Habibi, and H. D. Schotten, "The road towards 6G: A comprehensive survey," *IEEE Open J. Commun. Soc.*, vol. 2, pp. 334–366, 2021.
- [107] D. C. Nguyen, M. Ding, P. N. Pathirana, A. Seneviratne, J. Li, D. Niyato, O. Dobre, and H. V. Poor, "6G Internet of Things: A comprehensive survey," *IEEE Internet Things J.*, vol. 9, no. 1, pp. 359–383, 2022.
- [108] X. Wang, "System, method and apparatus for integrated local area locationing, tracking and communications," Sep. 2 2014, uS Patent 8,823,589.
- [109] C. De Lima, D. Belot, R. Berkvens, A. Bourdoux, D. Dardari, M. Guillaud, M. Iso-mursu, E.-S. Lohan, Y. Miao, A. N. Barreto *et al.*, "Convergent communication, sensing and localization in 6G systems: An overview of technologies, opportunities and challenges," *IEEE Access*, vol. 9, pp. 26 902–26 925, 2021.
- [110] Y. Li, J. Zhao, X. Jiang, and J. Lin, "An effective integrated communication and localization method based on digital phased array antenna," in *Proc. 7th IEEE Int. Conf. Comput. Commun. (ICCC)*. IEEE, 2021, pp. 2185–2189.
- [111] T. Mao, J. Chen, Q. Wang, C. Han, Z. Wang, and G. K. Karagiannidis, "Waveform design for joint sensing and communications in millimeter-wave and low terahertz bands," *IEEE Trans. Commun.*, vol. 70, no. 10, pp. 7023–7039, 2022.

- [112] J. Fan, X. Dou, W. Zou, and S. Chen, "Localization based on improved sparse Bayesian learning in mmWave MIMO systems," *IEEE Trans. Veh. Technol.*, vol. 71, no. 1, pp. 354–361, 2021.
- [113] M. Morelli and U. Mengali, "A comparison of pilot-aided channel estimation methods for OFDM systems," *IEEE Trans. signal process.*, vol. 49, no. 12, pp. 3065–3073, 2001.
- [114] A. Pratap, R. Misra, and S. K. Das, "Maximizing fairness for resource allocation in heterogeneous 5G networks," *IEEE Trans. Mobile Comput.*, vol. 20, no. 2, pp. 603–619, 2019.
- [115] W. Zhong, K. Xie, Y. Liu, C. Yang, and S. Xie, "Multi-resource allocation of shared energy storage: A distributed combinatorial auction approach," *IEEE Trans. Smart Grid*, vol. 11, no. 5, pp. 4105–4115, 2020.
- [116] H. Li, J. Xu, R. Zhang, and S. Cui, "A general utility optimization framework for energy-harvesting-based wireless communications," *IEEE Commun. Mag.*, vol. 53, no. 4, pp. 79–85, 2015.
- [117] T. Zhang, A. F. Molisch, Y. Shen, Q. Zhang, H. Feng, and M. Z. Win, "Joint power and bandwidth allocation in wireless cooperative localization networks," *IEEE Trans. Wireless Commun.*, vol. 15, no. 10, pp. 6527–6540, 2016.
- [118] N. C. Luong, X. Lu, D. T. Hoang, D. Niyato, and D. I. Kim, "Radio resource management in joint radar and communication: A comprehensive survey," *IEEE Commun. Surveys Tuts.*, vol. 23, no. 2, pp. 780–814, 2021.
- [119] J. Chen and A. Abedi, "A hybrid framework for radio localization in broadband wireless systems," in *Proc. IEEE Global Telecommun. Conf.* IEEE, 2010, pp. 1–6.
- [120] M. Ghorbanzadeh and A. Abdelhadi, *Practical Channel-Aware Resource Allocation*. Springer, 2022.
- [121] G. I. Tsiropoulos, O. A. Dobre, M. H. Ahmed, and K. E. Baddour, "Radio resource allocation techniques for efficient spectrum access in cognitive radio networks," *IEEE Commun. Surveys Tuts.*, vol. 18, no. 1, pp. 824–847, 2014.
- [122] H. Shajaiah, M. Ghorbanzadeh, A. Abdelhadi, and C. Clancy, "Application-aware resource allocation based on channel information for cellular networks," in *Proc. of IEEE Wirel. Commun. Netw. Conf. (WCNC)*. IEEE, 2019, pp. 1–6.
- [123] T. Erpek, A. Abdelhadi, and T. C. Clancy, "An optimal application-aware resource block scheduling in LTE," in *Proc. Int. Conf. Comput., Netw. Commun. (ICNC)*. IEEE, 2015, pp. 275–279.
- [124] Z. Kbah and A. Abdelhadi, "Resource allocation in cellular systems for applications with random parameters," in *Proc. Int. Conf. Comput., Netw. Commun.* IEEE, 2016, pp. 1–5.

- [125] H. Shajaiah, A. Abdelhadi, and C. Clancy, “An optimal strategy for determining true bidding values in secure spectrum auctions,” *IEEE Syst. J.*, vol. 13, no. 2, pp. 1190–1201, 2018.
- [126] Z. Wang, D. W. K. Ng, V. W. Wong, and R. Schober, “Robust beamforming design in C-RAN with sigmoidal utility and capacity-limited backhaul,” *IEEE Trans. Wireless Commun.*, vol. 16, no. 9, pp. 5583–5598, 2017.
- [127] M. Hemmati, B. McCormick, and S. Shirmohammadi, “Fair and efficient bandwidth allocation for video flows using sigmoidal programming,” in *Proc. IEEE Int’l Symp. Multimedia (ISM)*. IEEE, 2016, pp. 226–231.
- [128] Y. Zheng, J. Liu, M. Sheng, S. Han, Y. Shi, and S. Valaee, “Toward practical access point deployment for angle-of-arrival based localization,” *IEEE Trans. Commun.*, vol. 69, no. 3, pp. 2002–2014, 2020.
- [129] B. Li and X. Wang, “Rigid body localization and environment sensing with 5G millimeter wave MIMO,” in *Proc. IEEE 94th Veh. Technol. Conf. (VTC-Fall)*. IEEE, 2021, pp. 1–5.
- [130] Y. Shen and M. Z. Win, “Fundamental limits of wideband localization—Part I: A general framework,” *IEEE Trans. Inf. Theory*, vol. 56, no. 10, pp. 4956–4980, 2010.
- [131] F. P. Kelly, A. K. Maulloo, and D. K. H. Tan, “Rate control for communication networks: shadow prices, proportional fairness and stability,” *J. Oper. Res. Soc.*, vol. 49, no. 3, pp. 237–252, 1998.
- [132] I. C. Trelea, “The particle swarm optimization algorithm: Convergence analysis and parameter selection,” *Inf. Process. Lett.*, vol. 85, no. 6, pp. 317–325, 2003.
- [133] G. Kwon, A. Conti, H. Park, and M. Z. Win, “Joint communication and localization in millimeter wave networks,” *IEEE J. Sel. Topics Signal Process.*, vol. 15, no. 6, pp. 1439–1454, 2021.
- [134] X. Qi, S. Khattak, A. Zaib, and I. Khan, “Energy efficient resource allocation for 5G heterogeneous networks using genetic algorithm,” *IEEE Access*, vol. 9, pp. 160 510–160 520, 2021.
- [135] H. Hua, J. Xu, and T. X. Han, “Optimal transmit beamforming for integrated sensing and communication,” *IEEE Trans. Veh. Technol.*, 2023.
- [136] Y. Cao and Q.-Y. Yu, “Joint resource allocation for user-centric cell-free integrated sensing and communication systems,” *IEEE Commun. Lett.*, 2023.
- [137] Y. Li, Z. Wei, and Z. Feng, “Joint subcarrier and power allocation for uplink integrated sensing and communication system,” *IEEE Sensors J.*, 2023.
- [138] L. Zhao, D. Wu, L. Zhou, and Y. Qian, “Radio resource allocation for integrated sensing, communication, and computation networks,” *IEEE Trans. Wireless Commun.*, vol. 21, no. 10, pp. 8675–8687, 2022.

- [139] B. Li, X. Wang, Y. Xin, and E. Au, "Value of service maximization in integrated localization and communication system through joint resource allocation," *IEEE Trans. Commun.*, vol. 71, no. 8, pp. 4957–4971, 2023.
- [140] N. Zhao, Y.-C. Liang, D. Niyato, Y. Pei, M. Wu, and Y. Jiang, "Deep reinforcement learning for user association and resource allocation in heterogeneous cellular networks," *IEEE Trans. Wireless Commun.*, vol. 18, no. 11, pp. 5141–5152, 2019.
- [141] Y. Ju, H. Wang, Y. Chen, T.-X. Zheng, Q. Pei, J. Yuan, and N. Al-Dhahir, "Deep reinforcement learning based joint beam allocation and relay selection in mmwave vehicular networks," *IEEE Trans. Commun.*, vol. 71, no. 4, pp. 1997–2012, 2023.
- [142] Q. Liu, Y. Zhu, M. Li, R. Liu, Y. Liu, and Z. Lu, "DRL-based secrecy rate optimization for RIS-assisted secure ISAC systems," *IEEE Trans. Veh. Technol.*, 2023.
- [143] Y. Qin, Z. Zhang, X. Li, W. Huangfu, and H. Zhang, "Deep reinforcement learning based resource allocation and trajectory planning in integrated sensing and communications UAV network," *IEEE Trans. Wireless Commun.*, 2023.
- [144] A. Shastri, N. Valecha, E. Bashirov, H. Tataria, M. Lentmaier, F. Tufvesson, M. Rossi, and P. Casari, "A review of millimeter wave device-based localization and device-free sensing technologies and applications," *IEEE Commun. Surv. Tutor.*, vol. 24, no. 3, pp. 1708–1749, 2022.
- [145] B. Li, X. Wang, E. Au, and Y. Xin, "Joint localization and environment sensing of rigid body with 5G millimeter wave MIMO," *IEEE O. J. Signal Process.*, vol. 4, pp. 117–131, 2023.
- [146] W. C. Jakes and D. C. Cox, *Microwave mobile communications*. Wiley-IEEE press, 1994.
- [147] Y. S. Nasir and D. Guo, "Multi-agent deep reinforcement learning for dynamic power allocation in wireless networks," *IEEE J. Sel. Areas Commun.*, vol. 37, no. 10, pp. 2239–2250, 2019.
- [148] —, "Multi-agent deep reinforcement learning for dynamic power allocation in wireless networks," *IEEE J. Sel. Areas Commun.*, vol. 37, no. 10, pp. 2239–2250, 2019.
- [149] V. Konda and J. Tsitsiklis, "Actor-critic algorithms," *SIAM J. Control Optim.*, vol. 42, no. 4, pp. 1143–1166, 1003.
- [150] C. Qiu, H. Yao, F. R. Yu, F. Xu, and C. Zhao, "Deep Q-learning aided networking, caching, and computing resources allocation in software-defined satellite-terrestrial networks," *IEEE Trans. Veh. Technol.*, vol. 68, no. 6, pp. 5871–5883, 2019.
- [151] M. Clerc, "Particle swarm optimization," *Part. Swarm Optim.*, pp. 1–17, 2010.

- [152] S. P. Chepuri, N. Shlezinger, F. Liu, G. C. Alexandropoulos, S. Buzzi, and Y. C. Eldar, "Integrated sensing and communications with reconfigurable intelligent surfaces: From signal modeling to processing," *IEEE Signal Process. Mag.*, vol. 40, no. 6, pp. 41–62, 2023.
- [153] B. Zhao, M. Wang, Z. Xing, G. Ren, and J. Su, "Integrated sensing and communication aided dynamic resource allocation for random access in satellite terrestrial relay networks," *IEEE Commun. Lett.*, 2022.
- [154] P. Gao, L. Lian, and J. Yu, "Cooperative ISAC with direct localization and rate-splitting multiple access communication: A pareto optimization framework," *IEEE J. Sel. Areas Commun.*, vol. 41, no. 5, pp. 1496–1515, 2023.
- [155] S.-L. Shih, C.-K. Wen, and S. Jin, "CSI-embedded cooperative localization method for 3D indoor environments," *IEEE Commun. Lett.*, 2023.
- [156] J. Wang, Q. Gao, M. Pan, and Y. Fang, "Device-free wireless sensing: Challenges, opportunities, and applications," *IEEE netw.*, vol. 32, no. 2, pp. 132–137, 2018.
- [157] X. Mu, Y. Liu, L. Guo, J. Lin, and L. Hanzo, "NOMA-aided joint radar and multicast-unicast communication systems," *IEEE J. Sel. Areas Commun.*, vol. 40, no. 6, pp. 1978–1992, 2022.
- [158] Y. Zhou, H. Zhou, F. Zhou, Y. Wu, and V. C. Leung, "Resource allocation for a wireless powered integrated radar and communication system," *IEEE Wireless Commun. Lett.*, vol. 8, no. 1, pp. 253–256, 2018.
- [159] Z. He, W. Xu, H. Shen, D. W. K. Ng, Y. C. Eldar, and X. You, "Full-duplex communication for ISAC: Joint beamforming and power optimization," *IEEE J. Sel. Areas Commun.*, 2023.
- [160] G. Zhang, H. Zhang, L. Zhao, W. Wang, and L. Cong, "Fair resource sharing for cooperative relay networks using Nash bargaining solutions," *IEEE Commun. Lett.*, vol. 13, no. 6, pp. 381–383, 2009.
- [161] M. Ke, Y. Wang, M. Li, F. Gao, and Z. Du, "Distributed power allocation for cooperative localization: A potential game approach," in *Proc. 3rd IEEE Int. Conf. Comput. Commun. (ICCC)*. IEEE, 2017, pp. 616–621.
- [162] C.-G. Yang, J.-D. Li, and Z. Tian, "Optimal power control for cognitive radio networks under coupled interference constraints: A cooperative game-theoretic perspective," *IEEE Trans. Veh. Technol.*, vol. 59, no. 4, pp. 1696–1706, 2009.
- [163] A. Attar, M. R. Nakhai, and A. H. Aghvami, "Cognitive radio game for secondary spectrum access problem," *IEEE Trans. Wireless commun.*, vol. 8, no. 4, pp. 2121–2131, 2009.

- [164] Q. Ni and C. C. Zarakovitis, “Nash bargaining game theoretic scheduling for joint channel and power allocation in cognitive radio systems,” *IEEE J. Sel. Areas Commun.*, vol. 30, no. 1, pp. 70–81, 2011.
- [165] W. Yu and R. Lui, “Dual methods for nonconvex spectrum optimization of multicarrier systems,” *IEEE Trans. commun.*, vol. 54, no. 7, pp. 1310–1322, 2006.
- [166] S. P. Boyd and L. Vandenberghe, *Convex optimization*. Cambridge university press, 2004.
- [167] J. Chen, X. Wang, and Y.-C. Liang, “Impact of channel aging on dual-function radar-communication systems: Performance analysis and resource allocation,” *IEEE Trans. Commun.*, vol. 71, no. 8, pp. 4972–4987, 2023.
- [168] K. M. Braun, “OFDM radar algorithms in mobile communication networks,” Ph.D. dissertation, Karlsruhe, Karlsruher Institut für Technologie (KIT), Diss., 2014, 2014.

Appendix A

Proofs of Theorems in Chapter 3

A.1 The FIM of Channel Parameters in (3.38)

The expansion of FIM is dependent on the partial derivatives of the channel matrix concerning the channel parameters. The elements in (3.38) are expressed as

$$\frac{\partial \boldsymbol{\mu}[n]}{\partial \tau_l} = \frac{\mathbf{A}_R[n] \partial(\boldsymbol{\Gamma}[n]) \mathbf{A}_T^H[n]}{\partial \tau_l} \mathbf{F}[n] \mathbf{x}[n], \quad (\text{A.1})$$

$$\frac{\partial \boldsymbol{\mu}[n]}{\partial \theta_{t,l}} = \frac{\mathbf{A}_R[n] \boldsymbol{\Gamma}[n] \partial(\mathbf{A}_T^H[n])}{\partial \theta_{t,l}} \mathbf{F}[n] \mathbf{x}[n], \quad (\text{A.2})$$

$$\frac{\partial \boldsymbol{\mu}[n]}{\partial \phi_{t,l}} = \frac{\mathbf{A}_R[n] \boldsymbol{\Gamma}[n] \partial(\mathbf{A}_T^H[n])}{\partial \phi_{t,l}} \mathbf{F}[n] \mathbf{x}[n], \quad (\text{A.3})$$

$$\frac{\partial \boldsymbol{\mu}[n]}{\partial \theta_{r,l}} = \frac{\partial(\mathbf{A}_R[n]) \boldsymbol{\Gamma}[n] \mathbf{A}_T^H[n]}{\partial \theta_{r,l}} \mathbf{F}[n] \mathbf{x}[n], \quad (\text{A.4})$$

$$\frac{\partial \boldsymbol{\mu}[n]}{\partial \phi_{r,l}} = \frac{\partial(\mathbf{A}_R[n]) \boldsymbol{\Gamma}[n] \mathbf{A}_T^H[n]}{\partial \phi_{r,l}} \mathbf{F}[n] \mathbf{x}[n], \quad (\text{A.5})$$

$$\frac{\partial \boldsymbol{\mu}[n]}{\partial h_l} = \frac{\mathbf{A}_R[n] \partial(\boldsymbol{\Gamma}[n]) \mathbf{A}_T^H[n]}{\partial h_l} \mathbf{F}[n] \mathbf{x}[n]. \quad (\text{A.6})$$

Using the differential property of the Kronecker product, the derivative terms in (A.1-A.6)

can be expanded with the following notations

$$\begin{aligned}\mathcal{A}_x &= \left[-\frac{N_{Tx}-1}{2}, \dots, \frac{N_{Tx}-1}{2}\right], \\ \mathcal{A}_y &= \left[-\frac{N_{Ty}-1}{2}, \dots, \frac{N_{Ty}-1}{2}\right],\end{aligned}\tag{A.7}$$

$$\frac{\partial \Gamma[n]}{\partial \tau_l} = \text{diag}(0, 0, \dots, \sqrt{N_R N_T} \frac{-j2\pi n h_l}{N T_s \sqrt{\rho_l}} e^{-\frac{j2\pi n \tau_l}{N T_s}}, \dots, 0),\tag{A.8}$$

$$\frac{\partial \Gamma[n]}{\partial h_l} = \text{diag}(0, 0, \dots, \frac{1}{\sqrt{\rho_l}} e^{-\frac{j2\pi n \tau_l}{N T_s}}, \dots, 0),\tag{A.9}$$

$$\frac{\partial (\mathbf{A}_T^H[n])}{\partial \theta_{t,l}} = [0, 0, \dots, \frac{\partial \mathbf{a}_{t,n}(\theta_{t,l}, \phi_{t,l})}{\partial \theta_{t,l}}, \dots, 0],\tag{A.10}$$

$$\frac{\partial \mathbf{a}_{t,n}(\theta_{t,l}, \phi_{t,l})}{\partial \theta_{t,l}} = j \frac{2\pi}{\lambda_n} d_o \sin(\phi_{t,l}) \mathcal{D}_1 \cdot \mathbf{a}_{t,n}(\theta_{t,l}, \phi_{t,l}),\tag{A.11}$$

$$\mathcal{D}_1 = \begin{vmatrix} \cos\theta_{t,l} & \sin\theta_{t,l} \\ \mathcal{A}_x & \mathcal{A}_y \end{vmatrix},\tag{A.12}$$

$$\frac{\partial (\mathbf{A}_T^H[n])}{\partial \phi_{t,l}} = [0, 0, \dots, \frac{\partial \mathbf{a}_{t,n}(\theta_{t,l}, \phi_{t,l})}{\partial \phi_{t,l}}, \dots, 0],\tag{A.13}$$

$$\frac{\partial \mathbf{a}_{t,n}(\theta_{t,l}, \phi_{t,l})}{\partial \phi_{t,l}} = j \frac{2\pi}{\lambda_n} d_o \cos(\phi_{t,l}) \mathcal{D}_2 \cdot \mathbf{a}_{t,n}(\theta_{t,l}, \phi_{t,l}),\tag{A.14}$$

$$\mathcal{D}_2 = \begin{vmatrix} \sin\theta_{t,l} & -\cos\theta_{t,l} \\ \mathcal{A}_x & \mathcal{A}_y \end{vmatrix}.\tag{A.15}$$

The construction of $\frac{\partial (\mathbf{A}_R[n])}{\partial \theta_{r,l}}$ and $\frac{\partial (\mathbf{A}_R[n])}{\partial \phi_{r,l}}$ are similar to (A.10) and (A.13), by changing the transmitter parameters into receiver parameters.

A.2 The Entries in (3.48)

Using the derivative rules of the dot product, we can derive the following equations

$$\frac{\partial \zeta_0}{\partial p_i} = \frac{-p_i |\mathbf{p} - \mathbf{s}| + (p_i - s_i) |\mathbf{p} - \mathbf{s}|^{-1}}{|\mathbf{p} - \mathbf{s}|^2},\tag{A.16}$$

$$\frac{\partial \zeta_l}{\partial \kappa_i} = \frac{-p_i |\mathbf{p} - \boldsymbol{\kappa}| + (\kappa_i - s_i) |\mathbf{p} - \boldsymbol{\kappa}|^{-1}}{|\mathbf{p} - \boldsymbol{\kappa}|^2}, \quad (\text{A.17})$$

$$\frac{\partial [\mathbf{R}(2, :) \cdot \zeta_0 / \mathbf{R}(1, :) \cdot \zeta_0]}{\partial p_i} = \frac{1}{(\mathbf{R}(1, :) \cdot \zeta_0)^2} \mathcal{D}_3 \cdot \frac{\partial \zeta_0}{\partial p_i}, \quad (\text{A.18})$$

$$\mathcal{D}_3 = \begin{vmatrix} \mathbf{R}(1, :) \cdot \zeta_0 & \mathbf{R}(2, :) \cdot \zeta_0 \\ \mathbf{R}(1, :) & \mathbf{R}(2, :) \end{vmatrix}, \quad (\text{A.19})$$

$$\frac{\partial [\mathbf{R}(2, :) \cdot \zeta_l / \mathbf{R}(1, :) \cdot \zeta_l]}{\partial \kappa_i} = \frac{1}{(\mathbf{R}(1, :) \cdot \zeta_l)^2} \mathcal{D}_{4,l} \cdot \frac{\partial \zeta_l}{\partial \kappa_i}, \quad (\text{A.20})$$

$$\mathcal{D}_{4,l} = \begin{vmatrix} \mathbf{R}(1, :) \cdot \zeta_l & \mathbf{R}(2, :) \cdot \zeta_l \\ \mathbf{R}(1, :) & \mathbf{R}(2, :) \end{vmatrix}, \quad (\text{A.21})$$

$$\frac{\partial [\mathbf{R}(2, :) \cdot \zeta_l / \mathbf{R}(1, :) \cdot \zeta_l]}{\partial q_i} = \frac{1}{(\mathbf{R}(1, :) \cdot \zeta_l)^2} \mathcal{D}_{5,l} \cdot \zeta_l, \quad (\text{A.22})$$

$$\mathcal{D}_{5,l} = \begin{vmatrix} \mathbf{R}(1, :) \cdot \zeta_l & \mathbf{R}(2, :) \cdot \zeta_l \\ \partial \mathbf{R}(1, :) / \partial q_i & \partial \mathbf{R}(2, :) / \partial q_i \end{vmatrix}, \quad (\text{A.23})$$

$$\begin{aligned} \frac{\partial \mathbf{R}(1, :)}{\partial \mathbf{q}} &= \begin{bmatrix} 0 & -s_1 s_3 + c_3 s_2 c_1 & s_3 c_1 - c_3 s_2 s_1 \\ 0 & -c_3 s_1 + c_1 s_2 s_3 & -c_1 c_3 - s_1 s_2 s_3 \\ 0 & c_1 c_2 & -s_1 c_2 \end{bmatrix}^T, \\ \frac{\partial \mathbf{R}(2, :)}{\partial \mathbf{q}} &= \begin{bmatrix} -s_2 c_3 & s_1 s_3 + c_3 c_2 s_1 & c_3 c_2 c_1 \\ -s_2 s_3 & s_3 c_2 s_1 & s_3 c_2 c_1 \\ -c_2 & -s_2 s_1 & -s_2 c_1 \end{bmatrix}^T, \\ \frac{\partial \mathbf{R}(3, :)}{\partial \mathbf{q}} &= \begin{bmatrix} 0 & c_1 c_2 & -s_1 c_2 \\ -c_2 & -s_2 s_1 & -s_2 c_1 \\ 0 & 0 & 0 \end{bmatrix}^T. \end{aligned} \quad (\text{A.24})$$

and the notations in this part are the same as (3.8).

Appendix B

Proofs of Theorems in Chapter 6

B.1 Derivation of CRLB of $\eta_{k,m,m'}$

Here we show the proof of the device-free sensing model, and the device-based sensing can be derived similarly. Denote

$$\mathbf{H}_{k,m,n,m'} = \Omega(\tau_{k,m,n,m'}) \mathbf{A}_{k,m,r}(\phi_{k,m,m'}^{(s)}) \mathbf{A}_{k,m,t}^H(\theta_{k,m,m'}^{(s)}), \quad (\text{B.1})$$

where $\Omega(\tau_{k,m,n,m'}) = \frac{\sqrt{N_t N_r P_{k,m,n,m'} h_{k,m,n,m'}}}{\sqrt{\rho_{k,m,n,m'}}} e^{\frac{j2\pi\tau_{k,m,m'}}{NT_s}}$. By decomposing the $\mathbf{H}_{k,m,n,m'}$ onto each antenna, there is

$$\check{h}_{k,m,n,m',l_t,l_r} = \Omega(\tau_{k,m,n,m'}) \times \exp\left(\frac{2\pi}{\lambda_n} j\left(-\frac{N_t - 1}{2} + l_t\right) \times d \sin \theta_{k,m,m'} + \frac{2\pi}{\lambda_n} j\left(-\frac{N_r - 1}{2} + l_r\right) d \sin \phi_{k,m,m'}\right), \quad (\text{B.2})$$

where $l_t = 1, 2, \dots, N_t$ and $l_r = 1, 2, \dots, N_r$. Based on [98], when dealing with AWGN, the (p, q) -th elements in $\mathbf{J}_{\eta_{k,m,m'}}$ can be derived as

$$\mathbf{J}_{\eta_{k,m,m'}}(p, q) = \frac{2}{\sigma_s^2} \sum_{n=i_{k,m,m'}^{(s)}}^{i_{k,m,m'}^{(s)} + N_{k,m,m'}^{(s)}} \sum_{l_t=1}^{N_t} \sum_{l_r=1}^{N_r} \left\{ \frac{\partial(\check{h}_{k,m,n,m',l_t,l_r})^H}{\partial \eta_{k,m,m'}(p)} \cdot \frac{\partial \check{h}_{k,m,n,m',l_t,l_r}}{\partial \eta_{k,m,m'}(q)} \right\}^{\text{Re}}.$$

where $\eta_{k,m,m'}(q)$ is the q -th element of $\boldsymbol{\eta}_{k,m,m'}$, and the first summation is among all the subcarriers in the subchannels. Due to the difficulty of deriving the closed form with inverse processing

of \mathbf{J}_η , we adopt a similar approximation approach as in [167, 168]. For the three variables in $\eta_{k,m,m'}$, assuming the error source comes from the white noise, the estimation of each measurement is considered as independent, then we approximate with $\text{var}(\hat{\eta}_{k,m,m'}(i)) \geq \mathbf{J}_{\eta_{k,m,m'}}^{-1}(i, i)$, $i = 1, 2, 3$, as shown in (B.3).

$$\begin{aligned} \text{var}(\hat{\theta}_{k,m,m'}) &\geq \frac{\zeta_1}{N_{k,m,m'}^{(s)} P_{k,m,m'}} = \frac{3\sigma_s^2 \rho_{k,m,m'}}{16\pi^2 h_{k,m,m'}^2 N_{k,m,m'}^{(s)} N_r P_{k,m,m'}^{(s)} \cos^2 \theta_{k,m,m'} N_t (N_t + 1) (2N_t + 1)}, \\ \text{var}(\hat{\phi}_{k,m,m'}) &\geq \frac{\zeta_2}{N_{k,m,m'}^{(s)} P_{k,m,m'}} = \frac{3\sigma_s^2 \rho_{k,m,m'}}{16\pi^2 h_{k,m,m'}^2 N_{k,m,m'}^{(s)} N_t P_{k,m,m'}^{(s)} \cos^2 \phi_{k,m,m'} N_r (N_r + 1) (2N_r + 1)}, \\ \text{var}(\hat{\tau}_{k,m,m'}) &\geq \frac{\zeta_3}{N_{k,m,m'}^{(s)} (N_{k,m,m'}^{(s)} + 1) (2N_{k,m,m'}^{(s)} + 1) P_{k,m,m'}} , \quad \zeta_3 = \frac{3\sigma_s^2 \rho_{k,m,m'} N^2 T_s^2}{4\pi^2 h_{k,m,m'}^2 N_t N_r}. \end{aligned} \quad (\text{B.3})$$

B.2 Derivation of PEB from CRLB of $\eta_{k,m,m'}$

With the FIM of channel parameters, the $\text{PEB}_{k,m,m'}$ can be derived through the variable transformation tensor \mathbf{T} from $\eta_{k,m,m'}$ to $\mathbf{x}_{k,m'}^{(q)}$, as

$$\mathbf{J}_{\mathbf{x}_{k,m'}^{(q)}} = \mathbf{T} \mathbf{J}_\eta \mathbf{T}^T, \quad \mathbf{T} = \frac{\partial \boldsymbol{\eta}^T}{\partial \mathbf{x}_{k,m'}^{(q)}}, \quad (\text{B.4})$$

where $\mathbf{T} \in R^{3 \times 2}$ can be written as

$$\mathbf{T} = [\partial \tau_k / \partial \mathbf{x}_{k,m'}^{(q)}; \partial \theta_{k,m,m'} / \partial \mathbf{x}_{k,m'}^{(q)}; \partial \phi_{k,m,m'} / \partial \mathbf{x}_{k,m'}^{(q)}]. \quad (\text{B.5})$$

From (6.12-6.15), there are

$$\partial \tau_k / \partial \mathbf{x}_{k,m'}^{(q)} = \frac{1}{c} [\cos(\theta_{k,m,m'}) + \cos(\phi_{k,m,m'}), \sin(\theta_{k,m,m'}) + \sin(\phi_{k,m,m'})]^T \quad (\text{B.6})$$

$$\partial \theta_{k,m,m'} / \partial \mathbf{x}_{k,m'}^{(q)} = \frac{1}{d_{BS,k,m'}} [-\sin(\theta_{k,m,m'}), \cos(\theta_{k,m,m'})]^T, \quad (\text{B.7})$$

$$\partial \phi_{k,m,m'} / \partial \mathbf{x}_{k,m'}^{(q)} = -\frac{1}{d_{k,m',m}} [\cos(\pi - \phi_{k,m,m'}), \cos(\pi - \phi_{k,m,m'})]^T. \quad (\text{B.8})$$

With (B.3) and (B.6-8), $\mathbf{J}_{\mathbf{x}_{k,m'}^{(q)}}$ can be derived as

$$\begin{aligned} \mathbf{J}_{\mathbf{x}_{k,m'}^{(q)}}(1, 1) &= P_{k,m,m'}^{(s)} N_{k,m,m'}^{(s)} \left(\frac{\sin^2 \theta_{k,m,m'}}{\zeta_1 d_{BS,k,m'}^2} + \frac{\cos^2 \theta_{k,m,m'}}{\zeta_2 d_{k,m',m}^2} \right. \\ &\quad \left. + \frac{(\cos \theta_{k,m,m'} + \cos \phi_{k,m,m'})^2}{\zeta_3 c^2} (N_{k,m,m'}^{(s)} + 1)(2N_{k,m,m'}^{(s)} + 1) \right), \\ \mathbf{J}_{\mathbf{x}_{k,m'}^{(q)}}(2, 2) &= P_{k,m,m'}^{(s)} N_{k,m,m'}^{(s)} \left(\frac{\cos^2 \theta_{k,m,m'}}{\zeta_1 d_{BS,k,m'}^2} + \frac{\sin^2 \theta_{k,m,m'}}{\zeta_2 d_{k,m',m}^2} \right. \\ &\quad \left. + \frac{(\sin \theta_{k,m,m'} + \sin \phi_{k,m,m'})^2}{\zeta_3 c^2} (N_{k,m,m'}^{(s)} + 1)(2N_{k,m,m'}^{(s)} + 1) \right). \end{aligned} \quad (\text{B.9})$$

Then, with (B.9), there is

$$\text{PEB}_{k,m,m'} = \sqrt{\text{tr} \left\{ \mathbf{J}_{\mathbf{x}_{k,m'}^{(q)}}^{-1} \right\}} \approx \sqrt{\frac{1}{\mathbf{J}_{\mathbf{x}_{k,m'}^{(q)}}(1, 1)} + \frac{1}{\mathbf{J}_{\mathbf{x}_{k,m'}^{(q)}}(2, 2)}} = \frac{\zeta_{k,m,m'} (N_{k,m,m'}^{(s)})}{\sqrt{N_{k,m,m'}^{(s)} P_{k,m,m'}^{(s)}}}. \quad (\text{B.10})$$

The expression of $\zeta_{k,m,m'}$, with respect to bandwidth, the antenna array, channel gain, noise power, and position of sensing targets and users, can be obtained by substituting (B.9) into (B.10) and is not given due to limits of space.

B.3 Proof of Proposition 1

Proof of proposition 1. The objective function in P_1 in chapter 6 is written as $\sum_{k=1}^K \sum_{m=1}^{M_k} \ln(V_m - V_{m,\min})$, which is a sum of functions in form of

$$\psi_{k,m}(B_{k,m}^{(c)}, P_{k,m}^{(c)}, B_{k,i,m}^{(s)}, P_{k,i,m}^{(s)}) = B_{k,m}^{(c)} \log_2 \left(1 + \frac{P_{k,m}^{(c)} \xi_{k,m} B_0}{B_{k,m}^{(c)}} \right) + \sum_i \frac{\kappa_{k,i,m} P_{k,i,m}^{(s)\alpha} B_{k,i,m}^{(s)\beta}}{S_{k,m,\text{req}}}. \quad (\text{B.11})$$

Through calculating the Hessian matrix of $\psi_{k,m}(B_{k,m}^{(c)}, P_{k,m}^{(c)}, B_{k,i,m}^{(s)}, P_{k,i,m}^{(s)})$, it can be found that it's negative semi-definite respect to $B_{k,m}^{(c)}, P_{k,m}^{(c)}, B_{k,i,m}^{(s)}, P_{k,i,m}^{(s)}$, when $0 \leq \alpha \leq 1; 0 \leq \beta \leq 1$. Thus, the objective function in P_1 is concave since the linear combination of concave is concave. In addition, the constraints C1-C6 are determined over a convex set. Thus, the P_1 is a convex optimization problem.

B.4 Proof of Proposition 2

Given that the objective function outlined in \mathbf{P}_1 is both concave and injective, it satisfies all the Nash Bargaining axioms as delineated in [66]. When $V_{m,min} = 0$, the utility function in \mathbf{P}_1 is $\sum_{k=1}^K \sum_{m=1}^{M_k} \ln(V_{k,m} - V_{k,m,min}) = \sum_{k=1}^K \sum_{m=1}^{M_k} \ln(V_{k,m})$. The proportional fairness requires $\sum_{k=1}^K \sum_{m=1}^{M_k} \frac{V_{k,m} - V_{k,m}^*}{V_{k,m}^*} \geq 0$ [164], which can be achieved at $V_{m,min} = 0$.

Curriculum Vitae

Name: Biwei Li

Post-Secondary Education and Degrees: 2020 - Present, Ph.D.
Electrical and Computer Engineering
The University of Western Ontario
London, ON, Canada

2017 - 2019, M.Eng.
Computer and Communication Engineering
University of Science and Technology Beijing
Beijing, China

2013 - 2017, B.Eng.
Computer and Communication Engineering
University of Science and Technology Beijing
Beijing, China

Related Work Experience: Teaching Assistant
The University of Western Ontario
2020 - 2023

Research Assistant
The University of Western Ontario
2020 - Present

Publications:

- 1 **B. Li** and X. Wang, "Rigid body localization and environment sensing with 5G millimeter wave MIMO," in *Proc. IEEE 94th Veh. Technol. Conf. (VTC-Fall)*, Norman, OK, USA, 2021, pp. 1-5.
- 2 **B. Li**, X. Wang, E. Au and Y. Xin, "Joint localization and environment sensing of rigid body with 5G millimeter wave MIMO," *IEEE O. J. Signal Process.*, vol. 4, pp. 117-131, 2023.

- 3 **B. Li**, X. Wang, Y. Xin and E. Au, “Value of service maximization in integrated localization and communication system through joint resource allocation,” *IEEE Trans. Commun.*, vol. 71, no. 8, pp. 4957-4971, Aug. 2023.
- 4 **B. Li**, X. Wang, S. Ahn, S. Park and Y. Wu, “Successive resource allocation in multi-user ISAC system through deep reinforcement learning,” (*IEEE International Conference on Communications 2024*, accepted).
- 5 **B. Li**, X. Wang and F. Fang, “Maximizing the value of service provisioning in concurrent multi-user sensing over wireless networks through fairness guaranteed collaborative resource allocation,” (submitted to *IEEE Journal on Selected Areas in Communications*, under major revision).
- 6 **B. Li** and X. Wang “Value of service maximization in distributed ISAC system through spatial-aware resilient resource allocation,” (to be submitted).
- 7 R. Chen, **B. Li** and X. Wang, “Multi-camera collaboration for 3D visualization via correlated information maximization,” *IEEE Internet Things J.*, doi: 10.1109/JIOT.2023.3322698.